

Dynamics and Inhibition
of Class II
Fructose 1,6-bisphosphate Aldolase

by

Geneviève Labbé

A thesis
presented to the University of Waterloo
in fulfillment of the
thesis requirement for the degree of
Doctor of Philosophy
in
Chemistry

Waterloo, Ontario, Canada, 2009

©Geneviève Labbé 2009

AUTHOR'S DECLARATION

I hereby declare that I am the sole author of this thesis. This is a true copy of the thesis, including any required final revisions, as accepted by my examiners.

I understand that my thesis may be made electronically available to the public.

Abstract

It has been suggested for many decades that the essential and ubiquitous enzyme fructose 1,6-bisphosphate aldolase (FBA) could be a good drug target against bacteria and fungi, since lower organisms possess a metal-dependent (Class II) FBA, as opposed to higher organisms which possess a Schiff-base forming, metal-independent (Class I) FBA. The purpose of this doctoral project was to purify and study the inhibition of Class II FBA from pathogenic organisms. The capacity of various thiol compounds, as well as various derivatives of the metal-chelating compound dipicolinic acid, to inhibit the purified Class II FBAs from *Mycobacterium tuberculosis*, *Pseudomonas aeruginosa*, *Bacillus cereus*, and from the Rice Blast causative agent *Magnaporthe grisea*, was compared. The genes were subcloned in the *Escherichia coli* vector pT7-7 and the enzymes purified to near homogeneity, and characterized using a coupled assay. A small fed-batch fermentor was used to express the enzymes in *E. coli*, and yields of up to 2 grams of purified protein per liter of bacterial culture were obtained. The commercially available compound 2,3-dimercaptopropane sulfonate was found to be the most effective inhibitor against the aldolase from *M. tuberculosis*, with a second order binding rate constant of $500 \pm 4 \text{ M}^{-1}\text{s}^{-1}$, which is three times and twenty times higher than the constants obtained with dipicolinic acid and EDTA, respectively.

In an attempt to detect the enzyme dynamics during catalysis or inhibition, tryptophan residues were used as reporter groups and introduced by site-directed mutagenesis into the catalytic mobile loops and near the active site of the aldolases from *M. tuberculosis*, *P. aeruginosa* and *B. cereus*. The kinetic characterization of the mutants is described; as well as the effect of substrate binding on the steady-state and time-resolved fluorescence signals. Finally, the possibility of using the recombinant Class II FBP aldolases for industrial chemical synthesis was explored by measuring the enzymatic stability in organic solvents, at high temperatures and at different pH conditions. Surprisingly, the

commercial Class I enzyme from rabbit muscle was more stable than the metalloenzymes in most conditions tested. The results presented in this thesis will be useful for the future design of Class II FBP aldolase inhibitors.

Acknowledgements

I would first like to thank my supervisor Dr. J. Guy Guillemette, for his guidance, support, patience and understanding during the last 6 years. No one else could have pulled me back into pursuing another graduate degree and made it so ~~painless~~ enjoyable as well: I am forever grateful for this.

I would also like to thank our collaborators Dr. Gary I. Dmitrienko and Dr. Eric Jervis, as well as my advisory committee members Dr. Janet Wood, Dr. Michael Palmer, and Dr. John Honek, for their help and advice during my studies.

I thank Sarah de Groot, Jeremy Bezaire, Jason Yaeck, Dr. Anthony Krismanich, Liangchen Wang, Peggy Ramsaywak, Tim Rasmusson, Natasha Kruglyak, Christine How, Willis Lang, Gorica Milojevic, Diana Arsene, Ali Farsi, Val Goodfellow, Timothy Ramadhar, Miriam Heynen, and Dr. Stefan Siemann for working with me on this project; I had great pleasure in crossing your path and wish you all the best in your careers. I also thank Dr. Muhong Shang, Matthew D. Brown, Dr. Vassili Karanassios, Hamid Badiei, Dr. Jurgen Sygusch, and Mathieu Coincon for their work on this project.

I thank my labmates Dr. Don Spratt, Andrea Dupont, Erika Murray, Odi Israel, Valentina Taiakina, Yay Duangkham, Jennifer Lapierre and Elena Newman for their friendship and support. I hope we will have some cake in Petri dishes again from time to time...

I am also grateful to our Chemistry Department graduate secretary Cathy Van Esch for her kind help during my time at Waterloo.

I want to acknowledge the help from the educators at the University of Guelph Child Care and Learning Centre as well as from the staff for the YMCA after-school care at Ecole John McCrae in Guelph for caring for my son while I was pursuing this degree. I would also like to thank the University of Guelph and YMCA organization for their investment in providing quality childcare. Without that crucial community help, this thesis would never have been written.

Project funding was provided by NSERC.

Personal funding was also generously provided by three Ontario Graduate Scholarships, three UW President's Graduate Scholarships, two Travel Award for the ASBMB annual conferences in San Francisco and Washington, two UW Provost's/Faculty of Science Graduate Women's Incentive Fund Scholarships, and the GWC² Merck Frosst Biochemistry Award.

Je voudrais remercier mes parents Jean-Yves et Béatrice pour m'avoir donné les outils, le support et les encouragements nécessaire à la réussite de ma carrière. Votre amour et votre dévouement sont des sources d'inspiration constantes.

Finally, I would like to thank my husband, Dr Stephen Seah, and our son Mathieu for their love and unconditional support. I never thought that I would be (still) in school at the same time as my son, but I am confident that we will both do great things with our education when we grow up.

Dedication

*I would like to dedicate this thesis
to all the women in science and engineering,
and to those who support them.*

Table of Contents

List of Figures	xi
List of Tables	xv
Abbreviations	xvii
Chapter 1 Introduction.....	1
1.1 Biochemistry and drug discovery	1
1.2 Fructose 1,6-bisphosphate aldolase as a new drug target	5
1.2.1 Role of FBP aldolases	5
1.2.2 Phylogeny of FBP aldolases	6
1.2.3 Knock-out studies of Class II FBP aldolase	10
1.2.4 Why is FBP aldolase essential? – Glucose metabolism review	11
1.2.5 Possible alternative roles of FBP aldolases and their potential as vaccine targets	17
1.2.6 Summary: Justification for the choice of Class II aldolase as drug target.....	19
1.3 Class II FBP aldolase structure and mechanism.....	19
1.3.1 Aldolase groups and DHAP-dependant aldolases	20
1.3.2 Industrial use of FBP aldolases	22
1.3.3 TIM barrel, or ($\beta\alpha$) ₈ -barrel, enzymes superfamily	23
1.3.4 Structure of Class II FBP aldolase.....	25
1.3.5 Class II FBP aldolase mechanism	31
1.3.6 Catalytic loops.....	40
1.4 Inhibitors of FBP aldolase	44
1.4.1 Mechanism-based inactivators	44
1.4.2 Substrate analogue inhibitors	45
1.4.3 Inhibitors with high affinity for Class I aldolases	45
1.4.4 Inhibitors with high affinity for Class II aldolases	46
1.5 Target organisms	47
1.6 Summary	53
1.7 Project overview	54
1.8 Research objectives	55

1.9 Outline of the thesis	55
Chapter 2 Cloning, expression and purification of Class II FBP aldolases	57
2.1 Introduction.....	57
2.2 Procedures.....	59
2.2.1 Cloning of FBP aldolases in vector pT7-7.....	59
2.2.1.1 Materials	59
2.2.1.2 Bacterial strains.....	59
2.2.1.3 Genomic DNA	59
2.2.1.4 General molecular biology methods	60
2.2.1.5 PCR amplification of FBP aldolase genes	61
2.2.1.6 Cloning into the expression vectors pT7-7 and pT7-5.....	62
2.2.1.7 Removal of introns in <i>M. grisea</i> FBP aldolase	63
2.2.2 Growth and expression.....	64
2.2.2.1 Fermentor growth.....	64
2.2.2.2 Shake-flask growth for <i>E. coli</i> and <i>M. tuberculosis</i> aldolase overexpression.....	67
2.2.3 Enzymatic assays	68
2.2.4 Protein quantification.....	70
2.2.5 SDS-PAGE	70
2.2.6 Purification.....	70
2.2.6.1 Crude extract preparation.....	70
2.2.6.2 Ammonium sulfate fractionation	72
2.2.6.3 Chromatography	74
2.2.7 ESI mass spectrometry.....	78
2.3 Results.....	79
2.3.1 Cloning.....	79
2.3.2 Growth and expression.....	81
2.3.3 Purification.....	87
2.3.3.1 <i>M. tuberculosis</i> aldolase.....	88
2.3.3.2 <i>P. aeruginosa</i> aldolase	93
2.3.3.3 <i>B. cereus</i> aldolase.....	95
2.3.3.4 <i>M. grisea</i> aldolase	97
2.3.3.5 <i>H. pylori</i> aldolase	97

2.3.3.6 <i>E. coli</i> aldolase.....	98
2.3.4 Mass spectrometry results	100
2.4 Discussion	101
Chapter 3 Characterization of recombinant Class II FBP aldolases.....	109
3.1 Introduction	109
3.2 Procedures	112
3.2.1 Quaternary structure determination.....	112
3.2.2 Enzyme stability	112
3.2.2.1 Stability in assay solution at 4 °C.....	112
3.2.2.2 Temperature stability.....	113
3.2.2.3 Organic solvent stability.....	113
3.2.3 Determination of Michaelis-Menten parameters for FBP cleavage	113
3.2.4 Metal content determination.....	114
3.2.5 Metal replacement studies	114
3.3 Results	115
3.3.1 Quaternary structure.....	115
3.3.2 Optimum pH.....	118
3.3.3 Enzyme stability	119
3.3.4 Metal content and metal specificity.....	124
3.3.5 Kinetic parameters.....	131
3.4 Discussion	132
Chapter 4 Inhibition of Class II FBP aldolases	141
4.1 Introduction	141
4.2 Procedures	143
4.2.1 Inhibition screens.....	143
4.2.2 Inhibition assays (IC ₅₀ S)	144
4.2.3 Metal reactivation assays.....	144
4.2.4 Second order rate constants determination.....	145
4.3 Results	146
4.3.1 Inhibition screens.....	146
4.3.2 Inhibition model	158

4.4 Discussion	163
Chapter 5 Preliminary work on enzyme loop dynamics	171
5.1 Introduction.....	171
5.2 Methods.....	178
5.2.1 Site-directed mutagenesis	178
5.2.2 Expression and purification	180
5.2.3 Activity assays, protein assays, and SDS-PAGE	182
5.2.4 Steady-state fluorescence	182
5.2.5 Time-resolved fluorescence	183
5.3 Results.....	184
5.3.1 Cloning, purification and characterization.....	184
5.3.2 Equilibrium fluorescence studies	190
5.3.3 Time-resolved fluorescence	197
5.4 Discussion	204
Chapter 6 Original contributions and recommendations	209
6.1 Conclusions.....	209
6.2 Original contributions to research.....	210
6.3 Recommendations.....	211
Appendices	
Appendix A Plasmids, aldolase genes, and protein sequences	215
Appendix B Synthesized inhibitory compounds codes and molecular weights.....	239
Appendix C Derivation of time-dependent irreversible inhibition equations	243
References.....	249

List of Figures

Figure 1.1 Fructose 1,6-bisphosphate aldolase reaction.....	6
Figure 1.2 Biochemical pathways involving fructose-1,6-bisphosphate aldolase.....	7
Figure 1.3 The two different catalytic mechanisms of the Class I and Class II aldolases.....	8
Figure 1.4 Phylogenetic tree of Class II aldolases.....	9
Figure 1.5 Pathways for glucose degradation.....	13
Figure 1.6 DHAP-dependant aldolases and their substrates.....	21
Figure 1.7 TIM barrel structure.....	24
Figure 1.8 Structures of Class II FBP aldolases.....	26
Figure 1.9 Stereo image of the <i>E. coli</i> Class II FBP aldolase active site metals.....	28
Figure 1.10 Comparison of structural features of Class II FBP aldolases.....	29
Figure 1.11 <i>E. coli</i> Class II FBP aldolase active site.....	30
Figure 1.12 Proposed mechanism of the <i>E. coli</i> Class II FBP aldolase.....	32
Figure 1.13 Putative binding groove for the substrate GAP in the <i>E. coli</i> FBP aldolase.....	37
Figure 1.14 Spontaneous cyclization of D-fructose-1,6-bisphosphate and hydration of dihydroxyacetone phosphate in solution.....	39
Figure 1.15 Structure of the unligated <i>T. aquaticus</i> monomer and <i>E. coli</i> Class II FBP aldolase dimer colored according to B-factors.....	43
Figure 1.16 Class II FBP aldolase inhibitors.....	47
Figure 1.17 Sequence alignment of Class II FBP aldolases.....	48
Figure 2.1 Coupled enzymatic assay to monitor FBP cleavage.....	68
Figure 2.2 In-house technique for dialysis of a small volume of protein solution.....	79
Figure 2.3 Structure of the <i>M. grisea</i> aldolase gene.....	80
Figure 2.4 Harvested <i>E. coli</i> BI21(λ DE3) cells from 1.5 L fermentor culture.....	82
Figure 2.5 Culture growth and substrate feeding profiles.....	82
Figure 2.6 pH stat feeding control.....	83
Figure 2.7 Fermentor expression of <i>P. aeruginosa</i> FBP aldolase in <i>E. coli</i> BI21(λ DE3).....	84
Figure 2.8 Expression of <i>B. cereus</i> aldolase in fermentor culture and 1.5 mL cultures.....	85
Figure 2.9 Expression of the <i>M. tuberculosis</i> aldolase in the fermentor.....	85
Figure 2.10 Small-scale expression of the <i>H. influenzae</i> FBP aldolase.....	87

Figure 2.11 SDS-PAGE showing purification of the recombinant <i>M. tuberculosis</i> Class II fructose 1,6-bisphosphate aldolase from shake-flask grown cells.....	89
Figure 2.12 SDS-PAGE of the <i>M. tuberculosis</i> aldolase purification from fermentor-grown cells (induced with 0.5 mM IPTG).....	90
Figure 2.13 SDS-PAGE of the purification of the FBP aldolase from <i>M. tuberculosis</i> (fermentor-grown, induced with 2.5 mM IPTG).....	92
Figure 2.14 SDS-PAGE of the elution fraction from the Sepharose-Q column containing the <i>P. aeruginosa</i> aldolase	94
Figure 2.15 SDS-PAGE of the purified FBP aldolases.....	96
Figure 2.16 SDS-PAGE of the purification steps for the <i>E. coli</i> FBP aldolase	99
Figure 3.1 PAR structure	114
Figure 3.2 Quaternary structure determination of the recombinant <i>B. cereus</i> and <i>M. grisea</i> Class II FBP aldolases by gel filtration.....	116
Figure 3.3 Dimeric <i>M. grisea</i> FBP aldolase crystal structure.	117
Figure 3.4 Quaternary structure determination of the recombinant <i>P. aeruginosa</i> Class II fructose 1,6-bisphosphate aldolase by gel filtration.....	118
Figure 3.5 pH optimum of the purified Class II aldolases for the FBP cleavage reaction.....	119
Figure 3.6 Organic solvent stability of FBP aldolases.....	120
Figure 3.7 Temperature stability of the purified FBP aldolases.	121
Figure 3.8 Enzyme stability in assay mixture at 4 °C.....	123
Figure 3.9 Stability of the <i>B. cereus</i> and <i>P. aeruginosa</i> aldolases in the assay mixture at 4 °C.....	124
Figure 3.10 Effect of CoCl ₂ on the aldolases from <i>P. aeruginosa</i> and <i>H. pylori</i>	126
Figure 3.11 Activity of the <i>M. tuberculosis</i> aldolase in the presence of 2 μM of various divalent metals.....	129
Figure 3.12 Reactivation of the FBP aldolases from <i>P. aeruginosa</i> , <i>B. cereus</i> and <i>H. pylori</i> with divalent metals after EDTA treatment.....	130
Figure 4.1 Scheme of competitive reversible inhibition with associated rate constants.....	146
Figure 4.2 Compounds with characteristics related to the cyclic form of the substrate FBP used for the initial inhibitor screen.	147
Figure 4.3 Other commercially available molecules tested for inhibition	150
Figure 4.4 DPA derivatives and thiol-containing inhibitors	151
Figure 4.5 Cornish-Bowden plots of the inhibition data with the compounds 6 and 8.....	155

Figure 4.6 Progress curves of FBP cleavage by <i>M. tuberculosis</i> Class II aldolase in the presence of different metal-chelating inhibitors	156
Figure 4.7 Progress curve of FBP cleavage by <i>M. tuberculosis</i> Class II aldolase in the presence of compound 13 and added zinc chloride	157
Figure 4.8 Progress curves of FBP cleavage by the <i>M. tuberculosis</i> aldolase in the presence of 500 μ M DMPS	159
Figure 4.9 Tsou's test for competitive irreversible inhibition.....	160
Figure 4.10 Secondary plot of the apparent inhibition constants obtained with the <i>M. tuberculosis</i> aldolase in the presence of DMPS, as a function of the FBP concentration	162
Figure 4.11 PGH and sulfur-containing analogues	167
Figure 4.12 DMPS and AK4 docked into the <i>E. coli</i> Class II FBP aldolase active site.....	168
Figure 5.1 Targeted amino acids for tryptophan replacement in the <i>M. tuberculosis</i> Class II FBP aldolase.....	175
Figure 5.2 Targeted amino acids for tryptophan replacement in the <i>H. pylori</i> , <i>P. aeruginosa</i> and <i>B. cereus</i> Class II FBP aldolases	176
Figure 5.3 Targeted amino acids for site-directed mutagenesis	177
Figure 5.4 SDS-PAGE analysis of the purified MTI175W mutant.....	185
Figure 5.5 SDS-PAGE analysis of the purified MTN173W mutant	186
Figure 5.6 SDS-PAGE analysis of the purified MTY280W mutant	186
Figure 5.7 SDS-PAGE analysis of the purified BCI149W mutant	187
Figure 5.8 SDS-PAGE analysis of the purified PAF202W mutant.....	188
Figure 5.9 Fluorescence emission spectra of the <i>B. cereus</i> wild-type aldolase and its mutant BCI149W in the presence or absence of FBP	191
Figure 5.10 Fluorescence emission spectra of the wild-type aldolase from <i>B. cereus</i> (BC-WT) and of the mutant BCI149W in the presence of FBP or DMPS, in function of the excitation wavelength.	192
Figure 5.11 Absorption spectra of compound 6 and effect on fluorescence emission of <i>B. cereus</i> aldolase mutant I149W in function of the excitation wavelength.	193
Figure 5.12 Fluorescence emission spectra of mutant BCI149W enzyme in the presence of DMPS	194
Figure 5.13 Emission spectra of the <i>M. tuberculosis</i> aldolase and its mutants	195
Figure 5.14 Fluorescence emission spectra of the <i>M. tuberculosis</i> aldolase and its mutants in the presence of FBP and DMPS	196

Figure 5.15 Time-resolved fluorescence.....	201
Figure 6.1 Location of the Val-to-Gly substitution in the heat-sensitive <i>E. coli</i> Class II FBP aldolase (<i>ts8</i> mutation).....	213
Figure 6.2 Map of plasmid pT7-5.....	215
Figure 6.3 Map of plasmid pT7-7.....	218
Figure 6.4 Map of plasmid pT7-7/HIFBA.....	221
Figure 6.5 Map of plasmid pT7-7/HPFBA.....	223
Figure 6.6 Map of plasmid pT7-5/BCFBA.....	225
Figure 6.7 Map of plasmid pT7-7/MTFBA.....	231
Figure 6.8 Map of plasmid pT7-7/PAFBA.....	233
Figure 6.9 Map of plasmid pT7-7/MGFBA.....	235
Figure 6.10 Map of plasmid pT7-7/SPFBA.....	237

List of Tables

Table 2.1 Primers used to PCR amplify FBP aldolase genes	62
Table 2.2 Media composition	65
Table 2.3 Trace metals solution composition	65
Table 2.4 Cell weight obtained for fermentor and shake-flask bacterial cultures after recombinant aldolase expression	86
Table 2.5 Purification of the recombinant <i>M. tuberculosis</i> Class II fructose 1,6-bisphosphate aldolase (shake-flask grown)	89
Table 2.6 Purification table for the <i>M. tuberculosis</i> FBP aldolase (fermentor-grown, induced with 0.5 mM IPTG)	91
Table 2.7 Purification table for the <i>M. tuberculosis</i> FBP aldolase (fermentor-grown, induced with 2.5 mM IPTG)	93
Table 2.8 Purification table of the <i>P. aeruginosa</i> FBP aldolase	95
Table 2.9 Purification table for the <i>B. cereus</i> FBP aldolase	96
Table 2.10 Purification of the recombinant <i>M. grisea</i> Class II FBP aldolase	97
Table 2.11 Purification table of the <i>H. pylori</i> FBP aldolase	98
Table 2.12 Purification table for the <i>E. coli</i> FBP aldolase	100
Table 2.13 Mass spectrometry results for purified recombinant aldolases	101
Table 3.1 Kinetic parameters table for Class II FBP aldolases published by other groups	111
Table 3.2 Zinc content of the recombinant aldolases	125
Table 3.3 Kinetic parameters and quaternary structure of recombinant Class II aldolases (this study)	131
Table 4.1 Inhibition screen of compounds with FBP related structures	148
Table 4.2 Summary of IC ₅₀ values with DPA derivatives	152
Table 4.3 Summary of inhibition with thiol-containing compounds	153
Table 4.4 Second order rate constants for the binding of chelating inhibitors to the recombinant Class II aldolase from <i>M. tuberculosis</i>	163
Table 5.1 Primers used in site-directed mutagenesis	179
Table 5.2 Mass spectrometry results for the purified tryptophan mutants	188
Table 5.3 Purification results and kinetic parameters of the tryptophan mutants	189

Table 5.4 Peak fluorescence emission wavelengths of the native and mutated Class II FBP aldolases from <i>B. cereus</i> and <i>M. tuberculosis</i>	197
Table 5.5 Time-resolved decay constants and associated amplitudes	200
Table 6.1 Synthesized inhibitory compounds names and structures.....	239

Abbreviations

1,3-BPG	1,3-Bisphosphoglycerate
2PG	2-Phosphoglycerate
3PG	3-Phosphoglycerate
ADP	Adenosine diphosphate
AIDS	Acquired Immune Deficiency Syndrome
Amp	Ampicillin
ATP	Adenosine triphosphate
BC or BCFBA	<i>Bacillus cereus</i> Class II FBP aldolase (short from used in Figure legends)
bp	Base pair
BSA	Bovine Serum Albumin
CoA	Coenzyme A
CV	Column Volume
Da	Dalton
DEAE	Diethylaminoethyl
DHAP	Dihydroxyacetone phosphate
DMF	Dimethylformamide
DMSO	Dimethyl sulfoxide
DNA	Deoxyribonucleic acid
dNTP	2'-Deoxynucleotide triphosphate
DPA	Dipicolinic acid, or pyridine 2,6-dicarboxylic acid
DTT	Dithiothreitol
EC or ECFBA	<i>E. coli</i> Class II FBP aldolase (short from used in Figure legends)
<i>E. coli</i>	<i>Escherichia coli</i>
ED pathway	Entner-Doudoroff pathway
EDTA	Ethylenediaminetetra-acetate
EMP pathway	Embden-Meyerhof-Parnas pathway
F1P	Fructose 1-phosphate
F6P	Fructose 6-phosphate
<i>fba</i>	Fructose 1,6-bisphosphate aldolase gene
<i>fba-</i>	Fructose 1,6-bisphosphate aldolase-deficient strain

FBP	Fructose 1,6-bisphosphate
FBP aldolase	Fructose 1,6-bisphosphate aldolase
G6P	Glucose 6-phosphate
G acid	Glyceric acid
GAP	Glyceraldehyde 3-phosphate
Gluconic acid 6P	Gluconic acid 6-phosphate
<i>gnd</i> -	Gluconate 6-phosphate dehydrogenase-deficient strain
HI or HIFBA	<i>Haemophilus influenzae</i> Class II FBP aldolase (short from used in Figure legends)
HP or HPFBA	<i>Helicobacter pylori</i> Class II FBP aldolase (short from used in Figure legends)
IPTG	Isopropyl- β -D-thiogalactoside
k_{cat}	Catalytic constant
kDa	Kilodalton
K_M	Michaelis constant
LB broth	Luria-Bertani broth
MG or MGFBA	<i>Magnaporthe grisea</i> Class II FBP aldolase (short from used in Figure legends)
MT or MTFBA	<i>Mycobacterium tuberculosis</i> Class II FBP aldolase (short from used in Figure legends)
NAD ⁺	Nicotinamide adenine dinucleotide, oxidized form
NADH	Nicotinamide adenine dinucleotide, reduced form
NADP ⁺	Nicotinamide adenine dinucleotide phosphate, oxidized form
NADPH	Nicotinamide adenine dinucleotide phosphate, reduced form
NCBI	National Center for Biotechnology Information
NSERC	Natural Sciences and Engineering Research Council of Canada
OD	Optical density
PA or PAFBA	<i>Pseudomonas aeruginosa</i> Class II FBP aldolase (short from used in Figure legends)
PAR	4-(2-pyridylazo)-resorcinol
PDB	Protein Data Bank (http://www.rcsb.org)
PDTC	Pyridine- 2,6-bis(thiocarboxylic acid)
PEP	Phosphoenolpyruvate
PGH	Phosphoglycolohydroxamate

<i>pgi</i> -	Phosphoglucose isomerase-deficient strain
RAMA	Rabbit muscle (Class I) FBP aldolase
RBS	Ribosome binding site
RNA	Ribonucleic acid
rRNA	ribosomal RNA
SC or SCFBA	<i>Saccharomyces cerevisiae</i> (yeast) Class II FBP aldolase (short from used in Figure legends)
SDS-PAGE	Sodium dodecyl sulphate polyacrylamide gel electrophoresis
SP or SPFBA	<i>Streptococcus pneumoniae</i> Class II FBP aldolase (short from used in Figure legends)
TB	Tuberculosis
TB broth	Terrific Broth
TBP	Tagatose 1,6-bisphosphate
TIM	Triose phosphate isomerase
TLC	Thin layer chromatography
Tris	2-Amino-2-hydroxymethylpropane 1,3-diol
ts	Temperature sensitive
USRA	Undergraduate Student Research Award
UV	Ultraviolet
Vis	Visible
WHO	World Health Organization

The three letter and one letter abbreviations for amino acids are used throughout this thesis according to the IUPAC-IUB Joint Commission on Biochemical Nomenclature (J.C.B.N. 1984). Single letter abbreviations are also used for DNA bases.

Chapter 1

Introduction

1.1 Biochemistry and drug discovery

The central goal of the project described in this thesis is the discovery of a new drug against bacterial and fungal pathogens. The widespread recognition of microorganisms as disease agents in the mid-nineteenth century quickly led to better sanitation and large vaccination campaigns, reducing dramatically the number of deaths by infectious disease. The search for antimicrobial agents which could block essential cellular functions in microbes, but not in humans, followed. Today, thanks to the widespread availability of vaccination and antibiotics, less than 1% of all fatalities are caused by bacterial infections in the United Kingdom (WHO 2004), compared to up to three quarters of all fatalities in the mid-18th century England (Gage 2005; 1993).

Of these two major weapons we now have against microbes, vaccination remains the most cost-effective intervention measure in medicine, as for each \$1 in vaccination, \$5 to \$10 are saved in treatment (Kaufmann 2007). However, vaccination is not effective or practical for all microbial infections. For example, there is a vaccine offering good protection against the severe form of tuberculosis (TB) in children, but vaccination still cannot prevent the adult, pulmonary form of TB. There are also vaccines that are not used on a large scale because the risk of infection is too small to justify the cost and potential vaccine risks, as is the case for anthrax. Vaccinations have been ineffective in cases of AIDS and infections associated with immunosuppressive drugs used in organ transplants, wounds including massive burns, chronic diseases such as cystic fibrosis, or old age,

Chapter 1 Introduction

where the immune system is weakened and susceptible to secondary infections by opportunistic pathogens. Therefore, the need for drugs that can cure established microbial infections remains.

Today, there are two main methods for antimicrobial drug discovery: screening or design. The “golden age” of antibiotic discovery during which most drug classes in use today were discovered, occurred by screening from 1940 to 1960. Several advances during the subsequent years, particularly in molecular biology, brought the design of drugs within our reach. A major turning point, the discovery that protein sequences are encoded in genomic DNA, came in the 1940s. The subsequent development of the x-ray crystallography technique led to the elucidation of DNA structure and of the first enzyme structure in the 1950s. The new DNA cloning techniques combined with the genome sequencing efforts have greatly accelerated the biochemical study of drug-targeted proteins. It is now estimated that the human genome contains 20,000 to 25,000 protein-coding genes (International Human Genome Sequencing Consortium (I.H.G.S.C. 2004)), roughly 5 times as many as the number present in typical bacterial genomes (Wellcome Trust Sanger Institute (W.T.S.I. 2008)). We now see the beginning of systems biology and the bird’s-eye view of all the enzymatic reactions happening in one organism. With each technological advance, we improve our understanding of the complexity of life, and we find more opportunities for disease treatment.

In spite of these remarkably rapid advances in biological sciences, the number of antimicrobial agents has declined steadily since 1960. In fact, only two new classes of antibiotics were introduced between 1960 and the beginning of the 21st century: quinolones (nalidixic acid) in 1962 and phosphonates (fosfomycin) in 1969 (Walsh and Wright 2005). Current antibiotics have only four general targets in the cell: folate metabolism, ribosomes, envelope synthesis, and nucleic acid replication (Walsh 2003). Resistance to all these classes of antibiotics has already been observed (Franceschi and Duffy 2006). In addition to bacterial infections, the number of invasive fungal infections, such as those caused by *Candida albicans*, is also increasing due to the increased number

of AIDS patients and other immunocompromised patients. New drug-resistant fungal strains are also seen with higher frequency (Shao *et al.* 2007; Veiga-Crespo *et al.* 2007). Current medical antifungal agents are plagued by the development of resistance and cause side effects in patients, emphasizing the constant need for the development of new drugs (Pasqualotto and Denning 2008). It is important to note that it is harder to find suitable antifungal agents than antibacterial agents, because fungi are eukaryotes and thus share many enzymes and metabolic routes with plants and humans, resulting in toxic side-effects for the host. The number of validated drug targets in fungi is thus small in comparison with bacteria (Brown and Wright 2005). In addition to human pathogens, there are also numerous microbial plant pathogens, bacterial and fungal, that cause problems in agriculture. The oomycete *Phytophthora infestans* causing potato blight and the fungus *Magnaporthe grisea* causing rice blast, as well as numerous other strains, are responsible for important crop losses each year worldwide (Oerke 2004). New antifungal agents are therefore needed to counter both the rise of pesticide-resistant crop pathogens and the drug-resistant human pathogens.

The two approaches that can be used for drug discovery, screening of natural compounds (and of synthetic compounds libraries) or target-based design, have not been equally successful. The vast majority of drugs used today are actually derivatives of natural compounds discovered through phenotype-based screening (Brown and Wright 2005). This led major pharmaceutical companies to invest heavily in the techniques of High Throughput Screening. With the advances in genomics and computer modeling, the focus was shifted towards target-based drug discovery in the early 1990s. This approach has not been as successful as anticipated, in part because there are problems such as cell membrane permeability and intracellular modifications of drugs as some antimicrobials are prodrugs that are activated by intracellular enzymes. Most large pharmaceutical companies have now pulled out of antimicrobial research, as the financial return on investment is not high enough. Antibiotics are not used for long periods like drugs against chronic conditions, and the development

Chapter 1 Introduction

of resistance in the pathogens limits the useful life of the drugs (Nathan 2004). Over the last ten years, there were less than a dozen new antibacterial compounds produced by these companies that can significantly help to counter the problem of resistance. The major mechanism for drug resistance in bacteria is genetic change followed by natural selection. The bacteria can also acquire extrachromosomal DNA (usually plasmids) that includes genes that confer resistance to specific antibiotics. Five mechanisms of resistance have been identified (Black 1999). One mechanism is alteration of the target, for example the bacterial ribosomes, which prevents the effective binding of the antimicrobial agent. Another mechanism is the alteration of the membrane permeability, which occurs through changes in membrane proteins that are part of transport systems or membrane pores. A third mechanism is the development of enzymes which inactivate drugs, such as β -lactamases. Bacteria can also become drug-resistant through the alteration of an enzyme, for example by increasing its affinity for its substrate at the expense of the drug, as is seen in sulfonamide-resistance. A final mechanism is the alteration of a metabolic pathway, whereby bacteria can bypass the reaction inhibited by the antimicrobial agent. These resistance mechanisms are the reasons behind the constant need for new generations of drugs. Most of the “new” antibiotics produced in the last ten years are in fact 2nd, 3rd, or subsequent generation derivatives of natural compounds discovered decades ago (Monaghan and Barrett 2006).

Although structure-based drug design has not yet been very successful for the production of novel antibacterial or antifungal compounds, this approach was indeed successful in the design of inhibitors of viral and mammalian enzymes. In the case of AIDS, the structure of a protease led to the design of 5 marketed drugs (Franceschi and Duffy 2006). Inhibitors produced against the zinc-dependant mammalian enzyme carbonic anhydrase offer other examples (Krishnamurthy *et al.* 2008). Structure-based drug design has great potential for the production of new drugs. However, it is still a rather lengthy process, making it potentially better suited for academic than for industrial research. Due to

the long duration of the drug discovery process, the choice of the appropriate target at the outset is obviously critical. The subsequent sections in this chapter will introduce the target chosen for this project.

1.2 Fructose 1,6-bisphosphate aldolase as a new drug target

In this section, the distribution and role of fructose 1,6-bisphosphate aldolase among living organisms will be reviewed. The biological roles of the enzyme will be discussed, as well as the consequence of the reduction of its activity for bacterial and fungal growth. The potential and limitations of this enzyme as a new antibacterial and antifungal drug target will be outlined.

1.2.1 Role of FBP aldolases

The beginning of the scientific investigation of the metabolic pathways occurred around the beginning of the 20th century. The most common glycolytic pathway was elucidated between 1932 and 1939 (Meyerhof 1948), concomitant with the identification of central metabolic enzymes such as fructose 1,6-bisphosphate (FBP) aldolase (Meyerhof *et al.* 1936). FBP aldolases (E.C. 4.1.2.13) catalyze the reversible aldol condensation of dihydroxyacetonephosphate (DHAP) and glyceraldehyde 3-phosphate (GAP) (Figure 1.1) in glycolysis, gluconeogenesis, and the Calvin cycle (Figure 1.2).

The pathways of glycolysis and gluconeogenesis are universal and present in nearly all living organisms. The Calvin cycle is found in photosynthetic organisms and chemoautotrophic bacteria and allows the fixation of carbon dioxide into glyceraldehyde 3-phosphate, which can then be incorporated into other sugars (Voet and Voet 2004). Only 2 known prokaryotic genome sequences do not encode a homologue of the FBP aldolase, and it is possible that they encode an enzyme too divergent from known sequences for it to be identified by genomic analysis. The organisms

Chapter 1 Introduction

apparently lacking an FBP aldolase are the Archea *Thermoplasma acidophilum* and *Pyrobaculum aerophilum* (Verhees *et al.* 2003). Some FBP aldolases have a structural role in the cell in addition to their catalytic role, as will be briefly discussed in the following section.

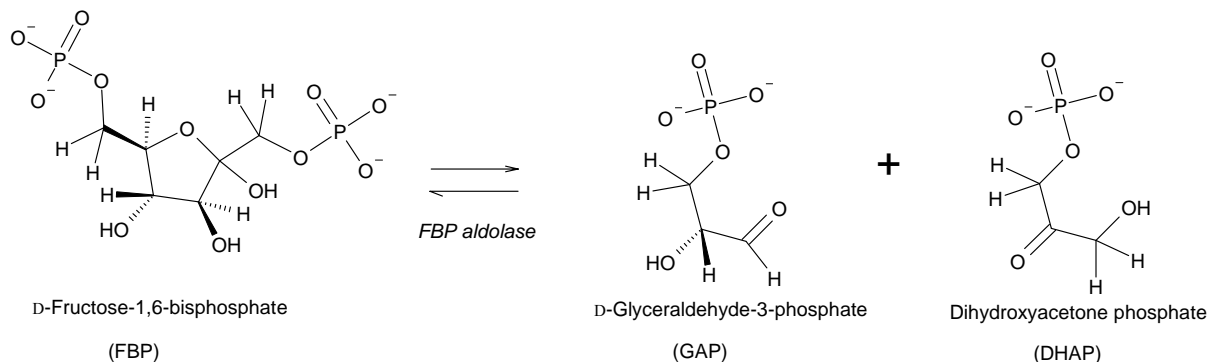


Figure 1.1 Fructose 1,6-bisphosphate aldolase reaction

1.2.2 Phylogeny of FBP aldolases

The FBP aldolases all adopt the $(\beta/\alpha)_8$ barrel fold, also known as the “TIM barrel” fold for the structure of triose phosphate isomerase (see section 1.3.2), but are divided into two groups depending on the reaction mechanism (Rutter 1964). The Class I aldolase forms a Schiff base using an active-site lysine residue with the carbonyl group of the substrate; whereas the Class II enzyme uses a divalent metal ion as an electron sink to stabilize the carbanion formed on the 3rd carbon of the substrate (Figure 1.3). Although the two classes of FBP aldolases share the same overall fold and catalyze the same overall reaction, they do not share any significant sequence homology or common catalytic residues. The locations of their active sites in the TIM barrel structure are also distinct, suggesting independent evolution (Sánchez *et al.* 2002). Recent reports also suggest that these

enzymes may have evolved independently from a common $(\beta/\alpha)_8$ barrel ancestor, like numerous other families of $(\beta/\alpha)_8$ barrel fold enzymes, based on structural alignments (Nagano *et al.* 2002).

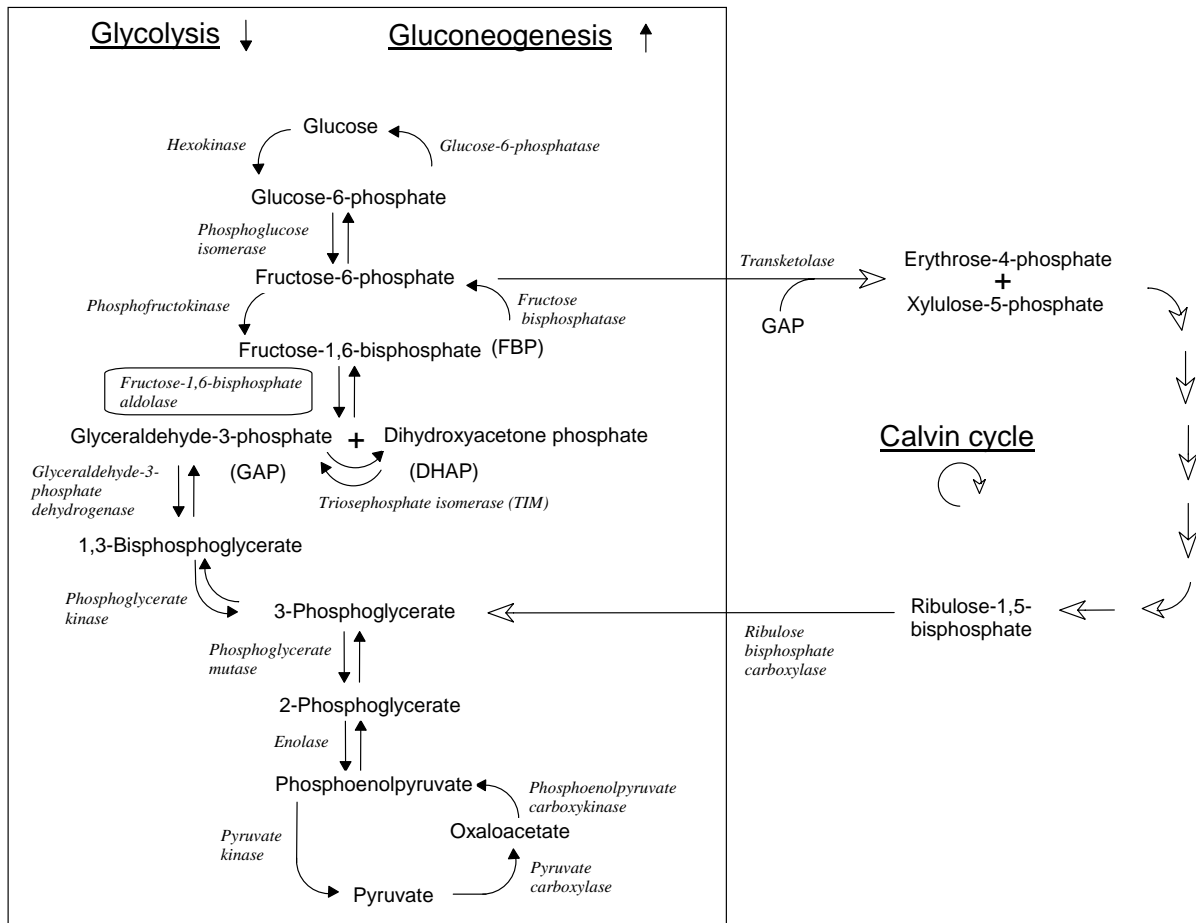


Figure 1.2 Biochemical pathways involving fructose-1,6-bisphosphate aldolase

The box represents the sugar metabolites and enzymes of glycolysis (the Embden-Meyerhof-Parnas pathway, from glucose to pyruvate) and gluconeogenesis (from pyruvate to glucose). The white arrows depict the reactions of the Calvin cycle (also called reductive pentose phosphate cycle) from photosynthetic organisms and chemoautotrophic bacteria, which are used to fix atmospheric carbon from CO_2 . The illustration was adapted from biochemistry textbook figures (Voet and Voet 2004).

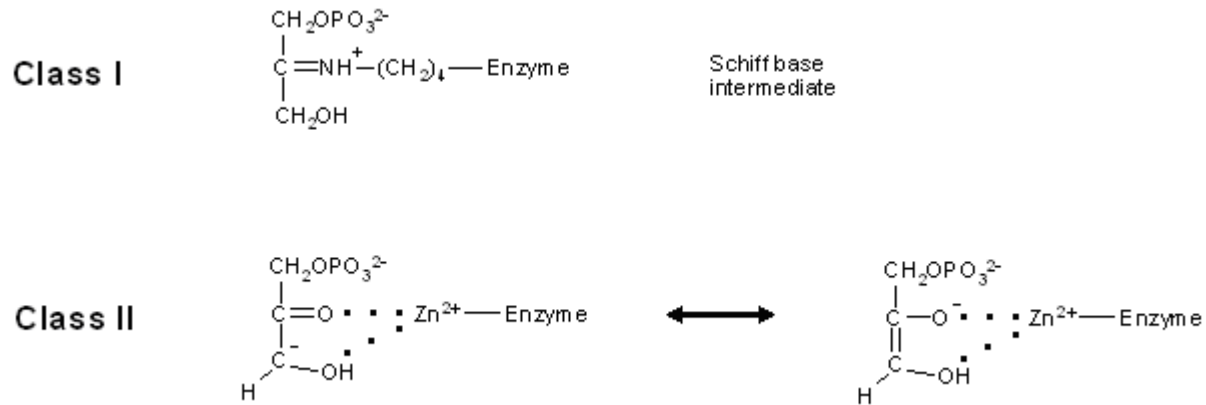


Figure 1.3 The two different catalytic mechanisms of the Class I and Class II aldolases

In Class I enzymes, the carbonyl function of the substrate and the amino group of a lysine side-chain in the active site condense to form a Schiff base intermediate. In Class II aldolases, the active site divalent metal acts as an electron sink that stabilizes the carbanion intermediate.

Only the Class I FBP aldolase is present in higher plants and mammals, but both classes can be present in lower organisms such as *Escherichia coli* and *Mycobacterium tuberculosis*. Some authors have suggested that the presence of two classes of aldolases in one organism is redundant and that higher organisms have eliminated one of them during evolution (Marsh and Lebherz 1992). In organisms that possess two aldolases, the expression of one of the enzymes is constitutive, whereas the expression of the other one can be induced by a change in the growing conditions (aerobic versus anaerobic, or autotrophically-grown versus heterotrophically-grown) (van den Bergh *et al.* 1996; Marsh and Lebherz 1992; Bai *et al.* 1974; Stribling and Perham 1973; Willard and Gibbs 1968b).

The distribution of Class II enzymes among microorganisms has been analyzed in several reports, and a phylogenetic tree of the Class II FBP aldolases from various lower organisms is presented below (Figure 1.4). The Class II enzymes are divided into the groups “A” and “B” depending in their amino acid sequences (Rogers and Keeling 2004; Plaumann *et al.* 1997). Several large insertions or

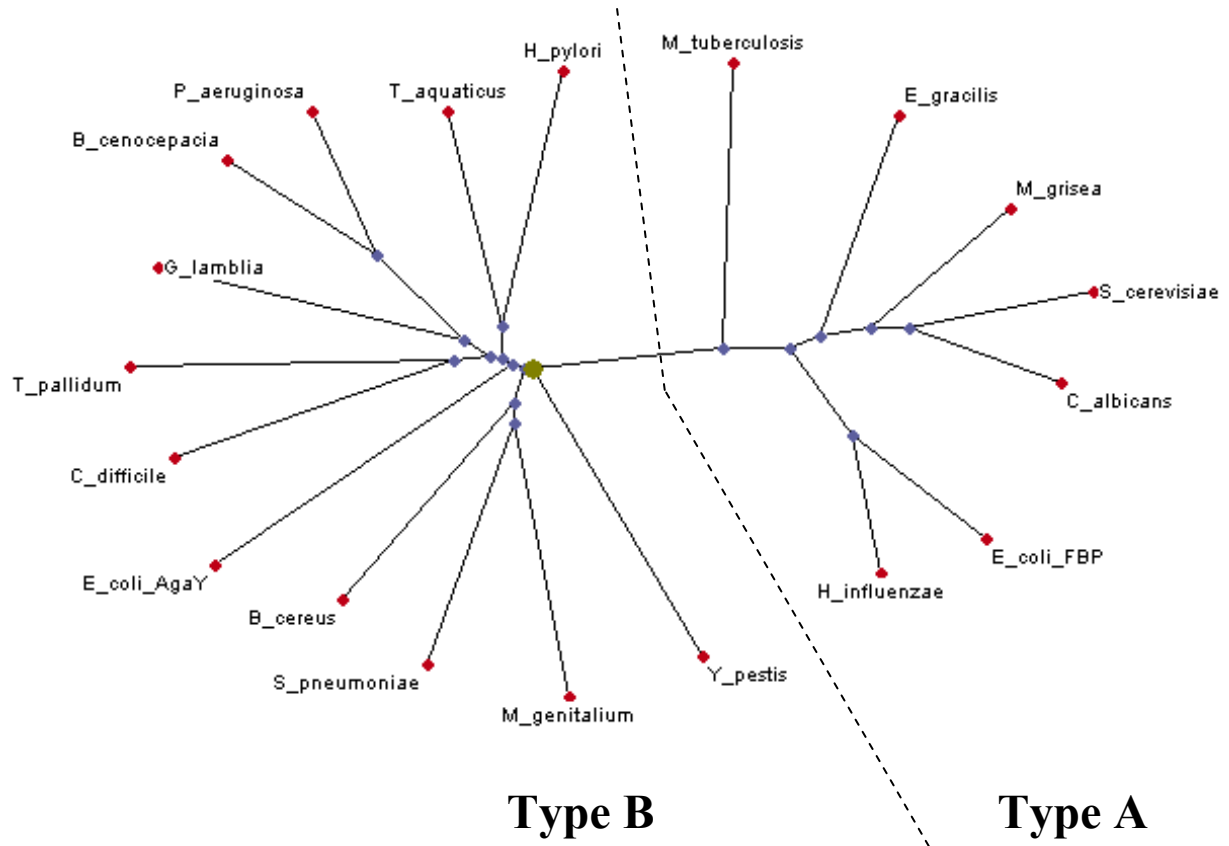


Figure 1.4 Phylogenetic tree of Class II aldolases.

The Class II enzymes are divided into the Type A and Type B subgroups as indicated by the dashed line (Plaumann *et al.* 1997). The sequence alignment was performed using ClustalW (Larkin *et al.* 2007), and the illustration was done with PhiloDraw (Choi *et al.* 2000). The *E. coli agaY* gene encodes a tagatose bisphosphate aldolase; most of the other aldolases have been shown to be specific for FBP. The source of the amino acid sequences were NCBI GeneBank and Protein Data Bank: *Haemophilus influenzae* Rd KW20 GeneID: 949539; *Helicobacter pylori* 26695 GeneID: 900140; *Bacillus cereus* ATCC 10987 GeneID: 1207675; *Mycobacterium tuberculosis* H37Rv GeneID: 886474; *Pseudomonas aeruginosa* PAO1 GeneID: 880792; *Magnaporthe grisea* GeneID: 2674368; *Streptococcus pneumoniae* Gene ID: 933499; *Candida albicans* SC5314 Protein ID: EAL04108.1; *Burkholderia cenocepacia* mc0-3 Gene ID: 6124318; *Escherichia coli* K12 MG1655 GeneID: 947415 PDB#1B57; *Escherichia coli* AgaY PDB#1GVE; *Saccharomyces cerevisiae* GeneID: 853805; *Thermophilus aquaticus* PDB#1RV8 Gene: AAF22441; *Giardia lamblia* PDB#2ISV; *Treponema pallidum* GeneID 2611197; *Yersinia pestis* GeneID 1176799; *Mycoplasma genitalium* GeneID: 875427; *Euglena gracilis* Protein ID CAA61912; *Clostridium difficile* GeneID: 4914942.

Chapter 1 Introduction

deletions separate the two groups (Sánchez *et al.* 2002). It has been noted that Group A contains mostly enzymes that function in glycolysis and gluconeogenesis; while group B is more heterogeneous and has aldolases with diverse metabolic roles and substrate specificities (Sauve and Sygusch 2001b). This will be explained in more detail in section 1.3.3.

1.2.3 Knock-out studies of Class II FBP aldolase

Attempts to disrupt the Class II FBP aldolase genes from *Mycobacterium tuberculosis*, *Escherichia coli*, *Streptomyces galbus*, *Bacillus subtilis*, *Pseudomonas aeruginosa* and *Candida albicans* by insertion or deletion mutagenesis have been unsuccessful, thereby suggesting that the Class II FBP aldolases are essential for the viability of these organisms (Rodaki *et al.* 2006; Gerdes *et al.* 2003; Jacobs *et al.* 2003; Kobayashi *et al.* 2003; Sassetti *et al.* 2003; Giaever *et al.* 2002; Sassetti *et al.* 2001; Wehmeier 2001). A study of RNA interference/RNA silencing in *Giardia lamblia* found no viable organism when the Class II FBP aldolase was targeted (Galkin *et al.* 2007). The gene was also part of the essential genes of a minimal bacterium genetically derived from *Mycoplasma genitalium* (Glass *et al.* 2006). The failure to create a viable knock-out mutation is, however, not a proof that the Class II FBP is essential, as it could instead be due to technical problems. A study where this gene would be introduced on a plasmid, and the subsequent knock-out of the genomic copy of the Class II FBP aldolase would prove that the gene is essential, if the plasmid cannot be cured from the knock-out organism. Such a study has to our knowledge not been performed with the Class II FBP aldolase.

It is interesting that in *E. coli* the Class II FBP aldolase is apparently essential, since this organism also possesses a Class I FBP aldolase (Thomson *et al.* 1998). Studies have shown that the Class II FBP aldolase in *E. coli* is constitutively expressed while the Class I FBP aldolase gene is only expressed in the presence of gluconeogenic substrates (Scamuffa and Caprioli 1980; Stribling

and Perham 1973). Thus, the organism is still viable when its Class I FBP aldolase gene is disrupted (Gerdes *et al.* 2003). *M. tuberculosis* also possess a Class I FBP aldolase which has been purified previously (Bai *et al.* 1982; 1974), but it is not yet known if that gene is essential for the viability of the organism. There is also no gene in the *M. tuberculosis* genome that shares sequence similarity to known Class I FBP aldolase (Camus *et al.* 2002; Cole *et al.* 1998).

Only two studies of transposon insertion have described the Class II FBP aldolase gene as “non-essential”: those done with *Haemophilus influenzae* and *Helicobacter pylori* (Salama *et al.* 2004; Akerley *et al.* 2002). However, details of the exact location of the insertion in the *fba* gene were not made available by the authors; there was only mention that there was a single “hit” obtained in the *H. pylori* aldolase gene. It is therefore possible that the transposon insertion did not completely inactivate the enzyme in those cases, as it is known that some essential genes tolerate insertions in specific areas (Gerdes *et al.* 2003), for example near the C-terminus of the protein.

1.2.4 Why is FBP aldolase essential? – Glucose metabolism review

Several studies have focused on mutant bacterial strains with low Class II FBP aldolase activity that is due to heat instability of the aldolase, or other unidentified reasons. The consequences of this bottleneck on metabolic processes were analyzed. To illustrate the interpretation of the results of these investigations, a metabolic map showing the different pathways for glucose metabolism in bacteria is presented below (Figure 1.5). This figure is adapted from a multi-genome comparisons study that has shown that the glycolysis pathway has high plasticity and versatility in lower organisms (Dandekar *et al.* 1999). The standard glycolysis, or Embden-Meyerhof-Parnas (EMP) pathway presented in Figure 1.2 is the common glucose degradation route, but other methods of glucose degradation such as the Entner-Doudoroff (ED) pathway can be used by prokaryotes as an alternative to classical glycolysis, for example in *Pseudomonas* species (Conway 1992; Lessie and

Chapter 1 Introduction

Phibbs 1984). In addition, there are alternate routes and bypasses to the reactions of glycolysis for glucose degradation, for example the pentose phosphate pathway, or hexose monophosphate shunt (Figure 1.5). Due to these alternate pathways, at least one *in silico* study concluded that the blocking of FBP aldolase as an antibiotic strategy may not be successful for some pathogens (Dandekar *et al.* 1999). However, the absence of a viable *fba* gene knock-out in several microorganisms (Section 1.2.3) as well as the growth inhibition observed in the following studies of mutants with low FBP aldolase activity, both indicate that developing antimicrobials against Class II FBP aldolase may be a good strategy, particularly because some critical cell processes appear to be strongly regulated in function of the concentration of metabolites and flux in glycolysis, as will be described below.

Analysis of the effect of low FBP aldolase activity on cell processes in the presence of glucogenic substrates (glucose, fructose, gluconate, ribose, etc.) showed growth inhibition and an accumulation of either FBP or triose phosphates (GAP and DHAP) in *E. coli* cells possessing heat-sensitive aldolase activity (Frey *et al.* 1975; Su *et al.* 1975; Bock and Neidhardt 1966a; 1966b), as well as in some yeast glucose-negative clones isolated from a mutagenized culture, which had lost over 95% of normal FBP aldolase activity (Lobo 1984). In *P. aeruginosa*, a mutant strain named ALD1 isolated from a mutagenized culture, and possessing less than 4% of wild-type Class II FBP aldolase activity, grew in Luria-Bertani or glutamate minimal media on supplementation with fructose or mannitol, but did not grow well on fructose or mannitol alone, and did not grow at all on glucose, gluconate, glutamate, glycerol, succinate, or lactate (Banerjee *et al.* 1985). High levels of triose phosphates were detected in the *P. aeruginosa* mutant ALD1 when grown on gluconate, which is consistent with the fact that the Entner-Doudoroff pathway is predominantly used in this organism. It was also observed that FBP accumulated when the strain was grown on fructose or mannitol (Banerjee *et al.* 1987).

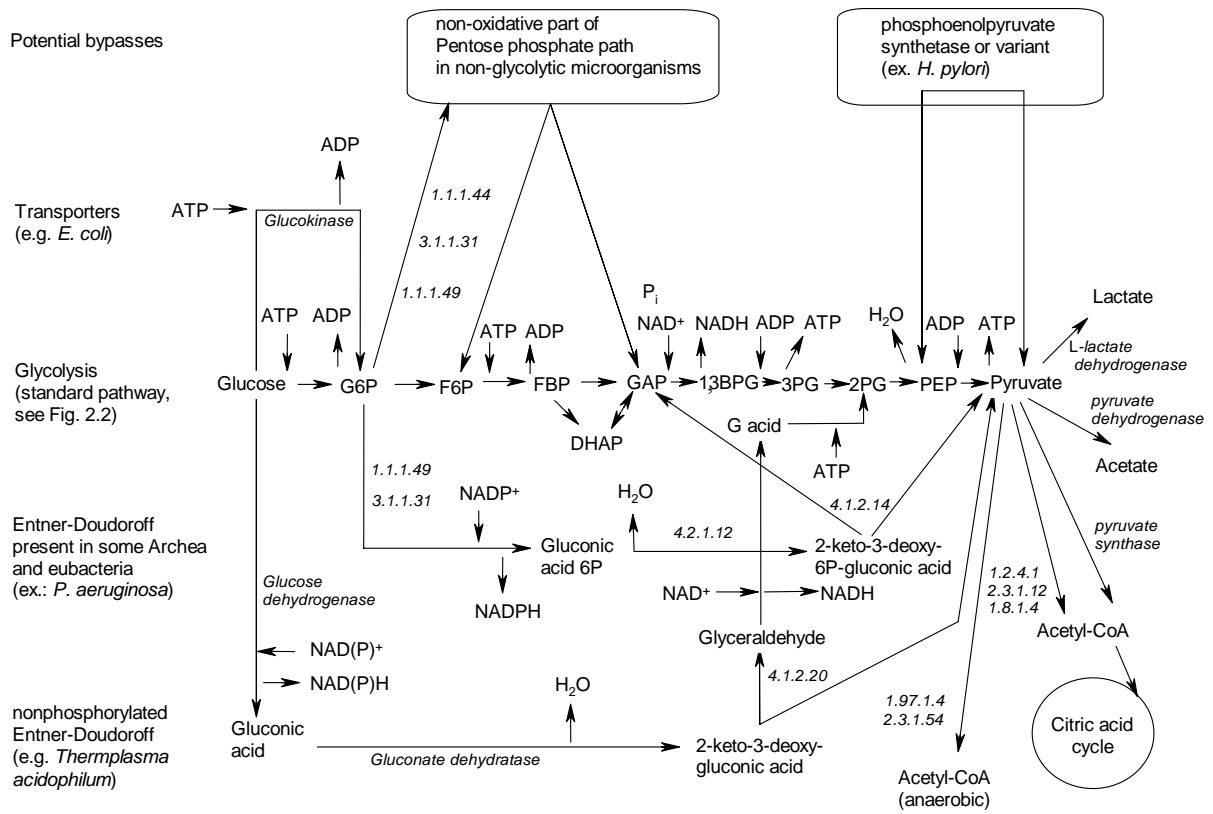


Figure 1.5 Pathways for glucose degradation

The alternative routes that bypasses (top) or are different (bottom) from the standard glycolytic pathway (centre) found in various species are shown. Paths and species examples are shown on the extreme left. The EC numbers given in the Entner-Doudoroff and Pentose phosphate pathways are representing the following enzymes: glucose 6-phosphate 1-dehydrogenase (EC 1.1.1.49), 6-phosphogluconolactonase (EC 3.1.1.31), 6-phosphogluconate dehydrogenase (EC 1.1.1.44), 6-phosphogluconate dehydratase (EC 4.2.1.12), 2-keto-3-deoxy-6-phosphogluconic aldolase (EC 4.1.2.14), 2-keto-3-deoxy-gluconate aldolase (EC 4.1.2.20). G acid stands for glyceric acid, and the enzymes and metabolites of the standard pathway of glycolysis are presented in more details in Figure 1.2. Figure adapted from (Dandekar *et al.* 1999).

The growth of mutant *E. coli* cells with heat-sensitive FBP aldolase activity has been shown to be blocked at non-permissive temperatures in the presence of glucogenic substrates, even when other carbon sources are present, because of the catabolite repression occurring on other pathways, where the presence of a utilizable carbon and energy source such as glucose severely inhibits the synthesis of new catabolic enzymes. The mutant cells were able to grow on the non-glucogenic substrates such

Chapter 1 Introduction

as glycerol and succinate (and alcohol for yeast), but failed to grow in glycerol-containing minimal media in the presence of even trace amounts of glucose. The depletion of ATP was ruled out to explain the growth inhibition effect in *E. coli*, however there is a 7- to 20-fold increase in the intracellular concentration of FBP upon shift to the non-permissive temperature when the cells are grown using glucose as the carbon source (Su *et al.* 1975; Bock and Neidhardt 1966b). In one of the reports (Bock and Neidhardt 1966b), the authors even suggested that the growth of *E. coli* on succinate and glycerol could be made possible by the presence of a “biosynthetic” FBP aldolase, which turned out to be an accurate prediction, as a Class I FBP aldolase expression was later found to be induced in *E. coli* in conditions of gluconeogenesis, i.e. in pyruvate or lactate-grown cells (Stribling and Perham 1973). The authors also acknowledged the possibility that the temperature-sensitive aldolase could still have enough residual activity to allow some hexose and pentose synthesis and allow the cell to grow on glycerol and succinate, without causing the accumulation of FBP which they said was the compound responsible for the inhibition of the Entner-Doudoroff pathway and other cell processes (Bock and Neidhardt 1966b).

The *E. coli* strains with a temperature-sensitive aldolase were found to immediately stop nucleic acid and phospholipid synthesis upon being shifted to the non-permissive temperature, but protein synthesis continued at a slower rate for a short period (Su *et al.* 1975; Bock and Neidhardt 1966a). The quick decline in stable RNA translation leads to cell growth inhibition (Singer *et al.* 1991a; Singer *et al.* 1991b). Recent studies have shown that the accumulation of phosphorylated metabolites in *E. coli* cells affect the concentration of initiating nucleoside triphosphate (iNTP) and of the rRNA translation initiation factor guanosine 5'-diphosphate 3'-diphosphate (ppGpp), in turn inhibiting the initiation of rRNA translation and thus stopping the production of ribosomes at the source, a phenomenon termed the stringent response (Schneider and Gourse 2003b; 2003a). This effect has been observed in *E. coli* when the carbon source is shifted from glucose to lactate (Winslow 1971),

and is similar to what is observed during starvation for amino acids (Neidhardt and Magasanik 1960). The cells can later resume growth when transferred into a medium without glucogenic substrates or when returned to a permissive temperature, in the case of FBP aldolase temperature sensitive (ts) strains. Two temperature-sensitive Class II FBP aldolase *Bacillus subtilis* mutants with a severe deficiency in RNA synthesis at non-permissive temperatures, were also isolated (Mitchell *et al.* 1992; Trach *et al.* 1988). In yeast, a knock-out of the *fba* gene resulted in a strain able to grow only in media where metabolites on both sides of the glycolysis block are present, for example media containing galactose and lactate (Schwelberger *et al.* 1989).

Revertants of the *E. coli* FBP aldolase (ts) strain have been obtained (Schreyer and Bock 1973), and genetic analysis showed that the mutation of other enzymes prevents the accumulation of phosphorylated metabolites and can restore growth on glucogenic substrates. Large numbers of spontaneous revertants with mutations affecting 6-phosphogluconate dehydrogenase activity (pentose phosphate pathway, EC 1.1.1.44, see Figure 1.5), or *fba⁻ gnd⁻* mutants, could be easily isolated by growth on gluconate at non-permissive temperature. An additional mutation in these *fba⁻ gnd⁻* strains in phosphoglucose isomerase (second enzyme in glycolysis, see Figure 1.2) could also partially restore the growth on glucose at non-permissive temperatures. The *fba⁻ gnd⁻ pgi⁻* mutants were found to degrade glucose predominantly via the Entner-Doudoroff pathway, but their growth on fructose was still strictly temperature-sensitive. The authors reported an important correlation between the temperature used for growth and the number of revertants obtained; it thus appears that the amount of residual activity of the FBP aldolase is critical for the revertant strains to arise without any mutagenesis and enrichment procedure. Spontaneous revertants were also obtained in yeast FBP aldolase (ts) mutants grown on glucose and a *P. aeruginosa* aldolase mutant grown on gluconate, but most of the revertants had regained the wild-type aldolase activity level (Banerjee *et al.* 1985; Lobo 1984).

Chapter 1 Introduction

In all the Class II FBP aldolase deficient organisms studied, it was noted that the growth inhibition occurred only when the mutants had less than 5% of the wild-type strain FBP aldolase activity. One of the *E. coli fba* revertants obtained by Bock and Neidhart had 5% of the wild-type activity, as opposed to less than 2% for the temperature sensitive strain h8 (Bock and Neidhardt 1966a). Another *E. coli* FBP aldolase temperature sensitive strain named ts8 could grow at 30 °C with only 10% of the wild-type FBP aldolase activity level, but not at 42 °C where the aldolase activity was virtually undetectable (less than 0.01% of wild-type activity level) (Singer *et al.* 1991a). In yeast, the *fba* mutants had 1 to 2% of the FBP cleavage and 2 to 5% of the triose phosphate condensation catalytic activity registered in the wild-type strain (Lobo 1984). The growth of a strain of *Candida albicans* with an engineered Class II FBP aldolase expression system was found to be significantly inhibited only when the quantity of active aldolase was less than 15% of that of the wild-type organism, and near-complete growth inhibition occurred only when that quantity dropped to below 4% of wild-type levels (Rodaki *et al.* 2006). This same team also tested the virulence of the engineered strain in mice, and found that the fungal burdens were at least 2 orders of magnitude lower for the mice infected with the conditional mutants, but these strains still established an infection in the mice. The mutant's virulence is thus partially but not completely attenuated. The authors of this study concluded that the effect of Class II FBP aldolase depletion appears static rather than cidal, and they did not find a synergistic effect of the aldolase depletion mutation with an azole antifungal. They also conclude that a drug inhibiting the aldolase activity could be protective but likely not cure systemically infected patients (Rodaki *et al.* 2006). One important caveat in this study is that they could not measure the actual level of FBP aldolase expression in the mutated *C. albicans* strain infecting the mice: it could have been close to 5% of the wild-type levels, thus allowing the mutant strain to grow. The authors themselves state that, although their results suggest the Class II FBP aldolase is not an attractive drug target, it may be because the activity is depleted slowly when

transcription is turned off. In other words, there may still be significant FBP aldolase activity under the conditions they employed. Thus, they did not rule out the aldolase as a good drug target in this fungus, since the transcriptional control of the FBP aldolase gene does not have the immediate and stringent effect that a potent inhibitor would have on the FBP aldolase activity level in the cell.

1.2.5 Possible alternative roles of FBP aldolases and their potential as vaccine targets

Some studies have indicated that Class II FBP aldolases could be a good vaccine target. A team from the University of Guelph successfully immunized chickens against *Clostridium perfringens* using recombinant His-tagged Class II FBA as a vaccine (Kulkarni *et al.* 2007). In the mammalian immune response to *Candida albicans* infection, Class II FBP aldolase was identified as one of the antigens that induce protective IgG2a antibody isotype in the sera from vaccinated animals (Fernandez-Arenas *et al.* 2004a; 2004b). Glycolytic enzymes associated with the cell surface of *Streptococcus pneumoniae*, one of which being the Class II FBP aldolase, were found to be antigenic in humans and to elicit protective immune response in the mouse (Ling *et al.* 2004). In *Paracoccidioides brasiliensis*, a fungal pathogen of humans, a Class II FBP aldolase was identified as an antigen in sera of patients with paracoccidioidomycosis (PCM) (da Fonseca *et al.* 2001). FBA Class II was also identified as a major protein released from *Streptococcus agalactiae*, and a possible candidate for use as a vaccine antigen (Fluegge *et al.* 2004). In *Giardia lamblia*, a protozoan causing diarrhea, the Class II FBP aldolase was one of 16 identified immunoreactive proteins (Palm *et al.* 2003). Some Class I FBP aldolases from parasitic worms and nematodes also attracted interest for their vaccine target potential (Marques *et al.* 2008; McCarthy *et al.* 2002).

The Class II FBP aldolase was shown to be well expressed in cells. Studies on *E. coli*, yeast and *C. albicans* showed that the growth of mutated cells still occurs when the FBP aldolase activity is

Chapter 1 Introduction

only 5% of the wild-type levels (see previous section). Class II FBP aldolase is in fact one of the most abundant soluble proteins in microbial cells, with an estimated 47,000 protein copies per cell in *E. coli* (Ishihama *et al.* 2008). It comprises 2% of all soluble proteins that have a pI between 4 and 7 in *C. albicans* (Yin *et al.* 2004). The protein was also found in the cell wall of *S. pneumoniae* (Portnoi *et al.* 2006) and in culture filtrates of *M. tuberculosis* (Rosenkrands *et al.* 2002). The fact that the enzyme is present in a 20-fold excess based on the growth requirements for its catalytic activity suggests that the protein may have another role in the cell in addition to that catalytic activity. On the other hand, it could be over-expressed simply to ensure it does not become a rate-limiting step in glycolysis, as suggested by some researchers (Schwelberger *et al.* 1989).

It is possible that the Class II aldolases have other roles in the cell aside from the reaction they catalyze (Carneiro *et al.* 2005). The participation of the enzyme in multi-protein complexes could also have been one influence in the evolutionary selection in favor of Class I aldolase in higher organisms, as enzymes of this Class have been shown to interact with F-actin and are localized along stress fibers in fibroblasts. It is therefore possible that Class I FBP aldolases play a structural role in the cytoskeleton in mammals in addition to their catalytic role in central metabolism (Wang *et al.* 1997). It is also known that the structural association of vertebrate FBP aldolases with other enzymes affect their catalytic efficiency (Pezza *et al.* 2003). In contrast, the Class II FBP aldolase does not appear to be involved in an essential multi-protein complex, as the yeast Class II aldolase can be replaced by the fruit fly Class I enzyme with no apparent ill effect (Boles and Zimmermann 1993). It would be interesting to see if a similar switch of a Class II aldolase in a human pathogen would affect its pathogenicity or survival in the host, since this cytoplasmic enzyme is immunoreactive. However at this time there is no evidence that Class II FBP aldolases have other roles besides their involvement in central metabolism.

1.2.6 Summary: Justification for the choice of Class II aldolase as drug target

We propose the glycolysis/gluconeogenesis pathway, at the core of all cells' central metabolism, may be a drug target. In this pathway, we are targeting an essential metabolic enzyme, Class II FBP aldolase, which is not found in eukaryotic cells. We propose that the blockage of this central pathway will inhibit the growth of the cell by shutting down its core metabolism and all synthetic pathways due to the accumulation of phosphorylated metabolites (Schneider and Gourse 2003b; Su *et al.* 1975; Bock and Neidhardt 1966b). This will result in the inhibition of ribosomal RNA transcription and effectively prevent ribosomes from being synthesized. An FBP aldolase inhibitor would be relevant especially in the case of human pathogens that obtain their carbon and energy requirements from nutrients in the human blood, where glucose is the principal energy source (ex. *H. pylori* (Mendz *et al.* 1994)). It is however likely that the inhibition of the Class II FBP aldolase will have a static rather than cidal effect on microorganisms, and that an effective eradication of the target pathogens may require other complementary drugs, for example RNA translation inhibitors. It is also possible that a FBP inhibitor may be ineffective in the case of organisms which (I) have access to other carbon sources providing metabolites for both sides of the FBP aldolase reaction, (II) do not experience strong catabolic repression, (III) do not exhibit stringent control over RNA synthesis when FBP or triose phosphates accumulate. In other words, as is the case with most drugs, *in vivo* testing will be necessary to assess the usefulness of FBP aldolase inhibitors for each target pathogen. On the positive side, a Class II FBP aldolase inhibitor would have great potential as a broad spectrum antibiotic.

1.3 Class II FBP aldolase structure and mechanism

Detailed knowledge of the structure and mechanism of the target enzyme is essential in structure-based drug design. In this section, the structural properties that allow the Class II FBP aldolases to

Chapter 1 Introduction

specifically bind to their substrates and catalyze aldol cleavage and condensation reactions to yield products stereospecifically will be reviewed. Several enzymes related to Class II FBP aldolases in terms of structure, mechanism or substrate specificity will also be briefly mentioned.

1.3.1 Aldolase groups and DHAP-dependant aldolases

The aldolases are classified into 5 groups regardless of mechanism but based on their substrate specificity: (1) DHAP-dependent aldolases comprising the FBP aldolases, the tagatose 1,6-bisphosphate (TBP) aldolases, the fuculose 1-phosphate aldolases (FucA), and the rhamnulose 1-phosphate aldolases (RhuA); (2) the pyruvate- or phosphoenol pyruvate-dependent aldolases such as N-acetylneuraminic acid aldolase and KDPG aldolase (EC 4.1.2.14, see Fig. 1.5); (3) transketolase and transaldolase, which are part of the pentose phosphate pathway and have a broad substrate specificity; (4) the 2-deoxy-D-ribose 5-phosphate (DERA) aldolase, which catalyses the condensation of acetaldehyde and GAP; and (5) glycine-dependant aldolases, for example the serine hydroxymethyltransferases and threonine aldolase (Fessner 2004; Seoane 2000; Takayama *et al.* 1997). Of particular interest are the four different DHAP-dependant aldolases. Each generate one unique aldol condensation product whose stereochemistry at C-3 and C-4 are different, as shown in Figure 1.6 (Takayama *et al.* 1997).

The four complementary DHAP-dependent aldolases have a high substrate specificity for DHAP, but a broad substrate specificity for the aldehyde acceptor in the aldol condensation reaction (Fessner *et al.* 1996). Some aldehydes that can be substrates for the Class II FBP aldolase from *E. coli* in addition to GAP include chloroacetaldehyde and methylglyoxal (Henderson *et al.* 1994).

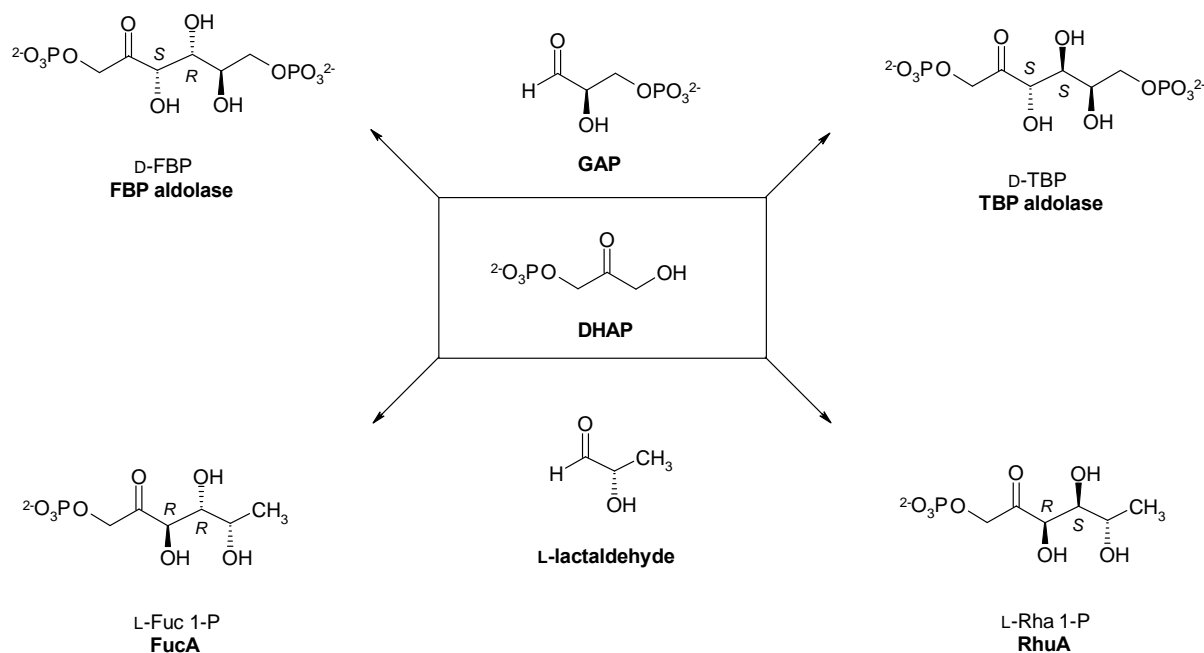


Figure 1.6 DHAP-dependant aldolases and their substrates

See details in the text. Figure adapted from (Takayama *et al.* 1997). Illustration made with the program MDL ISIS Draw (MDL Information Systems).

The Class II FBP and TBP aldolases are not evolutionarily related to the Class II FucA and RhuA, as they do not share the same structure. Both FBP and TBP aldolases have the TIM barrel fold, which will be described in the following section, whereas both FucA and RhuA exhibit a different alpha and beta (α/β) fold (PDB structures ID: 1DOS, 1GVF, 1FUA, and 1OJR, respectively (Kroemer *et al.* 2003; Hall *et al.* 2002; Blom *et al.* 1996; Dreyer and Schulz 1996). It is relevant to note that TBP aldolases, FucA and RhuA are not present in mammals or plants. The potential toxicity of a drug that mimics the DHAP structure would therefore be more likely to involve other DHAP-binding enzymes in higher organisms, such as the glycolytic enzymes Class I FBP aldolase and triose phosphate isomerase (Fig. 1.2), as well as glycerol-3-phosphate dehydrogenase, which is involved in lipid metabolism. Even if the overall fold of FucA and RhuA is not related to that of FBP aldolase, the availability of the structural information on the active site of these other Class II DHAP-

dependant aldolases can still be useful for inhibitor design, which will be discussed further in Chapter 4.

1.3.2 Industrial use of FBP aldolases

Being able to catalyze stereospecific C-C bond formation, FBP aldolases have been used for the synthesis of aza sugars important in the pharmaceutical industry as glycoprocessing inhibitors (Wong *et al.* 1995). It was suggested that the enzymes could also be useful for the production of C¹³-labelled sugars, deoxysugars, and high-carbon sugars, among many carbohydrate derivatives (Machajewski and Wong 2000). There have been studies comparing the prokaryotic Class I enzymes to the mammalian Class I enzyme from Rabbit muscle, and it was found that the prokaryotic enzymes were more stable at high temperatures and in the presence of organic solvents, and had different specificities for the aldehyde used in the condensation reaction (Schoevaart *et al.* 2000). There also have been suggestions that Class II enzymes could be better for industrial synthesis as they were shown to be more stable than the rabbit muscle enzyme in some cases (Von der Osten *et al.* 1989).

The information obtained on the range of accepted substrates for industrial synthesis is useful in rational ligand design, because it gives an idea of which ligands are capable of accessing/binding the active site. The consensus is that DHAP specificity is very strict; but DHA may also be used in the presence of arsenate, which mimics a phosphate ion (Schoevaart *et al.* 2001). A similar dependence on DHAP and inability to use DHA is observed in Fuculose 1-phosphate, and was explained structurally in that case by the requirement for the presence of the phosphate group to pull the DHAP molecule “down” so that its two oxygen atoms would not bind the catalytic zinc ion too tightly (Joerger *et al.* 2000). The aldehydes used in the condensation reaction for Class II aldolases are varied (Fessner and Walter 1997; Henderson *et al.* 1994): this gives an idea of potential steric clashes, which is helpful for ligand design. The absence of reaction with an alternate aldehyde substrate could

also be due to the displacement of the mobile loop, however, which doesn't mean that the aldehyde has a low affinity for the active site. Still, since the enzymes could potentially be useful for the pharmaceutical industry, it would be beneficial to investigate the stability and specificity of various Class II FBP aldolases.

1.3.3 TIM barrel, or $(\beta\alpha)_8$ -barrel, enzymes superfamily

The Class I and Class II FBP aldolases form two separate families in the 21 TIM barrel superfamilies of enzymes identified by structure-based sequence alignments (Nagano *et al.* 2002). The TIM barrel, or $(\beta\alpha)_8$ -barrel, structure (Figure 1.7) is one of the most common folds adopted by proteins, and is present in many enzymes involved in molecular or energy metabolism (Ishihama *et al.* 2008; Gerstein and Levitt 1997). A few important characteristics of the TIM barrel that are highly conserved across the different enzyme families: (1) the catalytically active residues are all located at the C-terminal ends of the β -strands and in the $\beta\alpha$ -loops. The global dipolar electrostatic field along the barrel axis is believed to create a positive potential at the catalytic face, which is optimal for the binding of negatively charged metabolites. (2) They often contain phosphate binding sites, as two-thirds of all enzymes with this structure have a phosphorylated substrate or cofactor. A structurally conserved phosphate-binding motif is present in some enzyme families, including both FBP aldolases families. (3) They often contain metal ion binding sites, as about half of all TIM barrel enzymes use divalent metal ions for catalysis (see section 1.3.8) (Sternier and Hocker 2005; Nagano *et al.* 2002). Several of these TIM barrel families have been suggested to have evolved from a common ancestor based on these conserved features.

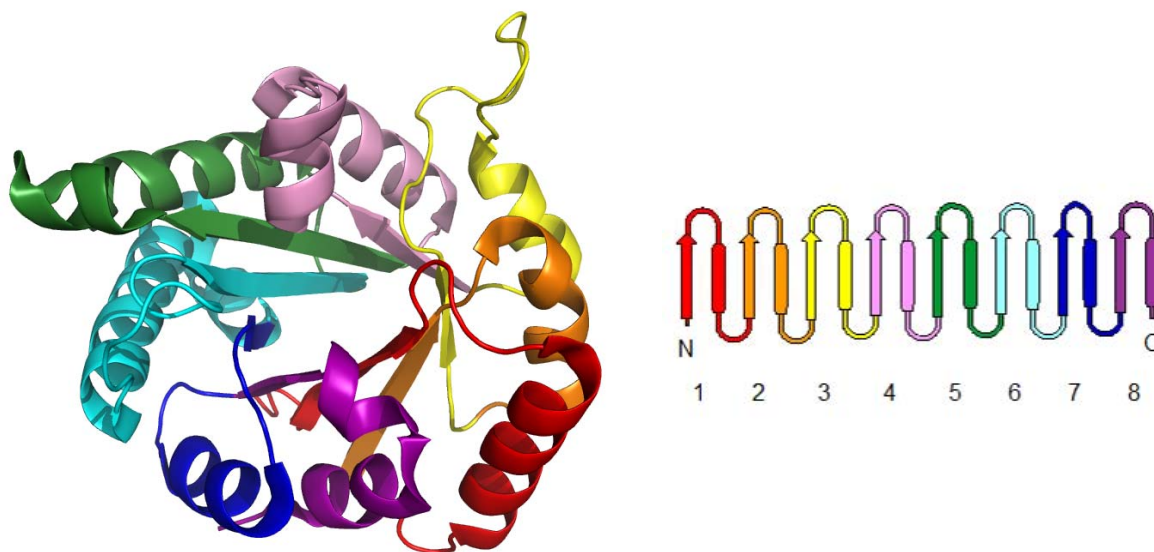


Figure 1.7 TIM barrel structure

The structure at left is that of the monomer of triose phosphate isomerase from chicken muscle (PDB ID: 1tim). The numbering of the β -sheets (arrows) and α -helices (cylinders) is shown on the right. The illustration on the left was produced with PyMOL (DeLano Scientific LLC).

Class II FBP and TBP aldolases are included in the same TIM barrel family, abbreviated as “ALD2” (Nagano *et al.* 2002). The mechanisms for substrate binding and discrimination between the stereoisomers in FBP and TBP aldolases are not well understood (Zgiby *et al.* 2000), but the stereospecificity of the *E. coli* TBP aldolase, AgaY, has successfully been altered towards FBP catalysis by directed evolution (Williams *et al.* 2003). The mutation of four amino acids in the evolved AgaY aldolase active site resulted in a 100-fold change in specificity for FBP over TBP. The location of the mutations suggest that they affect the position of the bound GAP as well as the DHAP enediolate plane relative to the incoming GAP, which allows the condensation reaction to occur on the opposite face of this molecule. It is not possible to distinguish TBP aldolases from FBP aldolases based on the amino acid sequence alone. The Class II FBP aldolase from *Thermus caldophilus* was even reported to have dual stereoselectivity (Lee *et al.* 2006).

1.3.4 Structure of Class II FBP aldolase

The structures of Class II FBP aldolases are shown in Figure 1.8. In addition to the core TIM barrel structure, there is a dimerization arm composed of two long antiparallel α helices (named $\alpha 10$ and $\alpha 11$ in *E. coli*, or $\alpha 8$ and $\alpha 8a$ in *Thermus aquaticus*) at the C-terminal end of the polypeptide chain. Mutagenesis experiments have confirmed that the enzyme is a functional dimer, with amino acid residues from both subunits required at each active site (Cooper *et al.* 1996; Qamar *et al.* 1996). Some enzymes are tetramers, or rather “dimer of dimers”, as in the aldolases from *T. aquaticus* (Sauve and Sygusch 2001a) and *T. caldophilus* (Lee *et al.* 2006), as well as for the TBP aldolase from *E. coli* (Hall *et al.* 2002). In the *T. aquaticus* tetramer, the interdimer interface was found to be three times smaller than the intradimer interface (Izard and Sygusch 2004). Other Class II FBP aldolases have also been determined by gel filtration to be either dimers or tetramers (Pelzer-Reith *et al.* 1994; Hill *et al.* 1976; Harris *et al.* 1969; Willard and Gibbs 1968a). An octameric Class II FBP aldolase was reported in *Synechocystis* sp. PCC6803, a cyanobacterium (Nakahara *et al.* 2003).

Various divalent metals such as Zn^{2+} , Co^{2+} , Fe^{2+} , and to a lesser extent Mn^{2+} and Ni^{2+} , have been shown to enable catalysis (Kobes *et al.* 1969). Some aldolase crystal structures have also been obtained with non-native metals such as cadmium (Hall *et al.* 2003) and yttrium (Izard and Sygusch 2004). Only one divalent ion per subunit is required for catalysis, but crystal structures of the *E. coli* and *T. aquaticus* aldolases have shown two mutually exclusive binding sites for this metal, as seen in Figure 1.9. One site is buried, and the other one is solvent-exposed, and the latter was determined to be the catalytically active metal position. The rotation of two histidine side-chains (His₁₁₀ and His₂₆₄ in *E. coli*) allows the metal to move between the two positions, which are 3.2 Å apart in the Zn^{2+} -dependant *E. coli* FBP aldolase (Blom *et al.* 1996) and 1.85 Å apart in the Co^{2+} -dependant *T. aquaticus* FBP aldolase (Izard and Sygusch 2004). The metal movement between the two sites is thought to be triggered by substrate binding.

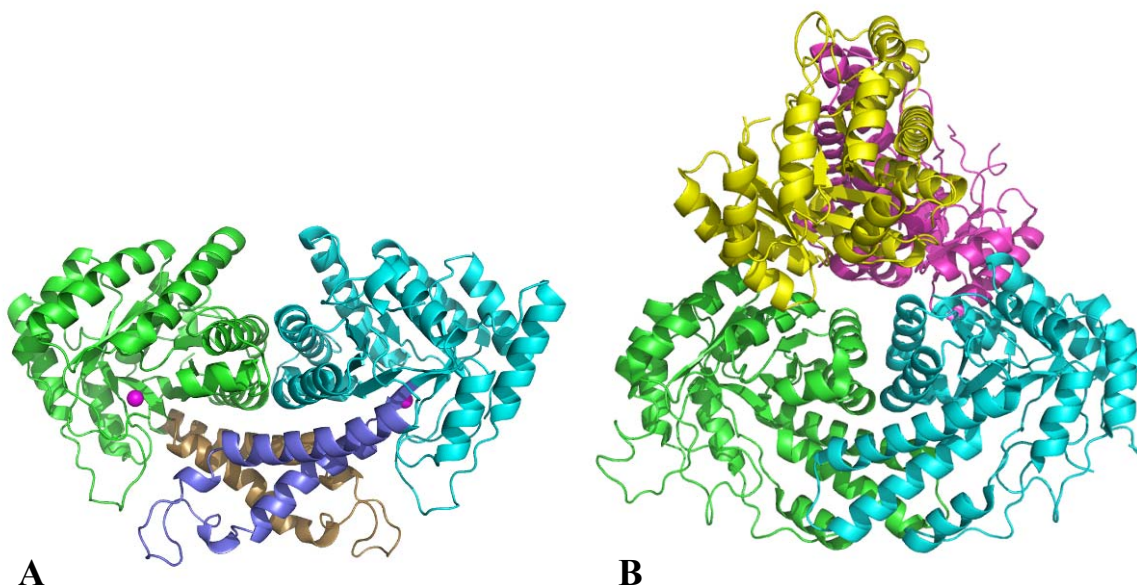


Figure 1.8 Structures of Class II FBP aldolases

In panel A, the *E. coli* dimeric aldolase (PDB ID: 1B57) is shown with the core TIM barrel of each subunit colored in green and cyan, respectively, and the active site zinc ions shown as pink spheres. The dimerization arms comprising the antiparallel α -helices 10 and 11 of each subunit are shown in brown and violet, respectively. In panel B, the *Thermus caldophilus* tetrameric aldolase (PDB ID: 2FJK) is shown with the four subunits positioned to highlight the “dimer of dimers” organization. One dimer is shown in green and cyan, and the other (perpendicular to the first dimer) is shown in yellow and pink. The illustrations were produced with PyMOL (DeLano Scientific LLC).

In addition to the catalytic metal ion, other metals have been identified in the *E. coli* crystal structures. A structural Zn^{2+} ion is found in the *E. coli* aldolase active site in the presence of the substrate analogue phosphoglycolhydroxamate (PGH), and a binding site for a monovalent cation (K^+ or NH_4^+) is also identified in some structures (Figure 1.9) (Hall *et al.* 2003).

There are two mobile loops in the active site of FBP aldolases that undergo a large conformational change upon ligand binding: these are the loops $\beta 5$ - $\alpha 7$ and $\beta 6$ - $\alpha 8$ in *E. coli*, which correspond to the residues 134-152 and 175-190 respectively in the *T. aquaticus* aldolase (Zgiby *et al.*

2002). The closure of these loops over the active site is coordinated, and the “closed” conformation required for catalysis has been suggested to be stabilized by the presence of the substrate phosphate moiety (Izard and Sygusch 2004). The loops and residues that participate in catalysis are identified in a sequence alignment of the *E. coli* and *T. aquaticus* FBP aldolases and highlighted in the *E. coli* enzyme structure (Figures 1.10 and 1.11).

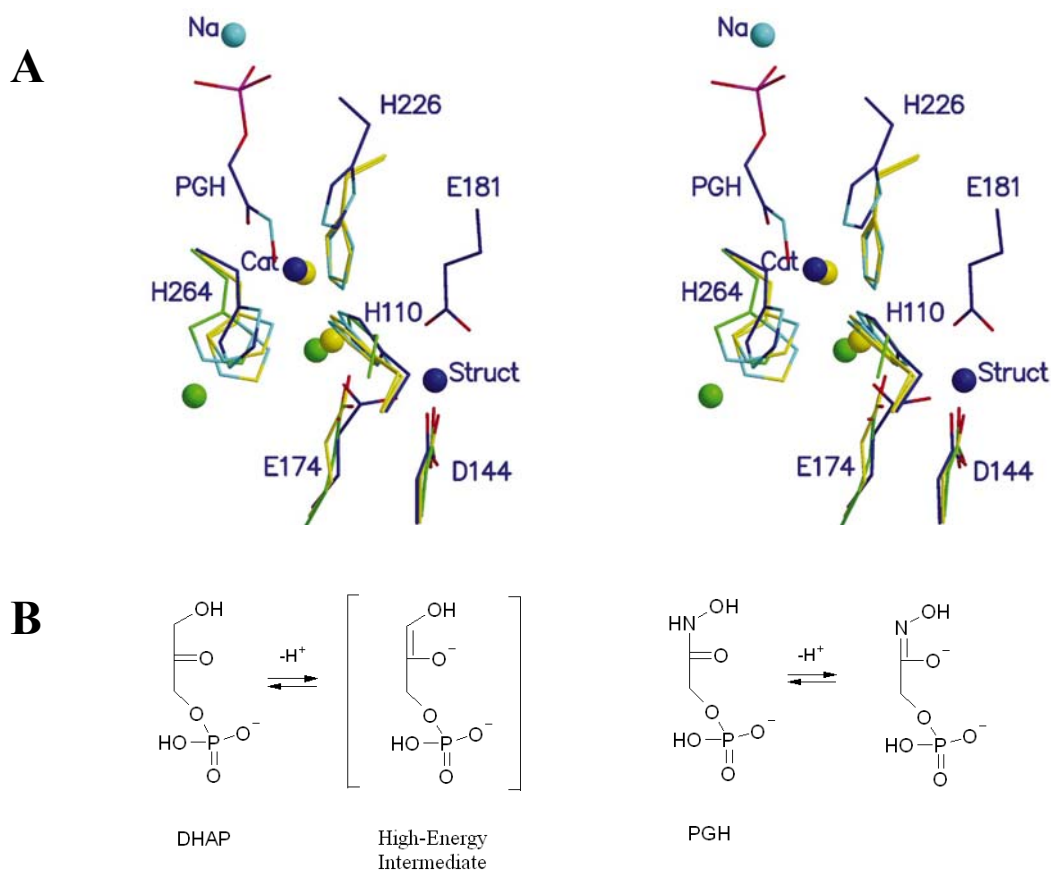


Figure 1.9 Stereo image of the *E. coli* Class II FBP aldolase active site metals

Panel A: The metal binding sites found in three *E. coli* Class II FBP aldolase structures (PDB IDs 1DOS, 1ZEN, and 1B57) are shown. The structures are overlaid, with the N, O and P atoms coloured cyan, red and purple, respectively. In the 1DOS structure, the mutually exclusive Zn_s and Zn_b are shown as yellow spheres and the C atoms of the ligands are also shown in yellow. In the 1ZEN structure, M1, M2 and C atoms are shown in green; M1 and M2 were identified as Zn^{2+} (centre, equivalent to Zn_b) and a monovalent cation such as K^+ , or possibly NH_4^+ (lower left). In the 1B57 structure where the enediolate analogue Phosphoglycolhydroxamate (PGH) is bound in the active site, the catalytic (Cat) and structural (Struct) Zn^{2+} and ligands are shown in blue and the activating Na^+ is in cyan. The Figure was published by (Hall *et al.* 2003), © 2003 International Union of Crystallography (<http://journals.iucr.org/>). Reproduced with permission. Panel B: The structures of the substrate DHAP, and of the inhibitor and reaction intermediate analogue PGH.

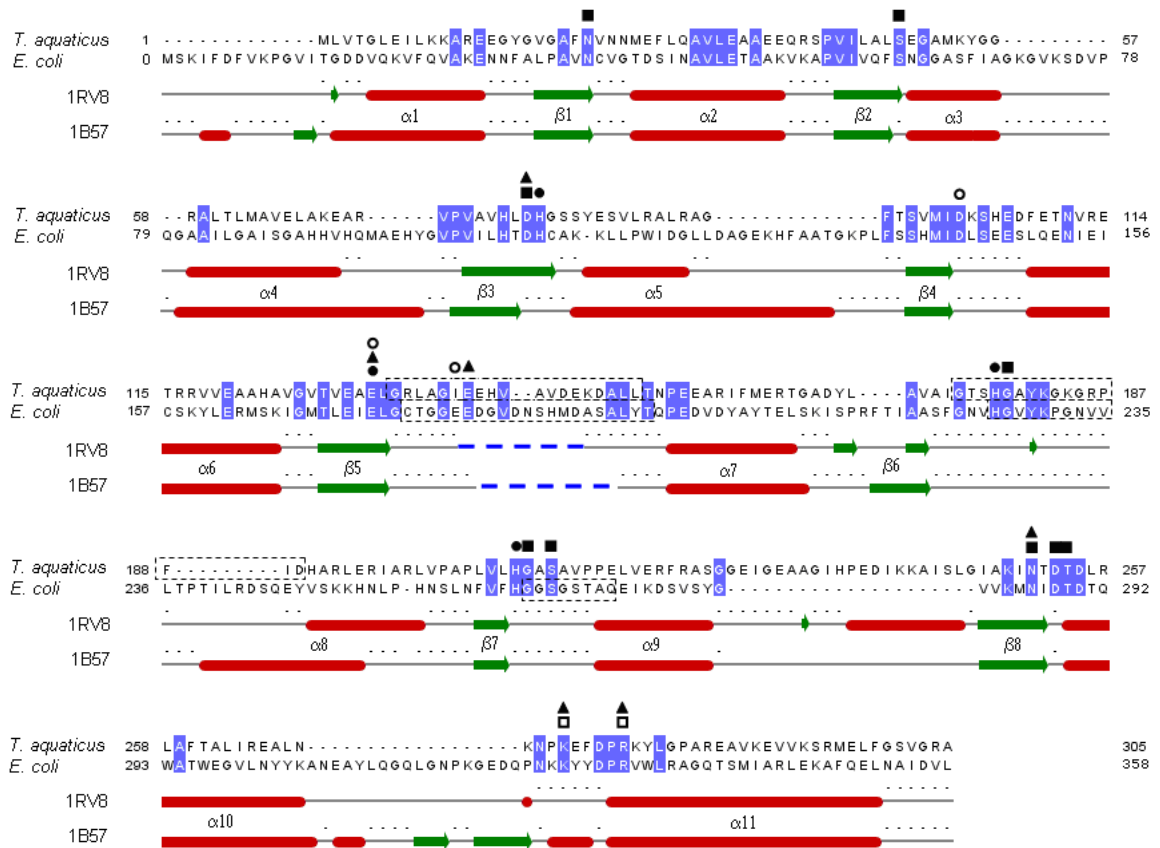


Figure 1.10 Comparison of structural features of Class II FBP aldolases

The sequences of the *T. aquaticus* and *E. coli* FBP aldolases (GeneID: AAF22441 and 947415, respectively) as well as the associated Protein Data Bank secondary structures 1RV8 and 1B57, are presented as indicated. The conserved residues are shaded in blue. The α -helices (red cylinders) and β -strands (green arrows) are identified following the numbering proposed for the *E. coli* enzyme (Cooper *et al.* 1996). The thick dashed blue lines correspond to the sections of missing electron density in the crystal structures. The mobile loops are indicated by dashed boxes around the sequences. The filled circles (●) indicate the catalytic divalent ion ligands (for the buried and exposed positions); the hollow circles (○) indicate the structural Zn^{2+} ligands in the *E. coli* enzyme structure (see Figure 1.9); the triangles (▲) indicate the residues involved in catalysis as characterized in the *E. coli* enzyme, and the squares (■) indicate the residues involved in substrate binding. The hollow squares (□) correspond to the substrate binding residues contributing to the active site of the adjacent subunit of the functional dimer. Note that the N-terminal methionine is absent from the mature *E. coli* FBP aldolase, which is why the sequence numbering starts with zero (0) in order to be consistent with the numbering used in the literature and in PDB sequences. The alignment was done using the ClustalW program (Larkin *et al.* 2007) and the graphic representation was done with Jalview (Clamp *et al.* 2004).

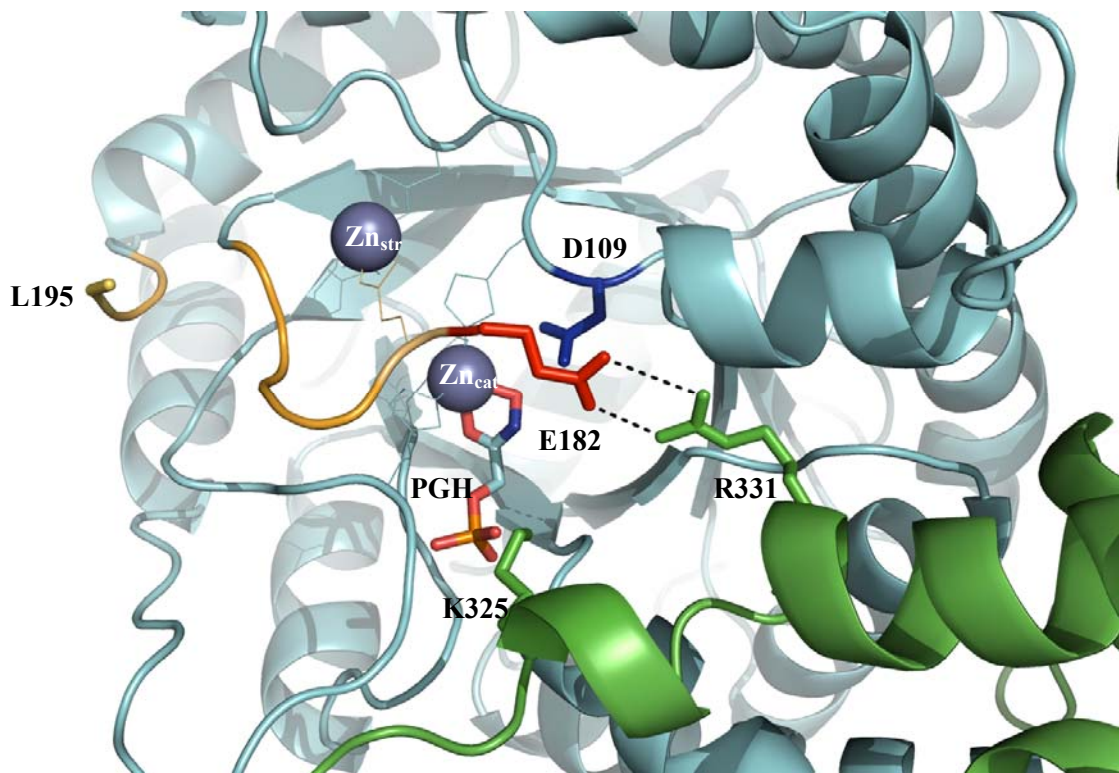


Figure 1.11 *E. coli* Class II FBP aldolase active site

The image is an enlarged view of the active site, looking down from the C-terminal end of the β sheets of the TIM barrel core. The two subunits of the dimeric enzyme are represented in cyan and green, with only a portion of the dimerization arm of the green subunit being visible. The catalytic and structural zinc ions are shown as dark grey spheres, with their amino acid ligands shown as lines. The phosphoglycolohydroxamate (PGH) inhibitor bound to the catalytic zinc ion is also shown in stick figure (carbons in cyan, nitrogen in blue, oxygens in red, phosphorus in orange; see structure in Fig. 1.9 B). The $\beta 5$ - $\alpha 7$ mobile loop backbone is shown in yellow, with the electron density missing between the residues Glu₁₈₂ (in red) and Leu₁₉₅ (far left, in yellow). The catalytic residue Asp₁₀₉ is shown in dark blue, and the adjacent subunit residues Lys₃₂₅ and Arg₃₃₁ are shown as green sticks. Note that the Glu₁₈₂ and Arg₃₃₁ functional groups have an ionic interaction in this crystal structure (shown as black dots). The figure was made with PyMOL (DeLano Scientific LLC) using the coordinates of the PDB structure 1B57.

1.3.5 Class II FBP aldolase mechanism

Aldol cleavage and aldol condensation occur through the formation of a carbanion by cleavage of a C-C or C-H bond. The base-catalyzed cleavage of these stable bonds is facilitated by stabilization of the resulting negative charge by the presence of the electron-withdrawing α -carbonyl group. The C-C-heteroatom system acquires a planar configuration which allows resonance stabilization of the negative charge by the formation of an enediolate. Class II aldolases further stabilize the enediolate by neutralizing its negative charge through bidentate coordination with a metal ion (Voet and Voet 2004).

The identities of the amino acids that participate in catalytic mechanism of the Class II FBP aldolase from *E. coli* have been elucidated mostly by the group of Dr. Alan Berry (U.K.) (Hall *et al.* 2003; Williams *et al.* 2003; Hall *et al.* 2002; Zgiby *et al.* 2002; Zgiby *et al.* 2000; Hall *et al.* 1999; Plater *et al.* 1999; Cooper *et al.* 1996; Qamar *et al.* 1996; Berry and Marshall 1993). The reaction mechanism proposed by this group is presented in Figure 1.12 (the amino acid residues that participate in catalysis are also shown in Figures 1.10 and 1.11). The enzyme follows an ordered mechanism (Hill *et al.* 1976; Rose *et al.* 1965) in the condensation reaction, with DHAP binding first to the active site, triggering a conformational change that brings the catalytic divalent metal from a buried position to a solvent-exposed position (Zn_5 site, Figure 1.9). DHAP forms a bidentate ligand to the divalent metal in this complex. The divalent metal acts as an electron sink, facilitating the 1-proS hydrogen abstraction (Rose and Rieder 1958) by Glu₁₈₂, a residue located on the $\beta 5$ - $\alpha 7$ large mobile loop, thus stabilizing the resulting enediolate intermediate. The second substrate, GAP, then binds to the active site and its carbonyl function is attacked by the enediolate carbanion, forming a new C-C bond between the two trioses. The side chain of the residue Asp₁₀₉ simultaneously protonates the GAP carbonyl to form an alcohol functional group, resulting in an enzyme-FBP complex. The product FBP is then released from the active site in the final step. All steps are fully

Chapter 1 Introduction

reversible. In the cleavage direction, GAP is the first product to leave the active site in an ordered mechanism.

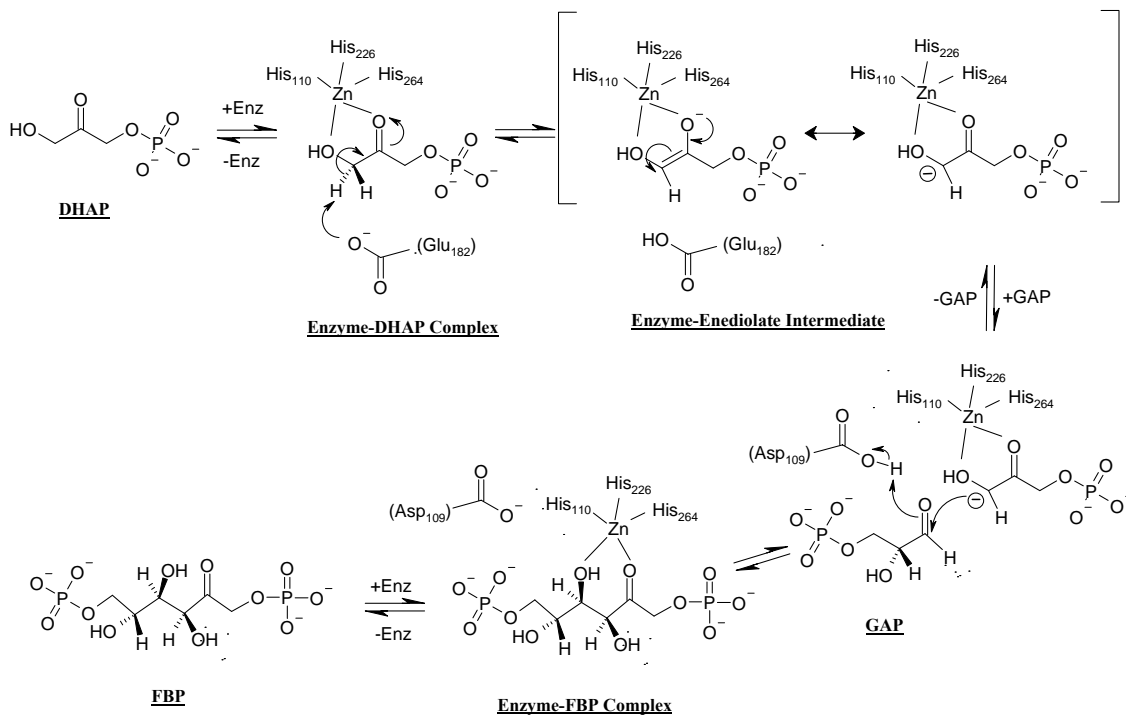


Figure 1.12 Proposed mechanism of the *E. coli* Class II FBP aldolase

The mechanism is shown in the condensation reaction direction, and all steps are fully reversible. The nomenclature for numbering the carbons of the substrates is as indicated on the left. See details in the text. Figure adapted from (Zgiby *et al.* 2002). Illustration made with the program MDL ISIS Draw (MDL Information Systems).

The zinc ligands in the proposed mechanism have been identified beyond any doubt after obtaining crystal structures of the enzyme with and without a substrate analogue (phosphoglycolhydroxamate, or PGH, see Figure 1.9), but *E. coli* enzyme mutants had also been produced earlier to identify some of these ligands. In particular, the mutant H110A had no detectable

activity, and had a zinc content of ~ 0.15 per dimer, as opposed to ~ 2 for the wild-type (Berry and Marshall 1993).

The residue Asp₁₀₉ was shown to be involved in one of the two proton exchanges of the catalytic mechanism through kinetic analysis of *E. coli* mutants. The mutant D109A had a k_{cat} 3,000 times lower than the wild-type enzyme for FBP cleavage, and carbanion formation could not be measured in the cleavage reaction. However, the rate of carbanion formation (production of the enediolate intermediate) was only ~ 8 times lower than the wild-type in the condensation direction, using DHAP as the substrate (Plater *et al.* 1999). Furthermore, the same study showed via Fourier transform infrared spectroscopy (FTIR) experiments that the D109A mutant is unable to polarize the carbonyl group of GAP. These results are consistent with the proposal that Asp₁₀₉ deprotonates the C-4 hydroxyl group of FBP in the cleavage direction (Figure 1.12). Interestingly, in the enzyme-PGH structure, the carboxylate group of Asp₁₀₉ has hydrogen bonds with the hydroxyl group of PGH (Hall *et al.* 1999), which indicates that this residue is in a position where it could interact with the C-1 hydroxyl function of DHAP (or C-3 hydroxyl in FBP), in addition to the GAP carbonyl group (see the structures of DHAP and PGH in Figure 1.9B). The equivalent conserved residue (Asp₈₀) in the *T. aquaticus* FBP aldolase structure also can form an hydrogen bond with the C-3 hydroxyl group of FBP when this substrate is modeled into the active site, based on the position of two sulfate ions in the crystal structure that are located in the putative FBP phosphate groups binding sites (Izard and Sygusch 2004).

The residues Arg₃₃₁ and Glu₁₈₂ are proposed to be involved in the binding of the GAP phosphate group and in proton exchange, respectively, based on kinetic analysis of enzyme mutants and on structural modeling (Zgiby *et al.* 2002; Qamar *et al.* 1996). These two residues form an ionic bond in the *E. coli* structure in complex with the substrate analogue PGH, which is the only crystal structure where Glu₁₈₂ is visible, as it is part of the $\beta 5$ - $\alpha 7$ mobile loop that is disordered in all crystal structures

Chapter 1 Introduction

obtained to date. There is no FBP aldolase structure available with an analogue of GAP or FBP bound in the active site, but the residue corresponding to Arg₃₃₁ in *T. aquaticus* (Arg₂₇₈ in that sequence) was shown to form an ionic bond to a sulfate ion positioned where the GAP phosphate group is believed to bind, adding some structural evidence to support the conclusions derived from kinetic analysis (Izard and Sygusch 2004). This conserved arginine residue is located in the α 10-loop- α 11 dimerization arm of the enzyme, and is part of the opposite subunit in the active dimer (see Figures 1.10 and 1.11). The *E. coli* mutants R331A and R331E showed respectively ~600-fold and ~1800-fold reductions in specificity ($k_{\text{cat}}/K_{\text{M}}$) for FBP compared to the wild-type enzyme, but only have ~8-fold reductions in specificity for DHAP based on the detection of carbanion formation from these substrates. The product inhibition by GAP during FBP cleavage was also significantly decreased for the mutant R331A compared to the wild-type, clearly pointing towards an interaction of Arg₃₃₁ with the FBP C-6 (or GAP) phosphate group (Qamar *et al.* 1996). The ionic bond between Arg₃₃₁ and Glu₁₈₂ in the crystal structure is thus thought to be a crystallization artifact (Zgiby *et al.* 2002).

The residue Glu₁₈₂ was mutated to an alanine, and the resulting mutant had a k_{cat} 300 times lower and a K_{M} 10 times lower than the wild-type enzyme in the FBP cleavage reaction, and an apparent k_{cat} ~60 fold lower than the wild-type enzyme for carbanion formation from DHAP. The kinetic analysis of this mutant suggests that it is responsible for the 1-proS proton abstraction from DHAP in the condensation reaction, and protonation of the carbanion in the cleavage reaction (Zgiby *et al.* 2002). The same study used a deuterium-labeled substrate, namely [1(S)-²H]DHAP, to show via kinetic isotope effect that proton abstraction from DHAP was the rate-limiting catalytic step in the E182A mutant, but not in the wild-type enzyme. It is relevant to note that in the mechanism proposed by Berry and collaborators (Figure 1.13), the Asp₁₀₉ and Glu₁₈₂ are not restored to their initial protonation state at the end of the catalytic cycle. One interesting possibility, based on the enzyme-

PGH crystal structure as well as the kinetic results obtained by Berry's group, would be that the Glu₁₈₂ residue is critical for loop closure and active site structure, instead of directly being responsible for proton exchange. In fact, the simultaneous mutation of four glycine residues located in the β 5- α 7 loop containing Glu₁₈₂ (G176A, G179A, G180A and G184A) results in a mutant which has similar kinetic parameters as the E182A mutant for FBP cleavage, but with an apparent k_{cat} ~30 times lower than E182A for carbanion oxidation from DHAP (Zgiby *et al.* 2002). Zgiby and collaborators mention that the pK_a of the Glu₁₈₂ side-chain should be perturbed from its normal value of ~4.3 and increased substantially to function as a proton abstractor in the condensation reaction, and they argue that loop closure may provide the necessary apolar environment for this to occur. This is consistent with the kinetic parameters obtained with the "loop" mutant described above, as the removal of the glycine residues is expected to severely restrict the flexibility of the β 5- α 7 loop and therefore affect the position of Glu₁₈₂ relative to the substrate, and likely hinder or prevent the formation of an apolar micro-environment for the Glu₁₈₂ side-chain in the active site. A crystal structure obtained with an FBP analogue, where the GAP binding site would be occupied and the mobile loop better defined, would nevertheless be helpful to confirm the role of Glu₁₈₂ in the proposed mechanism presented in Figure 1.12.

Several other acidic residues in the vicinity of the active site, which were potential proton donors or acceptors were mutated in the *E. coli* aldolase (namely, D144, D288, D290, D329, and E181), but these mutations had a less dramatic effect on catalysis (Zgiby *et al.* 2002; Plater *et al.* 1999). However, binding and catalysis were clearly affected by mutations of Asp₁₀₉ (described above), Glu₁₇₄, which is one of the buried zinc ion ligands in the absence of substrate (Zn₆ site, Figure 1.10), and Asn₂₈₆. The mutant N286D had an 8,000-fold reduction in k_{cat} for FBP cleavage compared to the wild-type enzyme, and carbanion formation from FBP or DHAP was equally affected (Plater *et al.* 1999). Product inhibition kinetics done with the mutant N286A, which had a ~200 fold higher k_{cat} for

Chapter 1 Introduction

FBP cleavage than the mutant N286D, showed that this residue is important for binding DHAP (or the DHAP-end of FBP). This residue has extensive contacts with the inhibitor PGH (and by analogy with DHAP) in the *E. coli* aldolase crystal structure 1B57, and is a ligand to a monovalent cation in the 1ZEN (ligand-free) crystal structure. Plater and collaborators also suggested that it could have an electrostatic role in the mechanism such as the repulsion of the carbanion intermediate. The mutation clearly affects catalysis more than binding, since the mutants' K_M for FBP and DHAP were only slightly increased (~10 fold or less). The mutation of a nearby conserved aspartate residue (D288A) had only a small effect on catalysis in comparison, with a ~4 fold reduction in k_{cat} for FBP cleavage compared to the wild-type enzyme. The Asp₂₈₈ residue was suggested to have a minor role in GAP binding (Plater *et al.* 1999), as shown in Figure 1.13. The equivalent conserved residue Asp₂₈₈ in the *T. aquaticus* FBP aldolase (Asp₂₅₃ in that sequence) is also proposed to bind to the C-4 hydroxyl group of FBP based on molecular modeling experiments (Izard and Sygusch 2004).

Other residues were identified as being important for substrate binding or enzyme structure by the kinetic analysis of various *E. coli* Class II FBP aldolase mutants. Asn₃₅, Ser₆₁, and Lys₃₂₅ are all part of the substrate-binding pocket according to a kinetic analysis of enzyme mutants (Zgiby *et al.* 2000) as well as the enzyme-PGH structure (Hall *et al.* 1999), as shown in Figure 1.13. Lys₃₂₅ interacts with the phosphate group of PGH (see Figure 1.11), but the mutant K325A had a similar substrate affinity for FBP and DHAP as the wild-type enzyme, with an apparent decrease in affinity for GAP. The catalytic efficiency of this mutant was significantly decreased for both the condensation and cleavage reactions (7- to 18-fold) compared to the wild-type, and as a result it was proposed that this residue is critical for the positioning of other catalytic residues in the *E. coli* FBP aldolase (Zgiby *et al.* 2000). Asn₃₅ is next to the catalytic residue Asp₁₀₉ and near the nitrogen atom of PGH (C-1 of DHAP), and product inhibition assays done with the mutant N35A which has only 1.5% of the catalytic activity of

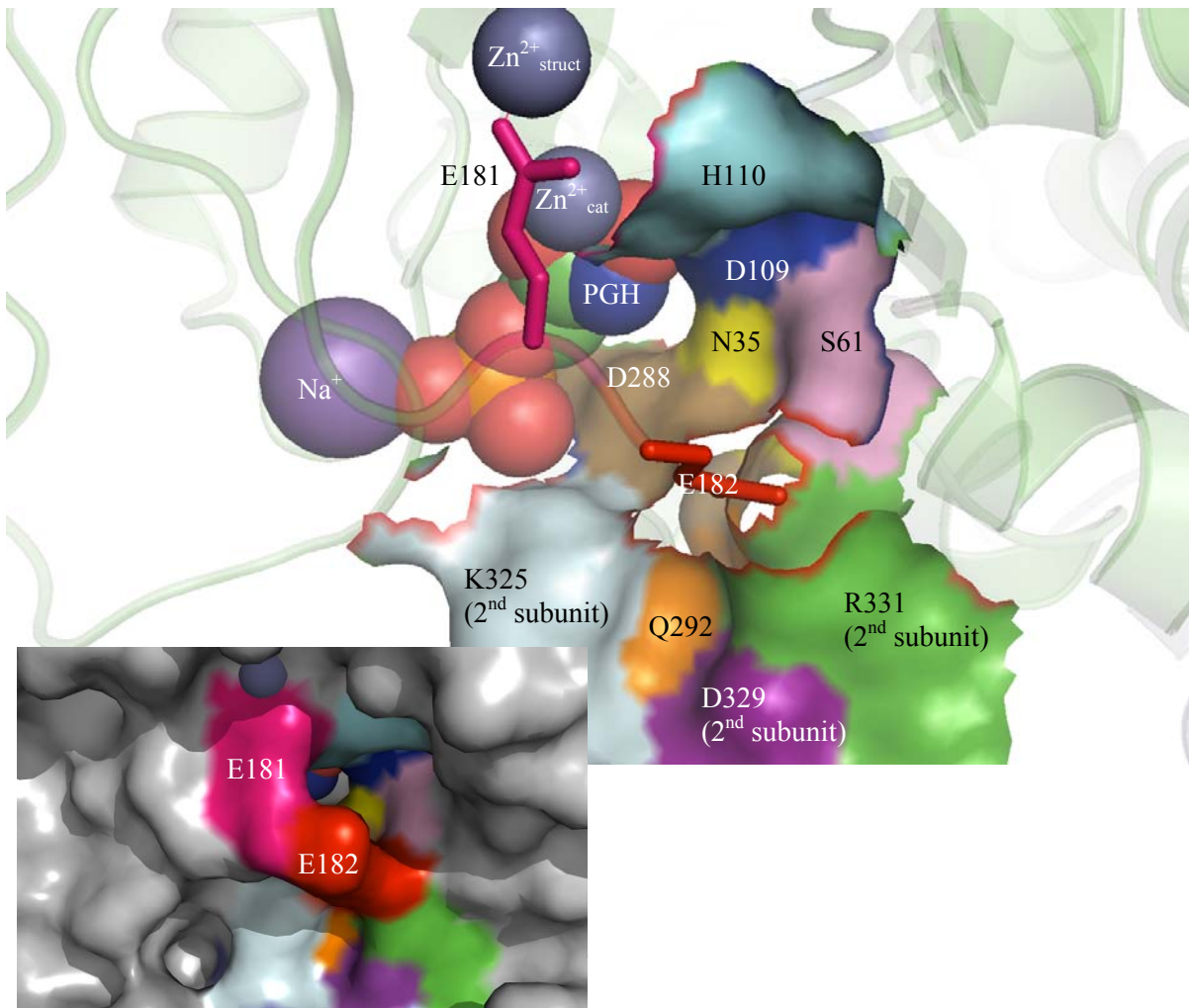


Figure 1.13 Putative binding groove for the substrate GAP in the *E. coli* FBP aldolase

The solvent accessible surface is shown in inset, and the main figure highlights the GAP binding surface, omitting the surface of the loop residues. The figure was done with PyMOL (DeLano Scientific LLC) using the coordinates of the PDB structure 1B57, and the viewing angle is similar to that of Figure 1.11, with a slight clockwise rotation of the molecule. The catalytic and structural Zn^{2+} ions are shown as dark grey spheres (top), and the Na^+ cation is shown as a purple sphere (left). The inhibitor PGH is shown in space-fill spheres (oxygen in red, phosphorus in orange, carbons in green and nitrogen in blue). The $\beta 5$ - $\alpha 7$ mobile loop residues are shown in magenta with Glu₁₈₁ (magenta) and Glu₁₈₂ (red) represented as large sticks. The putative GAP substrate-binding (and solvent-accessible) surface, which includes residues from both of the dimer subunits as indicated, is colored as follows: Arg₃₃₁ in green, Ser₆₁ in pink, Asp₁₀₉ in dark blue, Asn₃₅ in yellow, Asp₂₈₈ in brown, Lys₃₂₅ in pale cyan, Gln₂₉₂ in orange, Asp₃₂₉ in deep purple, and the catalytic zinc ligand His₁₁₀ in cyan. In the presence of GAP, the loop residue Glu₁₈₂ (centre) would be displaced to expose the guanidino group of Arg₃₃₁ located in the red-edged hole in the protein surface around the side-chain of Glu₁₈₂ (the surface of Glu₁₈₂ is omitted in the main Figure) (Zgiby *et al.* 2002).

Chapter 1 Introduction

the wild-type enzyme, showed that it is involved in binding both DHAP and GAP. The mutant S61A had a large increase in K_M in both the FBP cleavage and condensation reactions, and product inhibition assays showed that it had a decreased affinity for GAP, but a similar affinity for DHAP than the wild-type enzyme, indicating that Ser₆₁ is critical for GAP (or the C-4 to C-6 end of FBP) binding. Ser₆₁ is located between Asp₁₀₉, Asn₃₅ and Lys₃₂₅ in the active site; in fact, these residues form a water-exposed groove covered by the β 5- α 7 mobile loop residues Glu₁₈₁ and Glu₁₈₂ immediately next to PGH in the *E. coli* enzyme structure, as shown in Figure 1.13.

It is relevant to note that almost all the residues proposed to be involved in metal binding, substrate binding, and catalysis in the *E. coli* aldolase are completely conserved across all Class II FBP aldolases (see Figures 1.10 and 1.20), except for Ser₆₁, Glu₁₈₁, Asp₂₈₈, Lys₃₂₅, and Arg₃₃₁, which are strongly, but not completely, conserved. Most of these residues are involved in GAP binding and are less conserved among the Type B aldolases (Figure 1.4). The Type B group contains enzymes which have a more broad substrate specificity than the Type A enzymes, as mentioned previously (Section 1.2.2).

According to the large and relatively open GAP (substrate) binding area of the enzyme structure presented in Figure 1.13, it seems like the furanose form of FBP which predominates in solution (see Figure 1.14) could also fit in the active site and undergo linearization there to allow catalysis to occur on the linearized, or keto form, of FBP. The exact conformation(s) of FBP and DHAP that bind to the active site are relevant for inhibitor rational design. The proton transfer that happens during the linearization/cyclization of FBP could also be involved in changing the initial or final protonation state of Asp₁₀₉ and Glu₁₈₂ for true completion of the catalytic cycle (Figure 1.12). It is also possible that some of the mutants of active site residues that affect the kinetic parameters (for example, Lys₃₂₅) could be also impaired in the “linearization” of FBP, if the enzyme can in fact catalyze this reaction.

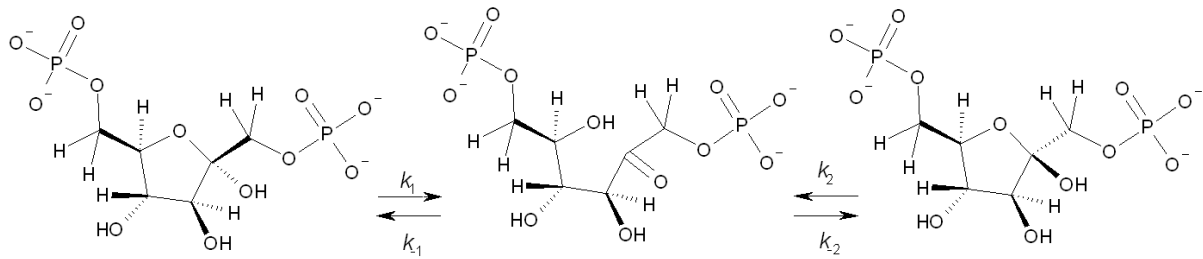
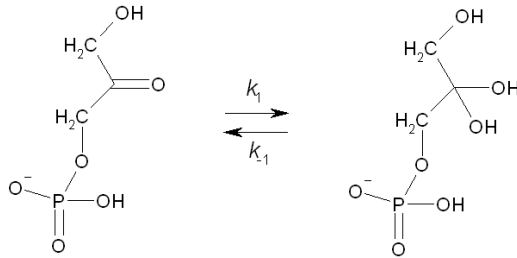
A**B**

Figure 1.14 Spontaneous cyclization of D-fructose-1,6-bisphosphate and hydration of dihydroxyacetone phosphate in solution

Panel A: The FBP molecule exists as an equilibrium of three conformations: α -D-fructofuranose-1,6-bisphosphate (on the left); linearized form (centre); and β -D-fructofuranose-1,6-bisphosphate (on the right). The β anomer is favored over the α anomer as they exist in a 4:1 ratio, and only $\sim 1.8\%$ of the molecules are in the linear form at equilibrium at 25°C . The tautomerization rates at 25°C are $k_1 = 5.3 \pm 0.4 \text{ s}^{-1}$; $k_{-1} = 55 \pm 6 \text{ s}^{-1}$; $k_2 = 21.0 \pm 1.5 \text{ s}^{-1}$; and $k_{-2} = 940 \pm 75 \text{ s}^{-1}$, and these rates were apparently not affected by pH in the range from 7 to 10 pH units and also not affected by the ionic strength of the solution or the presence of organic buffers. Panel B: DHAP exists in two forms in solution, carbonyl (left) and *gem*-diol hydrate (right), in proportions of $56 \pm 2\%$ and $44 \pm 2\%$ respectively at 25°C . The rate constants are $k_1 = 0.36 \text{ s}^{-1}$ and $k_{-1} = 0.45 \text{ s}^{-1}$ for the hydration and dehydration reactions, respectively (Szwergold *et al.* 1995).

There are several different reports regarding the anomeric specificities of the FBP aldolases. The yeast aldolase was found to possess an anomerase activity, but not the Class I enzymes or the *E. coli* Class II enzyme, based on rapid quench kinetic experiments (Schray *et al.* 1975). A more recent report stated that Class I aldolase catalyses the ring opening of the β anomer of FBP, and that only the

Chapter 1 Introduction

β anomer could bind productively to the muscle enzyme (Choi and Tolan 2004). Another report based on ^{13}C NMR spectra analysis also suggests that the keto (open-chain) form of FBP is the only one that binds to the active site and is used as a substrate by the *E. coli* Class II enzyme (Szwergold *et al.* 1995). However, this conclusion was based on the detection of the polarization of the carbonyl bond of the substrate, and this study was published before the enzyme structure was determined, along with the discovery that a conformational change occurs upon substrate binding to bring the buried zinc ion to its catalytically active position where it can polarize the carbonyl from DHAP. The same study concluded that the *E. coli* enzyme increased the enolization rate of DHAP by a factor of at least 10^3 relative to the uncatalyzed rate (Figure 1.14) (Szwergold *et al.* 1995). A recent crystal structure of the *T. aquaticus* FBP aldolase in the presence of ammonium sulfate has shown that there are two sulfate binding sites that are 10 \AA apart that correspond to the FBP phosphate binding sites (Figure 1.15). These binding sites can accommodate the structure of the linearized form of the substrate FBP, but not the cyclic forms. Considering that the spontaneous linearization rate of the predominant β -D-fructofuranose-1,6-bisphosphate is $\sim 21 \text{ s}^{-1}$ at $25 \text{ }^\circ\text{C}$, the anomerase activity would be irrelevant for the catalytic rate of the aldolases that have a turnover number below this value for FBP cleavage, as long as they can initially bind to the cyclic forms of FBP. Of all the Class II enzymes characterized to date, only the yeast FBP aldolase has a turnover number significantly higher than the spontaneous linearization rate, with an activity of $\sim 100 \text{ s}^{-1}$ at $30 \text{ }^\circ\text{C}$ (Belasco and Knowles 1983). The number and identity of substrate conformation(s) that can bind to the active site of most Class II aldolases thus still remain unclear.

1.3.6 Catalytic loops

The active site of the Class II FBP aldolases includes two mobile loops that are expected to bring the catalytic zinc ion to a solvent-accessible position and close over the substrate during catalysis, as

shown in Figures 1.11, 1.13, and 1.15. These loops form a large portion of the enzyme surface that is in contact with the substrate during catalysis (see Figure 1.13), and thus their structure and properties are very relevant for the rational design of ligands. Such loops are common features in TIM barrel enzymes, and their functions in substrate binding and catalysis were extensively studied in several enzymes, in particular in triose phosphate isomerase itself (Aparicio *et al.* 2003; Williams and McDermott 1995). It was also shown that loop movement can facilitate inhibitor binding in zinc-dependent metallo β -lactamases (Concha *et al.* 2000). There are several general reasons for loop motion during enzymatic catalysis. The movements may bring into position the amino acids participating in catalysis, as is proposed for the $\beta 5$ - $\alpha 7$ loop residue Glu₁₈₂ in the *E. coli* aldolase (Zgiby *et al.* 2002). Such movements may also exclude water molecules from the active site and create a hydrophobic environment in which the pK_as of ionizable groups are altered, as is also proposed for the Glu₁₈₂ residue carboxylate function. The loops can also protect reactive intermediates, as is the case for triose phosphate isomerase (Pompliano *et al.* 1990). It is possible that loop closure in the *E. coli* enzyme helps to prevent the DHAP carbanion from reacting with other substrates. The ionic interaction between Glu₁₈₂ and Arg₃₃₁ may not be a crystallization artifact, but instead could be a way to keep the carbanion isolated from the environment until GAP displaces the Glu₁₈₂ residue and the $\beta 5$ - $\alpha 7$ loop by binding to Arg₃₃₁ in the condensation reaction (Figures 1.11 and 1.13).

The Class II FBP crystal structures provide clear indications of loop movements, and previous studies have confirmed this through comparisons of the *E. coli* enzyme structures with and without PGH bound in the active site (Zgiby *et al.* 2002). The structures of apo- and substrate bound *T. aquaticus* fructose-1,6-bisphosphate aldolase have three regions of weaker electron density that show higher B-factors (see yellow and red colouring of the backbone in the structures shown in Figure 1.15). The regions of missing electron density in the *E. coli* and *T. aquaticus* structures are

Chapter 1 Introduction

also indicated in dashed boxes around the amino acid sequences in Figure 1.10. Izard and Sygusch (2004) argue that the closing and opening of the two active site loops has to be coordinated because of steric interference (Figure 1.15).

What controls the loop movements? Is it a natural motion of the enzyme, or are the movements influenced by the presence of substrate or inhibitor? In the case of TIM, Williams and McDermott report that the loop movements are not ligand-gated, but a natural motion of the protein with a time scale similar to that of catalytic turnover (Williams and McDermott 1995). However, for other enzymes such as metallo- β -lactamases, studies with tryptophan mutants showed that loops closed in presence of ligands (Garrity *et al.* 2004). The *E. coli* Class II FBP aldolase was studied by liquid state NMR and the loop movements did not seem to be coordinated by the presence of DHAP, as the backbone motions in the ns time scale were not significantly different from those of the free enzyme. However, structural changes in the β 5- α 7 loop were detected upon DHAP binding as 10 assigned residues from this loop had chemical shift and peak intensity perturbations in their NMR spectra (Hilcenko 2003). The enzyme movements in the presence of GAP were not studied. There were limitations reported to doing liquid NMR studies even with a 900 MHz machine, because of the large size of the dimer (78 kDa) and the limited stability of the *E. coli* aldolase. About 38% of the backbone resonances were successfully assigned in that study. Some regions like the α 10- α 11 loop and α 11 helix were not assigned, possibly because of flexibility (their dynamic behaviour seems to occur on ms time scale). It was concluded that a full NMR assignment using the standard triple resonance strategy is not feasible on this protein (Hilcenko 2003).

Tryptophan mutants were also constructed to detect movements induced by the presence of substrate in the *E. coli* Class II FBP aldolase. The native enzyme's combined four tryptophans' signal was shown to respond to DHAP binding at 10 °C or lower (but not at 20 °C). Attempts to identify

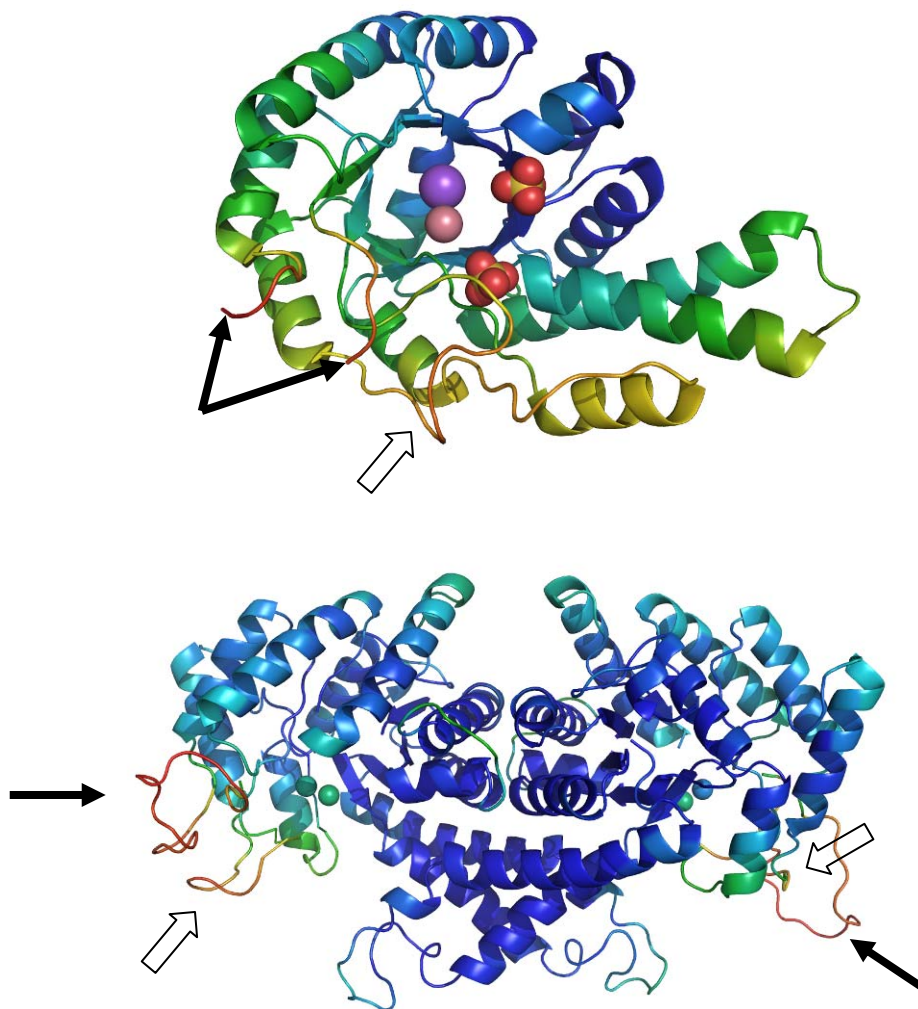


Figure 1.15 Structure of the unligated *T. aquaticus* monomer and *E. coli* Class II FBP aldolase dimer colored according to B-factors

The higher B factors are indicated by a more red colouring. In the *T. aquaticus* aldolase (top), the sulfate ions are shown in red and orange, the Na⁺ cation is shown in purple, and the Co²⁺ ion is shown in pink. In the *E. coli* aldolase structure (bottom), the two mutually exclusive Zn²⁺ positions are represented by green spheres. The active site loops are identified with black (β5-α7 loop) and white (β6-α8 loop) arrows. Note that a portion of the *T. aquaticus* β5-α7 loop is missing from the monomer structure. Figure done with PyMOL (DeLano Scientific LLC) using the coordinates of the PDB structures 1RV8a and 1DOS.

Chapter 1 Introduction

which tryptophan residue is responsible for the change in signal by mutating each residue were unsuccessful since the resultant enzymes were inactive (Hilcenko 2003). However, detection of movements by introducing tryptophan residues in the loops of FBP aldolase has not been attempted.

In summary, to date even though X-ray crystal structures suggest the possibility of loop movements upon substrate binding, this has not been confirmed using other techniques. It is possible that the loop movements are part of the natural enzyme motions and not dependent on the presence of substrate. It is therefore difficult to predict which structural characteristics of a novel ligand would be desirable in order to improve its binding to the active site through interactions with the mobile loops.

1.4 Inhibitors of FBP aldolase

In this thesis, the objective will be to gather as much structural and kinetic information as possible on Class II FBP aldolase in order to facilitate rational ligand design, which is a long-term goal of this multidisciplinary project. In this section, the compounds that are already known to inhibit the Class I and Class II FBP aldolases will be described, along with the structural basis for the inhibition. The inhibitors can generally be classified in two groups: the mechanism-based inactivators, and the substrate analogues. This latter category of inhibitor is especially relevant to inform novel ligand design.

1.4.1 Mechanism-based inactivators

The yeast Class II FBP aldolase was discovered to be inhibited by chelating agents soon after it was isolated, which led to the conclusion that this enzyme is metal-dependent (Warburg and Christian 1943). Numerous chelating agents have since been used to inhibit the Class II enzyme, including EDTA, cysteine, o-phenanthroline, and pyrophosphate (Jagannathan *et al.* 1956). The Class I enzymes can be inhibited in the presence of DHAP or FBP by sodium borohydride, which

irreversibly reduces the Schiff-base complex between the active site lysine and the substrate (Rutter 1964). These FBP aldolase inhibitors are of course not useful for medical treatment as they are not specific and can affect numerous other enzymes that are either metal-dependent, or form a Schiff-base intermediate.

1.4.2 Substrate analogue inhibitors

Several inhibitors that affect Class I FBP aldolases have been identified, and they are generally substrate analogues that are monophosphorylated or diphosphorylated, and that resemble the substrate DHAP or FBP. A previous review of the inhibitors of the Class I FBP aldolase (Gefflaut *et al.* 1995) stated that the presence of a hydrogen bond donor at position 3 is critical for the inhibitor affinity for the active site for phosphorylated compounds. Some other inhibitors are F1P and F6P, and some monophosphorylated alcohols with K_I/K_M ratios of ~50 to 500 for the Class I enzyme (Gefflaut *et al.* 1995). The presence of a second phosphate group increases the affinity significantly for longer chain compounds that are closer in size to FBP. Examples of potent inhibitors include hexitol-1,6-bisphosphate, D-arabinol-1,5-bisphosphate, 5-deoxy-FBP and D-glucitol-1,6-bisphosphate with K_I/K_M values close or lower than 1. The most potent Class I aldolase inhibitors described in that review were 2,6-naphthalenediol-bisphosphate derivatives ($K_I \sim 0.4 \mu\text{M}$) (Gefflaut *et al.* 1995).

1.4.3 Inhibitors with high affinity for Class I aldolases

Recent studies have focused on Class I FBP aldolase inhibitors as this enzyme is a potential drug target for protozoan parasites such as *Plasmodium falciparum* (malaria), *Leishmania mexicana* (leishmaniasis), and the family *Trypanosomatidae* (sleeping sickness) (Azéma *et al.* 2006; Dax *et al.* 2006). Some Schiff-base forming inhibitors of the Class I protozoan enzymes that have minimal

Chapter 1 Introduction

effects on the human and rabbit Class I aldolases, are hydroxynaphthaldehyde phosphate derivatives, with inhibition constants as low as 24 nM for the *T. brucei* aldolase (Dax *et al.* 2006; Dax *et al.* 2005; Blonski *et al.* 1997). Other reaction intermediates or substrate analogues which are also slow-binding inhibitors of the Class I FBP aldolases include β -dicarbonyl phosphorylated compounds (Blonski *et al.* 1998).

1.4.4 Inhibitors with high affinity for Class II aldolases

Very few potent Class II FBP aldolase inhibitors are known. The best known (and for more than 30 years, it was the only one known) is PGH (see structure in Figure 1.9b), with a K_I of 0.01 μ M for the yeast aldolase. It is not specific for Class II aldolase, however, since it has a K_I of 1 μ M for the rabbit muscle Class I aldolase, as well as a K_I of 3 μ M for the Rabbit muscle Triose phosphate isomerase (TIM) (Gavalda *et al.* 2005; Fonvielle *et al.* 2004; Lewis and Lowe 1973). PGH is also a potent inhibitor of other enzymes utilizing DHAP such as methylglyoxal synthase, L-rhamnulose-1-phosphate synthase, tagatose-bisphosphate aldolase, L-fuculose-1-phosphate aldolase, etc. (Kroemer *et al.* 2003; Hall *et al.* 2002; Marks *et al.* 2001; Fessner *et al.* 1996). Two new derivatives of PGH shown in Figure 1.16, phosphoglycoloamidoxime (PGA) and phosphoglycolohydrazide (PGHz), are more specific for the Class II FBA versus the Class I enzyme (K_I of 0.34-3.3 μ M for Class II enzymes, versus K_I of 370 μ M (PGHz) or >1 mM (PGA) for the rabbit FBA) (Fonvielle *et al.* 2004). However, they are also good inhibitors of the rabbit TIM, with K_I of 111 μ M (PGHz) and 4.5 μ M (PGA) (Gavalda *et al.* 2005), which makes these compounds likely toxic for humans.

N-sulfonyl hydroxamate derivatives were recently synthesized and tested as inhibitors of the Class II FBP aldolase (Gavalda *et al.* 2005). Two of these were competitive inhibitors specific for this enzyme (PGS1 and PGS2, Figure 1.16), as they were not significant inhibitors of the Class I

enzyme or TIM. They had a K_i of 350 and 100 μM , with the *E. coli* FBA, respectively. The authors concluded that a phosphate group, as opposed to a phosphonate group, was essential for binding of the compounds to the FBA active site.

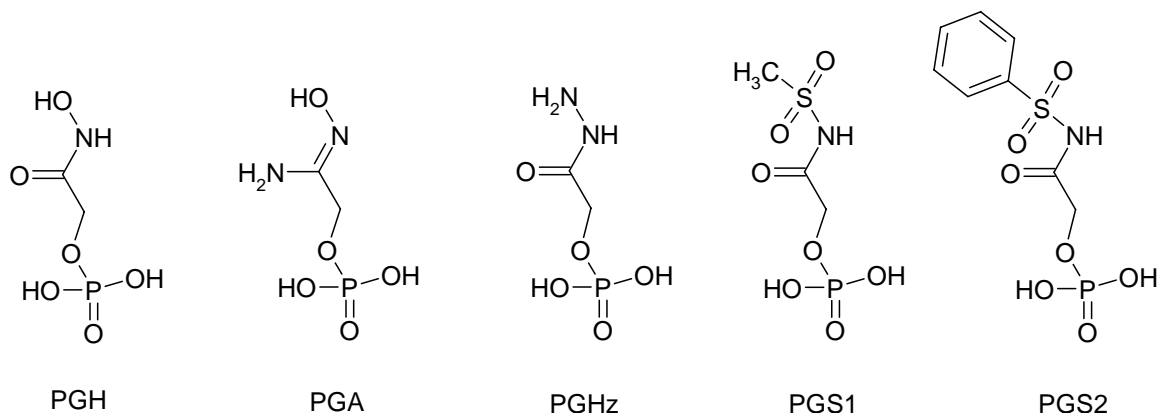


Figure 1.16 Class II FBP aldolase inhibitors

See details in the text. The PGH derivatives were synthesized and published in (Gavalda *et al.* 2005; Fonvielle *et al.* 2004).

To conclude this section, there is still a need for new leads in order to produce a potent and specific inhibitor of Class II FBP aldolases, as there is no ligand with sufficiently high affinity (nM range) that is specific for these enzymes. However, the recent synthesis of inhibitors that have a high affinity for the Class I *T. brucei* FBP aldolase, while not significantly inhibiting the human Class I enzyme, is proof that this goal is indeed achievable (Dax *et al.* 2006).

1.5 Target organisms

In order to test and improve the design of the first series of inhibitory compounds, the Class II FBP aldolases from six pathogenic organisms were cloned, purified and characterized. The Class II FBP aldolases were chosen to cover most of the evolutionary branches of the Class II aldolase

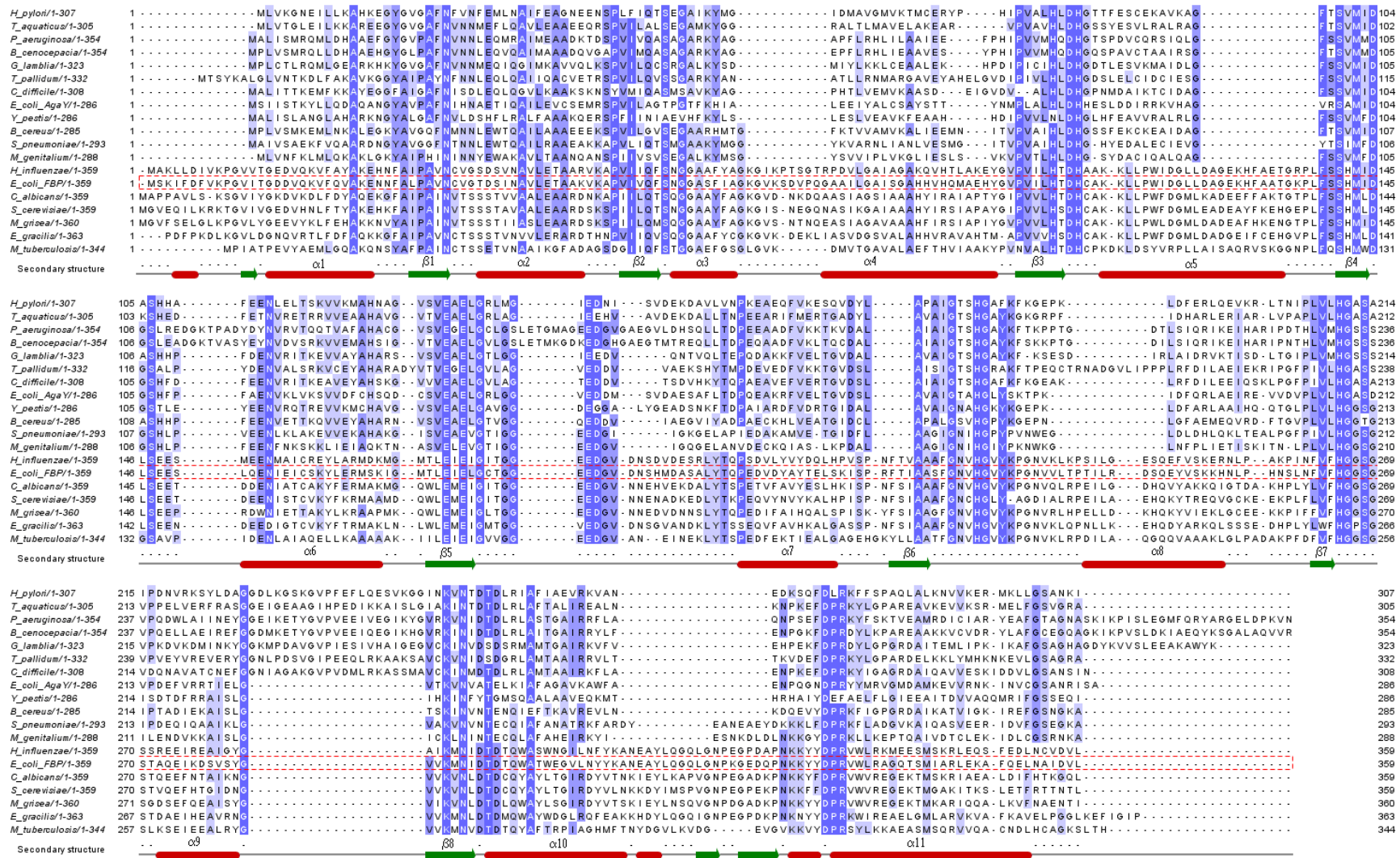
Chapter 1 Introduction

phylogenetic tree (Figure 1.4), with emphasis on the most devastating human and plant pathogens. The aldolases from *Mycobacterium tuberculosis*, *Pseudomonas aeruginosa*, *Bacillus cereus* (which has an amino acid sequence identical to that of *Bacillus anthracis*), *Helicobacter pylori*, *Magnaporthe grisea*, *Streptococcus pneumoniae*, and *Haemophilus influenzae* were cloned into *E. coli* overexpression vectors for this project. A sequence alignment of these aldolases, along with some of the best-characterized aldolases such as those from *E. coli* and *S. cerevisiae*, is presented below (Figure 1.17).

(Following page)

Figure 1.17 Sequence alignment of Class II FBP aldolases

The secondary structure for the *E. coli* Class II FBP aldolase (PDB ID 1B57, sequence framed with red dashed line) is indicated below the alignment. The secondary structure elements have been identified according to the *E. coli* aldolase structure reported by Cooper and collaborators (Cooper *et al.* 1996). The alignment was done using the ClustalW program (Larkin *et al.* 2007) and the graphic representation was done with Jalview (Clamp *et al.* 2004). The blue shading indicates >80%, >60%, and >40% conservation of residues within the alignment, with the darkest blue corresponding to the highest amino acid conservation. The source of the amino acid sequences were NCBI GeneBank and Protein Data Bank: *Helicobacter pylori* 26695 GeneID: 900140; *Thermophilus aquaticus* PDB#1RV8 GeneID: AAF22441; *Pseudomonas aeruginosa* PAO1 GeneID: 880792; *Burkholderia cenocepacia* GeneID: 6124318; *Giardia lamblia* PDB#2ISV; *Treponema pallidum* GeneID: 2611197; *Clostridium difficile* GeneID: 4914942; *Escherichia coli* AgaY (TBP aldolase) PDB#1GVF; *Yersinia pestis* GeneID: 1176799; *Bacillus cereus* ATCC 10987 GeneID: 1207675; *Streptococcus pneumoniae* Gene ID: 933499; *Mycoplasma genitalium* Gene ID: 875427; *Haemophilus influenzae* Rd KW20 GeneID: 949539; *Escherichia coli* K12 MG1655 GeneID: 947415 PDB#1B57; *Candida albicans* SC5314 Protein ID: EAL04108.1; *Saccharomyces cerevisiae* GeneID: 853805; *Magnaporthe grisea* GeneID: 2674368; *Euglena gracilis* Protein ID: CAA61912; *Mycobacterium tuberculosis* H37Rv GeneID: 886474. Note that the numbering of amino acids may not correspond to that used in PDB structures, as the N-terminal methionine is absent (cleaved off) in some of these proteins.



Chapter 1 Introduction

Mycobacterium tuberculosis is a human pathogen that is the causative agent of TB. According to the most recent statistics from the World Health Organization, tuberculosis is still one of the leading causes of death in developing countries and one of the most common infectious diseases in the world. Each year *M. tuberculosis* infects over 8 million people and causes more than 1.5 million deaths. It has been estimated that 1/3 of the world's population and 10% of Canadians have the latent form of tuberculosis and respiratory diseases in Canada (WHO 2004). In the latent stage the bacteria are less susceptible to the normal line of drugs recommended for the treatment of TB, hence the long duration of TB chemotherapy (6 to 8 months), which often results in patients not adhering to the drug treatment program (O'Brien and Nunn 2001).

In *M. tuberculosis*, which possesses both a Class I and a Class II FBP aldolase (see section 1.2.2), glucose is oxidized by EMP (94%) and the pentose phosphate pathway (6%) (Jayanthi Bai *et al.* 1975). The Class II enzyme has been shown to be constitutively expressed, and its expression is increased at low oxygenation level, a condition that is expected to occur during the bacteria's latent infection stage of lung tissues (Rosenkrands *et al.* 2002). These results are echoed by other studies showing that Class II FBP aldolase expression is up-regulated in response to stress in a variety of prokaryotes (Tomas *et al.* 2004; Wilkins *et al.* 2002; Marino *et al.* 2000; Schmid *et al.* 2000). In contrast, the Class I enzyme activity was detected only in high-oxygenation growth conditions (Bai *et al.* 1974). In addition, the absence of a Class II FBP aldolase gene (*fba*, Rv0363c) knock-out in a previous high-density mutagenesis study of *M. tuberculosis* (Sasseti *et al.* 2003; 2001) indicates that the gene could be essential for growth. Mutants of Class I *fba* were not identified in that study since the gene encoding this enzyme has not been identified in the genome, i.e. no homologues of known Class I FBP aldolases are present.

Pseudomonas aeruginosa is an opportunistic pathogen that infects immunocompromised individuals, including those undergoing cancer treatment, individuals with AIDS and those afflicted

with the genetic disease cystic fibrosis. Cystic fibrosis is the most common genetic disease among Caucasians in Canada, and by adulthood 80% of the patients are infected with *P. aeruginosa* (Saiman and Siegel 2004). In *P. aeruginosa*, mutations that reduce the FBP aldolase activity result in the lack of growth of the bacterium on minimal media with carbohydrate carbon sources (see section 1.2.4). Furthermore, the Class II FBP aldolase is essential for the synthesis of alginate, which is secreted by *P. aeruginosa* (Banerjee *et al.* 1985) and forms a coat that is partially responsible for bacterial resistance to therapy. One aspect of the pathogenesis of chronic lung infection in CF is the ability of *P. aeruginosa* to grow as a biofilm, which reportedly increases bacterial resistance to phagocytic killing and antibiotics. Of two, independent, pathways to biofilm formation, one is alginate-dependent (Lyczak *et al.* 2002). A drug disrupting the formation of alginate may increase bacterial sensitivity to both antibiotics and the immune system. The FBP aldolase from *P. aeruginosa* was recently suggested to be a potential drug target (Sakharkar *et al.* 2004).

Bacillus cereus and *Bacillus anthracis* both share the same Class II FBP aldolase and cause food poisoning and anthrax, respectively (Valjevac *et al.* 2005). The lung form of anthrax is deadly and cases have occurred as a result of biological warfare. Anthrax vaccines exist, but the low risk of the disease does not justify widespread vaccination protocols (Kaufmann 2007). However, drug-resistant strains of *B. anthracis* continue to appear and drugs are required in case of an anthrax attack (Brouillard *et al.* 2006).

Rice blast is the most devastating disease of rice and is caused by *Magnaporthe grisea* (also named *Pyricularia grisea* in its asexual state), an ascomycete fungus (Zhu *et al.* 2000). It is one of the most studied among phytopathogenic fungi (Soanes *et al.* 2002), and also causes serious disease on other grasses including wheat and barley. *M. grisea* is responsible for losses of 11-30% of the world's rice harvest each year, and has a very significant economic impact in agriculture

Chapter 1 Introduction

(Talbot 2003). Genetically resistant cultivars of rice generally become susceptible to blast after only a few growing seasons (Bonman *et al.* 1992), making the use and continued development of effective fungicides necessary. The genome of *M. grisea* was sequenced recently (Dean *et al.* 2005), and the gene of its Class II FBP aldolase made publicly available, making it an attractive target for this project. The *M. grisea* aldolase is closely related to the essential *S. cerevisiae* aldolase, according to amino acid sequence alignments (Figure 1.17).

Streptococcus pneumoniae is the most common bacterial cause of community-acquired pneumonia, a leading cause of mortality and morbidity (Alpuche *et al.* 2007). It is estimated that up to 1 million children die of pneumococcal disease annually in the world, and that pneumococci cause between 10% and 20% of all deaths among children in developing countries (Kaufmann 2007). The increase in antimicrobial resistance has raised concerns about the efficacy of available therapies, and a call for new therapeutic agents. *S. pneumoniae* is one of the best examples of the global emergence of antibiotic resistance (Adam 2002). Very recently, Song and co-workers (Song *et al.* 2005) in Korea reported an allelic replacement mutagenesis study which identified the Class II FBP aldolase gene as essential in *S. pneumoniae*, reinforcing our conviction that bacterial Class II FBP aldolases represent very attractive targets for totally new antibacterial agents.

Haemophilus influenzae is one of the most frequent causes of community-acquired pneumonia, and there is an increasing prevalence of antibiotic resistance in this pathogen (Alpuche *et al.* 2007). *H. influenzae* type b (Hib) causes bacteremia and acute bacterial meningitis in infants and young children (under 5 years of age), and the vaccination is very effective in preventing the disease. However, non-typable *H. influenzae* causes ear infections and sinusitis in children, and pneumonia in children and adults. The FBP aldolase from this organism is interesting because of its high sequence similarity to the Class II aldolases from *E. coli* and *M. tuberculosis* (Figure 1.17). By comparing the properties of those three enzymes, it may be easier to pinpoint the regions of the enzyme that are

critical for its specificity (for substrate and inhibitors) and catalytic efficiency, as well as its oligomeric state.

Helicobacter pylori is responsible for gastric ulcers and about half of all stomach cancers, and infects about 50% of the world's population (Brown 2000). The bacterial virulence factors promote the persistence of infection and chronic inflammation, as well as DNA damage which can lead to cancer in genetically susceptible hosts (McNamara and El-Omar 2008). An antibiotic could be economically viable, as there are antibiotic-resistant strains (Jafri *et al.* 2008).

Escherichia coli is a commensal bacterium which is part of the normal human intestinal microflora. However, some strains are pathogenic due to their acquisition of virulence factors, and can cause diseases such as dysentery, meningitis, diarrhoea, haemolytic uremic syndrome, and urinary tract infections (Kaper *et al.* 2004). The aldolase from *E. coli* will also be purified to have a better evaluation of our procedures compared with the available literature. The *E. coli* enzyme is the best-characterized Class II aldolase (Section 1.3).

1.6 Summary

Drug resistance is on the rise worldwide for bacterial and fungal pathogens, and novel drugs and drug targets are urgently needed. The metal-dependant Class II FBP aldolase has been shown to be an essential enzyme in prokaryotes under several growth conditions *in vitro*, and is a promising new target for rational drug design. It has been observed that the FBP aldolase activity level must decrease below 5% of wild-type levels before the effects on growth start to be significant, which means that only a very potent inhibitor would have a protective effect for animals or plants against pathogenic organisms *in vivo*. The active site of the *E.coli* Class II FBP aldolase has been extensively studied and the substrate binding pocket is well defined, excepted for the elements in the mobile loops that could be involved in substrate or inhibitor binding, which will require further investigation. No

Chapter 1 Introduction

specific and high affinity (nM range) inhibitor of Class II FBP aldolases is currently available, but some research groups are making progresses in this direction. The recent successful efforts towards the design of specific and potent inhibitors of the prokaryotic Schiff-base forming Class I FBP aldolase are encouraging, as they prove that it is possible to accurately target the active site of evolutionarily divergent aldolases even if they share the same substrate specificity. The Class II aldolases from several devastating human and crop pathogens will thus be studied for this project.

1.7 Project overview

In order to maximize our chances of finding an effective inhibitor against the microbial, metal-containing FBP aldolase (also called Class II FBP aldolase), we decided to study the enzymes from several microbes, including both human and plant pathogens. This thesis describes the cloning of the genes encoding these enzymes, their expression, purification and characterization. We took two approaches towards the production of a drug candidate against these enzymes. First, we screened numerous known and commercially available metal-binding chemicals, to evaluate their effectiveness as Class II FBP aldolase inhibitors. After identification of the most effective inhibitory chemicals, some derivatives were synthesized to increase their effectiveness, and the results of these efforts are also reported. Our second approach was to get a better understanding of the enzyme active site and the structural changes it undergoes during catalysis, in order to facilitate drug design. To achieve this we made mutants of some aldolases by introducing fluorescent probes, namely tryptophan residues, around the active site. Probe fluorescence was then monitored during catalysis and/or inhibition. We also attempted to test the microbial aldolases with different substrates to measure their specificity, or active site structures. In addition to being useful for inhibitor synthesis, the information on the specificity of microbial aldolases may lead to the commercial use of these enzymes as tools in commercial organic synthesis due to their ability to catalyse stereospecific C-C bond formation. In

conclusion, the results from these studies and recommendations for future directions towards the goal of novel drug discovery against Class II FBP aldolase are presented.

1.8 Research objectives

The purpose of this doctoral study is to put in place the foundation for a long-term study using the Class II FBP aldolases from several microorganisms as novel targets for inhibitor development. The overall objectives of this thesis are to:

- 1) Clone the genes encoding the Class II FBP aldolases from various pathogens and purify the over-expressed enzymes.
- 2) Characterize the enzymes in terms of metal utilization, stability, kinetic parameters and their susceptibility to inhibition by a range of metal-chelating synthetic compounds.
- 3) Gain a better understanding of the reaction mechanism of the Class II FBP aldolases.
- 4) Investigate possible links between structural features such as mobile loops, enzyme kinetics and inhibition parameters.
- 5) Make recommendations for the rational design of ligands that can inhibit the Class II aldolase, possibly leading to new antibacterial or antifungal agents.

The results presented in this project will facilitate future *in vitro* studies with the targeted enzymes, and recommendations are also made for further inhibitor development.

1.9 Outline of the thesis

This thesis consists of six chapters, with a common focus of laying down the groundwork necessary to achieve rational inhibitor development. The scope of each chapter is listed as follows:

Chapter 1 Introduction

Chapter 1 reviews the previous progress in rational drug design, the reasons behind our choice of fructose 1,6-bisphosphate aldolase as a new drug target, and the work done by other groups to better understand the structure-function relationship of this enzyme. Known inhibitors of this enzyme are also reviewed. The hypothesis, objectives and the scope of the thesis are also given in this chapter.

Chapter 2 presents the work done to clone and isolate the Class II FBP aldolases from various human and plant pathogens. Of particular interest is the use of a small bench-top fermentor to produce gram-scale amounts of purified enzyme.

Chapter 3 describes the characterization of the various recombinant enzymes in terms of structural and kinetic properties, their stability, and their metal content. The properties are compared with those previously published for the enzymes purified from their original hosts. The activity of the purified enzymes was also determined in the presence of various organic solvents and at elevated temperatures, to investigate the potential use of Class II aldolases in industrial organic synthesis.

Chapter 4 investigates the effectiveness of various inhibitory compounds, commercially available or synthesized by our group, on the aldol cleavage reaction. Models of inhibition are also proposed and recommendations for future inhibitor design are discussed.

Chapter 5 describes the design and purification of enzyme mutants for the purpose of investigating the loop movements during catalysis and inhibition. The preliminary results obtained with steady-state and time-resolved fluorescence experiments are discussed.

Chapter 6 presents the conclusions of this study, contributions of this research and recommendations for future work.

Chapter 2

Cloning, expression and purification of Class II FBP aldolases

2.1 Introduction

The objective in this chapter was to obtain, for each of the target enzymes, a reliable protein over-expression system and an efficient purification protocol, which would yield a large quantity of pure aldolase at sufficient concentration for characterization and possible structural analysis. Affinity tags were not used for the purification to prevent protein misfolding. We previously reported that several N-terminally-tagged constructs of the *M. tuberculosis* aldolase were misfolded (Ramsaywak *et al.* 2004; Ramsaywak 2003). Affinity tags may also interfere with enzymatic activity, metal binding capacity, or inhibitor binding. The *E. coli* expression vector, pT7-7 (Tabor and Richardson 1985), containing a T7 promoter and an ampicillin resistance gene, was used to express the native Class II FBP aldolases, as we have successfully used this system previously for the *M. tuberculosis* aldolase purification (Ramsaywak *et al.* 2004). For protein expression, a new protocol was developed to obtain higher cell yields using a 2-L working volume bench top fermentor, in collaboration with the laboratory of Dr. Eric Jervis in the Department of Chemical Engineering at the University of Waterloo. A similar protein purification protocol to the one for the *M. tuberculosis* enzyme, was used to purify the recombinant FBP aldolases with some modifications depending on each enzyme's properties. The yields of recombinant enzymes in *E. coli*, as well as the properties of these recombinant enzymes, will be compared with the results obtained by other investigators who purified the Class II FBP aldolase from the natural host in *Mycobacterium tuberculosis* (Bai *et al.* 1982;

Chapter 2 Cloning, expression and purification of Class II FBP aldolases

1974), *Pseudomonas putida* (Bang and Baumann 1978) and *Bacillus cereus* hosts (Sadoff *et al.* 1969).

The work presented in this chapter was performed in collaboration with chemical engineers Jeremy Bezaire and Jason Yaeck from the laboratory of Dr. Jervis (University of Waterloo) for the development of fermentation protocols. The cloning of the aldolases was performed by several undergraduate students under my supervision using oligonucleotides that I designed. The aldolases from *Bacillus cereus*, *Haemophilus influenzae* and *Helicobacter pylori* were cloned by Sarah de Groot; the *Pseudomonas aeruginosa* aldolase was cloned by Gorica Milojevic; and the *Streptococcus pneumoniae* aldolase was cloned by Natasha Kruglyak. In the case of the *Magnaporthe grisea* aldolase, the cloning of the gene including its introns was done by Sarah de Groot, and the introns were later removed using site-directed mutagenesis by Christine How. The purifications of the aldolases from *P. aeruginosa*, *E. coli*, *H. pylori*, and *M. tuberculosis* were also done with much help from Sarah de Groot, who was a 3-time NSERC summer undergraduate student research award (USRA) recipient.

An *E. coli* FBP aldolase overproducing strain was obtained from American Type Culture Collection (ATCC), and the purified *E. coli* enzyme was also generously provided by Dr. Jurgen Sygusch from the University of Montreal.

Part of the work described in this chapter has been published (Labbe *et al.* 2007; Ramsaywak *et al.* 2004).

2.2 Procedures

2.2.1 Cloning of FBP aldolases in vector pT7-7

2.2.1.1 Materials

All buffers and solutions were prepared with deionized Milli Q water (Millipore, Bedford, MA). Restriction enzymes were purchased from Fermentas (Glen Burnie, MD), unless otherwise indicated. Oligonucleotides were synthesized by Sigma-Genosys Canada (Oakville, ON). Purified genomic DNA from pathogenic bacterial strains was obtained from the American Type Culture Collection (ATCC, Manassas, VA), unless otherwise indicated.

2.2.1.2 Bacterial strains

The *E. coli* strain BI21(λ DE3) was obtained from Novagen (Madison, WI). The *E. coli* strain XL1 Blue was obtained from Clontech (Palo Alto, CA). The Subcloning Efficiency DH5 α Competent Cells were obtained from Invitrogen Canada Inc. (Burlington, ON). The *E. coli* FBP aldolase overexpression strain (pKEN-WTFDP8 Phagemid in *E. coli* XL1-Blue) was obtained from ATCC (Manassas, VA), Catalogue No.77472 (Henderson *et al.* 1994).

2.2.1.3 Genomic DNA

The genomic DNA from *P. aeruginosa* PAO1 (FBP aldolase GeneID **880792**) was kindly provided by Dr Stephen Y.K. Seah (University of Guelph, ON). The genomic DNA of other strains were purchased from the American Type Culture Collection (ATCC): *H. pylori* 26695 (FBP aldolase GeneID **900140**) ATCC catalog no 700392D; *B. cereus* ATCC 10987 (GeneID **2748113**), catalog no 10987D; *H. Influenzae* strain Rd KW20 (GeneID **949539**), ATCC catalog no 51907D; *S. pneumoniae* R6 (GenBank Accession No. **AE008341**) ATCC catalog no BAA-255D. The cDNA of *M. grisea* 70-

Chapter 2 Cloning, expression and purification of Class II FBP aldolases

15 containing the gene of Class II FBP aldolase was made available to the public as a result of the *Magnaporthe* Sequencing Project. We obtained the BAC vector containing the aldolase gene (Clone Name 20B24) from the Fungal Genetics Stock Center (School of Biological Sciences, University of Missouri, Kansas City, Missouri, USA). The aldolase has been given the GenBank protein accession no. **XP 369021**.

The construction of the *M. tuberculosis* FBP aldolase expression vector was completed prior to the start of this doctoral project and that work has been published (Ramsaywak *et al.* 2004; Ramsaywak 2003). The gene of Class II FBP aldolase was obtained using a cosmid from the *M. tuberculosis* H₃₇Rv genome library (MTY13E10, GenBank accession no. **Z95324**), which was a gift from Dr. Nadine Honoré (Pasteur Institute, Paris, France).

2.2.1.4 General molecular biology methods

The protocols and recipes described in the manual “Molecular Cloning” (Sambrook *et al.* 1989) were followed. DNA restriction digest was performed at the recommended temperatures and with the appropriate buffers as recommended by the manufacturer. Plasmid vectors used for ligation were dephosphorylated with alkaline phosphatase, and the alkaline phosphatase was heat-inactivated at 65 °C for twenty minutes following the dephosphorylation. DNA ligation reactions were incubated at 10 °C for 72 hours, and then desalted by dialysis against a 10% glycerol sterile solution, using MF-Millipore™ Membrane Filters (Millipore Corporation, Billerica, MA). Plasmid DNA were purified using the FlexiPrep™ kit (Amersham Pharmacia Biotech, Pisataway, NJ) according to the manufacturer’s instructions. The PCR products and DNA fragments were recovered from 1% agarose gels with the QIAquick gel extraction kit (Qiagen, Mississauga, ON). The ligation mixtures were transformed into *E. coli* DH5α competent cells (Invitrogen) or by electroporation into XL1-Blue cells (Clontech).

2.2.1.5 PCR amplification of FBP aldolase genes

FBP aldolase genes were amplified from bacterial genomic DNA using specific primers that also introduce restriction sites at the 5' and 3' ends to facilitate insertion into expression plasmids (Table 2.1). Typical PCR reactions is performed using using the PWO DNA polymerase kit (Roche, Laval, QC) with an initial denaturation of 1 min at 94 °C followed by 35 cycles of denaturation for 1.5 min at 95 °C, annealing for 1.5 min at 65 °C, and elongation for 2-3 min at 72 °C; and a final extension for 15 minutes at 72 °C. The *H. influenzae* aldolase was amplified using an annealing temperature of 45 °C instead of 65 °C. Due to the high GC content of the gene, PCR of the *P. aeruginosa* FBP aldolase gene requires PCR enhancer (Invitrogen, Carlsbad, CA) and a modified PCR amplification protocol. The reaction sequence included 32 cycles as follows: jump start at 85 °C; one cycle of denaturation at 94 °C for 90 seconds, annealing at 72 °C for 2 minutes and 30 seconds and elongation at 72 °C for 4 minutes; then 7 cycles where the annealing temperature decreased by one degree for each cycle (71 °C to 65 °C). In Cycles 9 through 32, the annealing temperature was maintained at 50 °C. The final extension was performed at 72 °C for 15 minutes. The protocol to amplify the *S. pneumoniae* aldolase was also modified. The reaction sequence included 21 cycles as follows: one initial cycle of denaturation at 94 °C for 5 minutes, then 6 cycles where the annealing temperature decreased by two degrees for each cycle (66 °C to 56 °C), consisting of: a denaturation at 94 °C for 30 seconds, annealing for 30 seconds and elongation at 72 °C for 2.5 minutes. This was followed by 15 cycles where the annealing temperature was maintained at at 56 °C: denaturation at 94 °C for 30 seconds, annealing at 56 °C for 30 seconds, and extension at 72 °C for 2.5 minutes. The final extension was done at 70 °C for 5 minutes.

Table 2.1 Primers used to PCR amplify FBP aldolase genes

Organism	Primers*	Introduced restriction sites
<i>P. aeruginosa</i>	PAEFOR: 5'-GGAATTCTGCATAT <u>ATGGCA</u> TCATCAGCATGCGCC-3' PAEREV: 5'-AAACTGCAG <u>CCCGGGTTAG</u> TTGACCTTCGGATCC-3'	<i>NdeI</i> <i>SmaI</i>
<i>H. pylori</i>	HPYFOR 5'-GGAATTCTGCATAT <u>ATG</u> TTAGTTAAAGCAATG-3' HPYLREV3 5'-GCTCGCTCATCCCAATAT <u>TCGAT</u> GTTACACTCTTTCCTTGTTG-3'	<i>EcoRI, NdeI</i> <i>ClaI</i>
<i>B. cereus</i>	BCERFOR1: 5'-TGAGCTCTA AGAAG GAGATATACATAT <u>GCCTTTAG</u> TTTCTA TGAAAGAAATGCTAAACAAAGCAC-3' BCEREV2: 5'-ACTCGGATCCCGGAATTTTATTCT TACG CTTACCGTTAGAA CCG-3'	<i>SacI, NdeI</i> <i>BamHI</i>
<i>M. grisea</i>	MGRISFOR1: 5'-ACGCATACTACCTTTTAAACAGGGCATA <u>ATGGGTGT</u> CTTCAG CGAGCTCGGTCTCAAGC-3' MGRISREV2: 5'-CATCATTACGAGCATCAAT <u>TCGAT</u> AGGTTGCGTGGAATTTA GATGGTG-3'	<i>NdeI</i> <i>ClaI</i>
<i>H. influenzae</i>	HINFOR 5'-GCGGAATTCTGAT <u>GGCTAA</u> ATTATTAGATATTGTGAAACCCGG-3' HINFREV2 5'-AACTATCGA <u>AGCTTGT</u> GGATTATAAAACATCAACACAATTTAA GTCTTCG-3'	<i>EcoRI</i> <i>HindIII</i>
<i>S. pneumoniae</i>	SpnefbaFOR: 5'-CAGGAGCCTGATCATAT <u>GGCA</u> ATCGTTTCAGCAG-3' SpnefbaR2: 5'-TTACTGCAGCTAGATTATGCTTT ACCTT CTGAA CCGAATACG-3'	<i>NdeI</i> <i>PstI</i>

*: The restriction sites are underlined, and the start and stop codons of the amplified genes are shown in bold. The ribosome binding site added to the BCERFOR1 primer is also shown in bold (see details in the text). N.B.: The HPYLREV3 primer binds to the genomic DNA downstream of the *H. pylori* aldolase gene location.

2.2.1.6 Cloning into the expression vectors pT7-7 and pT7-5

To ligate the gene in the *E. coli* expression vector pT7-7 (Tabor and Richardson 1985), both vector and insert were digested and subcloned into the appropriate cloning sites of the pT7-7 vector (see plasmid maps in Appendix A). For most constructs, the *NdeI* site was used at the N-terminus of the

Chapter 2 Cloning, expression and purification of Class II FBP aldolases

protein to obtain a native recombinant enzyme. However, the *NdeI* restriction site of the pT7-7 vector could not be used as the *H. influenzae* gene contains one such site. Some 5 extra amino acids (sequence MARIL) are therefore added at the N-terminus of the protein expressed by the resulting pT7-7/HIFBA plasmid because of the position of the *EcoRI* restriction site in the multiple cloning site of the pT7-7 vector. The 858 bp *fba* gene from *B. cereus* ATCC 10987 also contains a *NdeI* restriction site which prevented the use of the pT7-7 vector for native protein expression, so this gene was instead cloned in the vector pT7-5, NCBI Nucleotide ID=AY230150, (Tabor and Richardson 1985), using the *SacI* and the *BamHI* restriction sites. The ribosome binding site (RBS) missing from the pT7-5 vector was introduced by including the sequence of the RBS present in the pT7-7 vector in the primer used for the gene amplification (Table 2.1).

2.2.1.7 Removal of introns in *M. grisea* FBP aldolase

Three introns in the *M. grisea* FBP aldolase were removed by site-directed mutagenesis using PCR to allow for expression in *E. coli*. The FBP aldolase gene is 1345 bp in size. The gene contains three introns located at the following positions: 131-217 bp, 637-754 bp, and 982-1044 bp, respectively (Figure 2.3). We performed three sequential PCR reactions with different primer sets, verifying the removal of each intron by analytical digests and DNA sequencing after each reaction. PCR was performed using the *Pfu* DNA polymerase kit (Fermentas). The PCR product was used to transform *E. coli* strain DH5 α by heat shock, and then the transformed *E. coli* was grown on LB media containing ampicillin. The first intron (131-217 bp) was removed from the pT7-7/MGFBA3 expression vector using the DelMGI1F primer: 5'-CTCGTCGTCCACCATTATCGCCTCCCTTGA-3' and the DelMGI1R primer: 5'-TCAAGGGAGGCGATAATGGTGGACGACGAG-3'. An *NdeI/SalI* double digestion was used to verify that the first intron had been removed successfully. The second intron (637-754 bp) was removed from pT7-7/MGFBA1 using the DelMGI2F primer:

Chapter 2 Cloning, expression and purification of Class II FBP aldolases

5'-GGTGGTGAGGAGGATGGTGTCAACAACGAG-3' and the DelMG12R primer: 5'-CTCGTTGTTGACACCATCCTCCTCACCACC-3'. A *NdeI/SalI* double digestion was again used to verify that the second intron had been removed successfully. The third intron (982-1044 bp) was removed from pT7-7/MGFBA2 using the DelMG3FF primer: 5'-CGAGGAGAAGAAGCCTATCTTTTTTCGTCTTCCACGGTG -3' and the DelMG3RR primer: 5'-CACCGTGGAAGACGAAAAAGATAGGCTTCTTCTCCTCG-3'. A *NdeI/HindIII* double digestion was used to verify that the third intron had been removed successfully. DNA sequencing was used to confirm that all three introns had been removed successfully in the pT7-7/MGFBA expression vector.

2.2.2 Growth and expression

2.2.2.1 Fermentor growth

For large scale expression, a single colony of *E. coli* B121(λ DE3) transformed with one of the various pT7-7/FBA plasmids was used to inoculate a 1.5 mL culture of Luria-Bertani broth with 100 μ g/mL ampicillin, then grown at 37 °C overnight. This overnight culture was used to inoculate a 60 mL shake flask containing minimal media (Tables 2.2 and 2.3) supplemented with 100 μ g/mL ampicillin. This shake flask was grown for approximately 11 hours before being used to inoculate a 3 L continuous stirred tank reactor (CSTR) with a 1.15 L working volume of minimal media (Tables 2.2 and 2.3).

Table 2.2 Media composition

Media Component	Inoculum (g/L)	Fermentation Culture (g/L)	Feed Solution (g/L)
Na ₂ HPO ₄ (7 H ₂ O)	11.4	14.57	--
KH ₂ PO ₄	3	7.67	--
K ₂ HPO ₄	--	9.43	--
NH ₄ Cl	2	3.86	--
MgSO ₄ (7 H ₂ O)	0.49	0.43	8.10
CaCl ₂	0.01	0.087	0.30
FeSO ₄ (7 H ₂ O)	--	0.12	--
NaCl	1	--	--
Glucose	2	4.35	450.00
Trace metals	--	0.87 ml/L*	--
Ampicillin	0.1	0.1	--
Antifoam	--	--	8 - 16

* See Table 2.3

Table 2.3 Trace metals solution composition

Component	Amount (mg/L)
Citric acid	3840
FeSO ₄ (7H ₂ O)	55.6
ZnSO ₄ (7H ₂ O)	28.7
MnSO ₄ (H ₂ O)	16.9
CuSO ₄ (5 H ₂ O)	2.5
CoCl ₂	2.5
H ₃ BO ₃	6.2

Chapter 2 Cloning, expression and purification of Class II FBP aldolases

Dissolved oxygen, pH, temperature, and substrate feeding were controlled throughout the fermentation. Dissolved oxygen was measured using an AppliSens polarographic probe that was calibrated from 0 to 100% air saturation at 1 atm head-space pressure. Control of dissolved oxygen utilized manual adjustment of the air/O₂ flow rate and proportional-integral algorithm control of the stirrer speed on an ADI 1030 Bio Controller (Applikon Inc., USA). A minimum stir speed of 400 rpm was maintained to ensure a well mixed culture at all times. Air was fed from facility supplied compressed air. Oxygen was fed using compressed oxygen cylinders (Praxair, Kitchener ON). The maximum dissolved oxygen set-point was set to be 30% of air saturation. pH was measured using an AppliSens gel-filled pH sensor and maintained above a minimum value of 6.8 using software controlled additions of 5 N NH₄OH. Temperature was maintained at 37°C using proportional-integral algorithm control from an Applikon ADI 1030 Bio Controller using recirculated cooling water or an electrical heating pad as required. Substrate feed rate control was maintained using custom software developed in the LabView real time control environment (National Instruments, USA). This software allows the user to select from dissolved oxygen-stat, pH-stat, exponential, linear, and constant feeding methods. For this work, fed-batch substrate feeding control was accomplished using a pH-stat algorithm. In this system, the nitrogen source in the media is supplied by the base (NH₄OH) which is also used as the base to increase the pH when it falls below a fixed value (pH 6.8). A modified pH-stat control method induces the substrate feeding by detecting a change in the slope of the pH/time trend. A decrease in culture pH results from the consumption of glucose (here the sole carbon source) and the subsequent production of acetic acid (see glucose degradation pathways in Figure 1.5). A change in slope followed by an increase of the culture pH indicates that the acetic acid is consumed through the glyoxylate shunt and therefore that there is a starvation with respect to the primary carbon source. These instances of increasing pH induce pulsed substrate additions and hence automatically regulate culture feeding. The culture was induced at an OD₆₀₀ between 30 and 100 by

Chapter 2 Cloning, expression and purification of Class II FBP aldolases

adding isopropyl- β -thiogalactoside to a final concentration of 0.5-2.5 mM. At induction 0.2 mM ZnCl₂ was also added to prevent the formation of the inactive Class II FBP aldolase apoenzyme. The induction phase lasted approximately 3.5 hours, after which cells were harvested by centrifugation and stored at -80 °C. Between 55 g and 400 g of cells (wet weight) in ~ 1.5 to 2 L of bacterial culture were obtained for each construct.

2.2.2.2 Shake-flask growth for *E. coli* and *M. tuberculosis* aldolase overexpression

One colony of the *E. coli* BI21(λ DE3) strain transformed with the pKEN-WTFDP8 Phagemid (obtained from ATCC) was used to inoculate 2 flasks of 50 mL of LB broth supplemented with 100 μ g/mL of ampicillin which were incubated at 37 °C, 225 rpm, overnight. Then 6 flasks of 4 L capacity, containing 1 L of TB broth supplemented with 100 μ g/mL of ampicillin, were inoculated with 15 mL of this preculture. The bacteria were grown at 37 °C, 200 rpm for 3.25 hours before induction with 500 μ M IPTG when the cultures reached an OD₆₀₀ of ~1.1 to 1.3. The cells were harvested 3 hours later by centrifugation, frozen on dry ice, and kept at -80 °C.

The *M. tuberculosis* aldolase was overexpressed in shake-flasks by P. Ramsaywak as reported previously (Ramsaywak *et al.* 2004; Ramsaywak 2003). Briefly: a single colony of *E. coli* BI21(λ DE3) transformed with the plasmid pT7-7/MTFBA was used to inoculate a 50 mL culture of Luria-Bertani broth (Difco) with 100 μ g/mL ampicillin, then grown at 37 °C overnight. One litre of the same medium was inoculated with 10 mL of the overnight culture and grown at 37 °C to exponential phase, OD₆₀₀ of 0.6. Isopropyl- β -thiogalactoside was then added to a final concentration of 500 μ M, and 240 μ L of a solution of trace elements (FeSO₄·7H₂O (40 g/L), MnSO₄·H₂O (10 g/L), AlCl₃·6H₂O (10 g/L), CoCl₂·H₂O (4 g/L), ZnSO₄·7H₂O (2 g/L), Na₂MoO₄·2H₂O (10 g/L), CuCl₂·2H₂O (1 g/L), and H₃BO₃ (0.5 g/L)) was also added to each liter of culture. The temperature

was reduced to 18 °C and the cells were further grown for 3 hours. The cells were harvested and stored at -80 °C.

2.2.3 Enzymatic assays

The coupled assay used to monitor the aldol cleavage reaction is a modified version of the procedure described by (Blostein and Rutter 1963). We adapted the coupled assay (Figure 2.1) described for single cuvette monitoring for a more efficient 96-well plate spectrophotometer by adding bovine serum albumin (BSA) to prevent the aldolase and coupling enzymes from sticking to the ELISA 96-well plates. The assay volume, the quantities of NADH, and the amount of coupling enzymes were also optimized for these conditions.

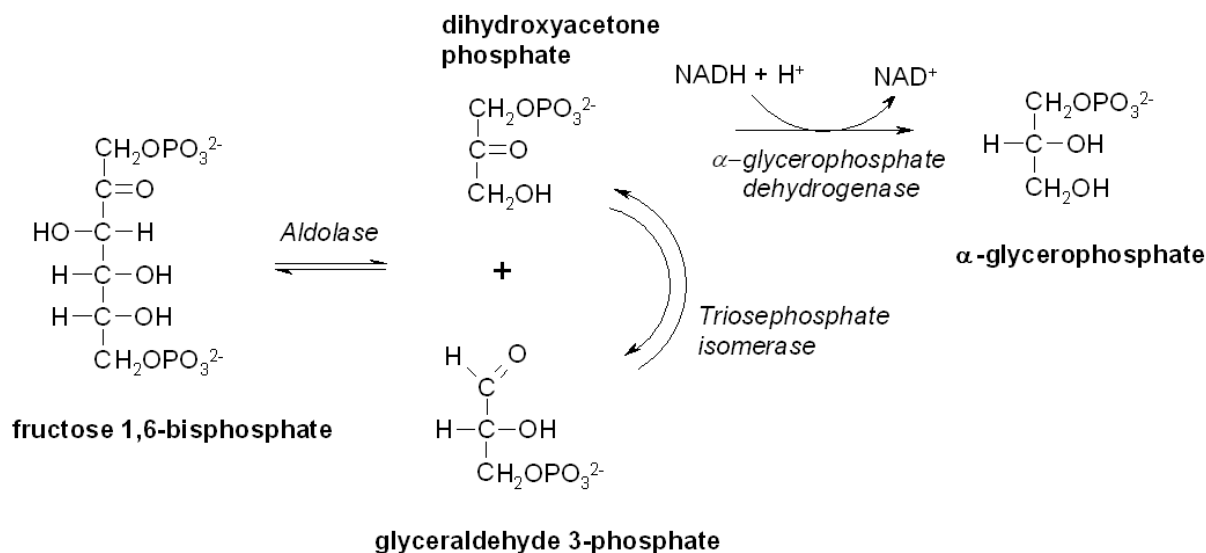


Figure 2.1 Coupled enzymatic assay to monitor FBP cleavage.

The assays were done in 96-well microtiter plates to maximize efficiency. The oxidation of NADH was monitored at a wavelength of 340 nm in a plate reader.

Chapter 2 Cloning, expression and purification of Class II FBP aldolases

The standard assay mixture (final volume 100 μ L) contained the FBP aldolase (0.003 to 0.020 U/mL), 0.3 mM NADH, 0.2 U/mL of rabbit muscle α -glycerophosphate dehydrogenase, 2.25 U/mL of rabbit muscle triose phosphate isomerase, 0.2 mg/mL BSA, 100 mM potassium acetate and 50 mM TRIS-HCl, pH 8. For the pH optimum determination, a 50 mM glycylglycine buffer was used instead of TRIS-HCl. Assays were performed at 30 $^{\circ}$ C in quadruplicate in 96-well flat bottom polystyrene plates (Corning, NY). The reaction was initiated by the addition of FBP (final concentration 4-3000 μ M) and monitored at 340 nm for 10 minutes on a 96-well plate reader (Spectramax 190, Molecular Devices, Sunnyvale, CA). Better results were obtained when the assay solutions were pre-warmed in the 96-well plate at the assay temperature (\sim 10 minutes) prior to mixing with the substrate. The molar extinction coefficient for NADH was determined with a standard curve in which the absorbance at 340 nm was plotted against NADH concentrations ranging from 0 to 350 μ M. The slope of the standard curve (0.00155 absorbance units per μ M) was used to calculate the activity of the Class II FBP aldolase in the following equation:

Equation 2.1: v (in U) = v (milliOD/min) * 1/1000 (OD unit/milliOD units) \div 2 (mol of NADH oxidized per mol of FBP cleaved) \div -0.00155 OD/ μ M (slope of NADH standard curve) * 0.0001 L (assay volume)

One unit (U) of aldolase activity is defined as 1 μ mol of FBP cleaved per min at 30 $^{\circ}$ C, unless indicated otherwise (some early assays were performed in 50 mM Hepes pH 7.3 at 28 $^{\circ}$ C). Kinetic parameters were estimated by fitting the data to the Michaelis-Menten equation using the least squares and dynamic weighting options of the Leonora software program (Cornish-Bowden 1995).

2.2.4 Protein quantification

Protein concentration was determined by the dye binding method of Bradford (Bradford 1976) using BSA as a reference standard.

2.2.5 SDS-PAGE

The purity of the preparations were estimated by SDS-PAGE on 12%-polyacrylamide gels according to the method of Laemmli (Laemmli 1970). All gels were stained with Coomassie Blue.

2.2.6 Purification

2.2.6.1 Crude extract preparation

M. grisea aldolase

The temperature was maintained at 4 °C throughout the purification. A portion of the harvested cells (55 grams of the fermentor-grown cells) were resuspended by adding buffer A (50 mM Tris-HCl buffer pH 7.5, 1 mM β -mercaptoethanol, 50 mM NaCl) containing 0.1 mg/mL DNaseI and 0.55 mg/mL lysozyme to obtain a total volume of around twice the pelleted cells initial volume (2x55=110 mLs). The cells were then lysed using a homogenizer and the lysate was centrifuged at 48,000 g for 25 minutes. To remove nucleic acids, 2 grams of protamine sulphate was added to the supernatant and the solution was stirred for 45 minutes. The crude cell extract was then centrifuged at 48,000 g for 25 minutes and the precipitate discarded.

M. tuberculosis aldolase

Fermentor-grown cells: Modifications to the protocol used for *M. grisea* aldolase: 41 grams of fermentor-grown cells were resuspended, and the Buffer A was composed of 50 mM sodium

Chapter 2 Cloning, expression and purification of Class II FBP aldolases

phosphate pH 7.0, 100 mM NaCl, with DNase and lysozyme added as described above. The cells were ruptured using a French Press (40 mL cell volume) from Carver (Wabash, IN).

Shake-flask grown cells: Modifications to the protocol used for *M. grisea* aldolase: 2.16 grams of cells were resuspended in 40 mL of buffer A (50 mM phosphate buffer pH 7.0, 1 mM β -mercaptoethanol, 0.1 M NaCl) containing 0.1 mg/mL DNaseI. The cells were lysed using a homogenizer. To remove the nucleic acids, 2% (w/v) protamine sulphate was added to the supernatant (0.1 mg of protamine sulfate per mg of protein).

P. aeruginosa aldolase

Modifications to the protocol used for *M. grisea* aldolase: 105 grams of fermentor-grown cells were resuspended, and the buffer A was composed of 50 mM sodium phosphate pH 7.0, 100 mM NaCl, 0.3 mM ZnCl₂, 1 mM β -mercaptoethanol, with 0.6 mg/ml lysozyme and 25 μ g/ml DNase added. 3.5 grams of protamine sulfate were used to precipitate nucleic acids.

B. cereus aldolase

Modifications to the protocol used for *M. grisea* aldolase: 103 grams of fermentor-grown cells were resuspended, and the Buffer A was composed of 50 mM sodium phosphate pH 7.0, 100 mM NaCl, 1 mM β -mercaptoethanol, with 0.1 mg/mL DNase and 0.55 mg/mL lysozyme added. 3.7 grams of protamine sulfate were used to precipitate nucleic acids.

H. pylori aldolase

Modifications to the protocol used for *M. grisea* aldolase: 32 grams of fermentor-grown cells were resuspended, and the Buffer A was composed of 20 mM Tris-HCl buffer pH 8.0, 100 mM NaCl, 1 mM β -mercaptoethanol, with 0.1 mg/mL DNase and 0.55 mg/mL lysozyme added. The cells were ruptured using a French Press (40 mL cell volume) from Carver (Wabash, IN).

Chapter 2 Cloning, expression and purification of Class II FBP aldolases

E. coli aldolase

Modifications to the protocol used for *M. grisea* aldolase: 47 grams of shake-flask grown cells were resuspended. Buffer A consisted of 50 mM Tris-HCl pH 8.0, 100 mM NaCl, 0.3 mM ZnCl₂, 1 mM β-mercaptoethanol, with 0.6 mg/mL lysozyme and 50 μg/mL DNase added. The cells were ruptured with a French Press (40 mL cell capacity) from Carver (Wabash, IN).

2.2.6.2 Ammonium sulfate fractionation

M. grisea aldolase

Solid ammonium sulfate was added to the supernatant to 40% saturation, and the solution stirred for an additional 40 minutes. The extract was then centrifuged at 48,000 g for 25 minutes and the pellet discarded. The supernatant was then brought to 80% saturation with ammonium sulfate, stirred for 1 hour and centrifuged following the same procedure. Following this extraction, the supernatant was discarded and the precipitate containing the enzyme was resuspended in buffer A. The solution was dialysed against buffer B (25 mM TRIS-HCl pH 7.5, 25 mM NaCl, 0.3 mM ZnCl₂, 1 mM β-mercaptoethanol) using a Spectra/Por 1 Membrane with a molecular weight cut-off of 6-8 kDa from Spectrum Laboratories, Inc (Rancho Dominguez, CA).

M. tuberculosis aldolase

Fermentor-grown cells: Modifications to the protocol used for the *M. grisea* aldolase: the buffer B was composed of 50 mM sodium phosphate pH 7.0, 100 mM NaCl.

Shake-flask grown cells: Modifications to the protocol used for the *M. grisea* aldolase: the ammonium sulfate cuts were 43.5% and 83.5%. The supernatant was discarded and the precipitate containing the enzyme was resuspended in 2.5 mL of buffer A (50 mM phosphate buffer pH 7.0,

Chapter 2 Cloning, expression and purification of Class II FBP aldolases

1 mM β -mercaptoethanol, 0.1 M NaCl). The excess salt was then removed from the sample using a PD-10 desalting column (Amersham Pharmacia Biotech) equilibrated with buffer A. The fractions containing the protein (total 4 mL) were pooled, flash-frozen in liquid nitrogen and stored at $-80\text{ }^{\circ}\text{C}$ overnight.

P. aeruginosa aldolase

Modifications to the protocol used for the *M. grisea* aldolase: the buffer B was composed of 50 mM sodium phosphate pH 7.0, 100 mM NaCl, 0.3 mM ZnCl_2 , 1 mM β -mercaptoethanol. The ammonium sulfate cuts were 40% and 60%, and the pellet from the 60% cut was resuspended in buffer B and dialyzed in the same buffer for chromatography.

B. cereus aldolase

Modifications to the protocol used for the *M. grisea* aldolase: the buffer B was composed of 50 mM sodium phosphate pH 7.0, 100 mM NaCl, 1 mM β -mercaptoethanol. The ammonium sulfate cuts were 40% and 60%, and the supernatant from the 60% cut was dialyzed against buffer B and concentrated with an Amicon fitted with a 10 kDa cut-off membrane for chromatography.

H. pylori aldolase

Modifications to the protocol used for the *M. grisea* aldolase: the buffer B was composed of 20 mM Tris-HCl buffer pH 8.0, 100 mM NaCl, 1 mM β -mercaptoethanol. The ammonium sulfate cuts were 40% and 60%, and the pellet from the 60% cut was dialyzed against buffer B and concentrated with an Amicon fitted with a 10 kDa cut-off membrane for chromatography.

Chapter 2 Cloning, expression and purification of Class II FBP aldolases

E. coli aldolase

Modifications to the protocol used for the *M. grisea* aldolase: the buffer B was composed of 50 mM Tris-HCl pH 8.0, 100 mM NaCl, 0.3 mM ZnCl₂, 1 mM β-mercaptoethanol. The ammonium sulfate cuts were 45% and 80%. After the 80% ammonium sulfate cut, the pellets were resuspended in buffer C: 100 mM Tris-HCl pH 7.5, 3 mM ZnCl₂. The protein was dialyzed against buffer C before chromatography.

2.2.6.3 Chromatography

M. grisea aldolase

The dialysed protein solution was centrifuged at 48,000 g for 25 minutes and the pellet was discarded. The protein sample was applied to a thermo-jacketed column (50 mm x 5 cm) containing 100 mL of DEAE Sepharose CL-6B resin (Amersham Pharmacia Biotech) equilibrated with buffer B and mounted on an ÄKTA Purifier HPLC system (GE Healthcare Bio-Sciences, Baie d'Urfé, QC, Canada). The aldolase was washed with 7 CV of buffer B at 1 mL/min, and eluted with a gradient of 25 mM to 500 mM NaCl over 10 CV at a flow rate of 3 mL/min. The fractions containing aldolase activity were pooled, and loaded in 3 mLs aliquots on a ResourceQ 6 mLs column also mounted on the ÄKTA Purifier. The enzyme was washed with 2 CV of Buffer C (25 mM TRIS-HCl pH 7.5, 25 mM NaCl), and eluted with a salt gradient of 25 mM to 500 mM NaCl over 10 CV at a flow rate of 5 mLs/min. The fractions containing activity were pooled and the purity of the preparation was estimated by SDS-PAGE on 12%-polyacrylamide gels. The purest fractions were either flash-frozen in liquid nitrogen in 50 µl aliquots and kept at -80 °C, or supplemented with glycerol to a final concentration of 50% and kept at -20 °C (both methods used for kinetic assays), or dialysed against a 85% saturated ammonium sulphate solution supplemented with 250 µM ZnCl₂ and kept at 4 °C (used for crystallographic trials).

Chapter 2 Cloning, expression and purification of Class II FBP aldolases

M. tuberculosis FBP aldolase

From fermentor-grown cells: The dialyzed enzyme was diluted with 50 mM sodium phosphate buffer pH 7.0 to bring NaCl concentration in the sample down to 90 mM before loading on the DEAE column (45 mLs of resin). The protein was extensively washed at 5 mL/min using 50 mM sodium phosphate buffer pH 7.0, 90 mM NaCl, until the OD₂₈₀ of the eluate was below 0.1 units. The gradient used for the elution was from 90 mM NaCl to 500 mM NaCl over 20 CV (in 50 mM sodium phosphate buffer pH 7), at 5 mL/min. Following this column, the purification was continued using a Bio-Scale CHT10 hydroxyapatite column (10 mm x 88 mm, 10 mL bed volume) from Bio-Rad (Mississauga, ON). The protein eluted from the DEAE column was thus pooled, concentrated with the Amicon apparatus (10 kDa cut-off membrane), dialyzed in 10 mM sodium phosphate buffer pH 6.8 using a Spectra/Por 1 Membrane with a molecular weight cut-off of 6-8 kDa from Spectrum Laboratories, Inc (Rancho Dominguez, CA). The dialyzed protein was loaded at 2 mL/min on the CHT10 column preequilibrated with buffer C (10 mM sodium phosphate buffer pH 7.2). The protein was washed with buffer C and then eluted using a gradient 0% to 20% buffer D (500 mM sodium phosphate buffer pH 7) over 12 column volumes at 5 mL/min. The fractions were then pooled, dialyzed in Buffer E (50 mM Tris-HCl pH 8.0, 200 mM NaCl) and concentrated to 0.75 mL before injection on a gel filtration column. The gel filtration was done on a thermo jacketed Sephacryl S-300 High resolution column 95 cm x 16 mm (Pharmacia, Uppola, Sweden; now operated under GE Healthcare). The protein was eluted with Buffer E at 1 mL/min at 4 °C, the active fractions were pooled and concentrated using an Amicon (Beverly, MA) with a 10 kDa cut-off membrane. The enzyme was then dialyzed against a 3.33 M ammonium sulfate solution in a Spectra/Por 1 Membrane (see above), and stored at 4 °C.

From shake-flask grown cells: The desalted protein solution was thawed, filtered through a 0.20 µm membrane and diluted to a volume of 5 mL with buffer A (50 mM phosphate buffer pH 7.0,

Chapter 2 Cloning, expression and purification of Class II FBP aldolases

1 mM β -mercaptoethanol, 0.1 M NaCl). The protein sample was applied to a thermo-jacketed column (16mm x 10cm) containing 20 mL of DEAE Sepharose CL-6B resin (Amersham Pharmacia Biotech) equilibrated with buffer A and mounted on a BioCad™ Sprint Perfusion Chromatography system (PerSeptive Biosystem). The protein was washed with 40 mL of buffer A and eluted by a linear salt gradient (0.1-0.5 M NaCl) over 4 column volumes at a flow rate of 1 mL/min. The peak fractions containing FBP aldolase activity were pooled and concentrated. The concentrated protein (2 mL) was injected onto a thermo-jacketed column (16 mm x 83 cm) containing 160 mL of Sephacryl S-200 superfine media (Amersham Pharmacia Biotech) equilibrated with buffer B (50 mM TRIS-HCl buffer pH 7.8, 200 mM NaCl, 200 μ M ZnCl₂ and 1 mM β -mercaptoethanol) and mounted on the BioCad™ system as described above. The protein was eluted with one column volume of buffer B at a flow rate of 1 mL/min and 2 mL fractions were collected. The appropriate fractions were pooled and concentrated prior to storage at 4 °C.

P. aeruginosa aldolase

The thermo-jacketed column containing 42 mLs of DEAE Sepharose CL-6B resin (Amersham Pharmacia Biotech) was pre-equilibrated with buffer B (50 mM sodium phosphate pH 7.0, 100 mM NaCl, 0.3 mM ZnCl₂, 1 mM β -mercaptoethanol), and the sample was loaded at 3 mL/min. The column was washed with 20 CV of buffer B at 1 mL/min, and then with 8 CV of the same buffer at 3 mL/min (until the OD₂₈₀ of the eluate was ~ 0.11 units). The protein was eluted with a gradient of 100 mM to 500 mM NaCl over 6 CV at 3 mL/min. The fractions containing the enzyme were pooled, dialyzed against buffer C (25 mM Tris-HCl pH 8, 100 mM NaCl, 0.3 mM ZnCl₂, 1 mM β -mercaptoethanol) and loaded on a Q Sepharose Fast Flow (Pharmacia, Uppola, Sweden; now operated under GE Healthcare) thermo-jacketed column containing 45 mLs of resin. The enzyme was eluted with a gradient from 100 mM to 500 mM NaCl in buffer D (25 mM Tris-HCl pH 8, 100 mM

Chapter 2 Cloning, expression and purification of Class II FBP aldolases

NaCl, 1 mM β -mercaptoethanol), at 3 mL/min. The fractions were pooled, dialyzed in an 80% saturated ammonium sulfate solution, in a Spectra/Por 1 Membrane (see above), and stored at 4 °C.

B. cereus aldolase

The enzyme was injected on a 160 mm x 20 mm thermo-jacketed column containing 50 mLs of DEAE Sepharose CL-6B resin (Amersham Pharmacia Biotech) equilibrated with buffer B (50 mM sodium phosphate pH 7.0, 100 mM NaCl, 1 mM β -mercaptoethanol) at a rate of 3 mL/min. The column was washed with buffer B and with a salt concentration increase at 120 mM NaCl until the OD₂₈₀ of the eluate was lowered to ~ 0.14 units. The protein was then eluted with a gradient from 120 mM to 500 mM NaCl over 6 CV, at a rate of 3 mL/min. The fractions were either flash-frozen in liquid nitrogen and kept at -80°C, or pooled, concentrated by filtration using Centriprep YM10 (Millipore, Billerica, MA), and dialyzed in an 80% saturated ammonium sulfate solution, in a Spectra/Por 1 Membrane (see above), and stored at 4 °C.

H. pylori aldolase

The enzyme was injected on a 160 mm x 20 mm thermo-jacketed column containing 50 mLs of DEAE Sepharose CL-6B resin (Amersham Pharmacia Biotech) preequilibrated with buffer B (20 mM Tris-HCl buffer pH 8.0, 100 mM NaCl, 1 mM β -mercaptoethanol), and the enzyme was washed off the column with buffer B in an absorbance peak immediately following that of the unbound sample. The fractions from this peak were pooled, supplemented with 0.1 mM CoCl₂ and dialyzed against a 3.9 M ammonium sulfate, pH 7.0, 0.1 mM CoCl₂ solution, and stored at 4 °C.

E. coli aldolase

The protein was injected on a Q Sepharose Fast Flow (Pharmacia, Uppola, Sweden; now operated under GE Healthcare) thermo-jacketed column containing 150 mL of resin, preequilibrated with buffer C (100 mM Tris-HCl pH 7.5, 3 mM ZnCl₂). The column was washed with buffer C for ~5 CV at a

Chapter 2 Cloning, expression and purification of Class II FBP aldolases

flow rate up to 2.5 mL/min. The protein was then eluted with a KCl gradient (0 to 1M KCl over 11.7 CV) at a flow rate of 2.5 mL/min. At this point the eluted enzyme was pooled and dialyzed against a 3.9 M ammonium sulfate solution at 4°C for storage. A portion of the pooled enzyme was later dialyzed against buffer D (50 mM Tris-HCl pH 7.0, 100 mM NaCl, 0.3 mM ZnCl₂) and then the salt concentration was diluted by half with the addition of buffer E (50 mM Tris-HCl pH 8.0). The protein was loaded on a ResourceQ 6 mLs column preequilibrated with buffer E. The enzyme was eluted with a gradient from 0% to 100% buffer F (50 mM Tris-HCl pH 7.0, 500 mM NaCl, 0.3 mM ZnCl₂) over 20 CV. The purest fractions (in buffer containing approximately 0.1 mM ZnCl₂) were pooled, flash-frozen in liquid nitrogen in small aliquots, and kept at -80 °C.

2.2.7 ESI mass spectrometry

The molecular mass of the Class II FBP aldolase monomers were determined by mass spectrometry at the WATSPEC Mass Spectrometry Facility at the University of Waterloo. Measurements were performed in positive ion mode on a Micromass Q-TOF Ultima™ Global mass spectrometer (Micromass) equipped with a Z-spray electrospray ionization source. Prior to ESI-MS analysis, a ~100 µL sample of each protein was dialyzed against milliQ water overnight (see in-house technique using a 1.5 mL plastic centrifuge tube in Figure 2.2) and brought to a concentration of 10 µM using a Microcon centrifugal YM-10 filter concentrator (Millipore). Proteins were denatured by 10-fold dilution in water/acetonitrile (50:50 [v/v] with 0.1% formic acid) before introduction into the ESI source with the aid of a syringe pump.

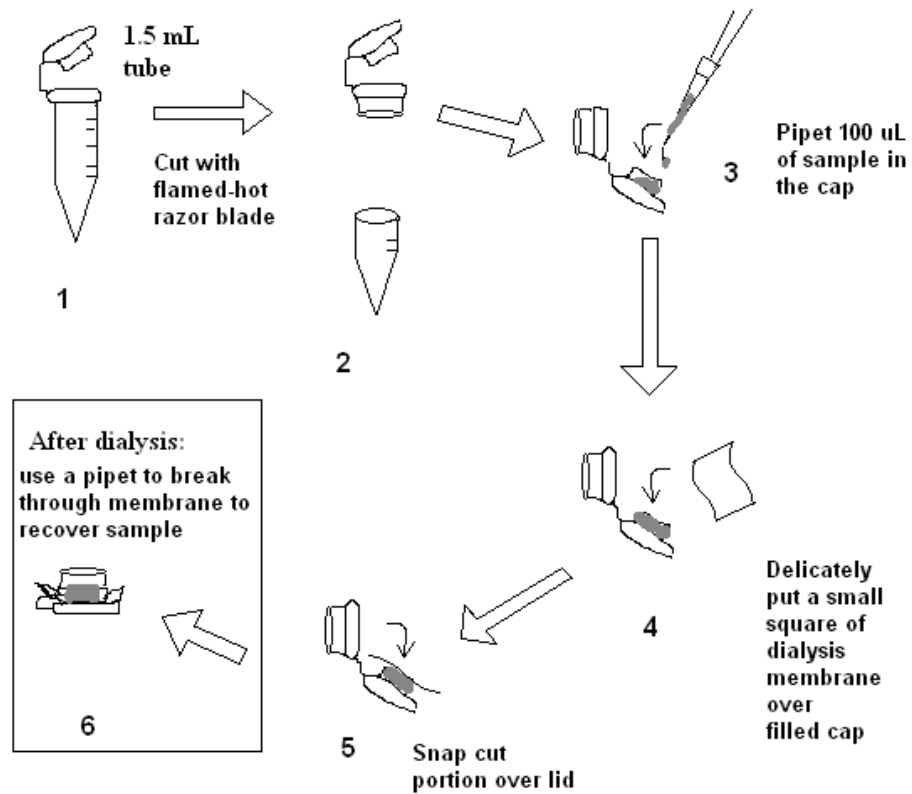


Figure 2.2 In-house technique for dialysis of a small volume of protein solution

2.3 Results

2.3.1 Cloning

In this study, the Class II aldolase genes from *B. cereus*, *H. influenzae*, *S. pneumoniae*, *M. grisea*, *H. pylori*, and *P. aeruginosa* were amplified from the organisms' genomic DNA and ligated into the expression vector pT7-7 (Tabor and Richardson 1985). The clones were verified by analytical restriction digestions and by sequencing to ensure there were no mutations present in the aldolase gene portion of the resulting expression vectors.

Chapter 2 Cloning, expression and purification of Class II FBP aldolases

The sequence of the FBP aldolase gene of *M. grisea* was identified and made publicly available as a result of the *M. grisea* genome sequencing project. The 1805 bp sequence, identified as a probable Class II FBP aldolase gene (also identified as hypothetical protein MG00223.4 in the Broad Institute website), constitutes of five exons (respectively 54, 131, 421, 229, and 302 bp) separated by four introns (406, 85, 116, and 61 bp). After sequence alignment analysis with other Class II FBP aldolases (Figure 1.17), and considering the ESTs overlapping the putative aldolase gene (made available online through the Program for the Biology of Filamentous Fungi supported by the Texas A&M University), we determined that the first putative exon containing the first 18 amino acids of the GenBank sequence was not part of the *fba* gene and so it was not included in our final construct. The last 1344 bp of the putative aldolase gene was cloned in the *E. coli* expression vector pT7-7, and the three introns present in the sequence were looped out by site-directed mutagenesis (Figure 2.3). The final construct pT7-7/MGFBA therefore expresses the native enzyme in *E. coli*, and the final gene sequence was also verified by sequencing.

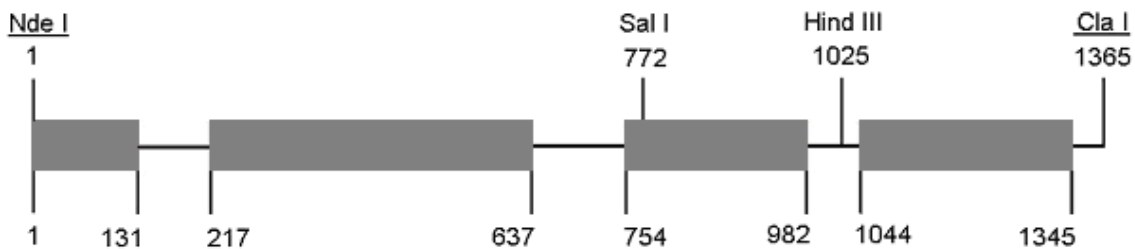


Figure 2.3 Structure of the *M. grisea* aldolase gene

The 4 exons are indicated by solid rectangles, and the non-coding sequences by a line. The restriction sites locations are indicated above the gene.

The *B. cereus* and *H. influenzae* aldolase genes contain *Nde*I restriction sites and therefore the genes cannot be easily inserted into the *Nde*I site of pT7-7. The *B. cereus* aldolase gene was cloned

Chapter 2 Cloning, expression and purification of Class II FBP aldolases in the plasmid pT7-5, with a primer (Table 2.1) that included the missing RBS site from this plasmid to make it equivalent to the vector pT7-7 (see resulting plasmid sequence in the Appendix A). The *H. influenzae* aldolase gene was cloned further in the multiple cloning site of the vector pT7-7 (in the *EcoRI* restriction site), such that the recombinant enzyme would be expressed with 5 additional amino acids at the N-terminus. The *H. influenzae* aldolase was however not yet purified, so only the cloning and small-scale expression tests for this enzyme are reported in this thesis.

2.3.2 Growth and expression

We chose to express the enzyme without affinity tags to avoid possible interference with the folding of the enzyme as previously mentioned. However, purification of native enzymes is often less efficient than that of tagged enzymes. To compensate for potential lower purification efficiencies, we decided to use a high cell density fermentation to increase product yield and then optimize purification procedures for litre volumes of concentrated crude cell extract. A 3 L bench-top fermentor with a 2 L working volume was used for expression of the recombinant aldolases in this study. Table 2.3 shows the yields of cells obtained in the fermentor, which are all above 55 g. This yield is at least 10-fold higher than in a typical batch culture of the same volume (see amount of cells obtained per volume in Figure 2.4).

A chart showing the culture growth and glucose feeding over time for a typical fermentation is presented in Figure 2.5. Fed-batch feeding was initiated automatically following 8 hours of batch culture, with subsequent feeding on demand using a pH-stat control strategy (Bezaire et al. *manuscript submitted*) (Figure 2.6). The cultures grown under these conditions have reached a maximum optical density of 268 (OD₆₀₀) and can routinely reach optical densities about 200 (OD₆₀₀).

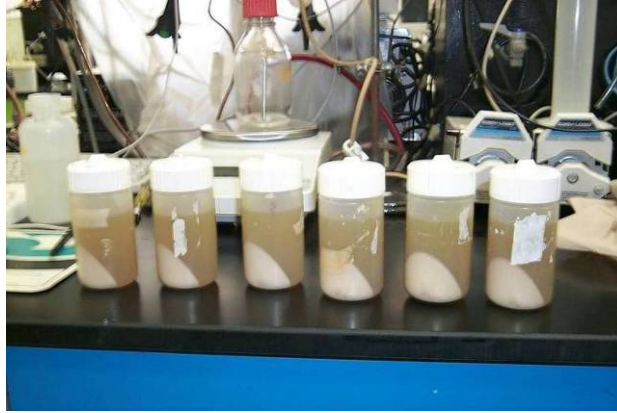


Figure 2.4 Harvested *E. coli* BI21(λ DE3) cells from 1.5 L fermentor culture

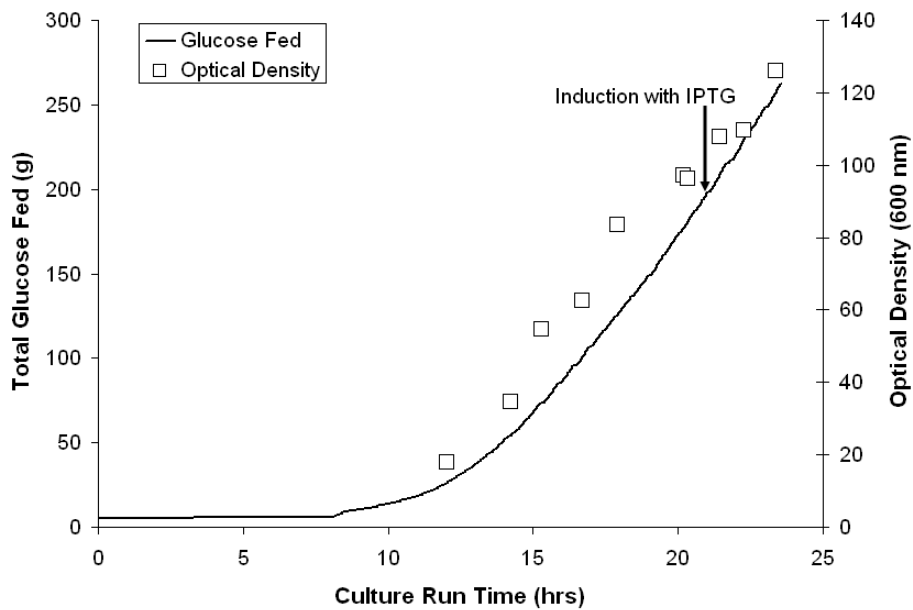


Figure 2.5 Culture growth and substrate feeding profiles

The amount of glucose added to the culture is indicated by a solid line, and the optical density of the culture measured from withdrawn aliquots is indicated by squares. The time of induction of recombinant protein expression by IPTG is indicated by an arrow.

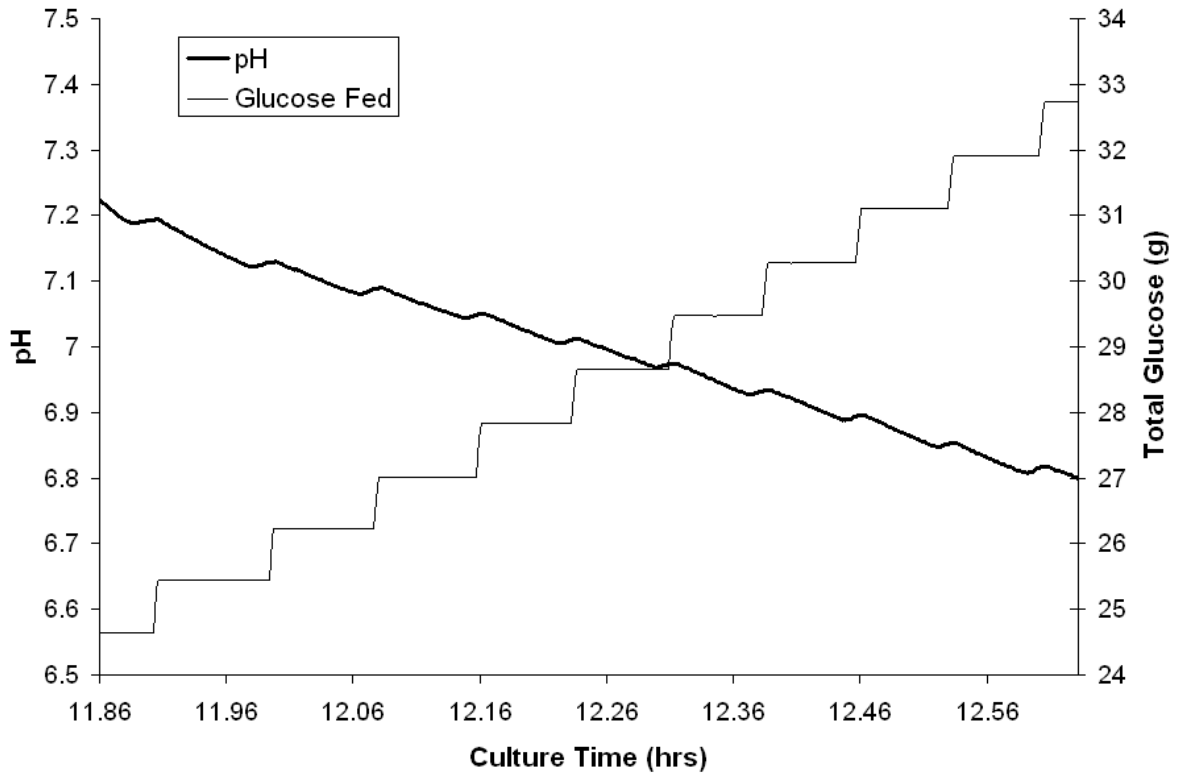


Figure 2.6 pH stat feeding control

The pH-stat control was able to induce automatic substrate feeding by detecting a change in slope in the pH trend that results from a switch between acetic acid production and consumption.

Expression of FBP aldolases grown in fermentor or by fed batch was compared. The overexpression of the aldolases in the growing cells was verified by SDS-PAGE (Figures 2.7-2.9). It was observed that the aldolase expression was not as high in fermentor-grown cells compared to shake-flask grown cells when the induction was done using 0.5 mM IPTG (see Figures 2.7 and 2.8). However, better results were obtained in high-density fermentor cultures when 2.5 mM IPTG was used for the recombinant protein induction (Figure 2.9).

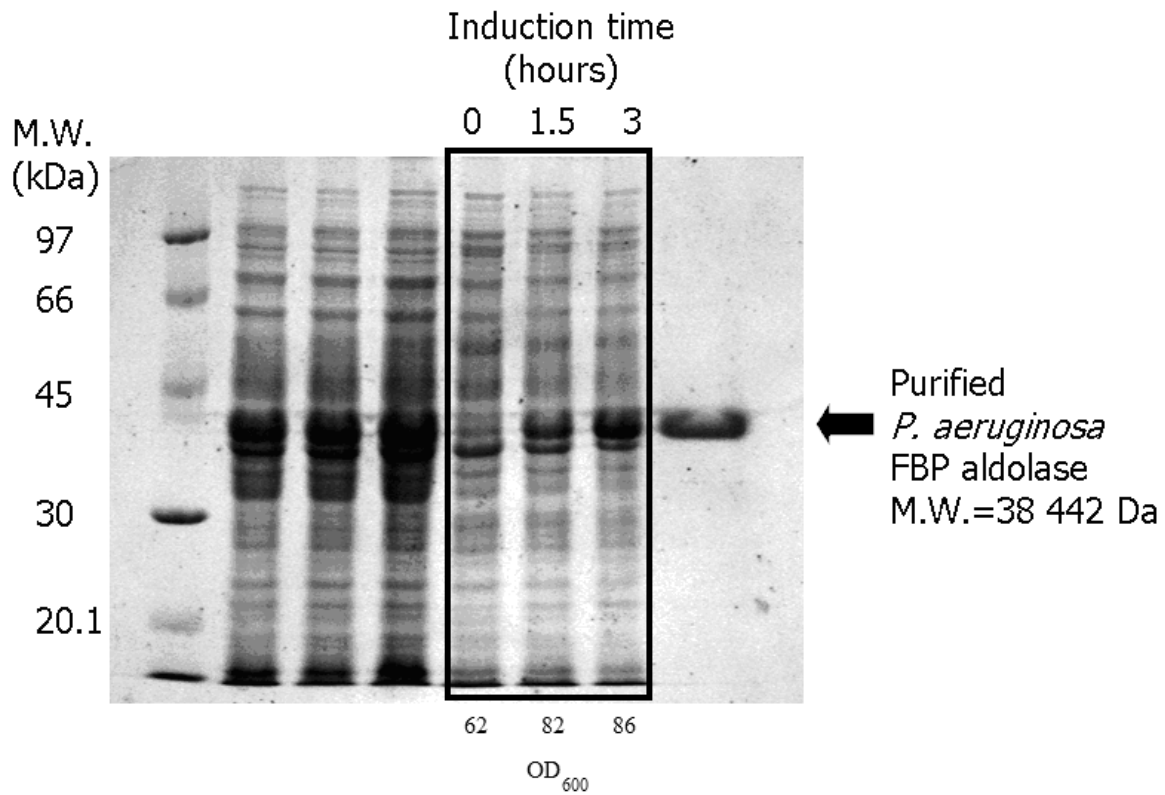


Figure 2.7 Fermentor expression of *P. aeruginosa* FBP aldolase in *E. coli* BI21(λDE3)

The first lane shows the molecular weight markers, and the lanes 2-4 show induced 1.5 mL cultures. The fermentor samples are in the box and the optical density is indicated under each lane. The last lane contains 5 µg of purified enzyme. The gel was stained with Coomassie Blue.

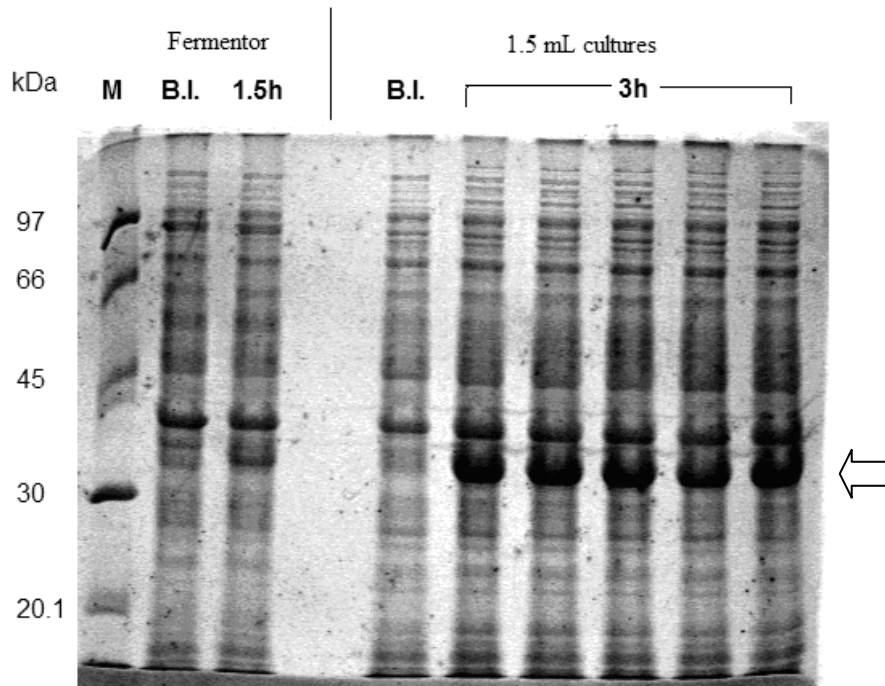


Figure 2.8 Expression of *B. cereus* aldolase in fermentor culture and 1.5 mL cultures

The induction times are indicated above the gel, and “B.I.” stands for “before induction”. The arrow on the right indicates the position of the overexpressed aldolase (M.W.: 30.7 kDa). The gel was stained with Coomassie Blue.

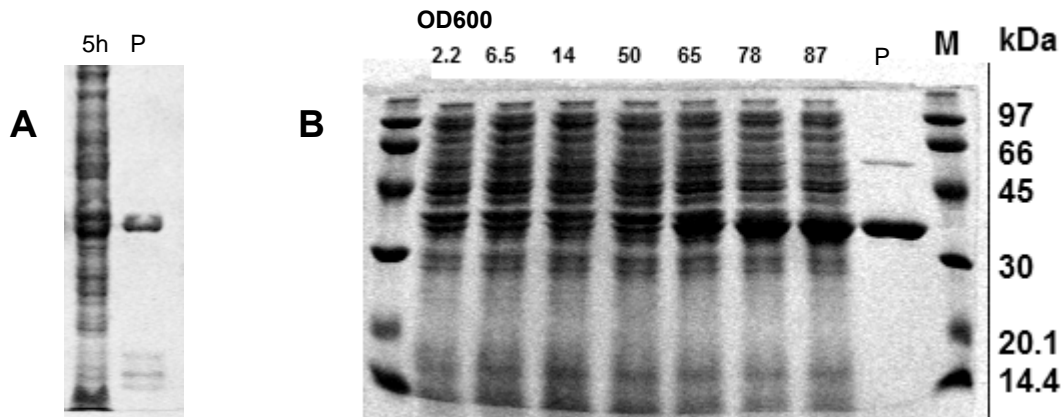


Figure 2.9 Expression of the *M. tuberculosis* aldolase in the fermentor

A) The culture was induced with 0.5 mM IPTG when the OD₆₀₀ reached 65, and was harvested 5 hours later (cell lysate shown in first lane). B) The culture was induced with 2.5 mM IPTG when the OD₆₀₀ reached 50 (5th lane), and was harvested 3 hours later (8th lane, at OD₆₀₀=87). The purified *M. tuberculosis* enzyme (1 μg for gel A and 2 μg for gel B) are shown in lanes P of the gels (M.W.: 36,413 Da). The gels were stained with Coomassie Blue.

Table 2.4 Cell weight obtained for fermentor and shake-flask bacterial cultures after recombinant aldolase expression

The *E. coli* cells weight is shown for the overexpression of the aldolases from *M. tuberculosis* (MTFBA); *P. aeruginosa* (PAFBA); *B. cereus* (BCFBA); *M. grisea* (MGFBA); *H. pylori* (HPFBA); and *E. coli* (ECFBA).

Construct	Fermentor culture <i>OD</i> ₆₀₀ at induction time	Fermentor yield grams of cells in ~2L, wet weight	Shake-flask yield g/L, wet weight (growth medium)
pT7-7/MTFBA	55	154	2.2 to 2.6 (LB)*
	65	160	
	50	151	
pT7-7/PAFBA	62	208	~5 (TB)
	71	190	
pT7-7/BCFBA	75	412	
pT7-7/MGFBA	30	75	
	96	275	
pT7-7/HPFBA	N/A	189	
pT7-7/ECFBA			~8 (TB)

*Cells grown in shake-flasks by P. Ramsaywak (Ramsaywak 2003)

The aldolases from *S. pneumoniae* and *H. influenzae* were only expressed in small scale cultures and have not been purified yet. The expression of the *H. influenzae* recombinant aldolase can be seen in Figure 2.10.

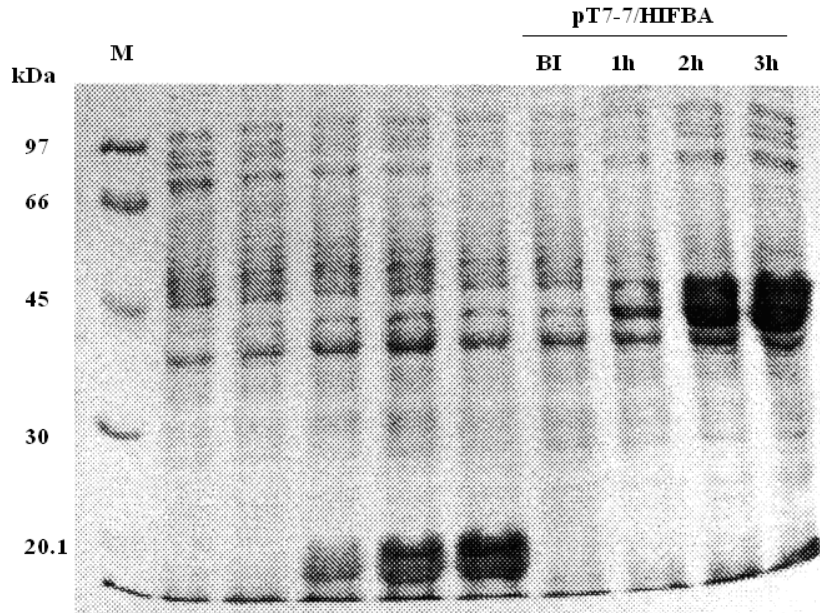


Figure 2.10 Small-scale expression of the *H. influenzae* FBP aldolase

The molecular weight markers are shown in the first lane. The last four lanes show the cultures of *E. coli* BI21(λ DE3) transformed with the plasmid pT7-7/HIFBA before induction (B.I.) and after 1, 2, and 3 hours of induction with 0.5 mM IPTG, respectively. The gel was stained with Coomassie Blue.

2.3.3 Purification

Purification of the different FBP aldolases involved the use of ammonium sulfate fractionation and anion exchange chromatography. To achieve higher than 95% purity, most of the aldolases require additional chromatographic steps that may include hydroxyapatite or gel filtration chromatography. The purification tables for each of the aldolases are shown in Tables 2.5 to 2.12. SDS-PAGE gels of the purified proteins are shown in Figures 2.15 and 2.16. It is noteworthy that between 200 mg and 300 mg of pure *P. aeruginosa*, *M. grisea*, and *B. cereus* aldolases were obtained from 55 g to 100 g (wet weight) of recombinant *E. coli* cells, after ammonium sulfate fractionation and anion-exchange chromatography.

Chapter 2 Cloning, expression and purification of Class II FBP aldolases

2.3.3.1 M. tuberculosis aldolase

The purification procedure for the *M. tuberculosis* enzyme produced by fermentor-grown cells was different than the one published previously (results shown in Figure 2.11 and Table 2.5) (Ramsaywak *et al.* 2004) in part because the expression level of the enzyme in the fermentor was lower than in the cells grown using batch culture. The results of the purification from fermentor-grown cells are shown in Figure 2.12 and Table 2.6. A similar enzyme purity of >95% was achieved, with a enzyme specific activity over 30 U/mg, but an additional chromatographic step was required and thus the yield went down from 14% (shake-flask grown cells) to 2.7% (fermentor-grown cells). When higher IPTG concentration used to induce expression in the fermentor grown cells, we could achieve an apparent 90% purity and a specific activity of 21 U/mg using one less chromatography step, with a 9% yield (Figure 2.13 and Table 2.7). The purified *M. tuberculosis* Class II FBP aldolase is very stable, as it was still fully active in elution buffer after 4 months at 4 °C, and retained all its activity after two weeks in a metal-free buffer.

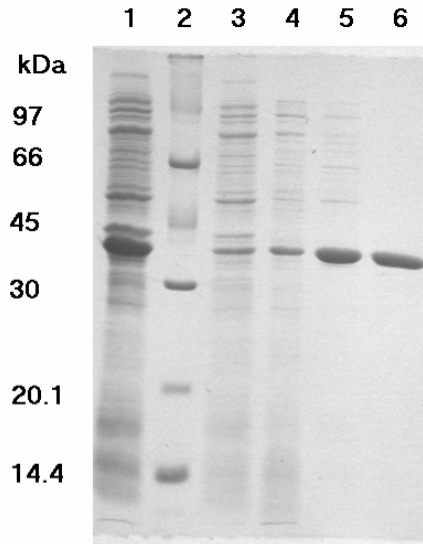


Figure 2.11 SDS-PAGE showing purification of the recombinant *M. tuberculosis* Class II fructose 1,6-bisphosphate aldolase from shake-flask grown cells

The lanes correspond to the following purification steps: 1) bacterial lysate (30 µg); 3) crude extract (10 µg); 4) ammonium sulphate fractionation (10 µg); 5) DEAE chromatography (5 µg); 6) size exclusion chromatography (5 µg). Lane 2 contains the molecular mass markers. The purified enzyme subunits have a molecular mass of 36,413 Da, as determined by ESI mass spectroscopy. The gel was stained with Coomassie Blue.

Table 2.5 Purification of the recombinant *M. tuberculosis* Class II fructose 1,6-bisphosphate aldolase (shake-flask grown)

One unit of activity corresponds to the cleavage of 1 µmol of FBP/min at 28 °C.

Step	Protein (mg)	Activity (units)	Yield (%)	Specific activity (µmol/min per mg)	Purification
1. Cell Extract	210	197	100	0.94	1
2. Ammonium sulphate	154	51	26.1	0.33	0.35
3. DEAE	2.80	30.6	15.4	10.9	11.6
4. Gel filtration	0.80	28.4	14.4	35.1	37.4

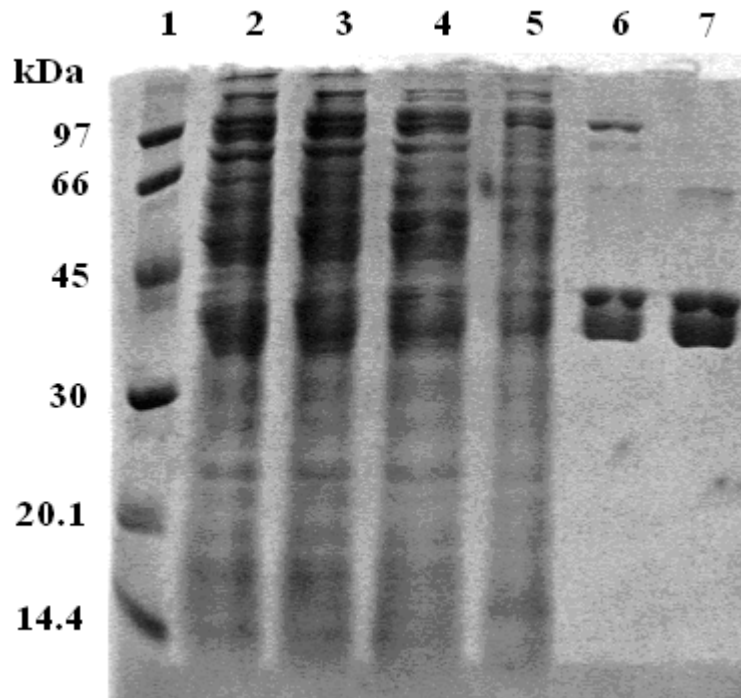


Figure 2.12 SDS-PAGE of the *M. tuberculosis* aldolase purification from fermentor-grown cells (induced with 0.5 mM IPTG)

The lanes correspond to the following purification steps: 2) crude extract (20 μg); 3) protamine sulphate (20 μg); 4) ammonium sulphate fractionation 40% (20 μg); 5) ammonium sulphate fractionation 80% (20 μg); 6) DEAE and Hydroxyapatite chromatography (5 μg); 7) gel filtration chromatography (5 μg). Lane 1 contains the molecular mass markers. The gel was stained with Coomassie Blue.

Table 2.6 Purification table for the *M. tuberculosis* FBP aldolase (fermentor-grown, induced with 0.5 mM IPTG)

One unit of activity corresponds to the cleavage of 1 μmol of FBP/min at 30 °C.

Step	Protein (mg)	Activity (U)	Yield (%)	Specific activity ($\mu\text{mol}/\text{min}/\text{mg}$)	Purification
1. Cell extract	3,890	6,370	100	1.64	1
2. Ammonium sulfate	1,380	3,720	58	2.7	1.6
3. DEAE	52	630	10	12	7.3
4. Hydroxyapatite and gel filtration	5.4	173	2.7	32	19.5

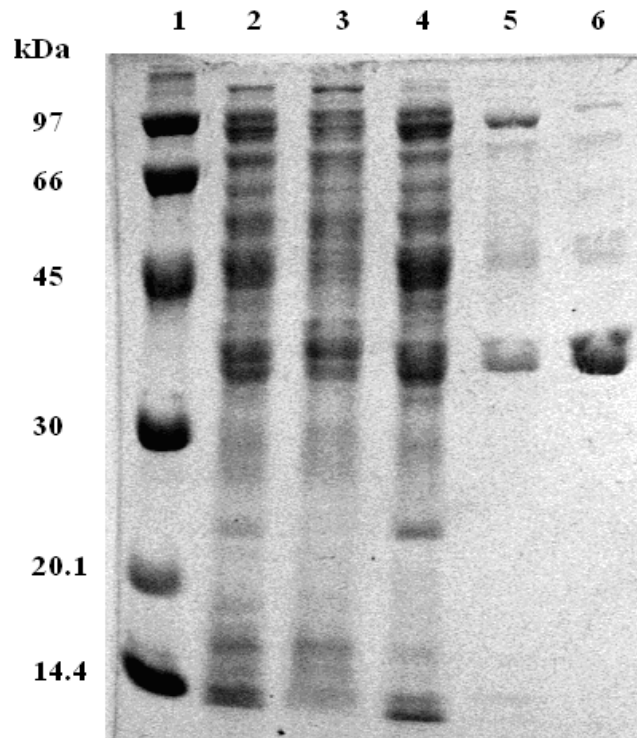


Figure 2.13 SDS-PAGE of the purification of the FBP aldolase from *M. tuberculosis* (fermentor-grown, induced with 2.5 mM IPTG)

The lanes correspond to the following purification steps: 2) crude extract (27 µg); 3) ammonium sulphate fractionation 43% (28 µg); 4) ammonium sulphate fractionation 83% (23 µg); 5) Sepharose Q chromatography (5 µg); 6) gel filtration chromatography (4 µg). Lane 1 contains the molecular mass markers. The gel was stained with Coomassie Blue.

Table 2.7 Purification table for the *M. tuberculosis* FBP aldolase (fermentor-grown, induced with 2.5 mM IPTG)One unit of activity corresponds to the cleavage of 1 μmol of FBP/min at 30 °C.

Step	Protein (mg)	Activity (U)	Yield (%)	Specific activity ($\mu\text{mol}/\text{min}/\text{mg}$)	Purification
1. Cell extract	5,400	6,770	100	1.25	1
2. Ammonium sulfate	1,702	4,040	60	2.4	1.9
3. Sepharose Q	230	1,320	19	5.7	4.6
4. Superdex 200	28	600	9	21	16.8

2.3.3.2 *P. aeruginosa* aldolase

It was observed that the amount of DEAE (anion exchange) resin used for the purifications has a bearing in the purity of the enzyme. This is because lower amounts of resin relative to the amount of loaded crude extract would result in less binding of contaminating proteins in the column. A good example is the purification we report for the *P. aeruginosa* aldolase, where only one anion-exchange chromatography step was sufficient to obtain a >95% pure enzyme (Figure 2.14, last lane). Attempts to purify the enzyme further using another anion-exchange column were not successful as the enzyme lost activity over time (Table 2.8). Over 2 grams of purified enzyme (1.8 U/mg) were obtained after the first anion exchange column, from 105 grams of fermentor-grown cells. The reported purification was done in Tris-HCl buffers containing added zinc chloride excepted for the Sepharose-Q (second anion-exchange) chromatography, where ZnCl_2 was not added. The final enzyme preparation had a specific activity of 1.4 U/mg, or 19 U/mg in the presence of 0.7 mM CoCl_2 (see metal titration curve

Chapter 2 Cloning, expression and purification of Class II FBP aldolases

in Chapter 3). A previous similar purification done in 50 mM sodium phosphate buffers (pH 7.0) not supplemented with ZnCl₂ yielded 1.7 grams of >95% pure enzyme from 90 grams of cells, with a specific activity of over 4 U/mg (or 27 U/mg in the presence of 0.7 mM CoCl₂) after the first anion exchange chromatography. The activity of this zinc-free preparation was stable for a least a year in 50% glycerol at -20 °C. It therefore seems that the Tris-HCl buffer with zinc chloride is not as good as sodium phosphate buffer in the case of this enzyme.

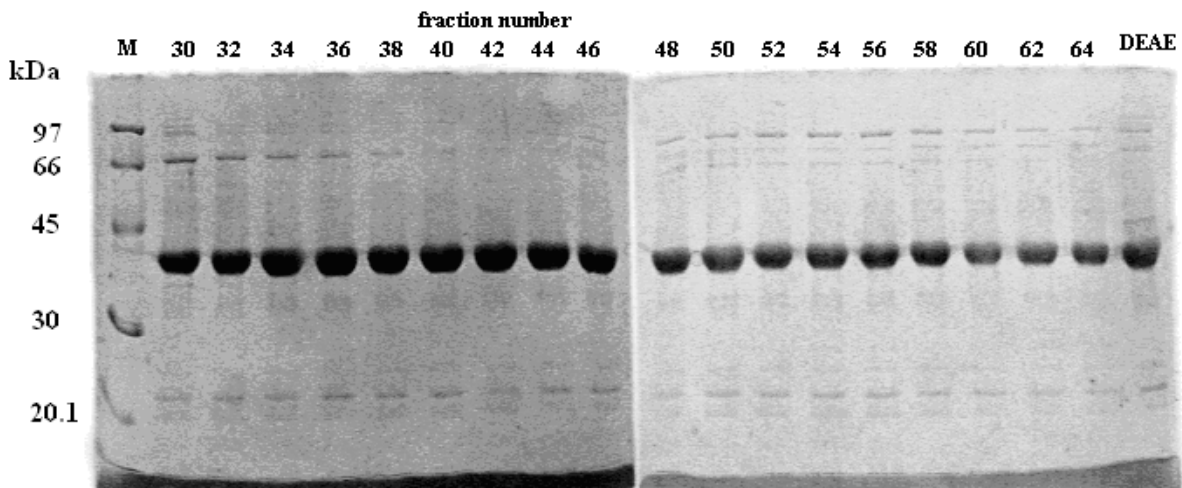


Figure 2.14 SDS-PAGE of the elution fraction from the Sepharose-Q column containing the *P. aeruginosa* aldolase

The fractions shown were kept in three separate pools (30-39; 40-45; 46-64). Only the pool made with the purest fractions (40-45) was used for kinetic assays. The low molecular weight contaminants visible on the gel were later eliminated during dialysis (see Figure 2.15). 11 µg of protein were loaded in each lane for the fractions 40 to 44. The last lane (DEAE) shows 13 µg of the enzyme after DEAE chromatography. The first lane (M) contains the molecular mass markers. The gel was stained with Coomassie Blue.

Table 2.8 Purification table of the *P. aeruginosa* FBP aldolase

Step	Protein (mg)	Activity (U)	Yield (%)	Specific activity ($\mu\text{mol}/\text{min}/\text{mg}$)	Purification
1. Cell extract	10,830	8,670	100	0.80	1
2. Ammonium sulfate	5,540	5,210	60	0.94	1.2
3. DEAE	2,151	3,872	45	1.8	2.25
4. Sepharose Q (only purest fractions)	305	427	4.9	1.4*	1.8

* The enzyme lost activity in storage before this chromatographic step.

2.3.3.3 *B. cereus* aldolase

The *B. cereus* aldolase was also purified to >95% purity (see Figure 2.15) using only one chromatographic step (Table 2.9). The purified enzyme was less stable than the *P. aeruginosa* aldolase as it lost almost a third of its activity after a few months, and after 3 years in storage (in saturated ammonium sulfate at 4 °C), the activity was around ~2 U/mg. A second purification was attempted from 54 grams of the cells obtained during the same fermentation, using buffers supplemented with 0.3 mM zinc chloride, and in which the enzyme was directly loaded on a DEAE column instead of being purified by ammonium sulfate cuts first. This modified procedure failed to produce an enzyme with a higher specific activity, as the eluted enzyme (1.07 gram) was ~60% pure and had a specific activity of about 2 U/mg. The procedure described in the methods section is therefore more effective, as it resulted in 210 mg of >95% pure enzyme with a specific activity of ~9 U/mg (Table 2.9).

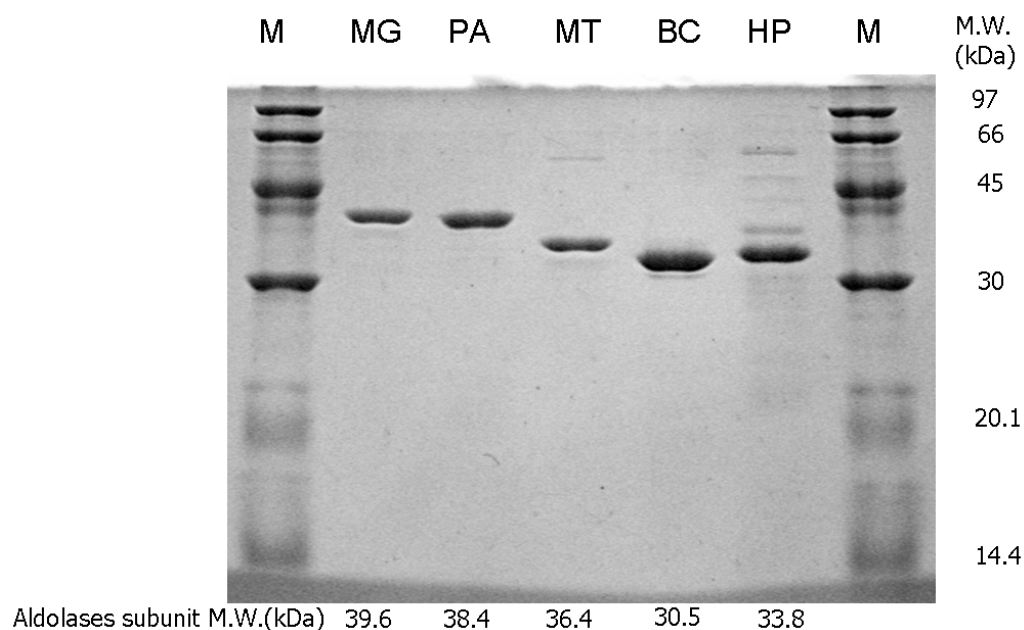


Figure 2.15 SDS-PAGE of the purified FBP aldolases

The first and last lanes (marked M) contain the low molecular weight markers, with sizes indicated on the right. The five middle lanes each contain 3 micrograms of purified recombinant FBP aldolases from the following organisms: *M. grisea* (MG); *P. aeruginosa* (PA); *M. tuberculosis* (MT); *B. cereus* (BC); and *H. pylori* (HP). The molecular weight of each recombinant aldolase is indicated at the bottom. The 12% acrylamide gel was stained with Coomassie Blue.

Table 2.9 Purification table for the *B. cereus* FBP aldolase

Step	Protein (mg)	Activity (U)	Yield (%)	Specific activity ($\mu\text{mol}/\text{min}/\text{mg}$)	Purification
1. Cell extract	7,510	8,300	100	1.1	1
2. Ammonium sulfate	520	1,800	22	3.4	3.1
3. DEAE	210	1,900	23	9.2	8.4

2.3.3.4 *M. grisea* aldolase

The enzyme was >95% pure (see Figure 2.15) after two anion exchange chromatographic steps (Table 2.10). We determined that the specific activity of the purified enzyme was ~70 U/mg. The enzyme is stable for over a year when precipitated in an ammonium sulfate solution and kept at 4 °C, or when snap-frozen in liquid nitrogen and kept at -80 °C, as described in the previous section.

Table 2.10 Purification of the recombinant *M. grisea* Class II FBP aldolase

The cell extract was prepared from 55 g wet weight of *E. coli* BI21(DE3) cells expressing pT7-7/MGFBA.

Step	Protein (mg)	Activity (U)	Yield (%)	Specific activity (μmol/min/mg)	Purification
1. Cell extract	5,510	63,300	100	11.5	1
2. Ammonium sulfate	2,490	39,100	62	15.7	1.4
3. DEAE	570	28,500	45	50.0	4.3
4. ResourceQ	265	18,600	29	70.3	6.1

2.3.3.5 *H. pylori* aldolase

The *H. pylori* aldolase did not bind to the DEAE column and was collected as the flow through. There is no improvement in binding when the column equilibration buffer pH was increased and it was observed that the enzyme is unstable and prone to aggregation. A second purification was performed with addition of 5 μM CoCl₂ in the purification buffers, by doing ammonium sulfate cuts and using a Resource Q column, and storing the enzyme in 50% glycerol at -20 °C, but again the

Chapter 2 Cloning, expression and purification of Class II FBP aldolases

enzyme had little activity (~1 U/mg) and was unstable. Attempts to reactivate the enzyme by addition of CoCl₂ or ZnCl₂ (by direct addition or dialysis at 4 °C) were not successful. Therefore the kinetic tests were done using the first preparation's flow-through from the DEAE column (Figure 2.15). The enzyme had about 50% of its activity remaining after 9 months when stored in 80% saturated ammonium sulfate, 0.1 mM CoCl₂ at 4 °C.

Table 2.11 Purification table of the *H. pylori* FBP aldolase

Step	Protein (mg)	Activity (U)	Yield (%)	Specific activity (μmol/min/mg)	Purification
1. Cell extract	1,830	1,300	100	0.7	1
2. Ammonium sulfate	540	320	25	0.6	0.9
3. DEAE	79	87	7	1.1	1.6
With added CoCl ₂ *		720		9.1	

* The activity of this fraction was also measured in the presence of 5 μM CoCl₂, which activates the enzyme by a factor ~8 (see metal titration curve in Chapter 3).

2.3.3.6 *E. coli* aldolase

The purity of the enzyme after each step of the purification can be seen in Figure 2.17, and the purification table is shown in Table 2.12. About 26 mg of ~95% pure enzyme were obtained from 46.5 grams of cells after the first anion exchange chromatography step (Figure 2.16, “pool A” in lane 6). The purified *E. coli* enzyme (Figure 2.16, lanes 9 and 10; Table 2.12 last row) which was flash-frozen in 50 mM Tris buffer pH 8.0 containing 0.3 mM ZnCl₂ gradually lost activity in storage at -80 °C over time (~50% loss after 2 weeks), so we instead used the purified enzyme (7 U/mg)

Chapter 2 Cloning, expression and purification of Class II FBP aldolases

generously provided by Dr. J. Sygusch (University of Montreal), which was stable when flash-frozen in 50 mM sodium phosphate, 200 mM NaCl, pH 7.9 and kept at -80 °C, for our kinetic assays.

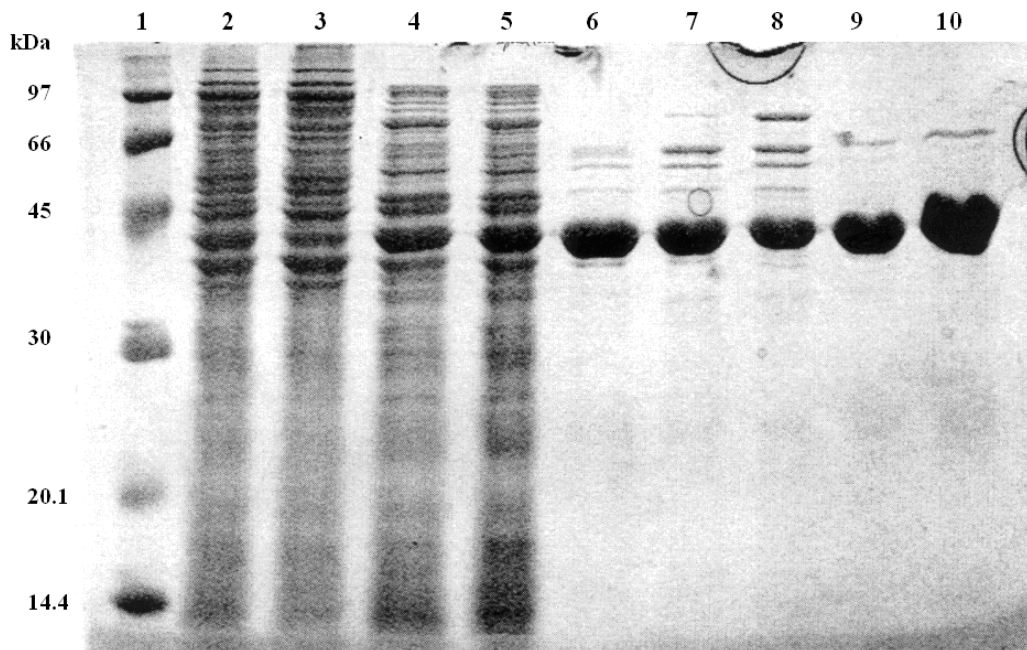


Figure 2.16 SDS-PAGE of the purification steps for the *E. coli* FBP aldolase

The lanes correspond to the following purification steps: 2) crude extract (20 µg); 3) ammonium sulphate fractionation 45% pellet (20 µg); 4) ammonium sulphate fractionation 45% supernatant (20 µg); 5) ammonium sulphate fractionation 80% pellet (20 µg); 6) to 8) Sepharose Q chromatography pools A, B, and C (5 µg); 9) ResourceQ chromatography (5 µg); 10) ResourceQ chromatography (10 µg). Lane 1 contains the molecular mass markers. The gel was stained with Coomassie Blue.

Table 2.12 Purification table for the *E. coli* FBP aldolase

Step	Protein (mg)	Activity (U)	Yield (%)	Specific activity ($\mu\text{mol}/\text{min}/\text{mg}$)	Purification
1. Cell extract	4,230	14,000	100	3.3	1
2. Ammonium sulfate	1,390	7,800	56	5.6	1.7
3. SepharoseQ (pool A)	26	N/A	N/A	N/A	N/A
(pools A, B, and C)	75				
4. ResourceQ*	1.8	68.4	1	38	11.5

N/A: the enzyme activity was strongly inhibited by the presence of 30 μM ZnCl_2 in the assay (from the purification buffer) and was around ~ 1 U/mg in the SepharoseQ elution pools.

* Only a portion (47%) of the SepharoseQ “pool A” was used for this step. The protein concentration for this step was estimated from the ResourceQ chromatography elution profile and from the SDS-PAGE (Figure 2.16).

2.3.4 Mass spectrometry results

The theoretical and measured molecular mass of the recombinant aldolases are shown in Table 2.13. Two peaks were obtained by ESI mass spectrometry for the aldolases from *B. cereus* and *M. grisea*, which correspond to the molecular weight of the entire cloned sequences, and the sequences minus the N-terminal methionine, respectively. The N-terminal methionine was thus not completely cleaved for these aldolases: this occurs frequently in the case of highly overexpressed recombinant enzymes. We could not get a reliable signal from the *H. pylori* aldolase on the mass spectrometer in spite of numerous attempts, and even when the enzyme was apparently $>90\%$ pure on a SDS-PAGE (Figure 2.15). This may be due to the aggregation problems we experienced with this enzyme; or possibly the enzyme degraded very quickly when dialyzed. The results shown are all

Chapter 2 Cloning, expression and purification of Class II FBP aldolases
equivalent to the expected molecular masses, within the error margin resulting from the mass spectrometer calibration procedure (+/- 3 Da), except for the *H. pylori* aldolase which is ~5 Da lower than expected for the sequence including the N-terminal methionine residue.

Table 2.13 Mass spectrometry results for purified recombinant aldolases

Aldolase	Theoretical M.W.*		Measured M.W. (Da)
	(+Met) (Da)	(-Met) (Da)	
<i>M. tuberculosis</i>	36,544	36,413	36,411
<i>P. aeruginosa</i>	38,574	38,443	38,440.5
<i>M. grisea</i>	39,776	39,645	39,775 and 39,644
<i>E. coli</i>	39,147	39,016	39,012.5
<i>B. cereus</i>	30,673	30,542	30,671 and 30,540
<i>H. pylori</i>	33,773	33,642	33,767.5

*The mass with and without the N-terminal methionine residue are shown

2.4 Discussion

The Class II aldolases from 6 microorganisms have been successfully cloned and expressed in *E. coli*. The aldolases from *M. tuberculosis*, *M. grisea*, *P. aeruginosa*, *B. cereus*, *H. pylori*, and *E. coli* have also been purified to near homogeneity. It is relevant to note that the amino acid sequence of the *B. cereus* FBP aldolase is completely identical to that of *Bacillus anthracis*, the causative agent of anthrax. However, the nucleotide sequences differ slightly: there are three nucleotides that are substituted in the aldolase gene when (855/858 nucleotides identical in the FBP aldolase gene, see Appendix A). The class II aldolases from *M. tuberculosis*, *B. cereus* and *P. putida* were previously isolated from the host organisms and partially characterized (Bai *et al.* 1982; Bang and Baumann 1978; Sadoff *et al.* 1969). The amino acid sequence of the *P. putida* FBP aldolase is

Chapter 2 Cloning, expression and purification of Class II FBP aldolases

96% identical to that of the *P. aeruginosa* PAO1 aldolase (see *P. aeruginosa* Protein ID: NP_249246.1, and *P. putida* Protein IDs: ZP_01637933.1; ZP_01715354.1 and NP_747063.1), so the results obtained in these previous studies will be considered in the evaluation of the recombinant enzymes reported here.

As mentioned in this chapter, we chose to express the native enzymes in *E. coli* without adding an affinity tag to avoid potential problems with improper folding the aldolases and/or metal incorporation, as problems were reported previously for N-terminally tagged Class II aldolases by our group and others (Ramsaywak *et al.* 2004; Wehmeier 2001). We chose to overexpress our enzymes in an *E. coli* strain that was not aldolase deficient, because our expression system is very effective and the small amount of native *E. coli* aldolase can be easily separated from our desired recombinant enzymes during the purification procedure. The native *E. coli* aldolase has a molecular weight of 39,016 Da and is not visible either on our purified enzyme SDS-PAGE gels, or detected by mass spectrometry analysis. However, if the aldolases were to be used as a vaccine component (see section 1.2.5), for example in the case of anthrax (Whiting *et al.* 2004), this overexpression system would obviously not be the best choice as there may still be traces of native *E. coli* enzymes, including the native FBP aldolase, in the purified protein preparations.

In most cases, half or more of the peak of enzyme activity eluted from the chromatography columns was discarded after visualization of the fractions on SDS-PAGE, and only the pure fractions were pooled (see example Figure 2.14). This was essential in order to limit the purification to a minimum number of steps and to achieve apparent purity of the enzymes in a timely manner, with the goal of conserving the highest specific activity in our samples. Our final yields were obviously diminished by this practice. Although only the purest fractions were pooled, the yields for the recombinant enzymes are superior to those of the purifications from the native hosts, as discussed below.

Chapter 2 Cloning, expression and purification of Class II FBP aldolases

It was observed that the amount of anion exchange resin used during the first chromatographic step in the purifications, was directly affecting the purity of the eluted enzyme, and thus affected the number of chromatographic steps that were subsequently required. For example, the *P. aeruginosa* aldolase was purified using the DEAE resin alone, because the amount of resin used was limiting and it seems the aldolase saturated the resin and prevented the binding of most contaminants. It would thus be worthwhile in the future to determine the optimal amount of anion exchange resin to use for a given amount of cell lysate, if the native enzymes were to be routinely purified

For the *M. tuberculosis* aldolase, a total of 6.1 mg of enzyme with a specific activity of 4 U/mg were previously obtained from 50 grams of cells from surface cultures of *M. tuberculosis* H₃₇Rv grown for 3 weeks. The purification consisted of ammonium sulfate fractionation, DEAE and gel filtration chromatography. A purification factor of 64 and a yield of 50% were reported (Bai *et al.* 1982; 1975). The authors state that the enzyme was stable when stored at -20 °C for 4 weeks. In comparison, the purest recombinant enzyme we obtained has a specific activity about 9 times higher than the aldolase purified from the native bacteria (35 U/mg), and the enzyme yield was also higher for the same number of chromatographic steps. A yield of 0.8 mg was obtained from only ~2 grams of *E. coli* cells. A higher enzyme yield was obtained from 41 grams of fermentor-grown cells, resulting in a total of 28 mg of purified aldolase with a specific activity of 21 U/mg. The expression of this enzyme in a recombinant host is clearly beneficial in terms of yield and enzymatic activity, in addition to it being safer and faster growing than the native host. The *M. tuberculosis* aldolase was however one of the most difficult recombinant enzymes to purify in this project, as it had a comparatively low level of expression and is co-eluted with other *E. coli* enzymes in the anion exchange chromatographic steps. The highest amount of *M. tuberculosis* aldolase purified (28 mg) is about ten times lower than that obtained for the *P. aeruginosa*, *M. grisea*, and *B. cereus* aldolases (200 mg to 300 mg each) from comparable quantities of fermentor-grown cells.

Chapter 2 Cloning, expression and purification of Class II FBP aldolases

No protein yield was reported for the previously purified *P. putida* aldolase (Bang and Baumann 1978), which is 96% identical to the *P. aeruginosa* enzyme. The authors report a 26- to 30-fold purification with a recovery of 70-75% after ammonium sulfate (40-60%) precipitation and DEAE chromatography, resulting in a final specific activity 4.9 to 5.7 U/mg in the presence of 0.7 mM CoCl₂. The activity of the preparation was reported to be completely dependent on the presence of added cobalt, and the activity decreased by 18% over 2 weeks at 4 °C. Similar purifications done from fermentor-grown cells in the present study yielded >95% pure enzyme with specific activities of 19 U/mg and 27 U/mg respectively in the presence of 0.7 mM CoCl₂. The use of a recombinant expression system is therefore clearly advantageous for this enzyme as well.

The vegetative cells and spores of *B. cereus* were previously grown in a 100-L fermentor to purify the FBP aldolase (Sadoff *et al.* 1969). The authors did not specify the total amount of cells obtained, but stated that they were resuspended in batches of 500 grams for the purifications. The yield was 59 mg of aldolase at 6.38 U/mg (71-fold purification and 38% activity yield from crude extracts) from spores; and 6.6 mg of aldolase at 57.9 U/mg (170-fold purification and 8% activity yield) from vegetative cells, after ammonium sulfate fractionation and 2 chromatographic steps. They state that the purified vegetative aldolase was unstable, but could be stabilized by the addition of 3 mM magnesium and 0.1 mM DTT. In the present study, 210 mg of pure recombinant enzyme with a specific activity of 9.2 U/mg was obtained after 1 chromatographic step less than the previous reported study, from 103 grams of fermentor-grown *E. coli* cells. The addition of Co²⁺ to the purified BCFBA did not increase the specific activity in our study. Sadoff and collaborators have reported inconsistent results for the effect of divalent metal ions on the purified BCFBA activity (Sadoff *et al.* 1969). As stated above, the enzyme they purified from vegetative *B. cereus* cells had a reported specific activity of 58 U/mg, a value significantly higher than that obtained for our recombinant enzyme. Sadoff and collaborators used a different coupled assay to determine the enzyme's activity,

Chapter 2 Cloning, expression and purification of Class II FBP aldolases

where glyceraldehyde-3-phosphate dehydrogenase is used to reduce NAD^+ . Their assays were done in the absence of triose phosphate isomerase, which results in the accumulation of the product DHAP in the assay as the FBP cleavage reaction proceeds. The different assay procedure could potentially explain the discrepancy with our value. The value that they reported for the K_M of BCFBA (2 mM) is also much higher than the one we determined using our NADH-linked assay (450 μM , see kinetic analysis in Chapter 3). By contrast, the K_M value reported for the *P. putida* aldolase by Bang and Baumann (30 μM) using the NADH-linked assay is equivalent to the one we determined for the closely related *P. aeruginosa* (34 μM , see Chapter 3). We subsequently purified PAFBA and BCFBA using buffers supplemented with 0.3 mM zinc chloride, but this did not increase the specific activity of either recombinant enzyme.

The use of a recombinant system is thus obviously useful in terms of yield of enzyme for a given amount of cells. However, the activity of the recombinant *B. cereus* aldolase is 6-fold lower than reported from vegetative cells from this organism. The correct protein folding may thus not be achieved or the native metals may not be accessible in the *E. coli* expression system for this enzyme. The *E. coli* expression is however better for the *M. tuberculosis* (35 U/mg) and *M. grisea* (70 U/mg) recombinant aldolases. The highest specific activity ever reported for a Class II FBP aldolase is 150 U/mg (100 s^{-1}) for the yeast enzyme assayed at 30 °C (Belasco and Knowles 1983). The aldolase from *M. grisea* shares 66% amino acid sequence identity with the yeast enzyme (Figures 1.14 and 1.17), has to our knowledge not been purified previously, and its specific activity is among the highest reported to date for FBP aldolases (Labbe *et al.* 2007).

We used an existing recombinant vector for the *E. coli* Class II aldolase. The *E. coli* enzyme activity obtained by the team who constructed the plasmid was 23.3 U/mg (Henderson *et al.* 1994), with an assay temperature of 25 °C. The activity we obtained using the same expression plasmid was

Chapter 2 Cloning, expression and purification of Class II FBP aldolases

higher (38 U/mg), but this may be due to the higher assay temperature (30 °C). Only 2 anion exchange chromatographic steps (SephacroseQ and ResourceQ) were needed to obtain ~1.8 mg of >95% purified enzyme from 46.5 grams of cells (14,000 U) in the procedure described here. This yield could have been improved by a factor 6 (~11 mg pure enzyme) if all the 76 mg obtained after the first chromatography step had been used in the second one, instead of only 12 mg. Henderson and collaborators started from 17,000 U in the crude extract, and obtained 8 mg of enzyme with a specific activity of ~17 U/mg after 2 anion exchange columns (DEAE and MonoQ). However an additional chromatofocusing step is required to obtain a higher purity (23.3 U/mg). The two purification methods using shake-flask grown cells with the same overexpression plasmid thus seem equivalent in terms of yield versus the number of purification steps. The purified enzyme was however unstable in the storage conditions employed here. The half-life of the *E. coli* aldolase was previously reported to be 60 days at 25 °C in Triethanolamine buffer containing 0.3 mM ZnCl₂ (Von der Osten *et al.* 1989); but we found that the enzyme had a half-life of only ~30 days at -80 °C in a similar buffer.

The expression and purification methods did not seem to be the major factor determining the final specific activity of the recombinant enzymes, as various conditions yielded purified enzymes with similar properties (within a factor ~2). It can be concluded that for Class II aldolases, the main factor influencing the specific activity and stability is the *E. coli* recombinant expression system itself. The aldolases from *B. cereus*, *B. anthracis*, *S. pneumoniae*, *H. pylori* and *P. aeruginosa* can be classified as “Type B” aldolases according to the classification of proposed by Plaumann and collaborators (Plaumann *et al.* 1997), whereas the aldolases from *M. tuberculosis*, *M. grisea* and *H. influenzae* are classified as “Type A” (Figure 1.4). The type B aldolases have a much lower specific activity than the type A enzymes in this recombinant system, and it is not known if this is an intrinsic property of the Type B enzymes, or if this is due to the inadequacy of the *E. coli* expression system for these enzymes, since many type B enzymes have been reported to use a divalent metal ion other than zinc.

Chapter 2 Cloning, expression and purification of Class II FBP aldolases

The recombinant enzyme from *P. aeruginosa* had a higher specific activity (4-fold) than reported when purified from the original host. However, the recombinant *B. cereus* aldolase activity was much lower (6-fold) than that reported earlier when the enzyme was purified from the host (Sadoff *et al.* 1969). It is particularly surprising that the *H. pylori* aldolase is the most unstable among the recombinant enzymes, since it is most related to a thermostable aldolase (that of *Thermus aquaticus*, see Figure 1.4). It would thus be interesting to try to purify the Type B enzymes from a *Pseudomonas* overexpression system for comparison.

The use of a fermentor allowed for the production of large amounts of cells in a conveniently small volume, but did not seem to be advantageous over batch cultures in terms of enzymatic yield, when the same amount of cells is used for the purifications. The expression level of the aldolases was usually lower in the fermentor, and this was attributed to the use of an insufficient amount of IPTG. This amount needs to be optimized according to the cell density of the fermentor culture to allow for the complete de-repression of the T7 RNA polymerase expression (under the control of the *lacUV5* promoter in the *E. coli* BL21(λ DE3) strain) which maximizes the recombinant gene expression.

The purified recombinant aldolases can be used for kinetic and inhibition assays, which will be the subjects of the two following chapters.

Chapter 3

Characterization of recombinant Class II FBP aldolases

3.1 Introduction

The purified recombinant Class II FBP aldolase enzymes were characterized to: i) compare their properties with those of the native enzymes, ii) gain the necessary information for design of inhibition kinetic assays (Chapter 4), and iii) investigate the potential of Class II enzymes for organic synthesis by comparison with the Class I rabbit muscle aldolase.

The kinetic parameters and optimum pH for the activity of the recombinant aldolases will be presented here and compared with those of other Class II aldolases previously characterized (Table 3.1). These properties for the *M. grisea* and *H. pylori* aldolases have to our knowledge not been determined previously. The temperature and organic solvent stability of the recombinant enzymes were also determined. The stability of the Class II aldolase in organic solvents was investigated only for the *E. coli* enzyme previously (Hao and Berry 2004; Hao 2003). The quaternary structure and metal content of the *M. tuberculosis* aldolase were determined previously by our group (Ramsaywak *et al.* 2004; Ramsaywak 2003), but the quaternary structure of the aldolases from *M. grisea* and *P. aeruginosa* were determined for the first time in this project. The metal content of the recombinant aldolases as well as their reactivation by various divalent metals will also be described here.

Some of the work presented in this chapter was performed by undergraduate students under my supervision. The metal titration and some of the kinetic characterization assays were done by NSERC summer Undergraduate Student Research Award (USRA) recipient Sarah de Groot. The

Chapter 3 Characterization of recombinant Class II FBP aldolases

organic solvent and temperature stability assays, as well as several assays to test the pH-dependence of the aldolases' kinetic parameters, were done by NSERC summer USRA recipient Timothy Rasmusson. The gel filtration chromatographies to determine the molecular weight of the aldolases from *B. cereus* and *M. grisea* were kindly performed by Dr. Stephen Seah (University of Guelph).

Table 3.1 Kinetic parameters table for Class II FBP aldolases published by other groups

Organism	Quaternary			Specificity	Reference
	Structure (subunits)	K_m (μM)	k_{cat} (s^{-1})	(k_{cat} / K_m) $10^2 \mu\text{M}^{-1} \text{s}^{-1}$	
<u>TYPE A</u>					
<i>Escherichia coli</i>	2	170	10.5	6	A
<i>Euglena gracilis</i>	2	175	14.1 †	8	B
<i>Saccharomyces cerevisiae</i>	2	370	57.5 ‡	16	C
<i>Mycobacterium tuberculosis</i>	**	80	2.5 †	3.1	D
<u>TYPE B</u>					
<i>Bacillus stearothermophilus</i>					
-Zn form	2	12	5.6 †	47	E
-Co form	2	4.55	10.4 †	230	E
<i>Clostridium perfringens</i>	2	300	41.7 ‡	14	C
<i>Saprospira thermalis</i>	4	190	27.5 ‡	14	F
* <i>Synechococcus</i> sp. PCC6301	4	160	21.8 ‡	14	F
<i>Synechocystis</i> sp. PCC6803	8	8	5.1 †	64	G
<i>Themophilus aquaticus</i>	4	305	25.3 †	8	H
<i>Bacillus cereus</i>	2	2000	29.5 †	1.5	I
<i>Pseudomonas putida</i>	N/A	30	3.7 †	12	J

N/A: not available. *Previously classified as *Anacystis nidulans*. ** Molecular weight > 200 kDa † Activity originally reported as U/mg. ‡ Activity originally reported as moles FBP cleaved per min per mole (i.e. per dimer or tetramer) of aldolase.

References: A (Plater *et al.* 1999); B (Pelzer-Reith *et al.* 1994); C (Rutter 1964); D (Bai *et al.* 1975); E (Hill *et al.* 1976); F (Willard and Gibbs 1968a); G (Nakahara *et al.* 2003); H (Sauve and Sygusch 2001b); I (Sadoff *et al.* 1969); J (Bang and Baumann 1978).

3.2 Procedures

3.2.1 Quaternary structure determination

The molecular weight of the native protein was determined by size exclusion chromatography. The Class II FBP aldolase from *M. grisea* (7 mg) and *B. cereus* (6 mg) were dialyzed in 50 mM phosphate buffer pH 7.0, 0.2 M NaCl and then injected onto a Superdex 200 HR (26 mm x 60 cm) column (Amersham Pharmacia Biotech) equilibrated with the same buffer (injection volume: 1.5 mL). The proteins were eluted at a flow rate of 3 mL/min at 25 °C. For reference, standards from a Molecular Weight Marker Kit (SIGMA) were used according to the manufacturer's instructions. Dextran Blue (2 mg/mL), β -amylase (3 mg/mL), alcohol dehydrogenase (5 mg/mL), BSA (10 mg/mL), carbonic anhydrase (3 mg/mL), and cytochrome C (2 mg/mL) were resuspended in the column equilibration buffer to the recommended concentration (in brackets), applied to the same column, and eluted using the same protocol.

For the the aldolase from *P. aeruginosa*, a Superdex 200 column (10 mm x 30 cm) was used. The enzyme (115 μ g) was dialyzed in 50 mM Tris-HCl, 10% glycerol, 100 mM NaCl, 1 mM DTT, pH 7.5 and the column was equilibrated with the same buffer. The injection volume was 50 μ L, and the proteins were eluted at a flow rate of 0.75 mL/min at 7 °C. The molecular weight markers (above) were resuspended in the column equilibration buffer, applied to the same column, and eluted using the same protocol.

3.2.2 Enzyme stability

3.2.2.1 Stability in assay solution at 4 °C

The assay mixture described in section 2.2.3 was prepared (one preparation large enough for 50 assays for each enzyme) and kept at 4 °C. Aliquots were withdrawn periodically to determine

their activity, and the assays were done in quadruplicate. In some cases, divalent metals were also added to the assay mixture at concentrations indicated in the results section.

3.2.2.2 Temperature stability

Concentrated samples of the different aldolases were diluted in 50 mM HEPES buffer with pH 7.3, and then divided into 50 μ L samples. The samples were incubated at the desired temperature using an Amplifon II Thermolyne PCR thermocycler for ten minutes, then placed on ice immediately for 20 minutes. Following this, 2.5 μ L of the sample were taken and the aldolase activity was assayed as described above, but with 50 mM HEPES buffer pH 7.3 (at 30 °C) instead of 50 mM Tris-HCl pH 8.0.

3.2.2.3 Organic solvent stability

Samples of concentrated aldolase were diluted in various concentrations of the desired organic solvent in water. The samples (15 μ L) were assayed for aldolase activity as outlined in the above paragraph at time 0 to confirm the enzyme activity. The samples were then incubated at room temperature for 3.5 hours, upon which another 15 μ L portion was withdrawn and assayed for aldolase activity. The Class I rabbit muscle aldolase (RAMA) and the Class II *S. cerevisiae* aldolase (SC) used in the assay were purchased from Sigma-Aldrich (Mississauga, ON).

3.2.3 Determination of Michaelis-Menten parameters for FBP cleavage

Assays were performed as described in section 2.2.3. The coupling enzymes were verified to be present in excess quantity, and therefore not limiting for the detection of the FBP cleavage rate. The *H. pylori* enzyme was tested in the assay mixture supplemented with 5 μ M CoCl₂. For the pH optimum determination, a 50 mM glycylglycine buffer was used instead of TRIS-HCl. The pH

Chapter 3 Characterization of recombinant Class II FBP aldolases

curves for each enzyme were done using 1.5 mM of FBP. A similar relative activity profile in function of pH was obtained for the aldolase from *B. cereus* using 4 mM FBP.

3.2.4 Metal content determination

The total zinc contents of the Class II FBP aldolases were determined spectrophotometrically using the chelator 4-(2-pyridylazo)-resorcinol (PAR, Figure 3.1) as described by Siemann and collaborators (Siemann *et al.* 2002). In a typical experiment, the aldolase (4-16 μ M) in Hepes 50 mM, pH 7.3, containing guanidine hydrochloride (4 M, unless otherwise indicated) was incubated at \sim 90 $^{\circ}$ C for at least 30 minutes, cooled on ice and supplemented with PAR (final concentration: 50 μ M). The absorbance in the range of 350-600 nm was recorded, using a Cary 1-Bio UV-Visible spectrophotometer (Varian, Mississauga, ON). A calibration curve was constructed using ZnCl_2 standards (0-10 μ M) by recording the absorbance at 495 nm under identical experimental conditions (see above). The data on the zinc content of the sample and its protein concentration provided the basis for establishing the stoichiometry with respect to the metal ion.

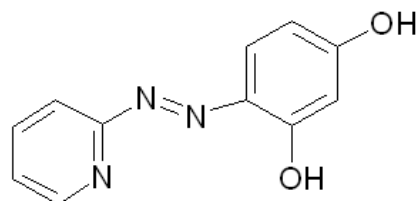


Figure 3.1 PAR structure

3.2.5 Metal replacement studies

The *M. tuberculosis* aldolase was incubated with 10 mM EDTA for 4 hours at 4 $^{\circ}$ C. The enzyme was then desalted using a PD-10 column previously equilibrated with 10 volumes of Chelex (Bio-Rad Corp.) (Himmelhoch *et al.* 1966) treated water followed by 2.5 volumes of Chelex-treated

50 mM Tris-HCl pH 7.4. The assay plates and the plastic vials used to prepare the assay mixture and the metal stock solutions were also previously treated with 10% Nitric acid for 15 minutes and then rinsed with Chelex-treated water. The metal stock solutions (~0.5 to 1.8 mM) were prepared by dissolving the metal chlorides in Chelex-treated water, except for ZnCl₂, MnCl₂ and CoCl₂ which precipitate under these conditions. The CoCl₂ and ZnCl₂ were dissolved in Chelex-treated 20 mM Tris-HCl pH 7.4, and the MnCl₂ was dissolved in Chelex-treated 20 mM Tris-HCl pH 7.4 and 10 mM DTT. The activity was tested using the coupled assay described in section 2.2.3., with divalent metals added to the assay mixture in the concentrations indicated in the results section.

P. aeruginosa, *H. pylori*, and *B. cereus* aldolases were inactivated with 1 mM EDTA (*P. aeruginosa* aldolase), 1.5 mM EDTA (*H. pylori* aldolase) or 5 mM EDTA (*B. cereus* aldolase) for 15 minutes at room temperature, then diluted into the assay mixture such that the final concentration of EDTA was 10 μM (*P. aeruginosa* aldolase), 15 μM (*H. pylori* aldolase) or 50 μM (*B. cereus* aldolase) in the assay. The divalent metals were added to the assay mixture in the concentration indicated in the results section. The metal stock solutions (5 mM) were prepared by dissolving the chloride salts in Chelex-treated 50 mM Tris-HCl pH 8.0, except for the ZnCl₂ and CoCl₂ solutions. The ZnCl₂ was made by dissolving the metal chloride to a concentration of 0.8 mM in 100 mM Tris-HCl pH 6.9. The CoCl₂ solution was made as described in the previous paragraph (lower pH to avoid oxidation and precipitation). The activity was tested using the coupled assay described in section 2.2.3.

3.3 Results

3.3.1 Quaternary structure

Gel filtration experiments revealed that the enzymes of *M. grisea* and *B. cereus* are dimeric (see Figure 3.2). The aldolases from *S. cerevisiae* and *E. coli*, which share 66% and 51% amino acid

Chapter 3 Characterization of recombinant Class II FBP aldolases

sequence identity respectively with the *M. grisea* enzyme (see Figures 1.4 and 1.17), are also dimeric (Baldwin *et al.* 1978; Harris *et al.* 1969). A crystal structure was solved by the laboratory of Dr. Sygusch (University of Montreal) for the *M. grisea* aldolase purified in our laboratory, in which the enzyme was also dimeric (Figure 3.3). The *M. tuberculosis* Class II aldolase has 39% sequence identity with the *M. grisea* enzyme, but has a tetrameric structure (Ramsaywak *et al.* 2004). The aldolase from *P. aeruginosa* is also tetrameric according to a gel filtration experiment (Figure 3.4).

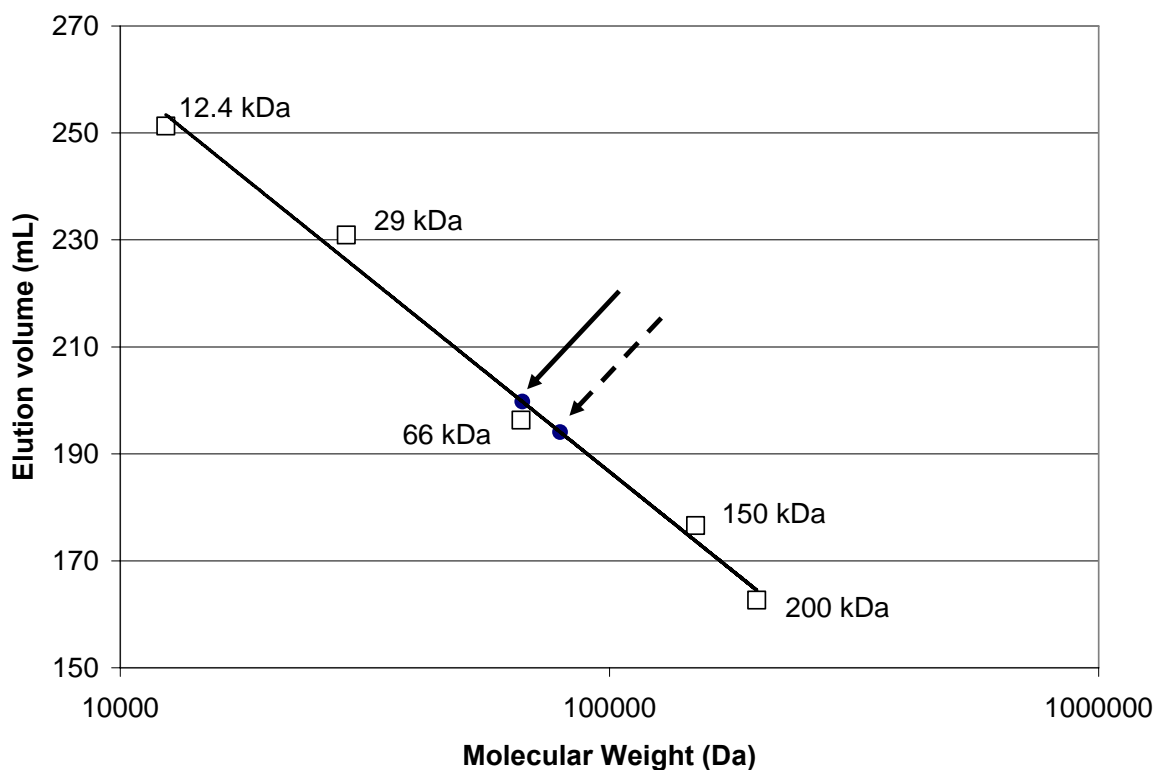


Figure 3.2 Quaternary structure determination of the recombinant *B. cereus* and *M. grisea* Class II FBP aldolases by gel filtration

Molecular mass standard consists of β -amylase (200 kDa), alcohol dehydrogenase (150 kDa), Bovine Serum Albumin (66 kDa), carbonic anhydrase (29 kDa), and cytochrome C (12.4 kDa) (squares). The solid and dashed arrows indicate the elution volume of the dimeric *B. cereus* (~66.4 kDa) and *M. grisea* (~79.3 kDa) aldolases, respectively (filled circles). The theoretical weight of the aldolase dimer is 61,346 Da for *B. cereus* and 79,288 Da for *M. grisea*.

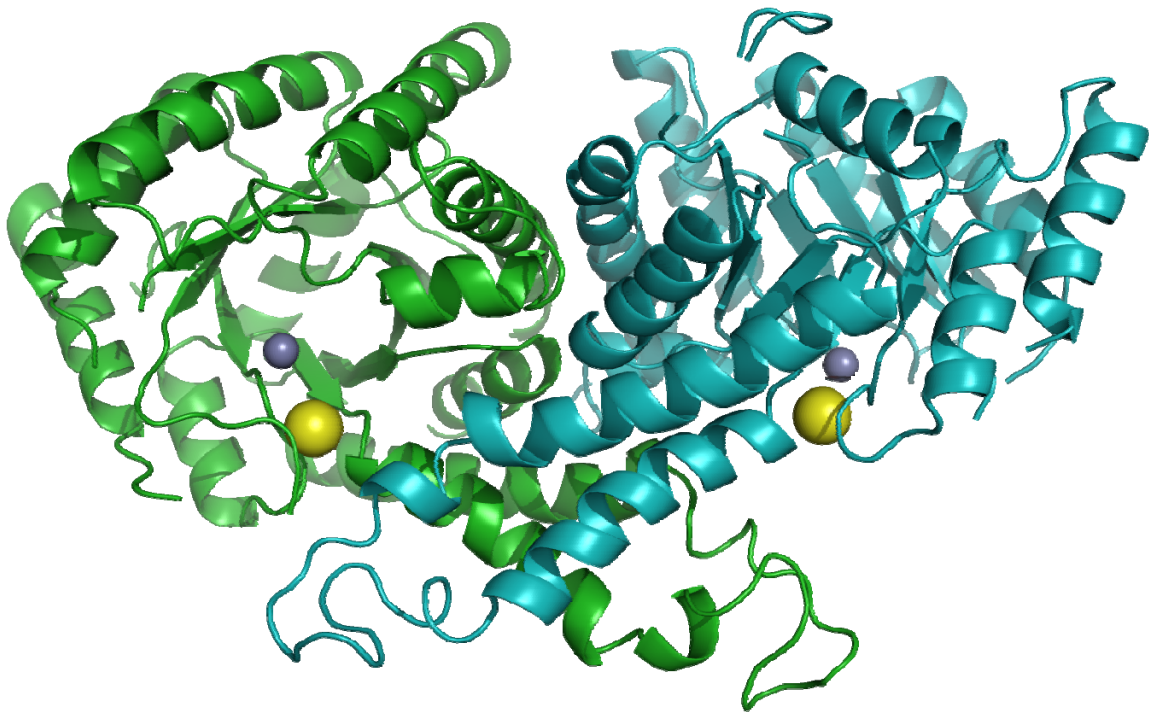


Figure 3.3 Dimeric *M. grisea* FBP aldolase crystal structure.

The structure was determined by Dr. Sygusch's laboratory (University of Montreal) using our purified enzyme. The dimer subunits are shown in green and blue, and the sodium and zinc ions are represented as yellow and grey spheres, respectively. The structure coordinates have not yet been deposited in the Protein Data Bank. The image was produced using PyMOL (DeLano Scientific, San Francisco, CA).

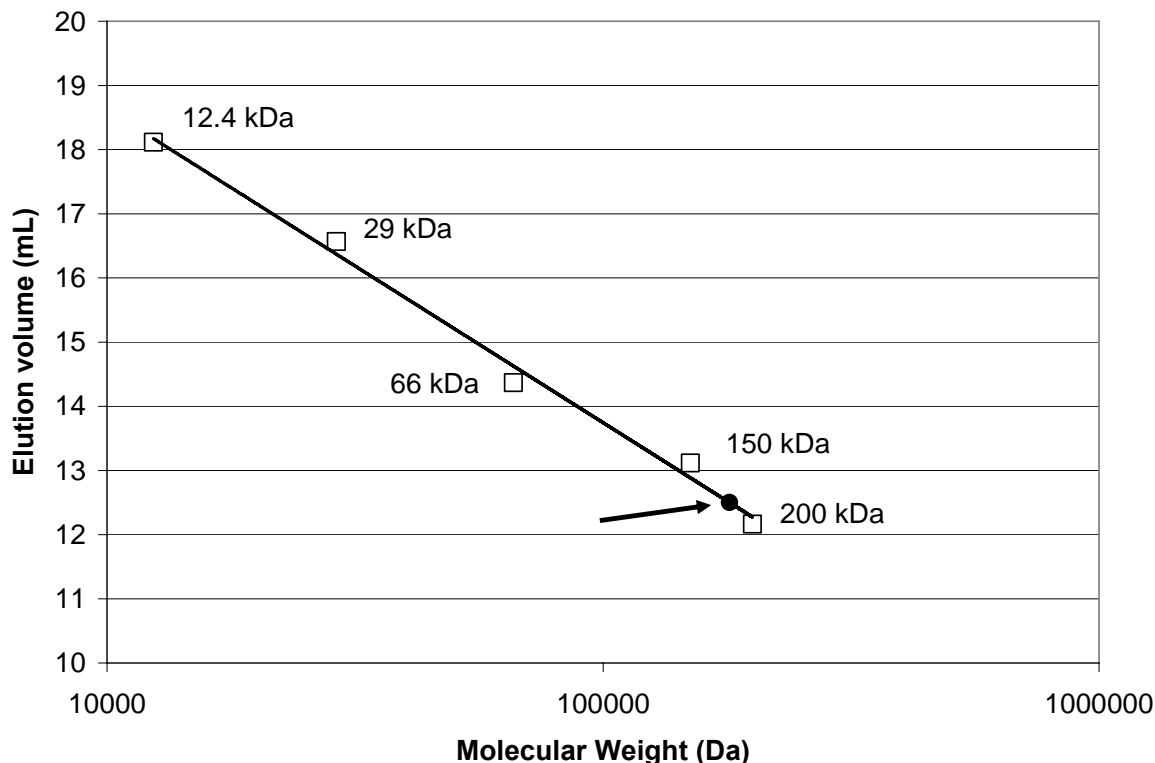


Figure 3.4 Quaternary structure determination of the recombinant *P. aeruginosa* Class II fructose 1,6-bisphosphate aldolase by gel filtration

Molecular mass standard consists of β -amylase (200 kDa), alcohol dehydrogenase (150 kDa), Bovine Serum Albumin (66 kDa), carbonic anhydrase (29 kDa), and cytochrome C (12.4 kDa) (squares). The arrow indicates the elution volume of the FBP aldolase under non-denaturing conditions (filled circle), showing that the enzyme has a tetrameric structure (~180 kDa). The theoretical weight of the tetrameric enzyme is 154 kDa.

3.3.2 Optimum pH

The pH optima of the recombinant aldolases for the FBP cleavage reaction were determined in glycylglycine buffer (Figure 3.5). Each point represents the relative activity of the enzyme at each pH value, determined by conducting assays in quadruplicate at a substrate concentration greater than 10 times the enzyme's K_M (except for the *B. cereus* aldolase, which was 3 times the K_M value, see

section 3.2.3). The aldolases from *M. grisea*, *B. cereus*, *H. pylori*, and *M. tuberculosis* all have a pH optimum between 7.75 and 8. However, the *P. aeruginosa* aldolase has a significantly different pH-activity curve with a pH optimum of 8.5.

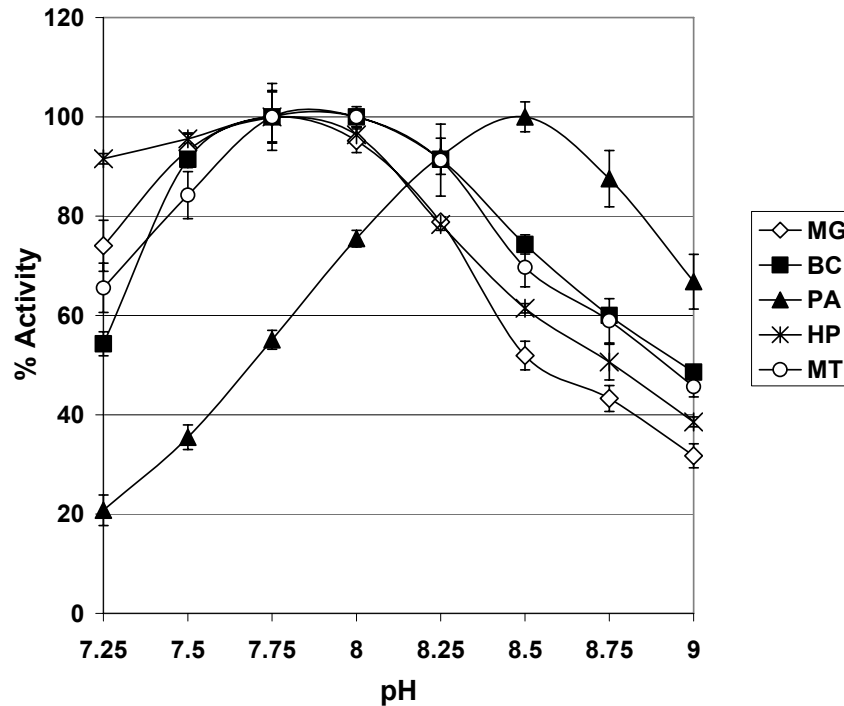


Figure 3.5 pH optimum of the purified Class II aldolases for the FBP cleavage reaction

The coupled assays were performed in 50 mM glycylglycine buffer. Each point represents the average of 4 replicates. Note that the *H. pylori* aldolase activity was tested in an assay mixture supplemented with 5 μ M CoCl_2 . All data were normalized relative to the highest activity recorded for each enzyme. The aldolases are identified in the legend according to their host organism: *M. grisea* (MG); *B. cereus* (BC); *P. aeruginosa* (PA); *H. pylori* (HP); and *M. tuberculosis* (MT).

3.3.3 Enzyme stability

The aldolases were characterized with respect to their tolerance to various organic solvents (Figure 3.6). The Class I rabbit muscle aldolase (RAMA) was also tested as a reference, since it is

Chapter 3 Characterization of recombinant Class II FBP aldolases

the most widely used FBP aldolase in organic synthesis. The results show that RAMA is the most stable overall in the five organic solvents tested, whereas the *M. grisea* aldolase is the most easily inactivated. The aldolases are most tolerant to DMSO (often up to 50% v/v) and least tolerant to t-butanol and acetonitrile (less than 20% v/v). RAMA and the aldolases from *B. cereus* and *P. aeruginosa* are stable in DMF and acetone at concentrations at or above 25% v/v.

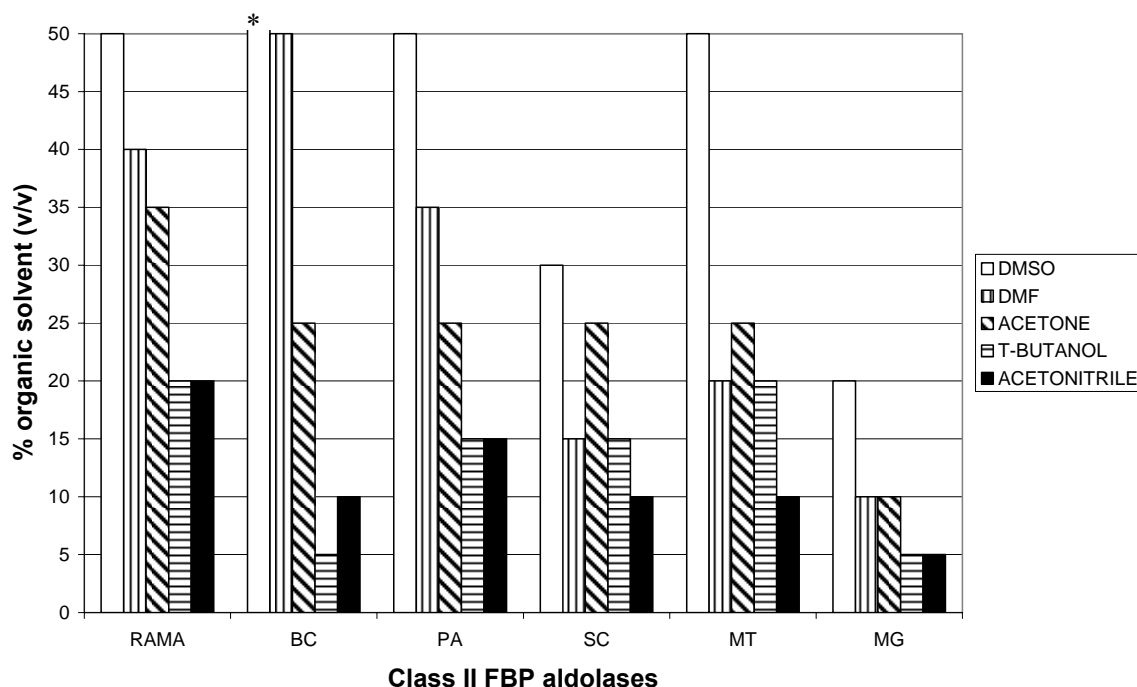


Figure 3.6 Organic solvent stability of FBP aldolases

The enzymes were pre-incubated in various solvent concentrations for 6 hours before being diluted in the assay mixture. Each bar indicates the highest concentration of organic solvent that results in the retention of more than 50% of the enzyme's activity (based on 4 replicates). The aldolases are identified according to their source organism: rabbit muscle and *S. cerevisiae* (RAMA and SC, respectively, purchased from Sigma-Aldrich, Mississauga, ON); *B. cereus* (BC); *P. aeruginosa* (PA); *M. tuberculosis* (MT); and *M. grisea* (MG). *The *B. cereus* aldolase was activated in DMSO.

The enzymes were also tested for their stability at higher temperatures. The results presented in Figure 3.7 show that the aldolase from *B. cereus* is very resistant to heat, as it retained almost half of

its activity after 10 minutes of incubation at 90°C. The other enzymes lost almost all their activity after a similar incubation at 60°C. The aldolase from *M. grisea* was again the least stable recombinant aldolase, as it lost 25% of its activity after 10 minutes of incubation at 45°C. The addition of 0.7 mM Co²⁺ during the incubation did not significantly increase the *P. aeruginosa* aldolase stability (results not shown). Note that the temperature stability of the *P. aeruginosa* and *B. cereus* aldolases were significantly reduced after long-term storage. When assayed 14 months later for example, the *B. cereus* aldolase only retained 16 ± 2% of its activity after 10 minutes of incubation at 70 °C, and had less than 2% activity after incubation at 80 °C.

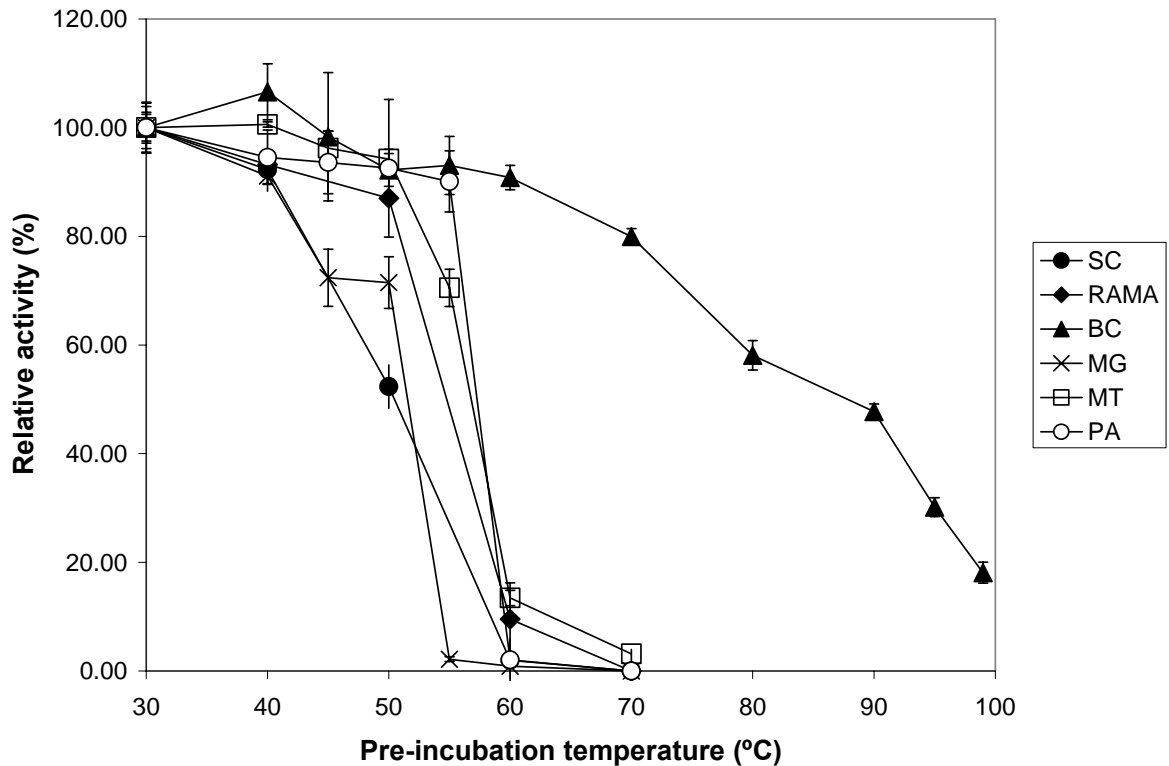


Figure 3.7 Temperature stability of the purified FBP aldolases.

The enzymes were pre-incubated for 10 minutes at the temperature indicated, cooled on ice, and assayed at 30°C. Each point represents the average of 4 replicates. The aldolases are identified according to their host organism as described in Figures 3.5 and 3.6.

Chapter 3 Characterization of recombinant Class II FBP aldolases

The stability of the aldolases at 4 °C was also monitored to ensure that the diluted enzyme would be stable while being kept on ice during the kinetic and inhibition tests done within the same day. The results shown in Figure 3.8 indicate that RAMA and the *M. tuberculosis* aldolase are stable for several days in these conditions, but that the other enzymes lose a significant amount of activity over 24 hours. The aldolases from *B. cereus* and *P. aeruginosa* are particularly unstable when diluted in the assay mixture, and lost over 95% of their activity after 24 hours. The stability of these enzymes were then tested by incubation in 5 μM of either ZnCl₂ or CoCl₂ (Figure 3.9). The results show that the aldolase from *P. aeruginosa* is stable for several days in the assay mixture supplemented with ZnCl₂. The aldolase from *B. cereus* was also significantly more stable in the presence of either metals, as it retained ~60% of its activity after 24 hours.

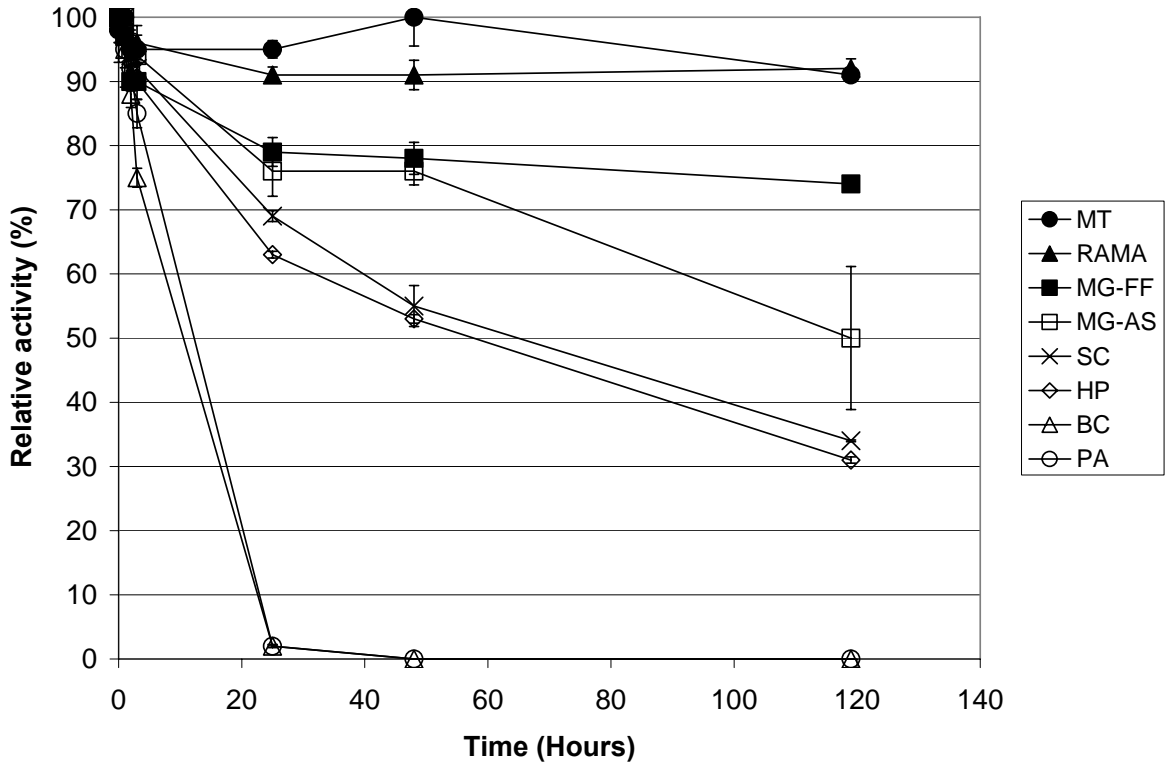


Figure 3.8 Enzyme stability in assay mixture at 4 °C

Each point represents the average of 4 replicates. The assay mixture was supplemented with 5 μM CoCl_2 in the case of the *H. pylori* aldolase (HP). The *M. grisea* aldolase originally stored both at 4 °C (in a saturated ammonium sulfate solution, MG-AS) and -80 °C (flash-frozen in liquid nitrogen, MG-FF) were tested as indicated. The other aldolases are identified according to their source organism: rabbit muscle and *S. cerevisiae* (RAMA and SC, respectively, purchased from Sigma-Aldrich, Mississauga, ON); *M. tuberculosis* (MT); *B. cereus* (BC); and *P. aeruginosa* (PA).

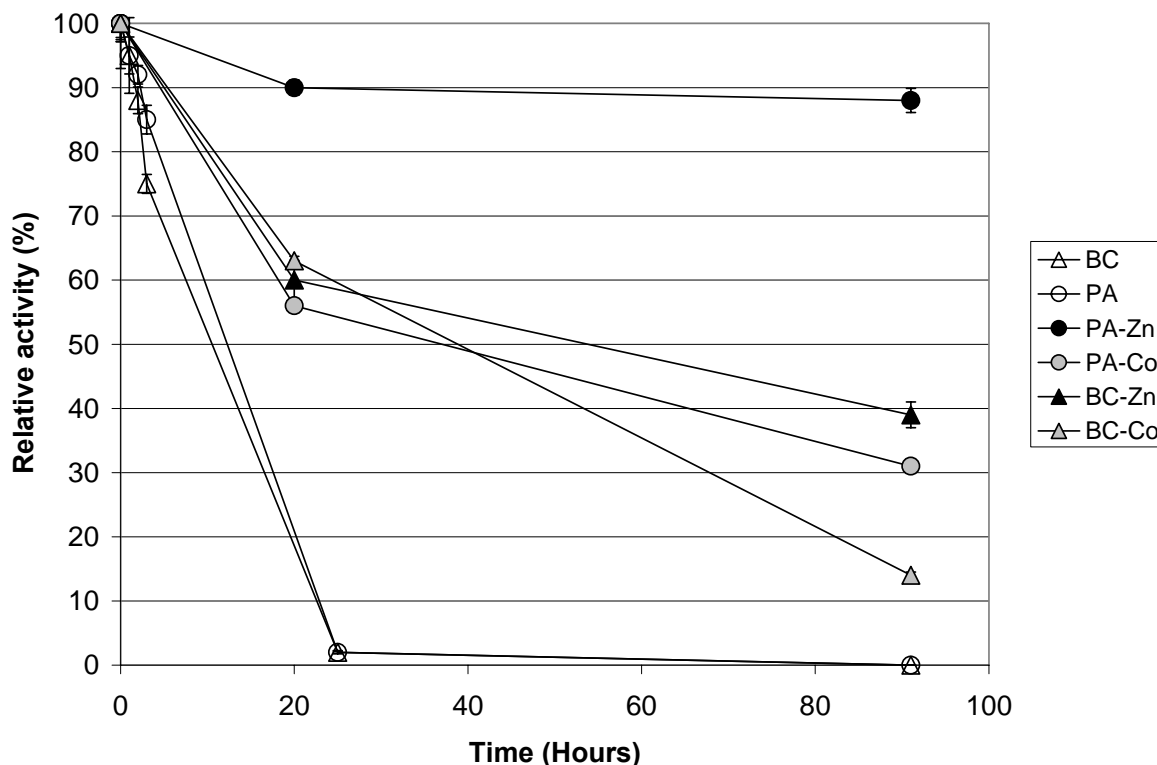


Figure 3.9 Stability of the *B. cereus* and *P. aeruginosa* aldolases in the assay mixture at 4 °C

The enzymes were incubated without metal (data from Figure 3.8, hollow symbols), and with 5 μM ZnCl_2 (PA-Zn and BC-Zn, solid black symbols) or 5 μM CoCl_2 (PA-Co and BC-Co, solid grey symbols). Each point represents the average of 4 replicates.

3.3.4 Metal content and metal specificity

The zinc content of the purified aldolases is shown in Table 3.2. The Zn^{2+} is tightly bound to the enzyme, and as a consequence the aldolases need to be denatured to release their Zn^{2+} ions. Using a colorimetric assay with PAR, we determined that the purified *M. grisea* aldolase had a zinc content 0.83 ± 0.05 per subunit. The enzyme had in that case been pre-incubated with 6 M guanidine-HCl for 30 minutes at 90 °C prior to the PAR addition. The other Class II type A aldolases from *E. coli*, *S. cerevisiae* and *M. tuberculosis* are also zinc-dependent (Ramsaywak *et al.* 2004; Scamuffa and Caprioli 1980; Harris *et al.* 1969). *M. tuberculosis* FBP aldolase zinc content was calculated to be

0.54 ± 0.09 per subunit using the PAR test after incubation at room temperature in 4M guanidine-HCl for 30 to 45 minutes (no heating). The PAR assay was later done after heating two other samples from separate *M. tuberculosis* purifications (specific activity 33 U/mg) at 93 °C for 30 minutes followed by a cooling on ice. The zinc content obtained by this method was 49.4 ± 0.8%.

Table 3.2 Zinc content of the recombinant aldolases

Source*	Zinc content (per subunit)	Denaturation conditions
<i>M. grisea</i>	0.83 ± 0.05	6 M Guanidine-HCl 90 °C for 30 minutes
<i>M. tuberculosis</i>	0.494 ± 0.008	4 M Guanidine-HCl 93 °C for 30 minutes
<i>B. cereus</i>	0.97 ± 0.10	4 M Guanidine-HCl 85 °C for 60 minutes and 25 °C for 4 days
<i>P. aeruginosa</i>	0.16 ± 0.02	4 M Guanidine-HCl 85 °C for 60 minutes and 25 °C for 4 days

*The *H. pylori* aldolase was not tested because Co²⁺ is added to the purified enzyme for stability.

The *B. cereus* aldolase had an apparent zinc content of 0.82 ± 0.08 per subunit immediately after the PAR test preceded by 1 hour incubation at 85 °C in 4M Guanidine-HCl. However 4 days later the absorbance of the enzyme samples left at room temperature in the presence of PAR had increased significantly and the zinc content was calculated to be 97 ± 10%. It seems like the enzyme was not fully denatured even after the heat treatment in denaturing conditions, and still retained some of its Zn²⁺. This is consistent with the high temperature stability of this enzyme, as shown in Figure 3.7. In a similar way, the *P. aeruginosa* FBP aldolase had an apparent zinc content of 0.08 ± 0.02 per subunit immediately after the same procedure, but 4 days later the absorbance was measured again and the zinc content was 0.16 ± 0.02 per subunit. It appears that the zinc ions take a long time to leach out of

Chapter 3 Characterization of recombinant Class II FBP aldolases

these type B enzymes. The zinc content of the *H. pylori* aldolase was not determined since the purified enzyme was stored in a solution supplemented with 5 μM CoCl_2 , in addition to being only ~90% pure.

The aldolases from *P. aeruginosa* and *H. pylori* were observed to be activated by CoCl_2 . These enzymes were titrated with this metal to determine the optimal concentration to be used in the kinetic assays (Figure 3.10). The activation curve obtained with the *P. aeruginosa* aldolase mirrors that presented by others for the *P. putida* aldolase, as they also had determined that an activation peak was reached at ~0.7 mM CoCl_2 (Bang and Baumann 1978). The *H. pylori* aldolase is also activated by this metal ion, but was increasingly inhibited when the CoCl_2 concentration was higher than 5 μM .

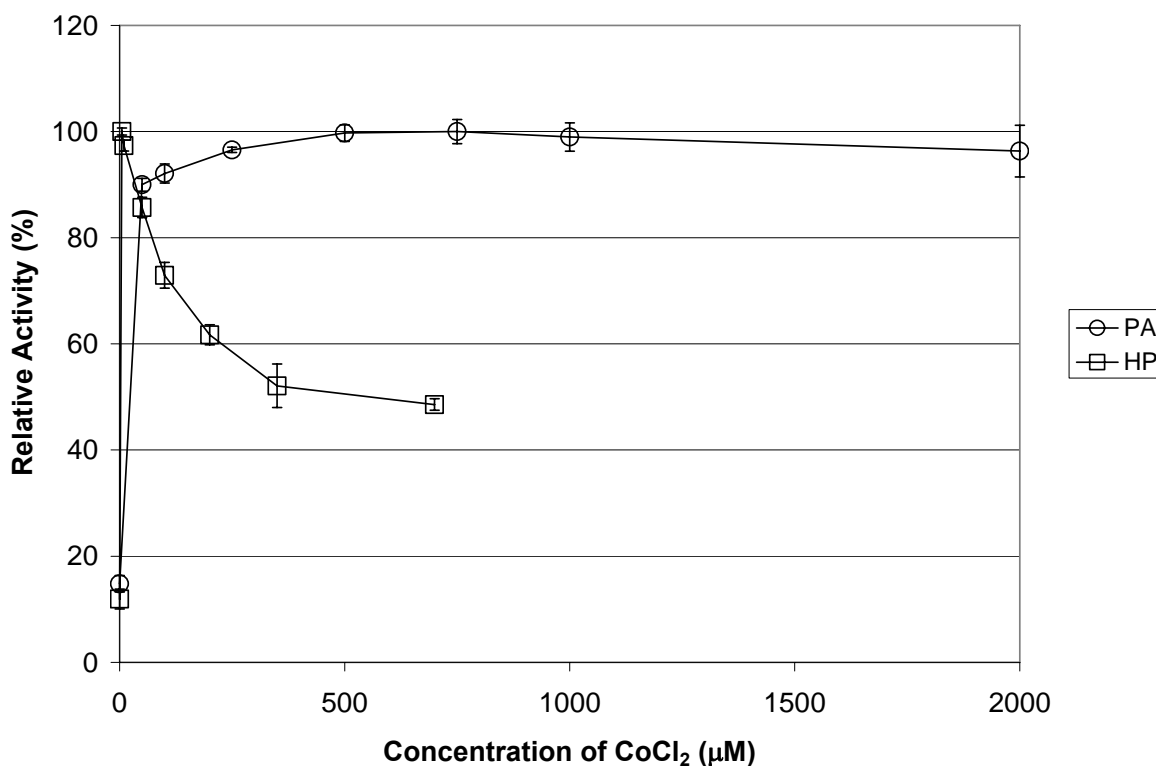


Figure 3.10 Effect of CoCl_2 on the aldolases from *P. aeruginosa* and *H. pylori*

The aldolases reached their activity peak at a CoCl_2 concentration of 0.75 mM (*P. aeruginosa*, circles) and 5 μM (*H. pylori*, squares) respectively.

Chapter 3 Characterization of recombinant Class II FBP aldolases

The metal specificity of the recombinant aldolases from *M. tuberculosis*, *B. cereus*, *P. aeruginosa* and *H. pylori* was further tested by treatment with a metal chelator, followed by reactivation with various divalent metals (Figures 3.11 and 3.12). It was observed that after a 2 hour incubation with 1 mM EDTA, *M. tuberculosis* aldolase is completely inactivated. When EDTA was removed from the enzyme using a desalting column, it was found to recover 80% of its activity when added to the assay mixture. It is possible that EDTA forms an inhibitory ternary complex with the metal ion and enzyme and the desalting column simply removes EDTA, allowing the enzyme to regain function. However, a more likely explanation would be that trace amounts of Zn^{2+} present in the assay described in section 2.2.3 are sufficient to reactivate the enzyme, making a metal-replacement study difficult to perform in the absence of a chelating agent. A typical assay would contain ~25 ng of *M. tuberculosis* aldolase per 100 μ l reaction, as well as 20 μ g BSA, which is a known zinc-binding protein (K_d of $10^{-7.6}$ M and $10^{-8.2}$ M, (Ohyoshi *et al.* 1999)). The BSA is likely to be the main source of extraneous zinc in this assay, but there could also be traces of zinc in the commercial coupling enzymes mixture and other assay components. Previous authors have noted that a zinc contamination as low as 1 ng/mL could fully reactivate the *S. cerevisiae* aldolase in a normal assay (Kobes *et al.* 1969). We therefore decided to do the metal replacement studies with a small amount of EDTA present in the assay mixture. The aldolases likely have a lower affinity for zinc than EDTA, as the dissociation constants determined previously (Henderson *et al.* 1994) for the two Zn^{2+} ions in the dimeric *E. coli* FBP aldolase are $K_1=10^{-8.9}$ M and $K_2=10^{-11.8}$ M, whereas the K_d of EDTA for zinc is approximately 10^{-16} M.

The aldolase from *M. tuberculosis* was inactivated by EDTA and desalted, leaving only a small amount of residual EDTA in the enzymatic assay. The enzyme had ~10% residual activity in the assay in the absence of added metal. Various divalent metals at a final concentration of 2 μ M were then used in the assay mixture. As a control, the enzyme not treated with EDTA was also tested by

Chapter 3 Characterization of recombinant Class II FBP aldolases

adding 2 μM of the same divalent metals to measure their effect (inhibitory or activating, see Figure 3.11). The results clearly show that the *M. tuberculosis* aldolase is a zinc-dependent enzyme, with CoCl_2 only producing a small activation (less than 30%) in the same conditions. The other metals did not significantly reactivate the enzyme relative to the control.

The aldolases from *P. aeruginosa*, *B. cereus* and *H. pylori* were in contrast more activated by the presence of CoCl_2 than ZnCl_2 after inactivation with EDTA (Figure 3.12). It is relevant to point out that there was a relatively high amount of EDTA (50 μM) in the assays done with *B. cereus* (Figure 3.12, Panel B), so the quantities of metal chlorides used for the reactivation (20 μM and 100 μM) were likely to be insufficient for a maximum reactivation. The instability of the *H. pylori* aldolase in the absence of metal also likely prevented its full reactivation. The results still indicate that CoCl_2 and CdCl_2 were able to significantly reactivate the *B. cereus* and the *H. pylori* aldolases. It is also interesting to note that MnCl_2 increased the activity of the *P. aeruginosa* aldolase by a factor 2.5 relative to its pre-inactivation activity level, whereas the CoCl_2 increased it by a factor 5.5. The results from these experiments (Figure 3.12) are only presented for qualitative purposes, as the addition of calcium chloride also partially reactivates the *B. cereus* and *H. pylori* aldolases, and appears to fully reactivate the *P. aeruginosa* aldolase to its pre-EDTA treatment activity level (Figure 3.12, Panel A). This indicates that the metal(s) trapped by the residual EDTA can be released using this protocol, as opposed to the protocol followed for the *M. tuberculosis* aldolase where CaCl_2 did not reactivate the enzyme (Figure 3.11). The levels of reactivation obtained with CaCl_2 in Figure 3.12 are assumed to indicate the limit under which the reactivation results cease to be valid.

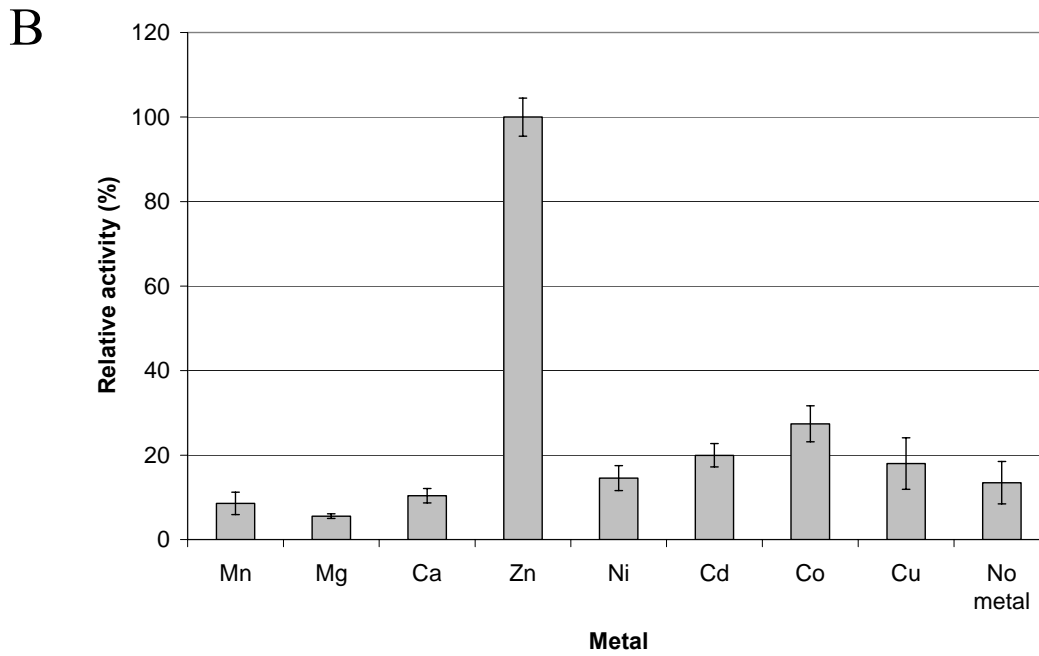
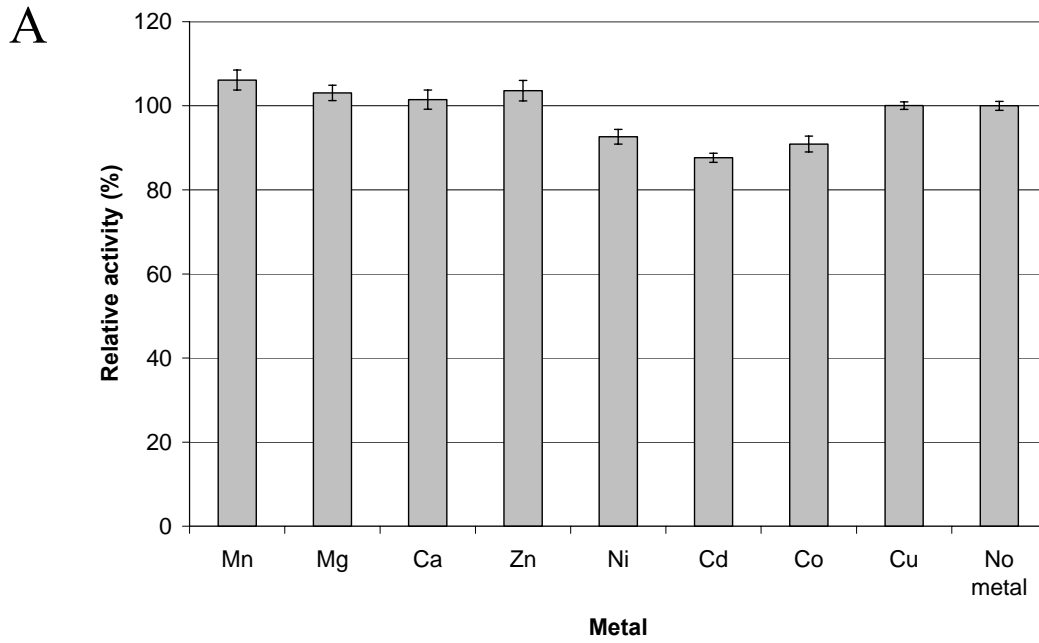


Figure 3.11 Activity of the *M. tuberculosis* aldolase in the presence of 2 μ M of various divalent metals

Chapter 3 Characterization of recombinant Class II FBP aldolases

Panel A: enzyme before EDTA treatment. Panel B: enzyme after EDTA treatment and desalting.

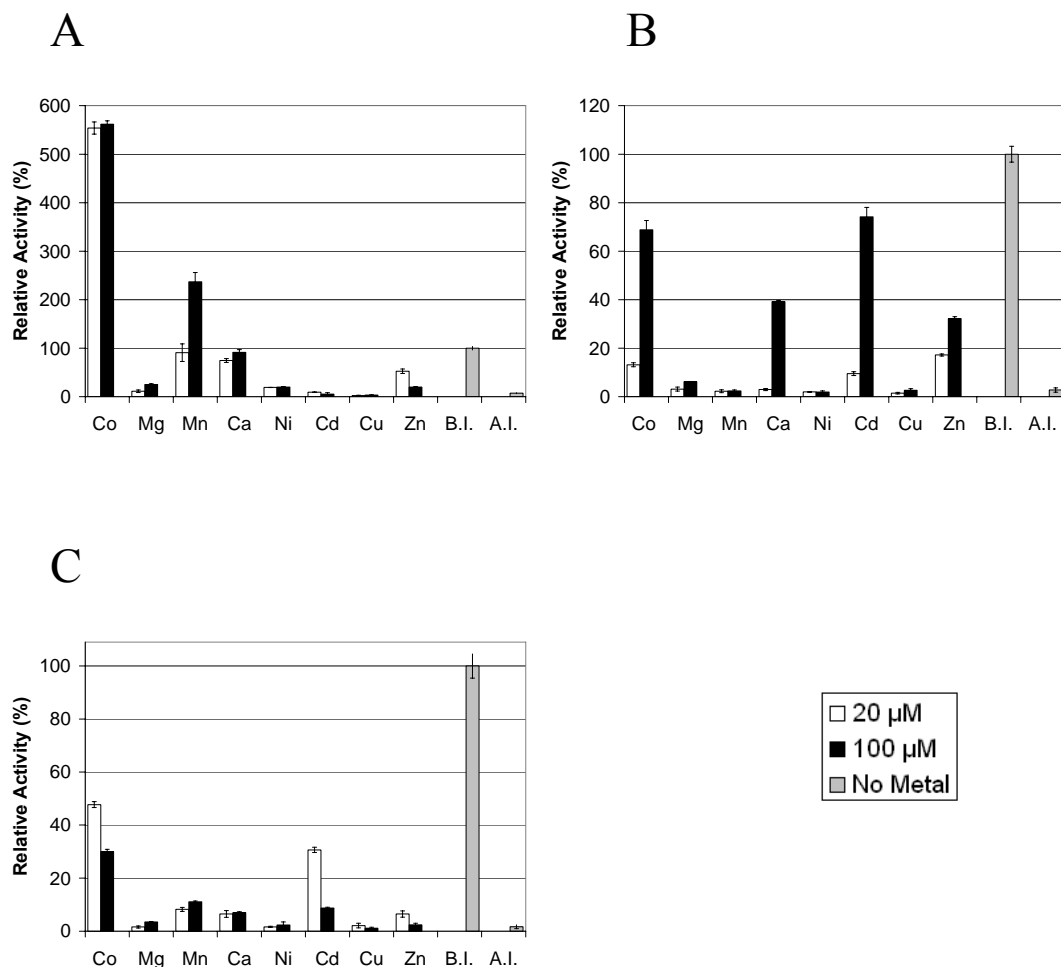


Figure 3.12 Reactivation of the FBP aldolases from *P. aeruginosa*, *B. cereus* and *H. pylori* with divalent metals after EDTA treatment

The divalent metals indicated at the bottom of the figure were added in the concentrations of 20 μM (white bars) or 100 μM (black bars). B.I. and A.I. stand for before and after inactivation, respectively, and these activities were measured without addition of divalent metal (solid grey bars). The assays measured before inactivation (B. I.) did not contain EDTA. Panel A: *P. aeruginosa* aldolase. The assay mixture contained 10 μM EDTA in addition to the divalent metal indicated. Panel B: *B. cereus* aldolase. The assay mixture contained 50 μM EDTA in addition to the divalent metal indicated. Panel C: *H. pylori* aldolase. Note that the sample before inactivation (B.I.) was assayed in the presence of 6 μM CoCl₂. The assay mixture for the other samples contained 15 μM EDTA in addition to the divalent metal indicated.

3.3.5 Kinetic parameters

The kinetic parameters determined using the coupled assay, in the presence of excess triosephosphate isomerase and α -glycerophosphate dehydrogenase, are presented in Table 3.3. The parameters were determined at pH 8.0, which is close to the Class II aldolases pH optimum (pH 7.75 to 8.0, Figure 3.5), except for the *P. aeruginosa* aldolase which is ~20% less active at pH 8.0 compared to its optimum pH 8.5. The highest k_{cat} was obtained with the *M. grisea* enzyme, but the aldolase from *M. tuberculosis* demonstrated the highest specificity for FBP, as the apparent second-order rate constant of the reaction, or $k_{\text{cat}}/K_{\text{m}}$, is $1.08 \times 10^6 \text{ M}^{-1}\cdot\text{s}^{-1}$ for this enzyme. The K_{M} of the *B. cereus* aldolase was found to be one order of magnitude greater than that of the other enzymes. The type B aldolases also have a significantly lower k_{cat} than the type A enzymes purified.

Table 3.3 Kinetic parameters and quaternary structure of recombinant Class II aldolases (this study)

Recombinant aldolase	Quaternary	K_{M} (μM)	k_{cat} (s^{-1})	Specificity
	Structure (subunits)			($k_{\text{cat}} / K_{\text{m}}$) $10^2 \mu\text{M}^{-1} \text{ s}^{-1}$
<u>TYPE A</u>				
<i>Magnaporthe grisea</i>	2	51 ± 1	45.7 ± 0.4	90 ± 2
<i>Mycobacterium tuberculosis</i>	4	27.9 ± 0.9	30.1 ± 0.3	108 ± 3
<u>TYPE B</u>				
<i>Pseudomonas aeruginosa</i>	4	35 ± 2	1.53 ± 0.02	4.4 ± 0.2
<i>Helicobacter pylori</i> *	2	66 ± 1	2.87 ± 0.02	4.35 ± 0.07
<i>Bacillus cereus</i>	2	450 ± 10	2.95 ± 0.03	0.66 ± 0.01

Activity determined in Tris-HCl pH 8.0, at 30 °C. Kinetic parameters were estimated by fitting the data to the Michaelis-Menten equation using the least squares and dynamic weighing options of the Leonora software program (Cornish-Bowden 1995). * Assays done in the presence of 5 μM CoCl_2 .

Chapter 3 Characterization of recombinant Class II FBP aldolases

A study on the aldol condensation reaction using GAP and DHAP as substrates was also attempted using a colorimetric method described by Roe and collaborators (Roe *et al.* 1949), with modifications introduced by Collins (Collins 1974). The method is based on the fact that the sugar FBP is reductive and can react with resorcinol in certain conditions to give a colored product that can be monitored spectrophotometrically at λ 520 nm. Unfortunately, it was found that the triose phosphates also react with resorcinol to a significant extent using this method, making a kinetic analysis unreliable due to background noise from the reactants. This problem had also been noted earlier by other authors (Lewis and Lowe 1977). An alternative method such as the oxidation of the carbanion intermediate by hexacyanoferrate (III) (Healy and Christen 1973) should instead be used for the aldol condensation kinetic analysis. This method however results in the indiscriminate detection of carbanion formation in both the aldol condensation and aldol cleavage reactions, and of course only allows the monitoring of the half reaction (the reagent oxidizes the enediolate intermediate shown in Figure 1.12). One other problem that we have noted with the hexacyanoferrate assay is that the extinction coefficient ($1,000 \text{ M}^{-1} \text{ cm}^{-1}$ at λ 420 nm) is ~ 6 times lower than that of NADH ($6,220 \text{ M}^{-1} \text{ cm}^{-1}$ at λ 340 nm), and this combined with the high concentration required to achieve a 100% turnover detection, results in the assays being done near the detection limits of the spectrophotometer, which in turn results in a high standard deviation. Alternatively, a stopped coupled assay using NADH as the reporter molecule described by (Lewis and Lowe 1977) could also be used to monitor the aldol condensation, although the procedure is work-intensive.

3.4 Discussion

The *M. grisea* aldolase was found to be dimeric in this study, like its close relative the yeast FBP aldolase. All other Class II Type A FBP aldolases characterized previously are dimers with

Chapter 3 Characterization of recombinant Class II FBP aldolases

molecular masses of approximately 80 kDa (Table 3.1), except for the *M. tuberculosis* FBP aldolase which was found to be a tetramer by our group (Ramsaywak *et al.* 2004).

The Class II Type B aldolase from *P. aeruginosa* was also determined to be a tetramer in this study. There are both dimeric and tetrameric Class II Type B aldolases, as shown in Table 3.1, and even an octameric enzyme (*Synechocystis* sp. PCC6803 FBP aldolase, (Nakahara *et al.* 2003)), as mentioned above in section 1.3.4. The recombinant *H. pylori* aldolase purified here was too unstable to allow the determination of its quaternary structure, but Sauv  and Sygusch (2001b) reported that the recombinant enzyme from that organism migrated like a tetramer on non-denaturing gels. In contrast, the recombinant *B. cereus* aldolase was found to be a dimer, as was reported for the enzyme purified from the native host (Sadoff *et al.* 1969).

Sauv  and Sygusch (2001b) suggested that a 21 amino acid insertion between the α -helix 9 and β -sheet 8 (see alignment in Figure 1.17) in Class II aldolases correlated with a tetrameric quaternary structure. While this is true for the *P. aeruginosa* and *B. cereus* Type B enzymes, the *M. tuberculosis* Class II aldolase (Type A) does not possess this insertion but is tetrameric. The quaternary structure of the type A Class II FBP aldolases therefore does not appear to correlate with the identifiable insertion in the amino acid sequence, contrary to the suggestion of Sauv  and Sygusch (2001b).

The Class I FBP aldolases have a broad optimal pH range, usually extending from 7 to 9 (Rutter 1964). In contrast, the Class II aldolases have a sharp pH optimum which usually peaks between pH 7.5 and 8 (Rutter 1964), and this was confirmed by the results obtained in this study. The aldolase from *P. aeruginosa* is an exception, as its pH optimum curve was found to be shifted towards more alkaline conditions, with a peak at pH 8.5. The pH optimum recorded for *P. aeruginosa* is identical to that recorded previously for the *P. putida* aldolase (Bang and Baumann 1978). The pH optimum recorded for the recombinant *M. tuberculosis* Class II aldolase in this study is also consistent with that

Chapter 3 Characterization of recombinant Class II FBP aldolases

reported previously for the enzyme purified from the native host (Bai *et al.* 1975; 1974). However, the *B. cereus* aldolase purified from its native host had a pH optimum between 8 and 9 (Sadoff *et al.* 1969), whereas the recombinant enzyme purified from *E. coli* had a pH optimum of 7.8 to 8.0. Sadoff *et al.* (1969) used a different coupled assay than the one used in the present study to determine the enzyme's activity. The assay involved the use of the coupling enzyme glyceraldehyde-3-phosphate dehydrogenase which reduces NAD⁺ in the presence of arsenate as the GAP product is formed. The different assay conditions could explain the discrepancy with our value. Alternatively, the protein may be post-translationally modified in the native host or the divalent metal used by the aldolase in its native host could also be different than the one present in the recombinant enzyme (which was found to have one zinc per subunit), as will be discussed below.

There have been reports that the Class II aldolase from *E. coli* is more stable than the Class I rabbit muscle aldolase (RAMA), and consequently that the Class II enzymes could be better suited for organic synthesis (Takayama *et al.* 1997; Henderson *et al.* 1994; Von der Osten *et al.* 1989). In this study however, we found that the recombinant Class II aldolases are usually less stable than RAMA in the coupled assay mixture and in various organic solvents. Only the *M. tuberculosis* and *P. aeruginosa* enzymes have a comparable stability to RAMA. However, the *P. aeruginosa* aldolase has to be stabilized by adding exogenous zinc chloride. The *B. cereus* aldolase was however found to be significantly more stable than RAMA at high temperatures. This organism is not thermophilic, but it produces thermotolerant spores that may necessitate enzymes with higher stability with regards to temperature. As mentioned above, Sauv e and Sygusch (2001b) have speculated that a 21 amino acid insertion between the α -helix 9 and β -sheet 8 (see alignment in Figure 1.17) in Class II aldolases potentially stabilized a tetrameric quaternary structure, and possibly conferred thermostability to the enzymes. However, the dimeric *B. cereus* does not possess this insertion and is significantly more thermostable than the tetrameric *P. aeruginosa* aldolase, which does have this insertion. The

Chapter 3 Characterization of recombinant Class II FBP aldolases

tetrameric quaternary structure therefore does not seem to confer a greater stability than the dimeric structure in the aldolases studied here, contrary to the suggestion by Sauvé and Sygusch (2001b). The higher temperature stability may instead result from the compact structure of the *B. cereus* enzyme, as it has the smallest subunit size amongst the enzymes tested (see Figure 2.15). Considering its exceptional temperature stability, it is very surprising that the *B. cereus* aldolase was found to be the most unstable when diluted in the enzymatic assay solution at 4 °C (Figures 3.8 and 3.9). The assay component which causes this instability has not been identified, but the fact that the enzyme is stabilized by the addition of divalent metal indicates that the *B. cereus* aldolase may bind its metal cofactor loosely. It may also be the case for the *P. aeruginosa* aldolase.

The recombinant Class II Type A aldolases from *M. grisea* and *M. tuberculosis* contain 0.8 and 0.5 Zn²⁺ ion per monomer as determined by the PAR assay. This is confirmed using ICP-MS in the case of the *M. tuberculosis* aldolase (Ramsaywak *et al.* 2004). The low zinc content for the *M. tuberculosis* enzyme may be due to the metal ions leaching out of the enzyme active site when exposed to a zinc-free buffer. The *Mycobacterium* enzyme prepared in a metal-free buffer still demonstrated a specific activity of 35 U/mg when transferred to the assay mixture. No extra metal was added to the assay mixture, however, this mixture was not metal-free, and the contamination with as little as 1 ng/mL Zn²⁺ in a similar assay mixture was previously reported to be sufficient to fully activate the yeast FBP aldolase apoenzyme (Kobes *et al.* 1969). The addition of ZnCl₂ to the assay did not increase the specific activity of the recombinant enzyme. The presence of substrate may result in a drastic increase of the affinity of the enzyme for zinc ions, as previously reported for metallo-β-lactamases (Wommer *et al.* 2002). Incubation of the *M. tuberculosis* aldolase with 1 mM EDTA completely abolished its catalytic activity, in agreement with observations by Bai and collaborators (Bai *et al.* 1974). The activity of the EDTA-inactivated enzyme was restored upon the addition of 2 μM Zn²⁺ and was restored to about 30% with the addition of 2 μM Co²⁺. The addition

Chapter 3 Characterization of recombinant Class II FBP aldolases

of Cu^{2+} , Ni^{2+} , Cd^{2+} , Mn^{2+} or Mg^{2+} did not reactivate the enzyme significantly. These results indicate that the *M. tuberculosis* and *M. grisea* Class II FBP aldolases are likely zinc-dependent enzymes, like the other Class II Type A FBP aldolases from *E. coli*, *G. lamblia*, and *S. cerevisiae* characterized previously (Galkin *et al.* 2007; Hall *et al.* 2003; Rutter and Ling 1958).

The recombinant *B. cereus* aldolase, a Type B enzyme, has a metal content of 1 Zn^{2+} ion per monomer. However, the other Type B aldolase from *P. aeruginosa* had a Zn^{2+} content of about 0.16 ion per subunit. The specific activity of this enzyme was increased by a factor 6 (Figure 3.10) in the presence of 0.7 mM cobalt chloride. Bang and Baumann (1978) had also reported that the partially purified *P. putida* aldolase's activity was completely dependent on the presence of added cobalt, and they obtained a specific activity of ~0.5 U/mg in the presence of 0.7 mM cobalt chloride, which is ~50-fold lower than the specific activity of the pure recombinant enzyme from *P. aeruginosa* in the same conditions reported in this thesis. The low zinc content and low activity (in the absence of CoCl_2) of the recombinant enzyme therefore does not appear to be a consequence of the use of an *E. coli* expression system. The specific activity of the recombinant *P. aeruginosa* aldolase was also increased more than twofold after EDTA inactivation followed by the addition of 100 μM manganese (II)-chloride. The zinc-dependent *E. coli* and yeast aldolases have also been reported previously to be activated by Mn^{2+} and Co^{2+} , although only Zn^{2+} could fully restore the yeast aldolase's activity (Stribling and Perham 1973; Kobes *et al.* 1969; Knox *et al.* 1948). It is unclear which metal ion the *P. aeruginosa* aldolase utilizes *in vivo*, because of the very high concentration of Co^{2+} required to fully activate it. The specific activity of the *B. cereus* aldolase was partially restored after EDTA inactivation by Co^{2+} and Cd^{2+} , in addition to Zn^{2+} , but not significantly restored by Cu^{2+} , Mn^{2+} , Mg^{2+} , or Ni^{2+} . The addition of Co^{2+} to the purified *B. cereus* aldolase did not increase the specific activity. Sadoff *et al.* (1969) have reported inconsistent results for the effect of divalent metal ions on the purified *B. cereus* aldolase activity. The enzyme they purified from vegetative *B. cereus* cells had a

Chapter 3 Characterization of recombinant Class II FBP aldolases

reported specific activity of 58 U/mg, a value significantly higher than that obtained for our recombinant enzyme (Sadoff *et al.* 1969), which is surprising considering that the recombinant enzyme's active sites appears fully occupied by zinc.

There are wide variations in the apparent catalytic parameters of both types of Class II aldolases, as can be seen in Tables 3.1 and 3.3. The observed turnover number of the mycobacterial enzyme is higher than those reported for other Class II Type A FBP aldolases, such as from *E. coli* (10.5 s^{-1}) or *Euglena gracilis* (14.1 s^{-1}) (Plater *et al.* 1999; Pelzer-Reith *et al.* 1994), but lower than the k_{cat} values reported for the FBP aldolase of *S. cerevisiae* (57.5 s^{-1}) (Kadonaga and Knowles 1983) (Table 3.1). Note that a specific activity of 150 U/mg (100 s^{-1}) was also reported for the yeast enzyme assayed at $30 \text{ }^{\circ}\text{C}$ (Belasco and Knowles 1983), which is over two times higher than the turnover number obtained in this study with the recombinant *M. grisea* aldolase (k_{cat} of 45.7 s^{-1} at $30 \text{ }^{\circ}\text{C}$), which shares 66% amino acid sequence identity with the yeast enzyme. The apparent K_{M} of the *M. tuberculosis* aldolase was the lowest among all the characterized Type A FBP aldolases, with K_{M} of 170, 175 and $370 \text{ }\mu\text{M}$ for the enzymes from *E. coli*, *E. gracilis*, and *S. cerevisiae*, respectively (Plater *et al.* 1999; Pelzer-Reith *et al.* 1994; Rutter 1964), and $51 \text{ }\mu\text{M}$ for the *M. grisea* enzyme characterized in this study, which gives the mycobacterial enzyme the highest catalytic efficiency ($k_{\text{cat}}/K_{\text{M}}$) for FBP cleavage.

Among the Type B FBP aldolases that have been characterized, most have an apparent K_{M} between 160 and $300 \text{ }\mu\text{M}$ for FBP (Sauve and Sygusch 2001b; Willard and Gibbs 1968a; Rutter 1964). However, the Co^{2+} form of the dimeric *Bacillus stearothermophilus* enzyme has an apparent K_{M} of $4.55 \text{ }\mu\text{M}$ for FBP, and the octameric Type B FBP aldolase from *Synechocystis* sp. PCC 6803 has a K_{M} of $8 \text{ }\mu\text{M}$ (Nakahara *et al.* 2003; Hill *et al.* 1976). The value reported by Sadoff and collaborators for the K_{M} of the *B. cereus* aldolase (2 mM) is much higher than the one we determined using our NADH-linked assay ($450 \text{ }\mu\text{M}$). By contrast, the K_{M} value reported for the *P. putida*

Chapter 3 Characterization of recombinant Class II FBP aldolases

aldolase by Bang and Baumann (30 μM) using the same coupled assay used in this study is equivalent to the one we determined (34 μM) (Bang and Baumann 1978; Sadoff *et al.* 1969). Although the *H. pylori* aldolase was cloned and expressed in *E. coli* and purified previously, no kinetic parameters were reported (Sauve and Sygusch 2001b). The K_M obtained in the present study for the *H. pylori* aldolase (66 μM) is in the same range as those obtained with the other recombinant aldolases except for the *Bacillus* enzyme. The k_{cat} of all three type B recombinant aldolases are between 1.5 s^{-1} and 3 s^{-1} , which is one order of magnitude lower than most k_{cat} values obtained for other type B enzymes (Table 3.1). There are at least two other type B enzymes which have a turnover number lower than 10 s^{-1} (*Bacillus stearothermophilus* and *Synechocystis* sp. PCC6803), but these aldolases also have very low K_M and thus their specificity for FBP is at least one order of magnitude higher than the type B enzymes characterized in the present project. It is unclear if these low values are the result of the expression of these type B aldolases in *E. coli*, or if the low turnover number is an actual characteristic of these aldolases.

One of the most variable regions between the two types of aldolases, as determined from the alignment reported by Sauvé and Sygusch (2001b), is the long flexible $\beta 5$ - $\alpha 7$ loop that was shown to close over the active site during catalysis in the *E. coli* FBP aldolase (see Figures 1.15 and 1.17). As described in section 1.3.5, this loop contains a glutamate residue critical for catalysis and was shown to undergo movements of more than 5 Å upon DHAP binding (Zgiby *et al.* 2002). The composition and length of this loop may play a major role in the aldolase catalytic efficiency. A 3D overlay alignment of the *E. coli* aldolase crystallographic structures with models of other type A aldolases threaded through the structure using the SwissModel software (Schwede *et al.* 2003) revealed that all the amino acids located within 7 Å of the zinc atom are completely conserved among Class II aldolases (~30 residues, see sequence alignments in Figures 1.10 and 1.17). The enzyme's kinetic parameters could be dependent on the residues present in the mobile loops, which close over the

Chapter 3 Characterization of recombinant Class II FBP aldolases

active site during catalysis and are missing from the crystal structures (Section 1.3.6). In the sequence alignments (Figures 1.10 and 1.17), there are notable differences in the composition of the small mobile loop (residues 224 to 238) of the *S. cerevisiae* FBP aldolase compared with the other type A aldolases. This loop contains a histidine residue which is a ligand for the active site zinc ion. This ion is mobile in a Class II FBP aldolase and moves from a buried position to a solvent-exposed position upon substrate binding (Figure 1.9). The sequence differences in this loop may partially account for the observed variation in kinetic parameters between the Class II FBP aldolases. The loop mobility will be the subject of Chapter 5.

A crystal structure was obtained for the *M. grisea* FBP aldolase purified in this study. The availability of the crystal structures of the other recombinant Class II FBP aldolases would be useful to identify the residues determining the quaternary structure and the specificity of these enzymes.

The lack of availability of an accurate and direct colorimetric assay to monitor the FBP aldolase activity is a serious hindrance for both the metal utilization analysis and for the aldol condensation reaction. A colored reporter substrate would be a useful tool for these purposes.

Chapter 4

Inhibition of Class II FBP aldolases

4.1 Introduction

In this project, a series of commercially available and synthetic compounds were to be screened to determine which ones can be used as starting points for rational ligand design for this enzyme. A few known inhibitors of Class II aldolases, all derivatives of the reaction intermediate analogue PGH, have been presented in section 1.4.4 (Figure 1.16, p.47) (Gavalda *et al.* 2005; Fonvielle *et al.* 2004; Lewis and Lowe 1973). However, as discussed in that section, PGH is a potent inhibitor of other enzymes which use DHAP as a substrate, and therefore it is likely to be toxic. Although some of the PGH derivatives appear to specifically inhibit the Class II aldolases, none of them possess the low nM-range inhibition capacity of the parent compound. The usual starting point for inhibitor design is the enzyme's natural substrate, but in this project the emphasis will be on compounds which first and foremost have some affinity for the metal ion that is unique to Class II aldolases, as the toxic cross-inhibition of Class I aldolases is to be avoided.

The effectiveness of a drug depends on ADME/Tox/PK/PD (adsorption, distribution, metabolism, excretion, toxicology, pharmacokinetics, pharmacodynamics) factors more than it depends on the affinity constant of the compound for its target (Whitesides and Krishnamurthy 2005) and that is beyond the scope of this doctoral project, even though drug design is indeed the long-term objective of this research. However, it is useful to have a general idea of which chemical structures have been successful in medicine, in order to guide the choice of a starting molecule for rational design. Even though the metal-chelating compounds listed in section 1.4.1 are not used to target specific enzymes

Chapter 4 Inhibition of Class II FBP aldolases

in medicine, some drugs possess metal-chelating functions such as a hydroxamic acid group, which is found in PGH. For example, several compounds used in clinical trials as metalloprotease inhibitors for cancer therapy have a hydroxamic acid function (Giavazzi and Taraboletti 2001). There are, however, significant side-effects associated with some of these drugs with hydroxamic functions (Rosenblum *et al.* 2003) and because of this, other metal-binding moieties such as thiols and carboxylates will be the focus of this project. Since possibly 2800 different proteins that are zinc-binding are encoded by the human genome (Andreini *et al.* 2006), the specificity of the zinc-chelating drugs is crucial to avoid toxicity.

Our chosen approach to obtain novel drug candidates that are non-toxic to humans or plants is to modify metal chelating compounds that specifically inhibit the Class II aldolase over the mammalian Class I aldolase. Ultimately the synthesized compounds should be specific inhibitors of the Class II enzymes and form a stable ternary complex with the enzyme and the active-site zinc, instead of promoting the release of the catalytic zinc ion (non-complexing inhibition). An example of structurally similar chelating inhibitors (D-cysteine and D-penicillamine) that display complexing versus non-complexing inhibition patterns with the zinc protease carboxypeptidase A, has been presented previously (Chong and Auld 2000).

In this chapter, the results of studies of several commercial and newly synthesized metal-binding compounds will be described in terms of their capacity to inhibit the Class II FBP aldolases from *M. tuberculosis*, *M. grisea*, *P. aeruginosa*, *B. cereus*, *S. cerevisiae* and *E. coli*. The Class I FBP aldolase from rabbit muscle was used as a negative control to assess the specificity of the compounds for the Class II enzymes. The inhibition kinetics of the most potent compounds with the aldolase from *M. tuberculosis* and the stability of the enzyme-inhibitor complexes will be discussed. The results will be compared with those obtained with other known Class II FBP aldolase inhibitors.

Some of the work presented in this chapter was performed by fellow graduate students, and by undergraduate students under my supervision. Some of the inhibition kinetic assays were done by M.Sc. student Peggy Ramsaywak, and by NSERC summer Undergraduate Student Research Award (USRA) recipient Sarah de Groot. The commercially available inhibitory compounds were obtained from Sigma-Aldrich (Mississauga, ON) and the other inhibitory compounds were synthesized in the laboratory of Dr. G.I. Dmitrienko (Dept. of Chemistry, University of Waterloo) by Ph.D. students Matt D. Brown and Anthony Krismanich, by USRA recipient Tim Rasmusson, and by post-doctoral fellow Muhong Shang. The molecular modeling was done with the help of Timothy Ramadhar.

4.2 Procedures

4.2.1 Inhibition screens

The standard assay mixture (final volume 100 μ L) contained the FBP aldolase (0.003 to 0.020 U/mL), 0.3 mM NADH, 0.2 U/mL of rabbit muscle α -glycerophosphate dehydrogenase, 2.25 U/mL of rabbit muscle triose phosphate isomerase, 0.2 mg/mL BSA, 100 mM potassium acetate, 5% v/v DMSO and 23.75 mM Hepes, pH 7.3 (see coupled reaction scheme presented in Figure 2.1). The molecular weights and laboratory codes of the compounds synthesized in Dr. Dmitrienko's laboratory are shown in Appendix B. The structure of each of the synthetic inhibitors was established by ^1H NMR (300MHz), ^{13}C NMR (75 MHz), and mass spectrometry. The purity of the compounds was assessed to be greater than 95% by examination of the ^1H NMR spectra. The molecules tested for inhibition (except compounds **4** and **6**, shown in Figure 4.2) were dissolved in 100% DMSO to produce 100 mM stock solutions. The compound **4** was instead dissolved in 50% DMSO, 50% 25 mM Hepes pH 7.3 to produce a 50 mM stock solution, and the compound **6** was dissolved directly in 50 mM Hepes, pH 7.3 to produce a 50 mM stock solution. DPA and compound **7** were further diluted with DMSO to a concentration of 20 mM prior to their addition to the assay mixture. The

Chapter 4 Inhibition of Class II FBP aldolases

compound EDTA was diluted in the Hepes buffer and tested in the same way but without DMSO. These compounds were incubated with the enzyme mixture for 15 minutes prior to the addition of the substrate FBP. Assays were performed at 25 °C in quadruplicate in 96-well flat bottom polystyrene plates (Corning, NY). The reaction was initiated by the addition of FBP (final concentration 30 or 200 μM) and monitored at 340 nm for 10 minutes on a 96-well plate reader (Spectramax 190, Molecular Devices, Sunnyvale, CA).

4.2.2 Inhibition assays (IC_{50}s)

The assays were done as described above, but in 50 mM Hepes buffer pH 7.3 at 28 °C. The FBP concentration was at least 10 times the enzyme's K_M . The concentration of inhibitor was varied depending on the amount of inhibition recorded, but inhibitor concentrations of 20, 50, 75, 100, 200, 500, and 1000 μM were typically used to determine the IC_{50}s . The enzymes were pre-incubated with the inhibitor for 15 minutes in the coupled assay mixture prior to the addition of the substrate FBP. The compound **6** was freshly dissolved prior to the kinetic assays as it became less potent during long-term storage in solution. The molecular weights and laboratory codes of the compounds synthesized in Dr. Dmitrienko's laboratory are shown in Appendix B. The commercial compounds tested were purchased from Sigma-Aldrich (Mississauga, ON) and were freshly diluted in buffer prior to the assays.

4.2.3 Metal reactivation assays

The assays were done as described in section 4.2.1, with the following modifications. The reaction was monitored in a 1 cm pathlength quartz cuvette in a Varian Cary 1 UV-Visible spectrophotometer (Varian, Mississauga, ON). The assay final volume was 1 mL, and the BSA was omitted from the reaction. The reaction was started by addition of 3 nM of *M. tuberculosis* aldolase to the cuvette containing 500 μM of FBP and 500 μM of inhibitor. Small volumes of a 1 mM ZnCl_2 solution were

subsequently added to reactivate the enzyme. The NADH coefficient of extinction used to calculate the aldolase activity was $6220 \text{ M}^{-1}\text{cm}^{-1}$.

4.2.4 Second order rate constants determination

The *M. tuberculosis* aldolase was used for these assays. Four replicates were done for each combination of substrate and inhibitor concentrations, and the reaction was monitored by absorbance readings every six seconds for 10 minutes using the coupled assay described in section 2.2.3. The assays were started by addition of the enzyme to the substrate and inhibitor mixture, without pre-incubation of the enzyme with the inhibitor. The FBP concentrations used were 25, 40, 60, 80, 120, 200, and 500 μM . The inhibitor concentrations were 20, 50, 100 and 500 μM of DMPS and DPA; 20, 50 and 500 μM of compound **6**; 20, 50 and 100 μM of compound **13**, and 50, 100 and 500 μM of EDTA. The Equations 4.1 and 4.2 (Morrison and Walsh 1988; Tsou 1988) presented below were fitted to each progress curve by non-linear regression using automatic outlier elimination (Rout coefficient Q set to 1% to exclude outliers, with no weighing) to obtain the apparent constants k or A using the GraphPad Prism software (GraphPad Software Inc, La Jolla, CA). A secondary plot of the apparent constant A multiplied by the inhibitor concentration versus the FBP concentration was then performed to obtain the constant k_{+0} for each inhibitor (Equation 4.3), again using non-linear regression with GraphPad Prism as described above. The equations are described in more detail in Appendix C.

Equation 4.1 (reversible inhibition)
$$[P]_t = v_s t + (v_0 - v_s) (1 - e^{-kt}) / k$$

Equation 4.2 (irreversible inhibition)
$$[P]_t = (v_0 / [I]A) (1 - e^{-[I]At})$$

When t approaches infinity, Equation 4.2 becomes:
$$[P]_\infty = (v_0 / [I]A)$$

Equation 4.3 (competitive irreversible inhibition)
$$A = k_{+0} / (1 + [S] / K_M)$$

Chapter 4 Inhibition of Class II FBP aldolases

where $[P]_t$ is the concentration of product formed at time t , v_0 is the initial velocity, v_s is the end velocity, $[I]$ is inhibitor concentration, $[S]$ is the concentration of substrate, K_M is the Michaelis constant, and k_{+0} is the second order rate constant for the binding of the competitive inhibitor (Figure 4.1). The description of the apparent constants k and A depends on the type of inhibition (Competitive, Noncompetitive or Uncompetitive, see Appendix C). Note that the constant k in Equation 4.1 is equivalent to $[I]*A$ in Equation 4.2.

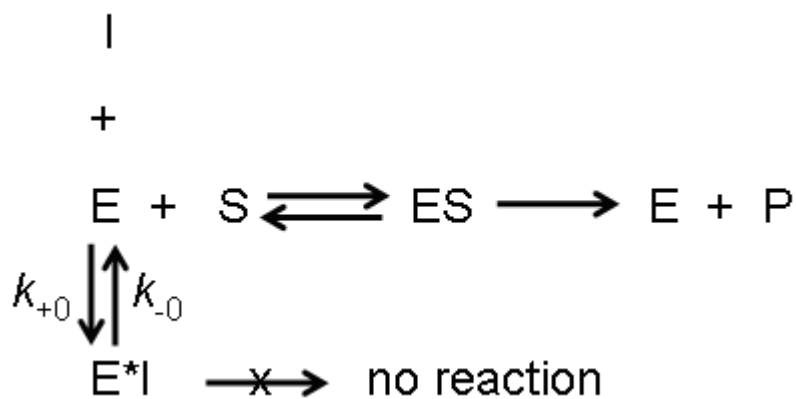


Figure 4.1 Scheme of competitive reversible inhibition with associated rate constants

4.3 Results

4.3.1 Inhibition screens

The first set of compounds (DPA and compounds **1** to **7**, Figure 4.2), as well as the metal chelator EDTA, were tested for their inhibition of the FBP cleavage reaction by the *M. tuberculosis* aldolase, and the results obtained with 1 mM of these compounds are presented in Table 4.1. The chelators EDTA and DPA completely inhibited the enzyme, whereas the DPA derivatives **1** and **6** partially inhibited the reaction (36% and 89% inhibition, respectively) after 15 minutes of pre-incubation. The remaining compounds were comparatively poor inhibitors.

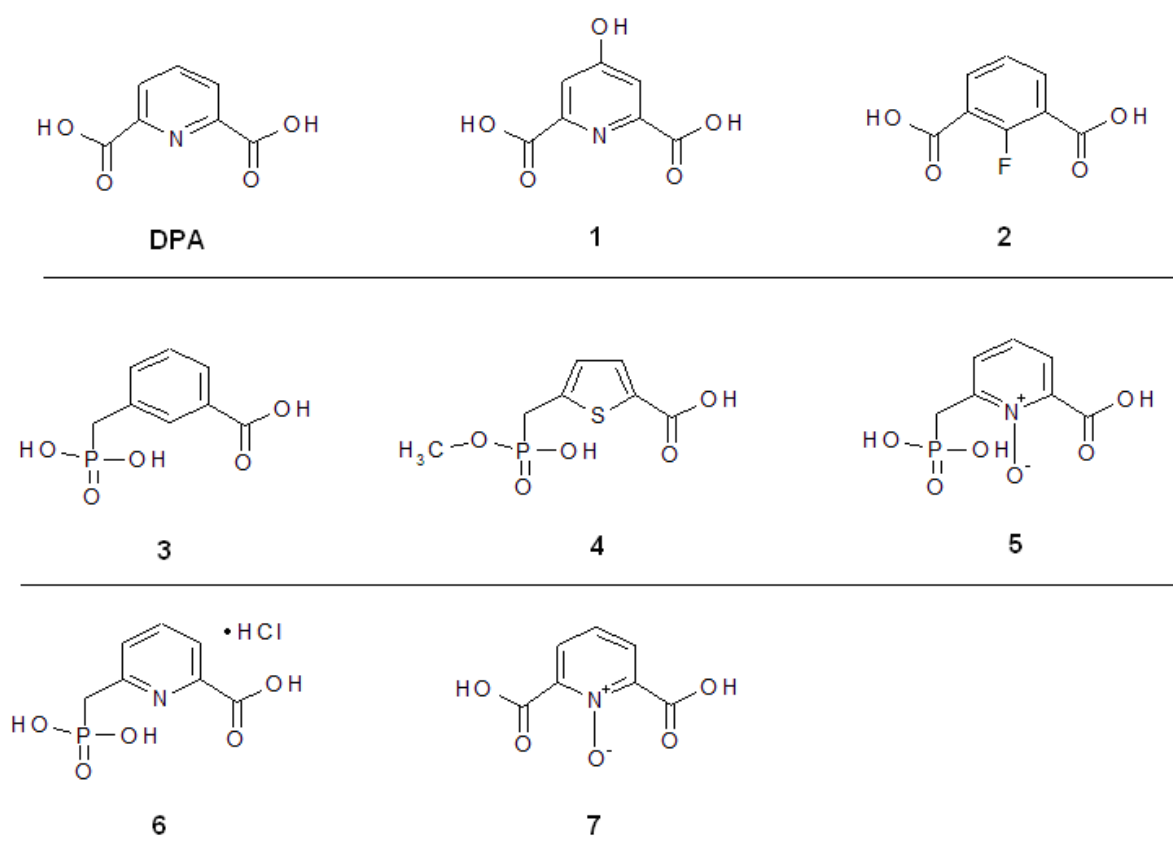


Figure 4.2 Compounds with characteristics related to the cyclic form of the substrate FBP used for the initial inhibitor screen.

The compounds were chosen because the negatively charged carboxylate and phosphonate groups overlap with those of the two phosphates of FBP in its furanose form (Figure 1.14). The compound DPA is pyridine-2,6-dicarboxylic acid (dipicolinic acid). The compounds **5** and **7** are N-oxides of the compounds **6** and DPA, respectively (see Appendix B).

Table 4.1 Inhibition screen of compounds with FBP related structures

The assays were done after a pre-incubation of 1 mM of the compound with the *M. tuberculosis* aldolase for 15 minutes. The concentration of FBP was 200 μ M.

Compound	% Inhibition
EDTA	100
DPA	100
1	36 \pm 1
2	8 \pm 6
3	11 \pm 2
4	0
5	16 \pm 4
6*	89 \pm 11
7	14 \pm 3

*assays done with 30 μ M FBP instead of 200 μ M FBP

The experiment was then performed to determine if the inhibition was reversible. The concentrated enzyme (100X compared to the assay concentration, or \sim 0.8 μ M of *M. tuberculosis* aldolase) was incubated with 1 mM of the inhibitors EDTA, DPA, and compound **1**, or 250 μ M of compound **6** for 15 minutes, in the presence of 5% v/v DMSO. The enzyme was only \sim 60% inhibited by the compounds **1** and **6** in these conditions. The aldolase was in contrast 100% inhibited by the pre-incubation with 1 mM EDTA and DPA under these conditions. The enzyme and inhibitor mixture was then diluted in the assay such that the inhibitor concentration was 10 μ M (or 2.5 μ M for compound **6**), and the reaction was immediately started by addition of FBP at a final concentration of 200 μ M. The *M. tuberculosis* aldolase recovered its full activity in all cases but with DPA, where only \sim 5% of the activity was recovered. Time-course assays were also done with 1 mM EDTA and

1mM compound **6**, and it was found that the enzyme gradually lost activity over time during the pre-incubation with the inhibitor.

After more aldolases were cloned and purified, several other potential inhibitory compounds were tested. Some were found to have no significant effect or were comparatively weaker inhibitors of the Class II aldolase reaction (Figure 4.3). These include nalidixic acid, which was probably inhibitory mostly to one of the coupling enzymes, as the rabbit muscle aldolase reaction was inhibited to a greater extent than those done with the Class II aldolases (~30% to 50% inhibition with 1 mM nalidixic acid). Another compound tested was 4-bromoisophthalic acid, which did not inhibit the aldolases from *M. tuberculosis*, *M. grisea*, or *B. cereus*, and only inhibited the *P. aeruginosa* aldolase by 10% at 1 mM concentration. Chelidonic acid was also tested and found to have no effect on the Class II aldolase reaction, but the structurally related chelidamic acid (compound **1**, see Appendix B) had an IC₅₀ of 1.3 mM for the enzymes from *M. grisea*, *P. aeruginosa*, and *B. cereus*, and an IC₅₀ of 0.3 mM for the aldolase from *M. tuberculosis* (this compound was however not tested with the Class I rabbit muscle enzyme). These results are consistent with those obtained in the first inhibitor screen, where the compounds based on the pyridine-2,6-dicarboxylic acid structure were found to be inhibitory, as opposed to the non-pyridine based structures. The thiol-containing reducing agent used in some Class II aldolase purification buffers, β-mercaptoethanol, did not cause any detectable inhibition at a concentration of 2 mM. The effect of 1 mM of tiopronin and 5-mercapto-1H-tetrazole-1-methanesulfonic acid was tested by pre-incubation of the *M. tuberculosis* aldolase for 15 minutes. Tiopronin was relatively potent and caused 50% inhibition (no effect on the Class I aldolase), but the second compound caused only a 10% inhibition (the second compound was not tested with the Class I aldolase).

In light of these results, the focus was then turned to DPA derivatives and thiol-containing compounds. The IC₅₀ values of such inhibitors after 15 minutes of incubation were then determined

Chapter 4 Inhibition of Class II FBP aldolases

with several aldolases (Figure 4.4 and Tables 4.2 and 4.3). It is relevant to note that the presence of metal in the assay was also found to significantly decrease the inhibitory capacity of the compounds, as less than 30% inhibition was observed after 15 minutes of incubation with 1 mM DPA or compound **6** for the *P. aeruginosa* aldolase in the presence of 0.7 mM CoCl₂, whereas the IC₅₀ values in the absence of metal were 200 μM or less.

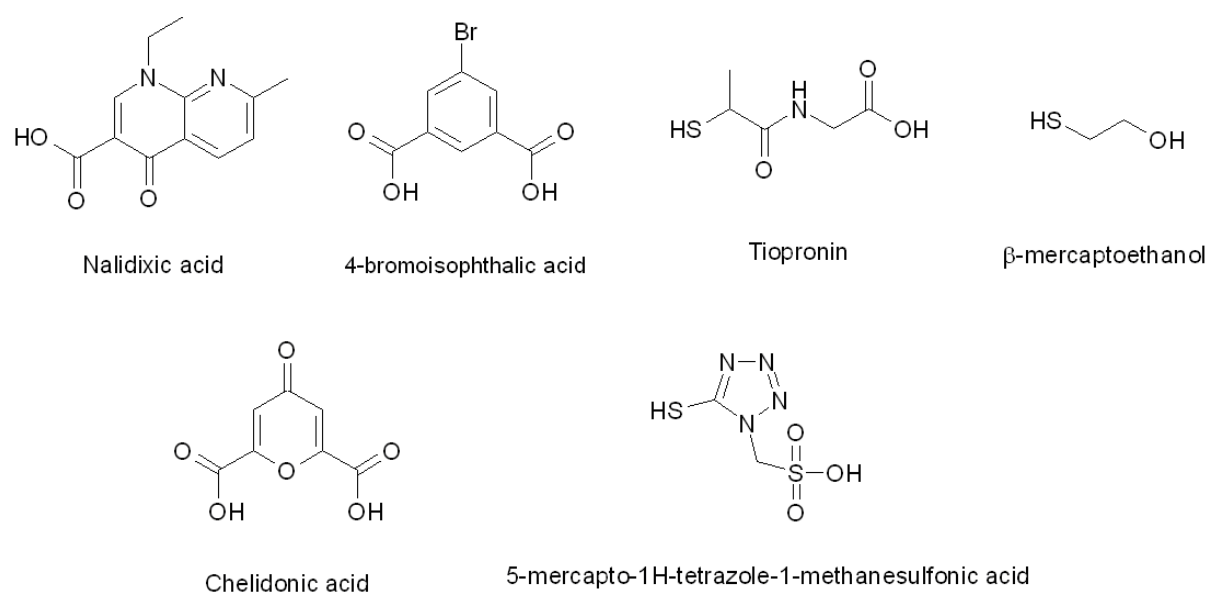


Figure 4.3 Other commercially available molecules tested for inhibition

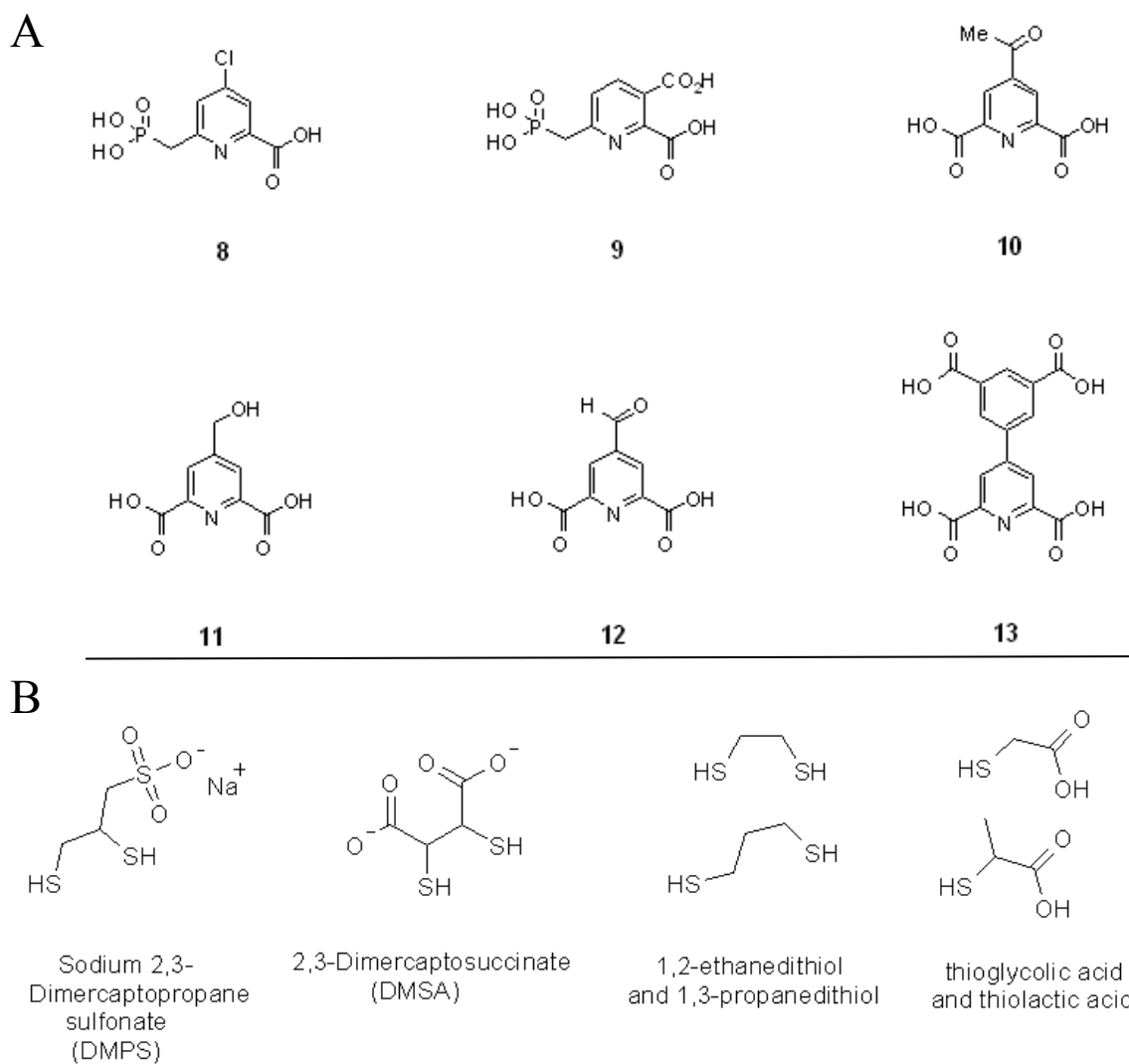


Figure 4.4 DPA derivatives and thiol-containing inhibitors

Panel A: Derivatives of pyridine-2,6-dicarboxylic acid (DPA) that were synthesized by our collaborators (see Appendix B). Panel B: commercial thiol-containing compounds. The thiol-containing compounds were investigated because some of them are already used for medical treatment in humans and animals (DMPS and DMSA), and they were also found to be inhibitors of another zinc metalloenzyme *in vitro* (Siemann *et al.* 2003).

Table 4.2 Summary of IC₅₀ values with DPA derivatives

Source Organism	IC ₅₀ (μM) obtained for each compound† (95% confidence interval)							
	DPA	6	8	9	10	11	12	EDTA
<i>M. grisea</i>	79 (74-84)	78 (68-92)	960 (880-1,050)	1,370 (1,320-1,420)	540 (480-630)	430 (400-470)	740 (710-770)	53 (45-66)
<i>M. tuberculosis</i>	28 (24-36)	57 (54-62)	650 (590-710)	560 (520-600)	190 (160-230)	110* (91-140)	81 (61-120)	48 (44-53)
<i>B. cereus</i>	150 (130-170)	78 (70-89)	1,050 (950-1,170)	1,100 (990-1,250)	N/I	170 (150-180)	740 (690-790)	8 (7-11)
<i>P. aeruginosa</i>	95 (81-120)	130 (100-180)	>1,000	>1,500	>1,000	270 (230-340)	240 (200-300)	41 (37-45)
<i>S. cerevisiae</i>	-	140 (120-160)	940 (870-1,020)	-	-	-	1,060 (1,000-1,100)	-
Rabbit muscle	N/I	N/I	N/I	-	N/I	680 (620-740)	N/I	N/I

†A one phase decay equation was fitted to the data by non-linear regression, and the 95% confidence interval for each IC₅₀ value is indicated in brackets

N/I: no inhibition

-: not determined

*The inhibition is affected by pH. This compound was also tested at a higher pH with the *M. tuberculosis* aldolase (assay at pH 8.0 instead of pH 7.3), and the IC₅₀ was found to be ~500 μM in these conditions. The other compounds were not tested at different pH.

Table 4.3 Summary of inhibition with thiol-containing compounds

Source Organism	% Inhibition obtained with each compound					
	Thiolactic acid 2 mM	Thioglycolic acid 2 mM	1,3- propanedithiol 2 mM	1,2- ethanedithiol 0.5 mM	DMSA 0.33 mM	DMPS 2 mM
<i>M. grisea</i>	N/I	Activates	N/I	27 ± 1	32.1 ± 0.9	100†
<i>M. tuberculosis</i>	16.7 ± 0.7	25 ± 3	16.1 ± 0.8	80 ± 10	28 ± 1	100‡
<i>B. cereus</i>	8.0 ± 0.3	16.5 ± 0.6	10.0 ± 0.7	-	N/I	-
<i>P. aeruginosa</i>	8.7 ± 0.3	15.2 ± 0.4	N/I	24.8 ± 0.5	N/I	-
<i>E. coli</i>	8.9 ± 0.4	24 ± 1	-	42 ± 3	N/I	-
Rabbit Muscle	-	-	-	N/I	N/I*	N/I

N/I: no inhibition

-:not determined

† IC₅₀ = (31 ± 3) μM‡ IC₅₀ = (5.2 ± 0.4) μM

* (25.9 ± 0.6) % inhibition with 2 mM DMSA

According to the data presented in Tables 4.2 and 4.3, the compounds tested appear to be generally no better than EDTA at inhibiting the Class II aldolases. However, these results were obtained after 15 minutes of pre-incubation in the absence of the substrate FBP. While performing similar experiments without pre-incubation with the inhibitory compounds, it was observed that the compounds were much less effective inhibitors when the substrate was present, pointing to a competitive mechanism. It was also observed that some compounds could inactivate the aldolases at a faster rate than others in the presence of the substrate. Some inhibitors were therefore assayed by varying both their concentration and the substrate concentration used to start the reaction, with and without the 15 minutes of pre-incubation of the enzyme with the inhibitor, as shown in Figure 4.5. However, the analysis showed that the competitive, uncompetitive, or mixed inhibition models did not fit the resulting data. Instead, the compounds exhibited a competitive and time-dependent pattern

Chapter 4 Inhibition of Class II FBP aldolases

of inhibition of the FBP cleavage reaction. The inhibition did not appear reversible under the assay conditions (reverse reaction too slow to be detected), but the enzyme could be reactivated upon the addition of zinc to the assay mixture. Some typical progress curves are reproduced below (Figures 4.6 and 4.7, see modified assay described in section 4.2.3). The inhibition experiments were from then on performed in the presence of substrate (no pre-incubation) and analyzed using a time-dependent inhibition model, which will be presented in the following section.

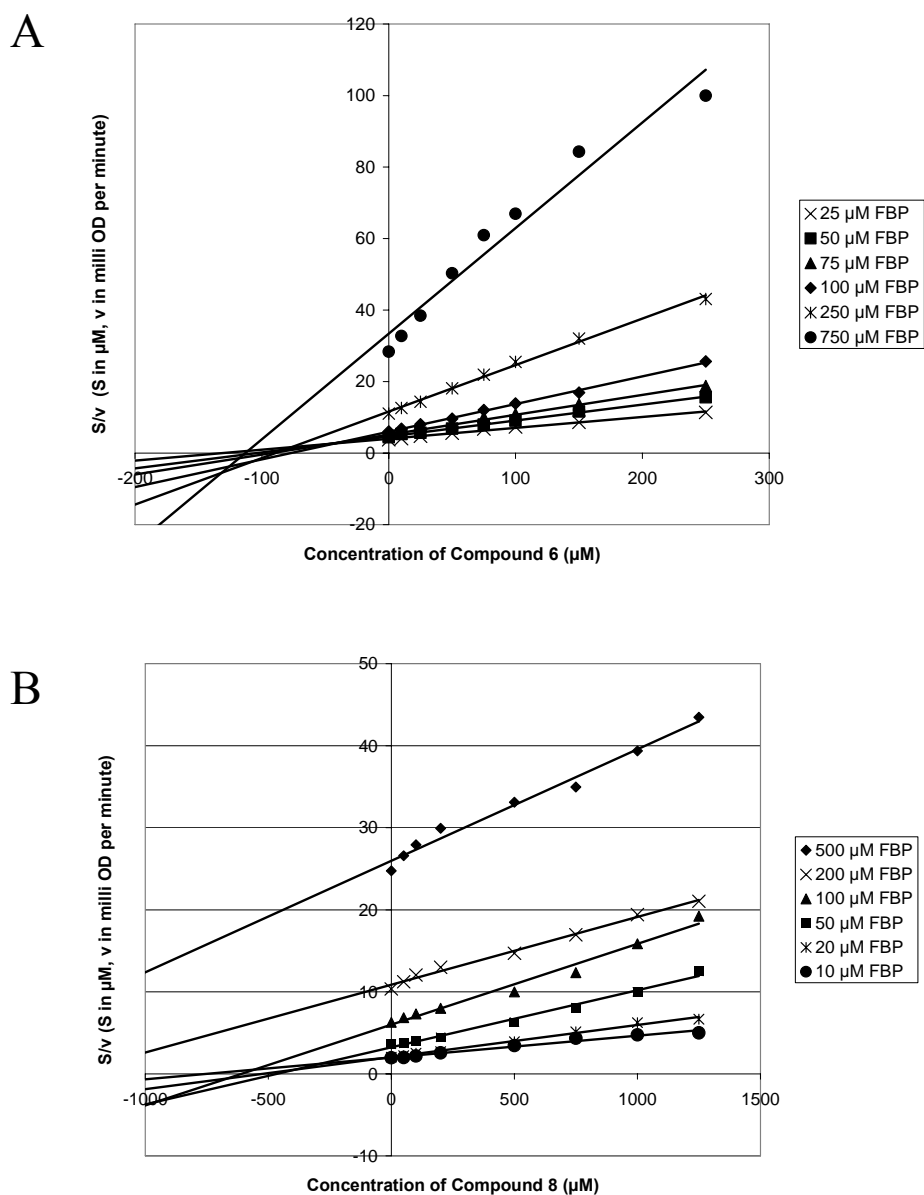


Figure 4.5 Cornish-Bowden plots of the inhibition data with the compounds **6** and **8**

Panel A: inhibition of the *M. grisea* FBP aldolase by the compound **6** (no pre-incubation period). Panel B: inhibition of the *M. tuberculosis* aldolase by compound **8** after 15 minutes of pre-incubation of the enzyme with the inhibitor. Each point represents the average of four replicates. The *M. grisea* aldolase had a $K_i=72 \mu\text{M}$ and $\alpha K_i=158 \mu\text{M}$ for compound **6** according to calculations done using the mixed inhibition equation and dynamic weighing options of Leonora. However the data obtained at higher substrate concentrations ($>100 \mu\text{M}$) and higher inhibitor concentration did not fit the mixed inhibition model and were excluded from these calculations, as can be seen in the figure by the plotted lines not passing through a single point in the upper left ($-x/+y$) quadrant in Panel A.

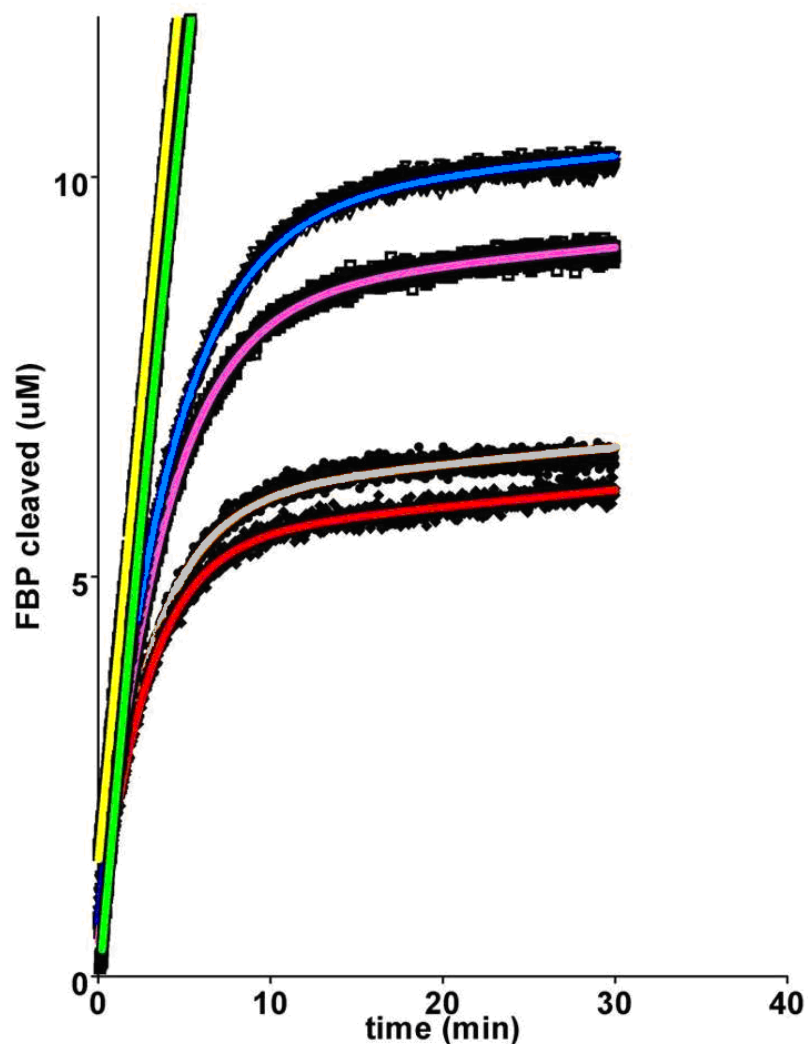


Figure 4.6 Progress curves of FBP cleavage by *M. tuberculosis* Class II aldolase in the presence of different metal-chelating inhibitors

3 nM of enzyme was used to start the reaction in the presence of 500 μ M FBP (yellow line) and the following compounds: Bovine serum albumin (3 μ M, green line); EDTA (5 mM, blue line); DMPS (500 μ M, pink line); DPA (500 μ M, grey line); and compound **13** (500 μ M, red line). After subtracting the background NADH oxidation from the data, the enzyme was calculated to be completely inactivated after 20 minutes.

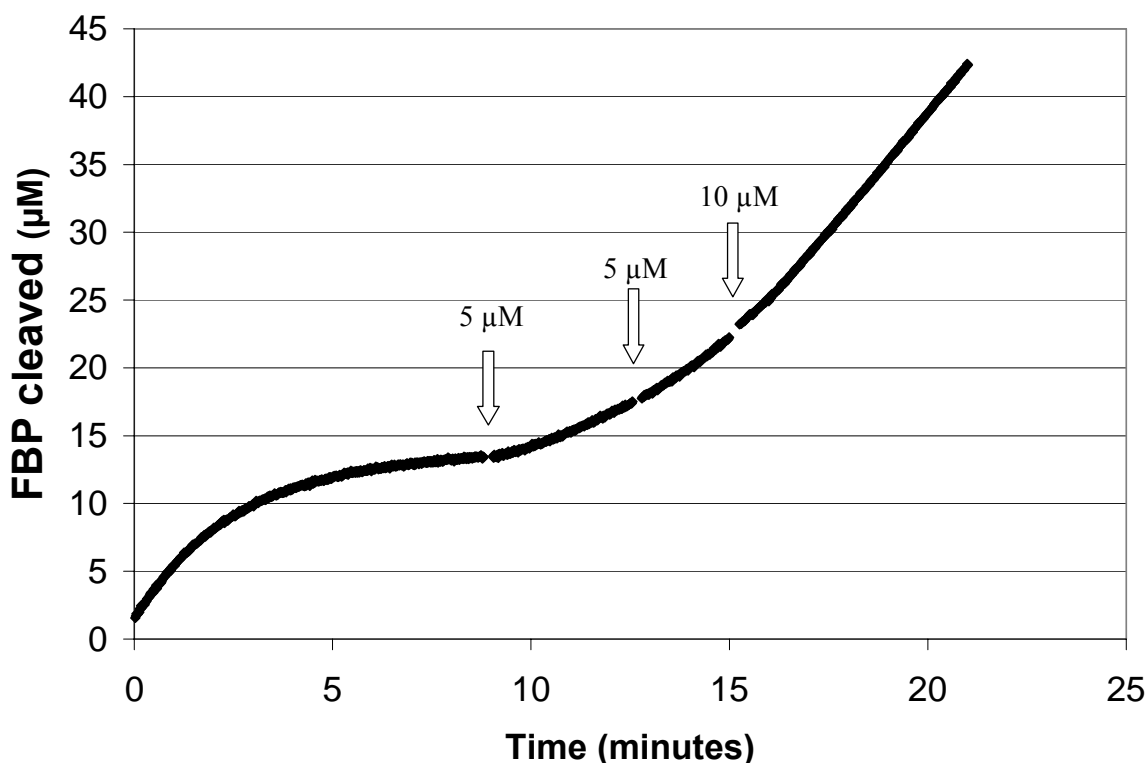


Figure 4.7 Progress curve of FBP cleavage by *M. tuberculosis* Class II aldolase in the presence of compound 13 and added zinc chloride

The enzyme's activity could be restored by addition of zinc chloride to the assay mixture, as shown in this graph obtained in the presence of 500 μM of compound **13**. The enzyme (3 nM) was added to the assay mixture with 500 μM FBP and 500 μM of compound **13** to start the reaction. The arrows indicate when the specified amounts of zinc were added, to a total of 20 μM zinc chloride. The starting velocity (over the first minute of reaction) was 3.9 μM FBP cleaved per min, after 8 minutes of reaction the inhibited enzyme had a residual activity of 0.3 μM FBP cleaved per minute, and the velocity after addition of 20 μM ZnCl₂ was 3.5 μM FBP cleaved per min (90% reactivation). The assay volume was not significantly changed by the addition of zinc chloride (2% increase). Similar results were obtained with the inhibitors DMPS (100% reactivation with 20 μM ZnCl₂ added) and DPA (68% reactivation with 40 μM ZnCl₂ added). This particular experiment was not attempted with EDTA because of the high concentration (~5 mM EDTA) required to inactivate the enzyme before 5% of the FBP substrate was cleaved in these conditions; see instead the metal reactivation study presented in Chapter 3 (Figure 3.11).

4.3.2 Inhibition model

In order to determine the inhibition mechanism of the inhibitors, we chose to use the enzyme from *M. tuberculosis*, as it generally was the most sensitive to the inhibitors during the initial screens (Tables 4.2 and 4.3). The most potent inhibitors from these screens (DPA, compounds **6** and **13**, and DMPS) were chosen for these studies, and EDTA was used for comparison.

The slow-binding inhibition progress curves can be fitted to Equation 4.1 (Morrison and Walsh 1988) (see Methods section) in the case of reversible inhibition. The inhibition of the Class II aldolases was shown to be reversible upon the addition of metal (Figure 4.7), but the end velocity (v_s) obtained in our assay conditions is too low to be detected. This could be due to the background NADH oxidation which is relatively high in our coupled assay, and this masks any potential small residual aldolase activity. The observed enzyme inhibition is therefore not distinguishable from irreversible inactivation, so we will consider the end velocity (v_s) in Equation 4.1 to be negligible and use instead the Equation 4.2 (Tsou 1988). An example of the Equation 4.2 fitted to the progress curves obtained for the cleavage of FBP by the *M. tuberculosis* aldolase in the presence of the inhibitor DMPS is shown in Figure 4.8. As is apparent in this figure, the initial velocity and the total amount of FBP cleaved cannot be easily determined using the coupled assay due to uncertainty on the initial absorbance of the NADH solution as well as the delay between the start of the reaction and the first absorbance measurement in the plate reader. The progress curves are therefore analyzed as a function of time with Equation 4.2 by non-linear regression to determine the apparent constant A, instead of simply using a plot of the total amount of FBP cleaved ($[P]_\infty$) until complete inactivation (at time approaching infinity), versus the initial velocity.

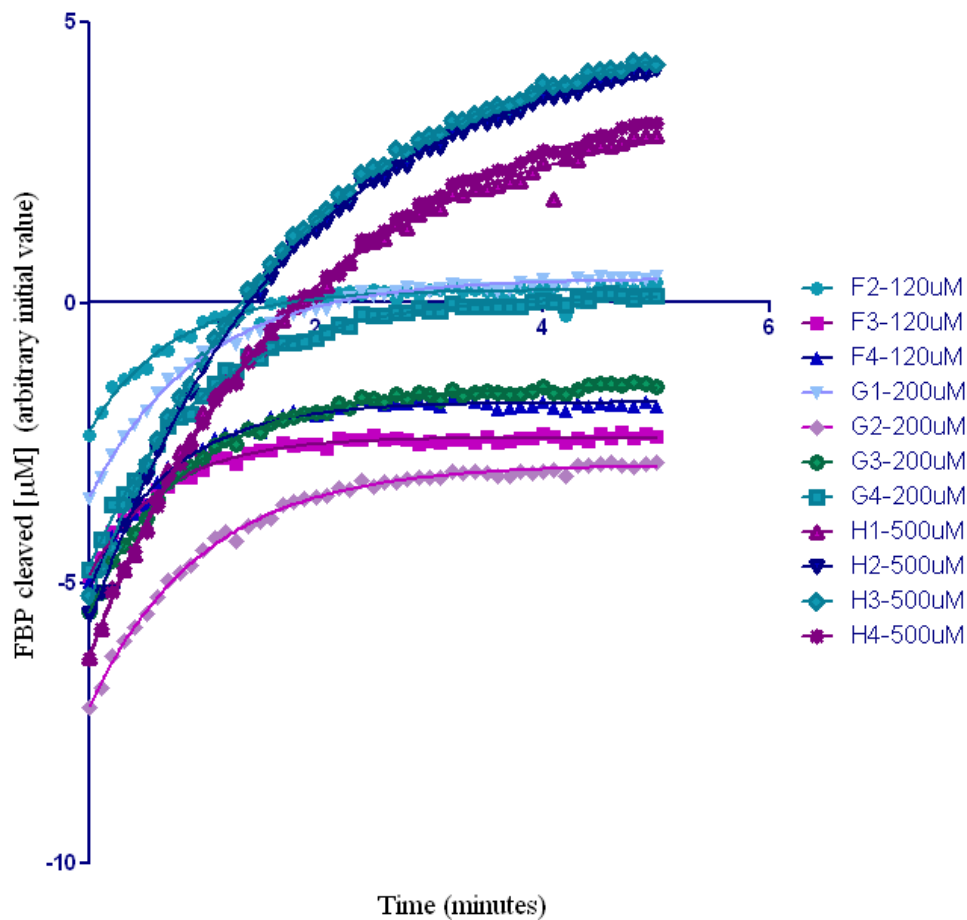


Figure 4.8 Progress curves of FBP cleavage by the *M. tuberculosis* aldolase in the presence of 500 μM DMPS

The initial FBP concentration for each curve is shown in the legend on the right. The initial absorbance value differed slightly for each curve due to the coupling assay procedure, so a variable representing the initial cleaved FBP concentration (arbitrary value) was included in the Equation 4.2 for the analysis. This modified Equation 4.2 was fitted to the data by non-linear regression (see resulting lines over each data set) using the GraphPad Prism software.

Tsou argues that the type of irreversible inhibition (Equation 4.2) can be distinguished by suitable plots of A and $[S]$ (Tsou 1988) (see Appendix C). In the case of competitive inhibition (Figure 4.1), A is defined by Equation 4.3, and thus a plot of $1/A$ versus $[S]$ should give a straight line. A typical plot obtained with two metal chelating inhibitors is shown in Fig 4.9.

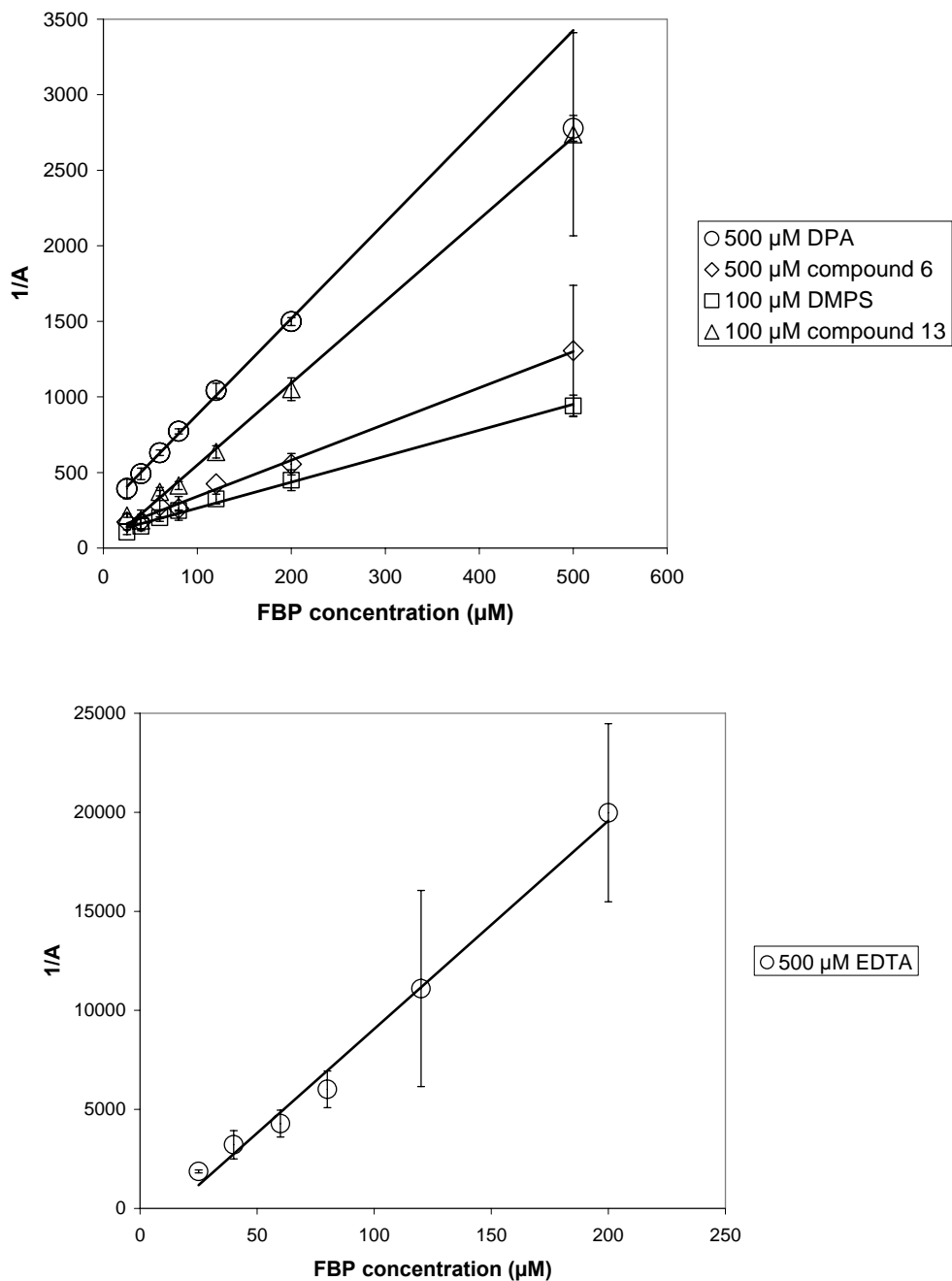


Figure 4.9 Tsou's test for competitive irreversible inhibition

The apparent constant A was obtained by fitting Equation 4.2 (Tsou 1988) using non-linear regression to the progress curves obtained with the *M. tuberculosis* aldolase, in the presence of different inhibitors (compounds and concentrations indicated in the legend) and various concentrations of FBP. Each point represents the average value of 4 replicate assays. Straight lines indicate that the inhibition is competitive with respect to the substrate FBP (see Appendix C).

Since the inhibition appears irreversible under the assay conditions used, the apparent K_I cannot be determined for a one-step inhibition mechanism (Figure 4.1), as it would represent the ratio of the forward and reverse inhibitor binding rate constants (k_{+0}/k_{-0}). The binding capacity of the inhibitors will instead be compared using their second order binding rate constant k_{+0} (Equation 4.3, Figure 4.1). This constant can be directly obtained from the ordinate intercepts in Figure 4.9, but the high standard deviation observed on the apparent rate constant A at higher substrate concentrations called for the use of a more robust approach. An example of a secondary plot used to calculate the second order rate constant from several data sets for each inhibitor is presented in Figure 4.10. The rate constants obtained with the most potent inhibitors are presented in Table 4.4.

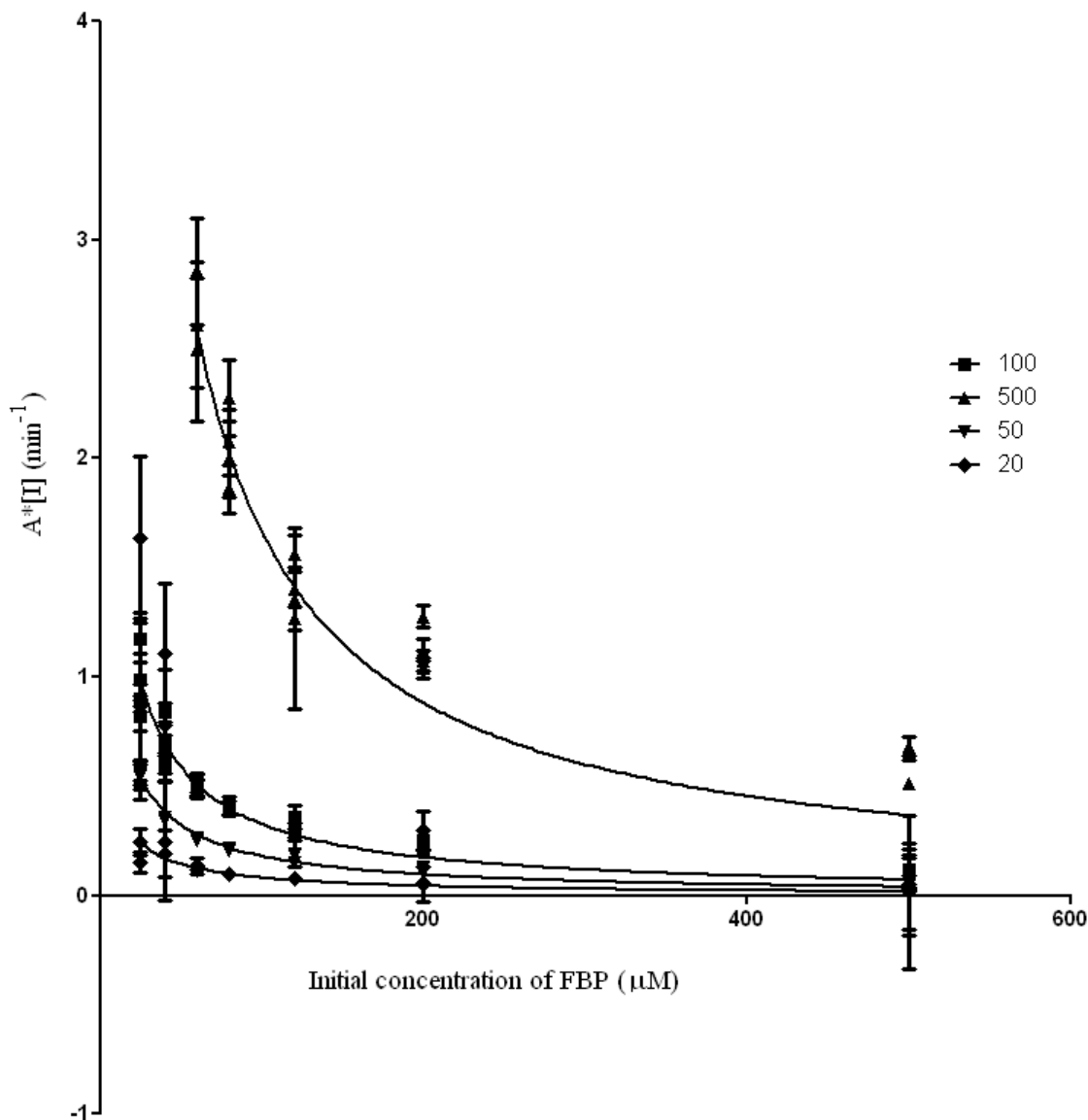


Figure 4.10 Secondary plot of the apparent inhibition constants obtained with the *M. tuberculosis* aldolase in the presence of DMPS, as a function of the FBP concentration

The concentrations of DMPS used (in μM) are indicated in the legend on the right. The Equation 4.3 defining the apparent constant A according to Tsou (1988) for competitive inhibition (see text) was fitted to the data by non-linear regression using the GraphPad Prism software. The equation was fitted independently to the data from each inhibitor concentration (shown as lines on the Figure), and the global parameters were also calculated. The apparent A constants multiplied by the inhibitor concentration ($A*[I]$, represented by k in Equation 4.1) were obtained from 95 progress curves and are shown with their error bars representing the standard deviation. Of those 95 points, 80 were analyzed, and 15 were outliers. The global R^2 value was calculated to be 0.9911.

Table 4.4 Second order rate constants for the binding of chelating inhibitors to the recombinant Class II aldolase from *M. tuberculosis*

Each value is calculated from a secondary plot (see Figure 4.10, Equation 4.3) using the apparent constant A (Equation 4.2) obtained for multiple assays done simultaneously in a microtiter plate in the presence of various concentrations of FBP and inhibitor.

Inhibitor	k_{+0} $M^{-1} s^{-1}$	R ² value of secondary plot
DPA	151 ± 2	0.9866
6	479 ± 9	0.9686
13	277 ± 7	0.9092
DMPS	500 ± 4	0.9911
EDTA	25 ± 1	0.9153

As can be seen from the results presented in Table 4.4, the inhibitors DMPS and compound **6** can inactivate the Class II FBP aldolase from *M. tuberculosis* ~20 times faster than EDTA, and ~3 times faster than DPA in the presence of the substrate FBP, whereas the inhibitor **13** can inactivate the enzyme almost 2 times faster than DPA in the presence of FBP. The apparent second order rate constants obtained for the irreversible reaction with these inhibitors are over 3 orders of magnitude lower than the second order rate constant determined for the FBP cleavage reaction for the *M. tuberculosis* aldolase ($k_{cat}/K_m = 1.08 \times 10^6 M^{-1} \cdot s^{-1}$, see Table 3.3).

4.4 Discussion

Although the Class II FBP aldolases are potential targets for antimicrobial therapy there have been few potent Class II FBP aldolase inhibitors reported in the literature. The molecule PGH has been reported to inhibit the yeast Class II aldolase with K_I of 0.01 μM but it also inhibits the rabbit

Chapter 4 Inhibition of Class II FBP aldolases

muscle Class I aldolase and other enzymes utilizing DHAP as substrate, such as methylglyoxal synthase, L-rhamnulose-1-phosphate synthase, tagatose-bisphosphate aldolase, L-fuculose-1-phosphate aldolase, etc. (Kroemer *et al.* 2003; Hall *et al.* 2002; Fessner *et al.* 1996; Mildvan *et al.* 1971). Derivatives of PGH such as, phosphoglycoloamidoxime (PGA) and phosphoglycolohydrazide (PGHz) (Figure 1.16, p.47), are more specific for the Class II FBA (Fonvielle *et al.* 2004), but are also good inhibitors of the rabbit TIM, which makes these compounds likely toxic for humans.

In order to create more specific inhibitors for the Class II aldolases, compounds that have potential zinc chelating groups were tested. The results were compared with the general metal ion chelators, EDTA and thiol containing compounds. The molecule 2,6-pyridinedicarboxylic acid (or dipicolinate, DPA, Figure 4.2) was the most potent inhibitor according to our initial compound screen (Table 4.1). Derivatives of DPA were then synthesized and IC_{50} values were determined with a wider range of FBP aldolases. IC_{50} values are generally similar with DPA and compound 6, which differs from DPA by the substitution of the carboxylate with a phosphomethyl group at the 6-position of the pyridine ring. Addition of other substituents (in compounds 8 to 12) resulted in higher IC_{50} values for most enzymes. Two exceptions are compounds 11 and 12, respectively with hydroxymethyl and formyl substituents in position 4 of the pyridine ring, which had IC_{50} s comparable to DPA and Compound 6 with the *M. tuberculosis* aldolase. The generally poorer inhibition observed with compounds 8 to 10 in *M. tuberculosis* aldolase does not appear to be due to steric hindrance in the active site of the enzyme since Compound 13, with a 3,5-dicarboxyphenyl substituent in position 4 of the pyridine ring was later found to be better than DPA in inhibiting this enzyme.

Upon further analysis, it was noticed that the inhibition by these compounds was weaker in the presence of the FBP substrate, implying a competitive mechanism. A time-dependent analysis of reaction progress curves of the cleavage of FBP by the *M. tuberculosis* aldolase in the presence of the most potent inhibitors showed that compounds 6, 13, and DMPS were better competitive inhibitors

than DPA, according to their second-order binding rate constants. EDTA was comparatively a weak inhibitor of the enzyme in the presence of substrate, being 6 times less potent than DPA.

The results have been analyzed using a one-step inhibition model (Figure 4.1). Other researchers have pointed out that a two-step model is also possible for this type of competitive and irreversible inhibition, where the first step is a reversible equilibrium between the free enzyme and the EI complex, and the second step is an irreversible inactivation (Leytus *et al.* 1984). They argue that the primary data appears similar for both models, and that the progress curves for both models can be analyzed using equations with a similar format as Equation 4.2, or $P=(j/k)*(1-e^{-kt})$. However, a plot of the apparent first-order constant k obtained at high inhibitor concentration, versus the concentration of inhibitor, can differentiate between the one-step and two-step models. The concentrations of inhibitors used in our study were not high enough to allow us to rule out a two-step model for our inhibitors excepted in the case of DMPS, which appeared to be a one-step process. Some researchers have shown that chelating inhibitors with a one-step inhibition process were bound to the active site, whereas others following a two-step process were removing the metal ion from the active site (Chong and Auld 2000; Bardsley and Childs 1974). In our study, the enzymes were reactivated by the addition of small amounts of zinc (i.e. ~10 times less zinc than the inhibitor concentration), which indicates that either the inhibitors are forming an unstable ternary complex with the active site and the zinc ion (one-step process), or they remove the metal ion from the active site (two-step process). The practical consequences are the same in both cases in our study, in that the inhibitors do not have a sufficient affinity for the active site to form a stable complex in the presence of extraneous zinc. Interestingly, an unstable ternary complex between DPA and cobalt carbonic anhydrase has been observed previously by absorption spectroscopy (Hirose and Kidani 1981). In contrast, the inhibitor PGH was shown to form a stable complex with the cobalt-dependant *Bacillus stearothermophilus* Class II FBP aldolase, as the inhibited enzyme was not reactivated in the presence of excess cobalt

Chapter 4 Inhibition of Class II FBP aldolases

(Lewis and Lowe 1977). Our data however shows that some chelating inhibitors, such as DMPS and Compound 6, are better able to compete with the substrate FBP for the access to the active site zinc in the *M. tuberculosis* aldolase in comparison with DPA or EDTA, which means that some of the studied compounds have a higher affinity for the active site than others.

The compound DMPS was modeled into the active site of the *E. coli* FBP aldolase in complex with PGH (Figure 4.12). Although the compounds appear to form equivalent interactions with the active site amino acids compared to PGH, the sulfur-zinc bonds are not of an optimal length (the average length for sulfur-Zn²⁺ bonds is 2.3 ± 0.2 Å in protein structures (Tamames *et al.* 2007)) because DMPS is one carbon atom “shorter” than PGH or the substrate DHAP (see Figures 1.9b and 4.11). It is also relevant to note that the zinc-chelating functions of the inhibitory compounds are still solvent-accessible in the closed-loop form of the enzyme (see the opening in the surface of the enzyme indicated by arrows at the bottom of the Figure 4.12, panels A to C, which corresponds to the GAP binding site). Therefore extraneous metal ions could access the active site through that opening and interact with an inhibitor bound in the active site, possibly weakening its interaction with the catalytic zinc, if the interaction is not optimal. In an attempt to create a similar molecule that was closer in structure to the substrate DHAP, a derivative of DMPS with a sulphonate group and a longer main chain (Compound AK4) was also modeled into the *E. coli* aldolase active site (Figure 4.11 and Figure 4.12, panels C and F). The zinc-sulfur bonds were indeed slightly shorter after minimization, but the Compound AK4 seemed to have a smaller number of strong interactions with the active site amino acids (dashed lines in Figure 4.12, panels D to F). Other derivatives that have a longer chain that would extend into the putative GAP binding site could form a more stable complex with the enzyme in the presence of extraneous zinc, as the zinc-chelating functions could then be shielded from the solvent in the closed loop enzyme structure. Indeed, longer-chain FBP analogues containing metal chelating functions have been shown recently to be very potent inhibitors of the *S. cerevisiae*,

Chapter 4 Inhibition of Class II FBP aldolases

H. pylori and *M. bovis* Class II aldolases, with K_i as low as 13 nM (Fonvielle *et al.* 2008). It is relevant to note that the amino acid sequences of the Class II FBP aldolases from *M. bovis* and *M. tuberculosis* are identical, and therefore the inhibition results can be applied to both aldolases.

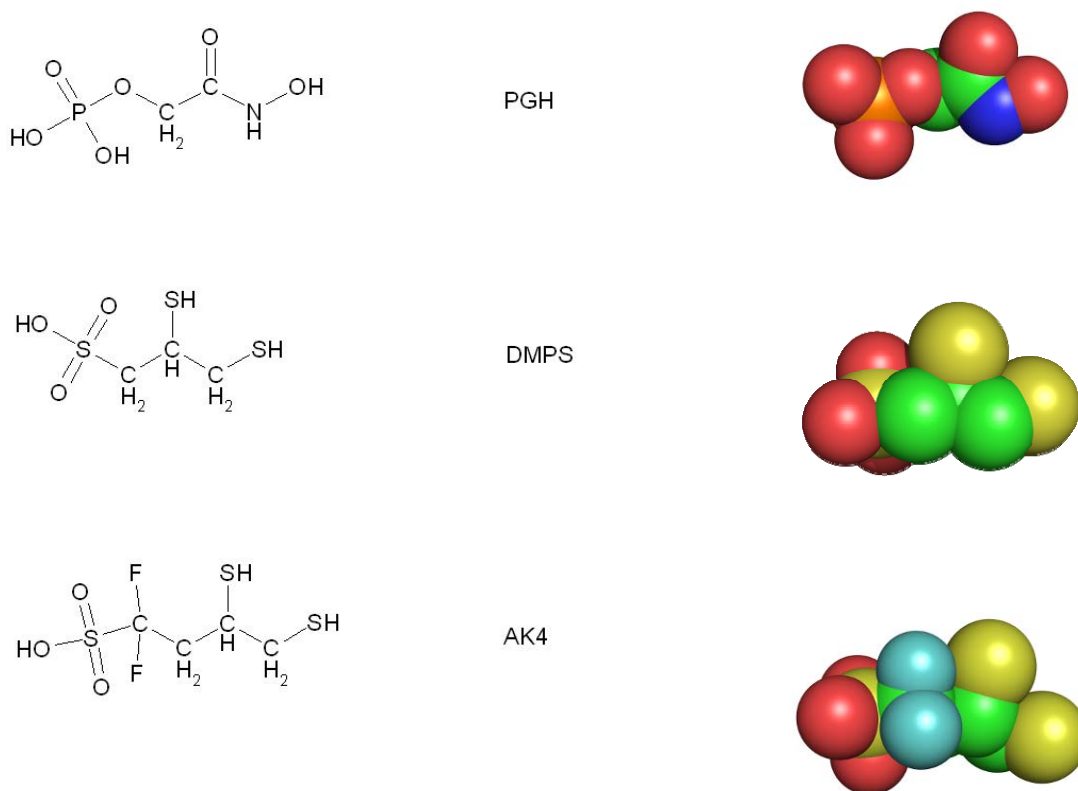


Figure 4.11 PGH and sulfur-containing analogues

The images were produced using MDL ISISTM/Draw 2.5 (MDL Information Systems, Inc.) and PyMOL (DeLano Scientific, San Francisco, CA). In the space-fill representations on the right, the carbons are pink, the oxygens are red, the sulfurs are yellow, the fluorines are cyan, the phosphorus is orange, and the nitrogen is dark blue.

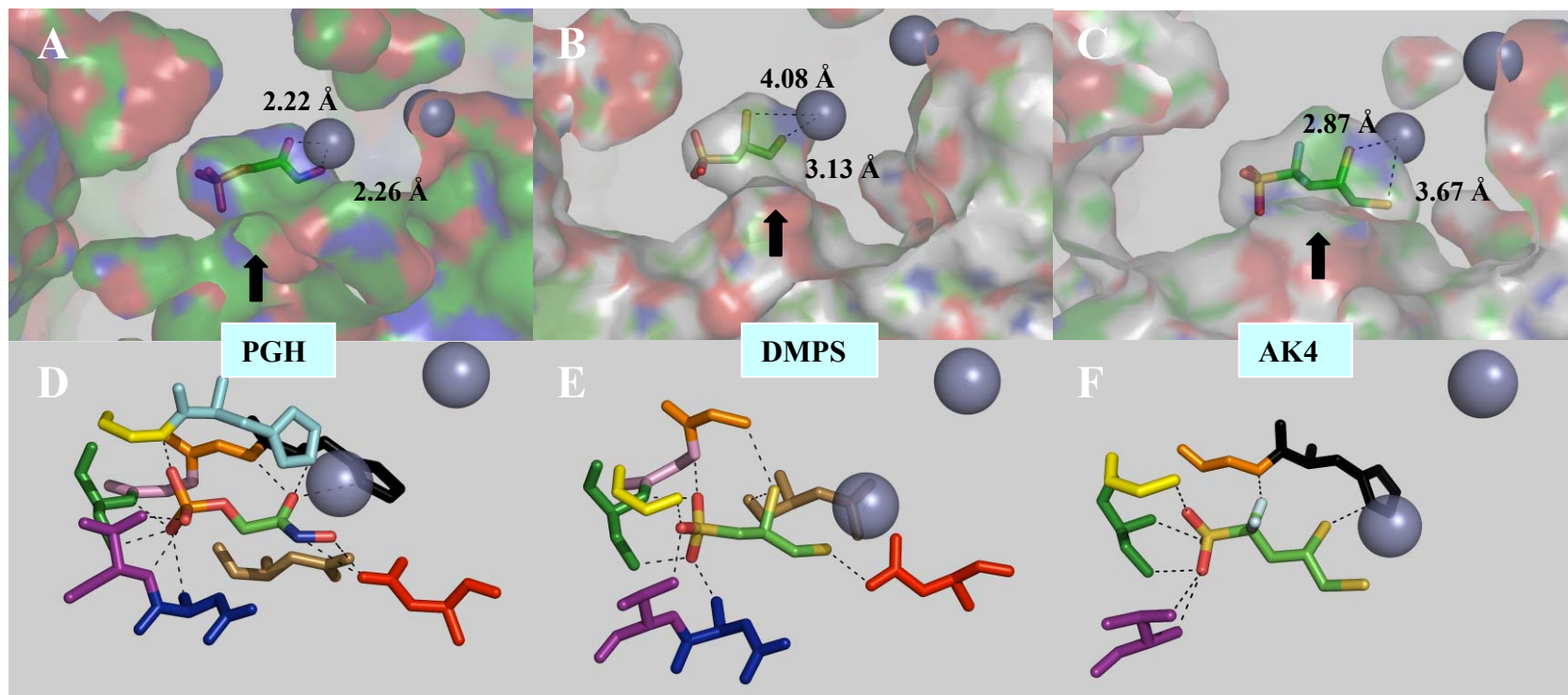


Figure 4.12 DMPS and AK4 docked into the *E. coli* Class II FBP aldolase active site

The compounds DMPS (Panels B and E) and AK4 (Panels C and F) were positioned in the space occupied by the inhibitor PGH in the *E. coli* Class II FBP aldolase PDB structure 1B57 (Panels A and D) and a sphere of 6 Å around the inhibitor was minimized (20, 000 iterations) using the MMFF94 force field in Sybyl (Tripos, St-Louis, MO). The catalytic and structural (right) zinc ions (see Figure 1.9) are represented as grey spheres. The solvent-accessible surface of the enzyme is colored according to electrostatic charges, and the molecules DMPS and AK4 are represented as sticks. Only a 30 Å-thick slab of the structure is shown, and the plain light grey area represents the interior of the protein. The black arrows indicate the opening in the surface which allows solvent and substrate access to the catalytic Zn^{2+} ion. The distances between the catalytic Zn^{2+} ion and the ligands from the inhibitors are indicated in Panels A to C. In Panels D, E, and F, the interactions (2.5 to 3.2 Å) between the inhibitors and the active site residues are shown as black dashes. The active site residues forming bonds with the inhibitors are shown as sticks: Asp₁₀₉ is in red, His₂₂₆ in cyan, Gly₂₂₇ in yellow, His₂₆₄ in black, Gly₂₆₅ in orange, Gly₂₆₆ in pink, Ser₂₆₇ in green, Asn₂₈₆ in brown, Asp₂₈₈ in blue, and Thr₂₈₉ in purple. The images were produced using PyMOL (DeLano Scientific, San Francisco, CA).

Chapter 4 Inhibition of Class II FBP aldolases

The inhibition model proposed for the Class II FBP aldolase inhibitors characterized in this study will now be compared with the inhibition model described for PGH. The compound PGH was first reported to have a K_i of 0.05 μM for Class II FBP aldolase (Lewis and Lowe 1973). PGH was later shown to display a time-dependent competitive inhibition pattern as seen in our study in the presence of high FBP concentrations, and the PGH K_i was then calculated to be 1.2 nM for the *B. stearrowthermophilus* aldolase (Lewis and Lowe 1977). However, the PGH inhibition was reversible, as enzyme activity is not completely inhibited after the equilibrium was reached between the enzyme and the inhibitor, in contrast to what was observed in the present study. As mentioned above, the presence of a divalent metal did not affect the inhibition by PGH, but the presence of divalent ion completely restored the activity of the enzyme inhibited by EDTA in the Lewis and Lowe (1977) study, as was observed here with the Class II enzymes. However, after exhaustive dialysis of the PGH-inactivated *B. stearrowthermophilus* enzyme, 1/3 of the activity could be restored upon the addition of excess metal. Lewis and Lowe (1977) reported a ~90% inhibition of the aldolase after a 15-minutes reaction with 500 μM FBP in the presence of 2 μM PGH. In contrast, a similar level of inhibition in our study was obtained using 500 μM of the most potent inhibitory compounds (DMPS, Compound 6 and 13, and DPA), which indicates that these compounds are at least 250 times less potent than PGH, not considering the lower K_M for FBP of the Co^{2+} -containing *B. stearrowthermophilus* aldolase (4.55 μM , see Table 3.1) compared to that of the *M. tuberculosis* aldolase (28 μM , Table 3.3). Lewis and Lowe (1977) further calculated the PGH k_{+0} (see Figure 4.1) to be $4 \pm 3 \times 10^5 \text{ M}^{-1} \text{ s}^{-1}$ and its k_{-0} to be $4.3 \pm 0.9 \times 10^{-4} \text{ M}^{-1} \text{ s}^{-1}$. The k_{+0} (or k_{on}) of PGH is therefore ~1000 times higher than the k_{+0} constants calculated for DMPS and Compound 6, which are the most potent inhibitors identified in the present study. This is consistent with the PGH K_i being at least 3 orders of magnitude lower than the $\text{IC}_{50\text{S}}$ obtained in the present study for DPA, DMPS, and Compounds 6 and 13.

Chapter 4 Inhibition of Class II FBP aldolases

The PGH derivatives synthesized in recent years (including PGA, PGHz, PGS1, and PGS2, see Figure 1.16) were reported to be strictly competitive with the substrate, but their behavior in the presence of excess divalent metal was not reported. The reported K_i values were also determined using initial velocities in the presence of substrate and inhibitor, with no mention of time-dependence or reversibility of the inhibition (Fonvielle *et al.* 2008; Gavalda *et al.* 2005; Fonvielle *et al.* 2004). A crystallographic structure of the *H. pylori* Class II FBP aldolase in complex with a newly synthesized biphosphorylated FBP analogue inhibitor containing a N-substituted hydroxamate function was recently obtained (Fonvielle *et al.* 2008). This novel and powerful inhibitor, with a reported K_i of 13 nM for the *H. pylori* aldolase, and a K_i of 264 μ M for the Class I rabbit muscle aldolase, has an improved selectivity for the Class II aldolases and is able to form a stable ternary complex with the enzyme like the compound PGH. The authors reported that the zinc chelation by this inhibitor was not optimal and could be improved. The use of metal-chelating substrate analogues, like the ones reported in the present study, is therefore very promising for the development of new drugs targeting the Class II FBP aldolase.

Chapter 5

Preliminary work on enzyme loop dynamics

5.1 Introduction

The active site of the Class II FBP aldolases includes two mobile loops: the $\beta 6$ - $\alpha 8$ loop that is expected to bring the catalytic zinc ion to a solvent-accessible position, and the $\beta 5$ - $\alpha 7$ loop which is expected to close over the substrate during catalysis, as shown in Figures 1.11, 1.13, and 1.15. These loops form a large portion of the enzyme surface that is in contact with the substrate during catalysis (see Figure 1.13), and thus their structure and properties are very relevant for the rational design of ligands. Interestingly, the length and amino acid sequence of these loops varies widely among the Class II aldolases, as can be seen in sequence alignments (Figures 1.10 and 1.17). The composition of these mobile loops may provide a structural basis to explain the wide variation in the Class II FBP aldolase kinetic parameters (Tables 3.1 and 3.3), since the other active site amino acids involved in metal and substrate binding, as well as catalysis, are highly conserved (see section 1.3.5).

The Class II FBP crystal structures provide clear indications of loop movements, and previous studies have confirmed this through comparisons of the *E. coli* enzyme structures with and without PGH bound in the active site (Zgiby *et al.* 2002). The structures of apo- and substrate bound *T. aquaticus* fructose-1,6-bisphosphate aldolase have three regions of weaker electron density that show higher B-factors (see yellow and red colouring of the backbone in the structures shown in Figure 1.15). It is however not known at this time whether the loop movements are influenced by the presence of the FBP substrate (i.e. ligand-gated), or if they occur spontaneously (natural motion of the protein).

Chapter 5 Preliminary work on enzyme loop dynamics

The loop movements of other enzymes, such as metallo- β -lactamase, hypoxanthine-guanine-xanthine phosphoribosyltransferase, and asparaginase, have been successfully studied by stopped-flow and/or steady-state tryptophan fluorescence (Garrity *et al.* 2004; Munagala *et al.* 2001; Aung *et al.* 2000). These studies have linked the fluorescence quenching, and subsequent return to resting value, of a tryptophan residue inserted into an active site mobile loop, under single-turnover conditions, with the enzyme turnover rate. In the asparaginase study, the fluorescence emission spectrum of the enzyme was also shown to be red-shifted in the presence of increasing concentration of substrate (Aung *et al.* 2000). Other studies have used time-resolved tryptophan fluorescence to study loop movements and global conformational changes in enzymes in the presence of ligands, for example in mutants of fructose-1,6-bisphosphatase (Wen *et al.* 2001).

In the case of the *E. coli* Class II FBP aldolase, NMR studies were attempted to examine movements upon DHAP binding (Hilcenko, 2003, also see section 1.3.6). It was concluded that the β 5- α 7 loop did not change from an open to a closed conformation upon DHAP binding (FBP or GAP binding were not studied), and that the time scale of motion of a few ns for the loops β 5- α 7 and β 6- α 8 means that loop closure cannot be rate-limiting (Hilcenko, 2003). A fluorescence-based investigation of the loop movements in the same enzyme was not possible because the enzyme possesses 4 native tryptophan residues which could not be completely substituted without the loss of enzyme function (Hilcenko, 2003). The substitution of the native tryptophans was desirable because it was observed that the native *E. coli* Class II FBP aldolase fluorescence spectra changed upon DHAP binding. It was also reported that the mutation D183W (next to the catalytic E182 in the β 5- α 7 loop) results in over a 100-fold decrease in k_{cat} and a four-fold decrease in K_M in the *E. coli* enzyme, and this low activity prevented the study of this mutant for fluorescence changes upon substrate binding (Hilcenko, 2003). In contrast, the mutant M190W (M190 is also found within the *E. coli* aldolase β 5- α 7 loop) has similar kinetic properties as the wild type enzyme (Hilcenko, 2003).

The fluorescence changes observed upon DHAP binding for this mutant (which possessed a total of 5 tryptophan residues) were however similar to those observed with the wild-type *E. coli* aldolase, and it was concluded that the difference in fluorescence intensity did not come from the inserted W190 residue. It is noteworthy that the fluorescence changes upon binding of FBP or GAP were not studied by these authors.

In light of these results, and based on the Class II FBP aldolase sequence alignment (Figure 1.17), the recombinant aldolase from *H. pylori* (containing no native tryptophan residue), as well as the aldolases from *M. tuberculosis*, *P. aeruginosa*, and *B. cereus* (each possessing one native tryptophan residue) were chosen as templates for site-directed mutagenesis and intrinsic fluorescence studies. The following six mutations are proposed:

- *M. tuberculosis* FBP aldolase (Class II, type A), with a single native tryptophan residue (W130) in the hydrophobic core of the barrel (see Figure 5.1):
 - 1) Y280W – Residue is next to the substrate binding site (near C6-phosphate of substrate, close to the dimer interface in the *E. coli* FBP aldolase structure)
 - 2) N173W – Within the mobile $\beta 5$ - $\alpha 7$ loop
 - 3) I175W – Within the mobile $\beta 5$ - $\alpha 7$ loop
- *H. pylori* FBP aldolase (Class II, type B) with no native tryptophan residue (see Figure 5.2a):
 - 4) F185W – in the middle of the mobile $\beta 6$ - $\alpha 8$ loop, which contains one catalytic zinc ligand.
- *P. aeruginosa* FBP aldolase (Class II, type B) with a single native tryptophan residue (W240) at the dimer interface (see Figure 5.2b):
 - 5) F202W – in the middle of the mobile $\beta 6$ - $\alpha 8$ loop, which contains one catalytic zinc ligand.

Chapter 5 Preliminary work on enzyme loop dynamics

- *B. cereus* FBP aldolase (Class II, type B) with a single native tryptophan residue (W30) at the dimer interface (see Figure 5.2c):
 - 6) I149W – Within the mobile β 5- α 7 loop

The residues chosen as targets are not conserved across all Class II FBP aldolases, as shown in Figure 5.3. The other mutations (I149W, N173W and I175W) are all located on the large catalytic loop near the position of the residue M190 in *E. coli* (see Figure 5.3), which was previously mutated to a tryptophan with no adverse effect on the enzyme kinetics, as described above. The mutations F185W, F202W, and Y280W are conservative and are not expected to adversely affect the structure of the enzymes.

In this chapter, the mutagenesis, purification and kinetic characterization of these Class II FBP aldolase tryptophan mutants will be reported. The preliminary steady-state and time-resolved fluorescence studies results for the enzymes in the presence of substrate and inhibitors will also be presented and discussed.

Some of the work presented in this chapter was performed by undergraduate students under my supervision. The site-directed mutagenesis was performed by Sarah de Groot, except for the mutagenesis for MTY280W which was done by Willis Lang. The aldolase mutants were purified with the help of Diana Arsene, Sarah de Groot, Natasha Kruglyak and Willis Lang. The fluorescence experiments were also done with assistance from Diana Arsene and Natasha Kruglyak.

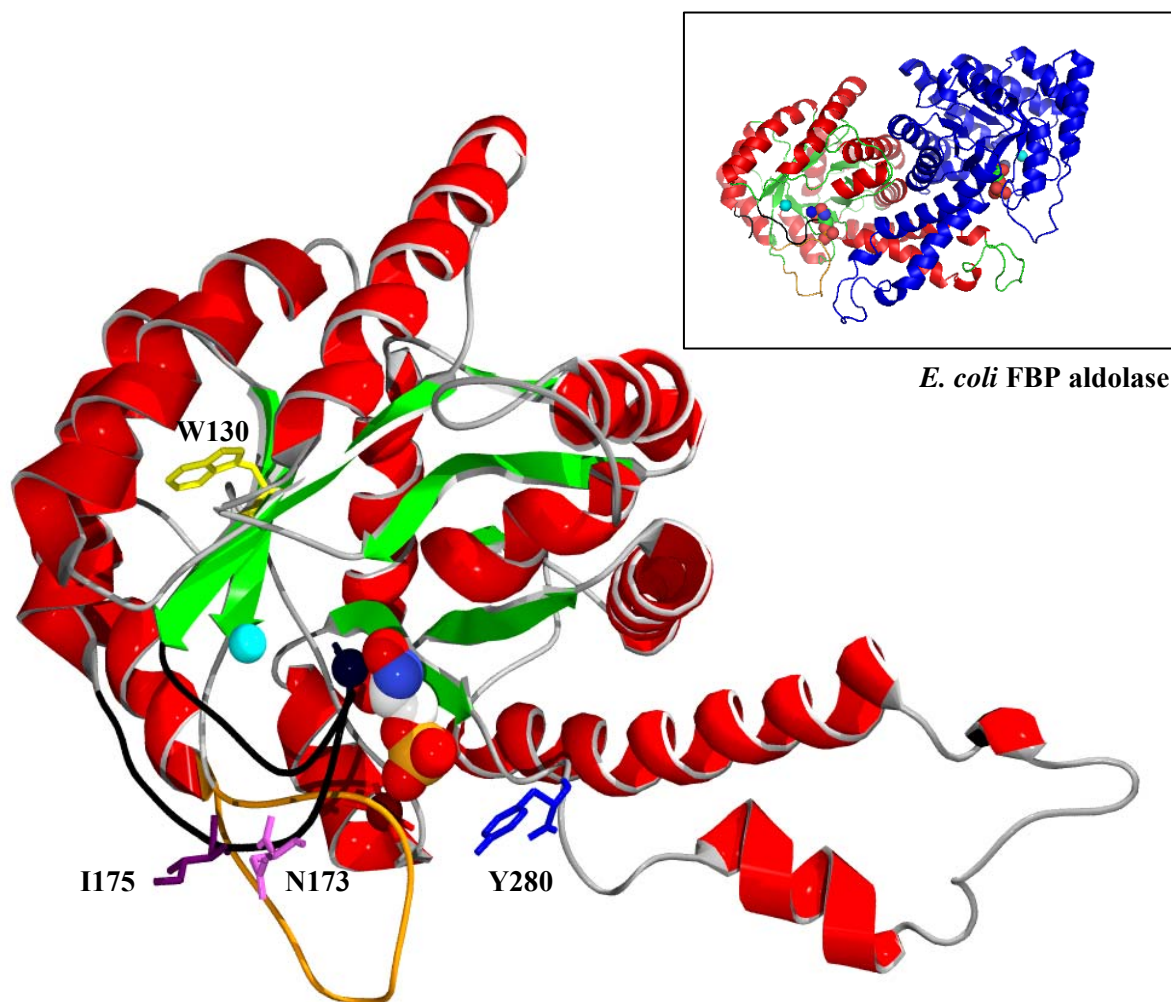


Figure 5.1 Targeted amino acids for tryptophan replacement in the *M. tuberculosis* Class II FBP aldolase

The image is a model of the *M. tuberculosis* Class II FBP aldolase monomer, created by threading its amino acid sequence onto the *E. coli* FBP aldolase structure with PGH bound (PDB entry 1B57, shown in inset with the other subunit in blue) using the online program SWISS-MODEL (www.expasy.ch) (Schwede *et al.* 2003; Guex and Peitsch 1997; Peitsch 1995). The β strands are in green and the α helices are in red. The large mobile loop ($\beta 5$ - $\alpha 7$) is in the closed position and is shown in black. The small mobile loop ($\beta 6$ - $\alpha 8$, containing one of the catalytic zinc ligands) is shown in orange. The native tryptophan (W130) is shown in yellow (buried in the hydrophobic core of the barrel). The targeted residues N173, I175, and Y280 are shown in pink, purple and blue sticks, respectively. The catalytic zinc is indicated by a black sphere, with the inhibitor PGH chelating it in space-fill representation (oxygens in red, carbons in white, phosphorus in orange, nitrogen in blue) along with the sodium ion associated with the phosphate group (dark red sphere). The structural zinc ion is shown as a cyan sphere. The image was done using DeepView/Swiss-PdbViewer (Guex and Peitsch 1997), POV-Ray™ for Windows (Persistence of Vision Raytracer Pty. Ltd.), and PyMOL (DeLano Scientific LLC). After the submission of this thesis, a structure of the *M. tuberculosis* Class II aldolase was published (Pegan *et al.* 2009)

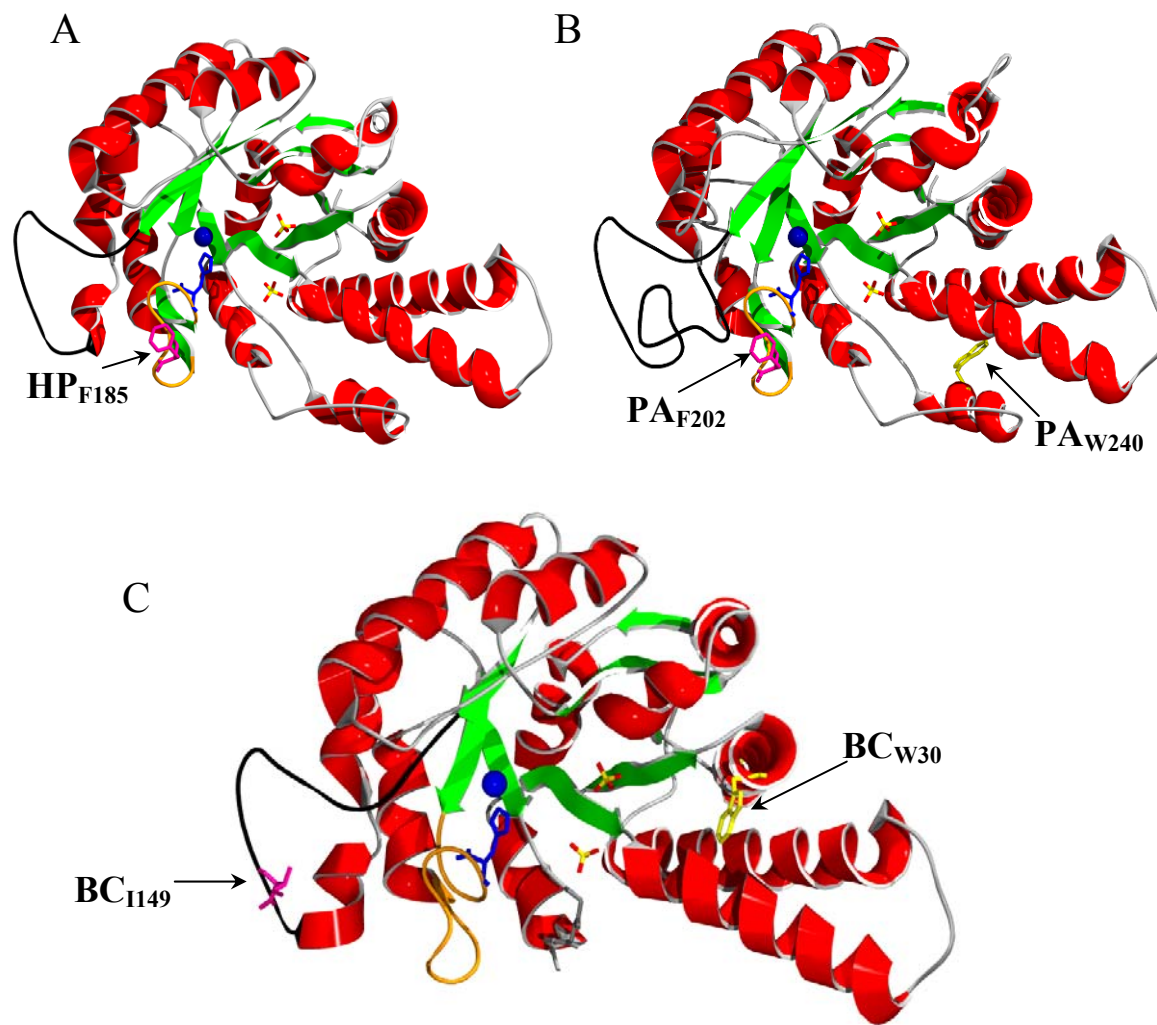


Figure 5.2 Targeted amino acids for tryptophan replacement in the *H. pylori*, *P. aeruginosa* and *B. cereus* Class II FBP aldolases

Models of the Class II FBP aldolase monomers from *H. pylori* (Panel A); *P. aeruginosa* (Panel B); and *B. cereus* (Panel C). The sequence of each monomer was threaded on the *T. aquaticus* FBP aldolase structure (PDB entry 1RV8) with a catalytic cobalt (blue sphere) in the buried position and 2 sulfate molecules (shown as yellow and red sticks) in the putative binding sites for the substrate's phosphate groups, using the online program SWISS-MODEL (www.expasy.ch) (Schwede *et al.* 2003; Guex and Peitsch 1997; Peitsch 1995). The β strands are in green and the α helices are in red. The large mobile loop ($\beta 5$ - $\alpha 7$) is in the open position and is shown in black. The small mobile loop ($\beta 6$ - $\alpha 8$, containing a catalytic zinc histidine ligand, shown as blue sticks) is colored in light orange. The native tryptophans (PAFBA W240 and BCFBA W30) are shown as yellow sticks. The loop residues targeted for mutagenesis (HPFBA F185, PAFBA F202, and BCFBA I149) are shown as pink sticks. The images were done using DeepView/Swiss-PdbViewer (Guex and Peitsch 1997) and POV-Ray™ for Windows (Persistence of Vision Raytracer Pty. Ltd.).

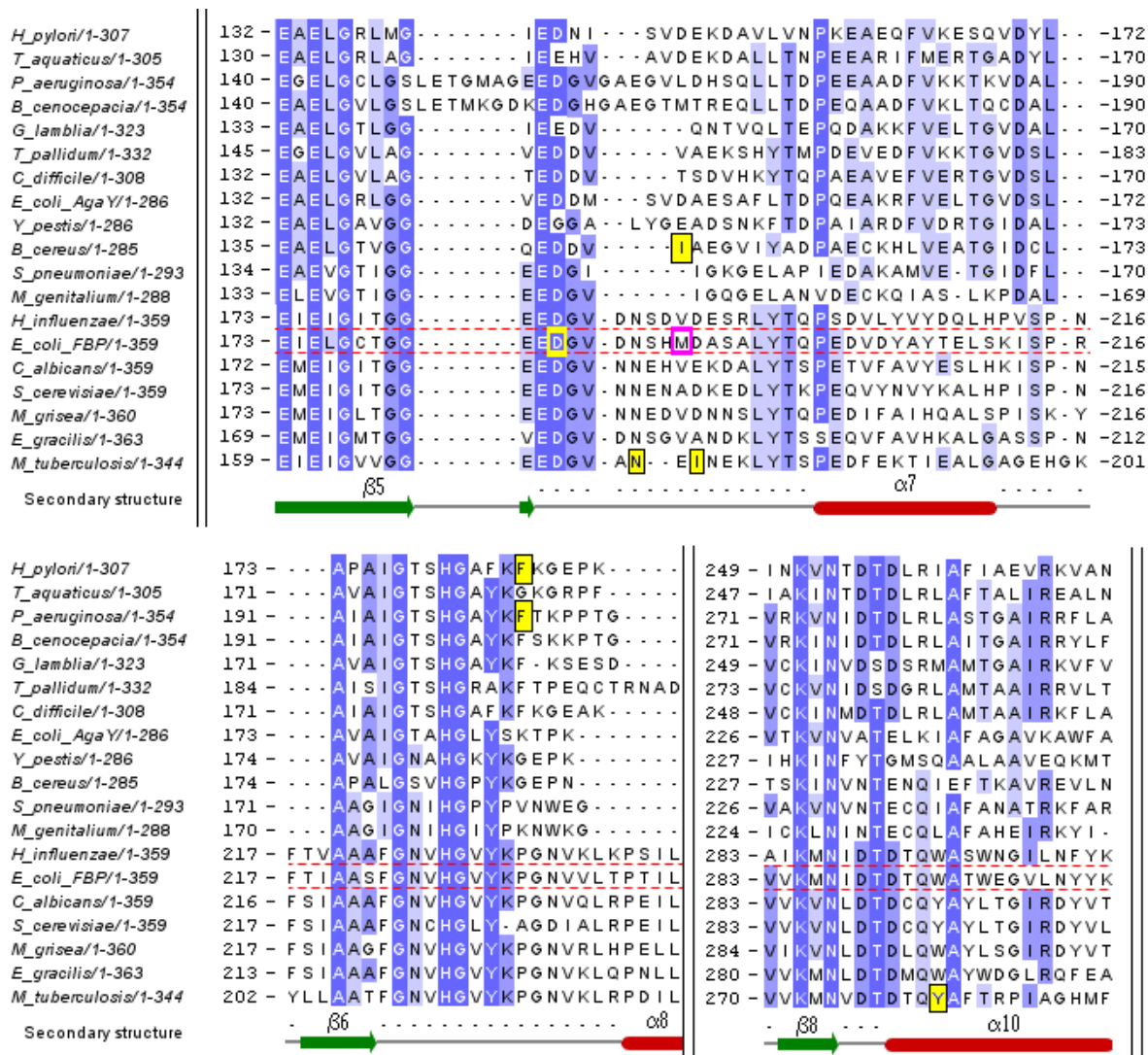


Figure 5.3 Targeted amino acids for site-directed mutagenesis

The figure shows portions of the Class II aldolases alignment presented in Figure 1.17. The targeted amino acids in the sequence of the aldolases from *H. pylori*, *P. aeruginosa*, *B. cereus* and *M. tuberculosis* are shown in filled yellow boxes. The residues D183 and M190 in the *E. coli* FBP aldolase sequence (mutated to tryptophans by other authors, see text) are also shown in yellow and pink boxes, respectively. Note that the numbering of amino acids may not correspond to that used in PDB structures, as the N-terminal methionine is absent (cleaved off) in some of these proteins.

5.2 Methods

5.2.1 Site-directed mutagenesis

The plasmids pT7-7/MTFBA, pT7-7/PAFBA, pT7-7/HPFBA and pT7-5/BCFBA (see Chapter 2 and Appendix A) were used as templates for the site-directed mutagenesis reactions. The primers used for each mutant are presented in Table 5.1. The PCR was performed using the Pwo DNA Polymerase kit (Roche Diagnostics) on an Endurance TC-512 Thermal cycler (Techne, Burlington, NJ). A two-stages site-directed mutagenesis protocol was used (Wang and Malcolm 1999). The first 5 cycles were done using two separate mixtures including either the forward or reverse primer, to promote maximal annealing of the primers with the template plasmid. After these five cycles, the two mixtures containing the forward and reverse primers were combined for the last 12 cycles. The initial denaturation for one minute at 94 °C, and the cycles consisted of a denaturation for 1.5 minute at 95 °C, annealing for 1.5 minute at 65 °C, and extension for 3 minutes at 72 °C. The final extension was done at 72 °C for 15 minutes.

Table 5.1 Primers used in site-directed mutagenesis

The mutations used to introduce the tryptophan codon (TGG), as well as the silent mutations used to insert or remove a restriction site, are shown in bold. The positions of the restriction sites (added or removed as indicated) are underlined.

Mutant	Primers	Restriction sites (added or removed)
MTY280W	MTY280WF: 5'-CACCGACACCCAGT TGGGCGTT CACCCGC-3' MTY280WR: 5'-GCGGGTGA ACGCC ACTGGGTGTCGGTG-3'	<i>Mlu</i> I (removed)
MTI175W	MTI175WF: 5'-GAGG ACGGCGT CGCGAACGAGT TGGA ACGAGAAGCTGTAC-ACC-3' MTI175WR: 5'-GGTGTACAGCTTCTCGTT CCACT CGTTCGC GACGCCGTC -CTC-3'	<i>Tth</i> 111I or <i>Psy</i> I (added)
MTN173W	MTN173WF: 5'-GAGG ACGGCGT CGCGT TGG GAGATCAACGAGAAG-3' MTN173WR: 5'-CTTCTCGTTGATCT CCCACGC G GACGCCGTC CCTC-3'	<i>Tth</i> 111I or <i>Psy</i> I (added)
BCI149W	BCI149WF2: 5'-CGGACAAGAAGAC GACGTC T TGGG GCTGAAGGCGTAATT-TAC-3' BCI149WR2: 5'-GTAAATTACGCCTTCAG CCCAG ACGTCGTCTTCTTGTCCG-3'	<i>Aat</i> II (added)
PAF202W	PAF202WF: 5'-CACCAGCCAC GCGCA TACAAGT TGG ACCAAGCCGC-3' PAF202WR: 5'-GCGGCTTGGT CCACT TGTA TGCGCC GTGGCTGGTG-3'	<i>Nar</i> I (removed)
HPF185W	HPF185WF: 5'-GGGACAAGCCAC GCGCCT TAAAT TGGA AAGGCGAGCC-3' HPF185WR: 5'-GGCTCGCCCT CCATT TAAAG GCGCC GTGGCTTGT-3'	<i>Nar</i> I (added)

In order to assess the success of the mutagenesis, the primers were designed to incorporate silent mutations to add or remove restriction sites from the templates (Table 5.1). For the mutant MTY280W, a *Mlu*I site was removed. The wild-type gene has another *Mlu*I site (Appendix A), yielding two fragments of 497 bp and 2989 bp when the plasmid is digested. After the mutation, only

Chapter 5 Preliminary work on enzyme loop dynamics

the linear plasmid (3486 bp) is obtained after *Mlu*I digestion. For the mutants MTI175W and MTN173W, a *Tth*111I site was added (*Tth*111I shares the same recognition sequence as *Pst*I). The vector pT7-7/MTFBA already contains this restriction site, such that after mutation the digestion yields two fragments of 777 bp and 2709 bp. An *Aat*II restriction site was added for the mutant BCI149W. The pT7-5/BCFBA vector also has an *Aat*II restriction site, such that after the mutation, the digestion of the vector gives two fragments of 1727 and 1525 base pairs. For the mutant PAF202W, a *Nar*I site was removed. Before mutation, the *Nde*I and *Nar*I double digestion of the pT7-7/PAFBA vector yields a 597 bp fragment, which is not present after mutation. Finally, a *Nar*I site was added for the mutant HPF185W.

5.2.2 Expression and purification

The mutated aldolases were expressed and purified using the methods described in Chapter 2. The mutant PAF202W was expressed in a fermentor as described in section 2.2.2.1. The mutants BCI149W, MTY280W, MTN173W and MTI175W were expressed in shake-flasks as described in section 2.2.2.2. The mutants were purified using the same methods as the corresponding native enzymes (see section 2.2.6), with the following modifications:

The mutant BCI149W was purified from 11 g of cells from a 3 L culture grown in LB broth supplemented with 0.1 mM ZnCl₂, and 0.36 g of protamine sulfate was used to precipitate nucleic acids. After ammonium sulfate fractionation, the anion-exchange chromatography was done using a 100 mls bed volume DEAE sepharose CL 6B column. The protein was washed with 10 CV of buffer B (50 mM Tris-HCl, 0.1 M NaCl, 0.2 mM ZnCl₂, pH 8.0) until the OD₂₈₀ was less than 0.12, before the start of the elution gradient which was from 100 mM to 400 mM NaCl over 5 CV. The active fractions were pooled, dialyzed against a 3.9 M ammonium sulfate solution, and stored at 4 °C.

Chapter 5 Preliminary work on enzyme loop dynamics

The mutant PAF202W was purified from 48 g of cells. Buffer A was composed of 50 mM Tris-HCl, 0.1 M NaCl, pH 8.0, with 0.1 mg/mL DNase I and 0.5 mg/mL lysozyme added. 0.94 g of protamine sulfate was used to precipitate nucleic acids. Buffer B used to dialyze the protein after ammonium sulfate fractionation was composed of 50 mM Tris-HCl, 0.1 M NaCl, pH 8.0. The first anion exchange chromatography was done using a thermo-jacketed column (16mm x 10cm) containing 20 mL of DEAE Sepharose CL-6B resin. The protein was washed with 10 CV of buffer B and eluted using a gradient from 100 mM to 500 mM NaCl over 10 CV at a flow rate of 1 mL/min. The active fractions were pooled and supplemented with glycerol to a final concentration of 50%, and stored at -20 °C. The protein was then loaded (70 mg per run) on a 6 mL ResourceQ column pre-equilibrated with buffer C (50 mM Tris-HCl, 0.1 M NaCl, 1 mM β -mercaptoethanol, pH 8.0), washed with 5 CV of the same buffer, and eluted using a gradient of 100 mM to 500 mM NaCl over 20 CV at a flow rate of 5 mL/min. The active fractions were pooled, supplemented with glycerol to a final concentration of 50%, and stored at -20 °C.

The mutants MTY280W and MTN173W were purified from ~4 g of cells grown in TB broth. The enzymes were purified as described in Chapter 2 for the native *M. tuberculosis* aldolase grown in shake-flask. The DEAE column had a bed volume of 24 mL (16 mm x 12 cm), and the gel filtration column used was a 124 mL bed volume HighLoad 16/60 Superdex 200 column (Amersham-Pharmacia Biotech). The 3 most active elution fractions (2 mL each) of the purified enzymes were either frozen in liquid nitrogen and stored at -80 °C (MTY280W), or supplemented with glycerol to a final concentration of 50% and stored at -20 °C (MTN173W). The mutant MTN173W was then further purified by loading the pooled gel filtration fractions onto a 1 mL ResourceQ column (Pharmacia LKB Biotechnology) pre-equilibrated with buffer C (50mM TRIS-HCl, 100mM NaCl, pH 7.8). The protein was washed with 13 CV using buffer C, and then eluted with a gradient from

Chapter 5 Preliminary work on enzyme loop dynamics

100 mM to 500 mM NaCl over 40 CV. The 4 most active fractions (1 mL each) were supplemented with glycerol to a final concentration of 50% and stored at -20 °C.

The mutant MTI175W was purified from 20.5 g of cells grown in LB broth. The purification procedure was as described above for the mutant MTN173W, excepted that the protein eluted from the gel filtration column was split into two pools, and further purified using a 6 mL Resource Q column (in two subsequent runs) for the last anion-exchange chromatography step, instead of using the 1 mL ResourceQ column. The active fractions were pooled, supplemented with glycerol to a final concentration of 50% and stored at -20 °C.

5.2.3 Activity assays, protein assays, and SDS-PAGE

The enzymatic assays and the kinetic parameters determination were done as described in section 2.2.3. The characterization of the *M. tuberculosis* FBP aldolase mutants was done at 30 °C using 50 mM Hepes pH 7.3 as the assay buffer, instead of 50 mM Tris-HCl, pH 8.0. The *B. cereus* and *P. aeruginosa* aldolase mutants were assayed in 50 mM Tris-HCl, pH 8.0. Protein concentration was determined by the dye binding method of Bradford (Bradford 1976) using BSA as a reference standard. The purity of the preparations were estimated by SDS-PAGE on 12%-polyacrylamide gels according to the method of Laemmli (Laemmli 1970). All gels were stained with Coomassie Blue.

5.2.4 Steady-state fluorescence

The *M. tuberculosis* wild-type aldolase and its mutants I175W, N173W, and Y280W were dialyzed in 1L of dialysis buffer (50 mM Hepes buffer, pH 7.3, with 5 μ M ZnCl₂) overnight at 4 °C. Dialysis tubing with 6-8,000 molecular weight cut-off was used in each case to remove the glycerol. The dialyzed samples were then concentrated using VivaSpin columns (Viva Science) with a 10,000 Da cut-off, followed by Nanosep 10,000 Da cut-off columns (PALL Life Sciences), to a total volume of less than 100 μ l. A Bradford assay and NADH enzyme-coupled assay was performed to

determine the specific activity of each enzyme sample to be used in the fluorescence studies. The concentrations of enzyme used in the presence of 5.3 mM FBP and 4.2 mM DMPS were: 8.5 mg/mL (230 μ M) for the wild-type *M. tuberculosis* aldolase; 2.8 mg/mL (77 μ M) for MTI175W mutant; 1.7 mg/mL (47 μ M) for the MTN173W mutant; and 0.9 mg/mL (25 μ M) for the MTY280W mutant. The enzyme concentrations were 1.2 times higher for the scans taken prior to the addition of FBP and DMPS (100 μ L of each enzyme solution were used for the first scan, then 10 μ L of FBP stock and 10 μ L of DMPS stock were added for the second scan). The specific activity immediately prior to the fluorescence scans was 9.1 U/mg for the wild-type enzyme, and 17.3 U/mg, 14.2 U/mg, and 4.1 U/mg for the I175W, N173W and Y280W mutants, respectively.

Prior to starting the emissions scans, the following parameters were adjusted: excitation slit 1 and 2 on the fluorimeter (PTI, Photon technology International, Birmingham, NJ) were opened to 1 mm and 2 mm, respectively. The emission slits were then adjusted; emission slit 1 and 2 were opened to 1 mm and 2 mm, respectively. The lamp was warmed up at 75 Watts. The excitation wavelength was set to 295 nm, to avoid excitation of native tyrosine residues in the enzyme sample. The emission scan was performed from 300 to 450 nm, using a 2 nm step-size and 0.5 second integration. Only one scan was taken for each sample, which were placed in a 90 μ l quartz cuvette.

5.2.5 Time-resolved fluorescence

A Pulsed Diode LED (PDL 800-B light source with a sub-nano second pulsed LED PLS-301 plug-in head, PicoQuant) was used as the light source (excitation wavelength of 298 nm, minimum pulse width of 0.45 ns). The detector was a FluoTime 100 Compact Fluorescence Lifetime Spectrometer (PicoQuant GmbH, Berlin, Germany). All samples were run in a 90 μ l quartz cuvette, which was tilted in the “magic” 54.7 $^{\circ}$ angle position to compensate for emission anisotropy. Time Harp 200 software was used to collect the data. Data was collected up to a 5,000 photon count for

Chapter 5 Preliminary work on enzyme loop dynamics

each trial, unless otherwise indicated, and the fluorescence emission was recorded over ~135 ns (34 ps per channel). A light-scattering colloidal silica solution (Ludox) was used to record the instrument response function. To eliminate some of the background signal attributed to light scattered by the buffer (50 mM Hepes, pH 7.3, with 5 μ M ZnCl₂), a 320 nm filter was used. An exponential function was then fitted to the data using the Marquardt algorithm in the FluoroFit software (PicoQuant GmbH, Berlin, Germany), and the parameters were altered until a minimal χ^2 value was obtained.

The BCI149W mutant had a concentration of 0.73 mg/mL (24 μ M) and a specific activity of 3 U/mg. The *B. cereus* wild-type aldolase had a concentration of ~32 mg/mL (~1 mM) and a specific activity of ~6.6 U/mg. The enzymes were diluted by ~10% after the addition of 5.3 mM FBP.

Due to the limited amount of the *M. tuberculosis* aldolase and its mutants, the samples used for time-resolved fluorescence spectroscopy were the same ones used for steady-state fluorescence studies (see enzyme concentrations in section 5.2.4). The samples used with the 320 nm emission filter for these time-resolved fluorescence studies were the same samples previously used without the filter, which had been flash-frozen in liquid nitrogen (after addition of 5.3 mM FBP and 4.2 mM DMPS) and stored at -80 °C for 6 days.

5.3 Results

5.3.1 Cloning, purification and characterization

The proposed mutants were all generated by site-directed mutagenesis. The success of the mutagenesis was verified by performing appropriate restriction digests and by gene sequencing. The mutants were then purified, except for the mutant HPF185W, which was not studied because the native *H. pylori* FBP aldolase was too unstable in our hands (see section 2.3.3.5). The SDS-PAGE of the purified proteins are shown in Figures 5.4 to 5.8, and the molecular weight of the enzymes are

shown in Table 5.2. A summary of the purification and characterization results is presented in Table 5.3.

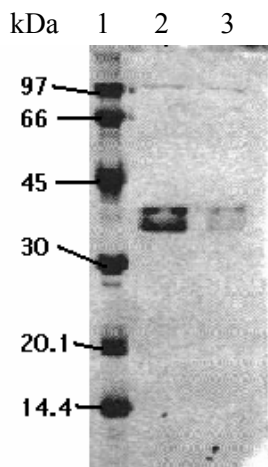


Figure 5.4 SDS-PAGE analysis of the purified MTI175W mutant

Lane 1 contains the molecular weight markers. Lanes 2 and 3 contain respectively 1.4 μg and 0.6 μg of the purified *M. tuberculosis* aldolase I175W mutant. The gel was stained with Coomassie Blue.

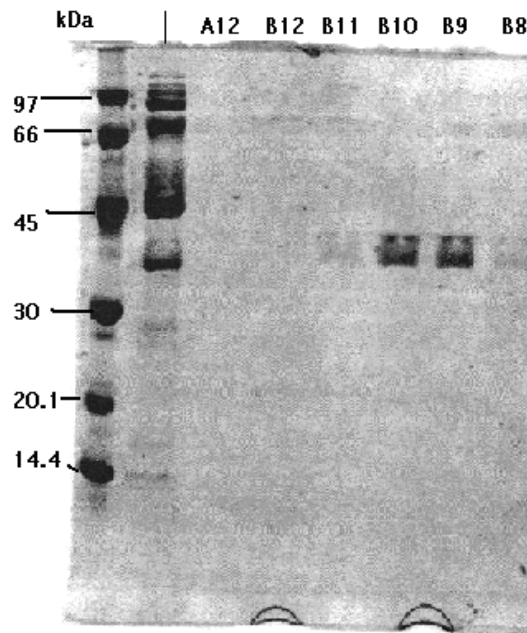


Figure 5.5 SDS-PAGE analysis of the purified MTN173W mutant

The molecular weight markers are shown in the extreme left lane. The lanes B10 and B9 each contain ~1.2 μg of the purified *M. tuberculosis* aldolase N173W mutant. The gel was stained with Coomassie Blue.

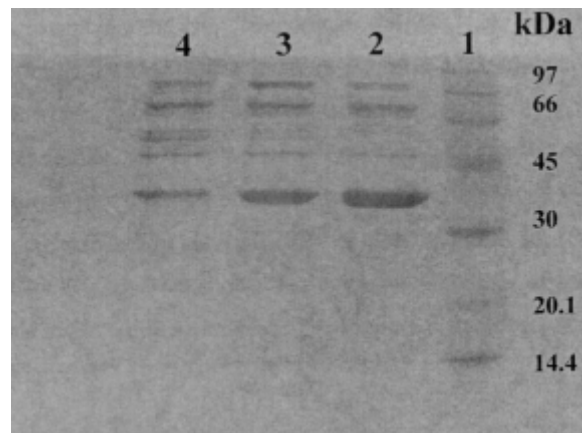


Figure 5.6 SDS-PAGE analysis of the purified MTY280W mutant

Lane 1 contains the molecular weight markers, and lanes 2 to 4 contain 20 μL aliquots from the 3 most active fractions (total volume of 2 mL each) eluted from the gel filtration column. Lane 2 contains approximately 3 μg of the purified *M. tuberculosis* aldolase Y280W mutant. The gel was stained with Coomassie Blue.

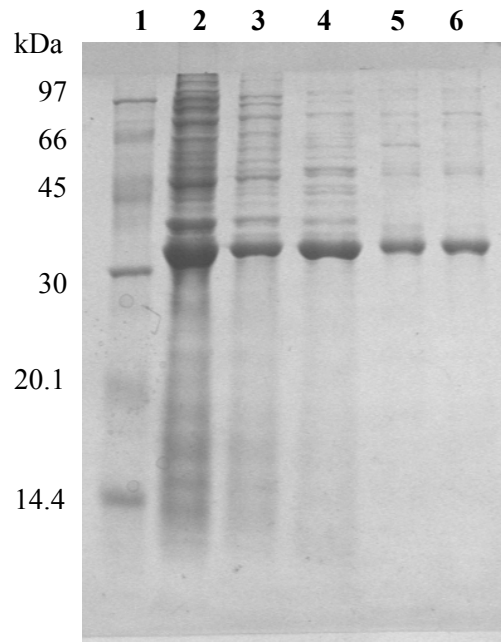


Figure 5.7 SDS-PAGE analysis of the purified BCI149W mutant

Lane 1 contains the molecular weight markers; lane 2 = 20 μg of crude extract; lane 3 = 10 μg of 40% ammonium sulfate cut supernatant; lane 4 = 5 μg of 60% ammonium sulfate cut supernatant. The purified *B. cereus* aldolase I149W mutant is shown in lanes 5 and 6: lane 5 = 5 μg of DEAE fractions pool D; lane 6 = 5 μg of DEAE fractions pool E. The gel was stained with Coomassie Blue.

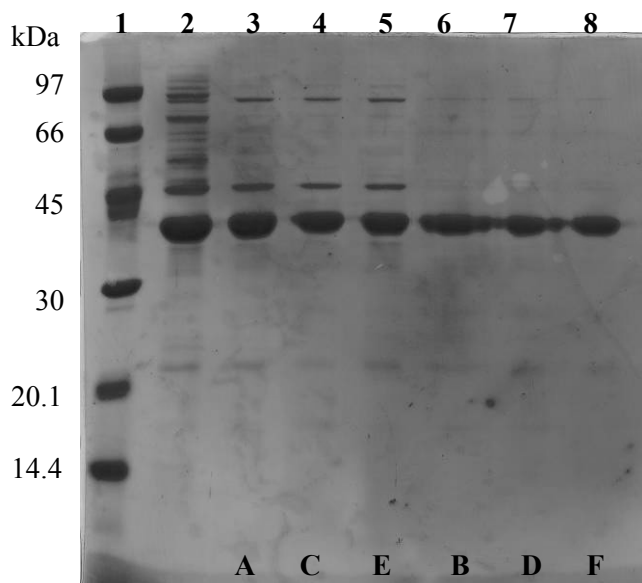


Figure 5.8 SDS-PAGE analysis of the purified PAF202W mutant

Lane 1 contains the molecular weight markers; lane 2 contains $\sim 7 \mu\text{g}$ of the DEAE fractions pool; and lanes 3 to 8 contain $\sim 2 \mu\text{g}$ of the purified *P. aeruginosa* aldolase F202W mutant (pools A to F, as indicated at the bottom of the gel). The gel was stained with Coomassie Blue.

Table 5.2 Mass spectrometry results for the purified tryptophan mutants

Aldolase	Theoretical M.W.*		Measured M.W.† (Da)
	(+Met) (Da)	(-Met) (Da)	
<i>M. tuberculosis</i> Y280W	36,567	36,436	36,432 (major, 100%) and 25,802 (minor, 43%)
<i>M. tuberculosis</i> N173W	36,617	36,485	36,482.5
<i>M. tuberculosis</i> I175W	36,618	36,486	36,483.5
<i>P. aeruginosa</i> F202W	38,610	38,479	38,482
<i>B. cereus</i> I149W	30,746	30,615	30,613.5 (major, 100%) and 30,649.5 (minor, 28%)

*The mass with and without the N-terminal methionine residue are shown

†When more than one peak was obtained, the relative intensity of each signal is indicated in brackets.

Table 5.3 Purification results and kinetic parameters of the tryptophan mutants

Aldolase†	Total Protein (mg)	Percent Yield (%)	Specific Activity ($\mu\text{mol FBP}/\text{min}/\text{mg}$)	K_M ($\mu\text{M FBP}$)	k_{cat} (s^{-1})
<i>MT wild-type</i>	0.80	14.40	35.1	20.3 ± 0.3	21.0 ± 0.1
MTY280W	1.50	2.00	2.60	90 ± 7	1.38 ± 0.04
MTI175W	1.55	2.17	31.8	20 ± 2	19.9 ± 0.4
MTN173W	0.33	4.71	27.8	17 ± 2	16.6 ± 0.3
<i>BC wild-type</i>	210	23	9.2	450 ± 10	2.95 ± 0.03
BCI149W (C to E)	100	19	3 to 4.7	730 ± 50	2.40 ± 0.07
<i>PA wild-type</i>	305	4.9	1.4	35 ± 2	1.53 ± 0.02
PAF202W (A to F)	309	4.8	0.7 to 0.98	$45 \pm 2^*$	0.45^* to 0.63^*

† Results for the wild-type enzymes are those presented in Chapters 2 and 3 and are included as a reference. The *M. tuberculosis* aldolase (wild-type and mutants) kinetic parameters presented in this Table were determined in 50 mM Hepes pH 7.3, whereas the other enzymes were assayed in 50 mM Tris-HCl pH 8.0. Kinetic parameters were estimated by fitting the data to the Michaelis-Menten equation using the least squares and dynamic weighting options of the Leonora software program (Cornish-Bowden 1995). *Enzyme lost activity rapidly.

The enzymes with mutations in the large catalytic loop (MTN173W, MTI175W, and BCI149W) have kinetic parameters similar to the corresponding wild-type enzymes. The mutant PAF202W, which had a mutation in the small loop participating in the catalytic zinc coordination, rapidly lost activity after its purification and was not used for fluorescence experiments. The mutant MTY280W, with a mutation near the C6 phosphate binding site and dimerization interface, had a $k_{\text{cat}} \sim 15$ times

Chapter 5 Preliminary work on enzyme loop dynamics

lower than the wild-type enzyme (the lower purity of the enzyme is partially responsible for the lower k_{cat}), but only a 4-fold increase in its K_M for FBP cleavage. The purified mutants all had the expected molecular weight according to the ESI-MS results (Table 5.2), and all have their N-terminal methionine cleaved. The minor peak at 30,649.5 Da (enzyme + 36 Da) obtained with the BCII49W mutant, and the peak at 25,802 Da obtained with the MTY280W mutant may be due to the presence of contaminating proteins, as several contaminating proteins can be seen on the SDS-PAGE gels of the purified fractions (see Figures 5.6 and 5.7). The mutant MTY280W is only ~70% pure, and the BCII49W is ~90% pure. The MTN173W and MTI175W mutant enzymes were purified by the extra anion-exchange purification step resulting in 95% pure enzyme. The small amount of purified *M. tuberculosis* aldolase mutants obtained (1.5 mg or less) will only allow for preliminary fluorescence studies.

5.3.2 Equilibrium fluorescence studies

The fluorescence spectrum of the wild-type aldolase from *B. cereus* has a maximum intensity around 323 nm, consistent with the burial of the tryptophan residue (W30) at the dimer interface (Figure 5.2 Panel C). The native tryptophan residue of this aldolase does respond to FBP binding as there is a small blue shift (4 nm) in the fluorescence peak in the presence of substrate for the wild-type enzyme. No significant shift in fluorescence is observed for the mutant BCII49W, which has two tryptophan residues (Figure 5.9 and Table 5.4). The emission peak of BCII49W occurs at a higher wavelength than the wild-type enzyme (peaks at 339 nm and 323 nm, respectively) which is consistent with the water-exposed position of the tryptophan residue inserted in the large mobile loop, compared to the hydrophobic environment of the native *B. cereus* aldolase tryptophan (Figure 5.2 Panel C). The inserted W149 has a much higher fluorescence emission than the native W30 in the mutant (see the relative fluorescence intensity versus the enzyme concentration of the wild-type and mutant *B. cereus* aldolases in Figure 5.10), and therefore makes the highest contribution to the overall

fluorescence spectrum of BC149W. This may explain why the small blue shift in the fluorescence of the native tryptophan upon substrate binding is not detectable in the mutant. The excitation scan of these enzymes is presented in Figure 5.10, showing that the presence of DMPS did not affect the excitation spectra of BC149W. However, it was observed that DPA-based inhibitors absorb light in the tryptophan excitation range and do affect the fluorescence emission of the aldolases (Figure 5.11). Therefore the inhibitor DMPS was used instead for subsequent fluorescence studies.

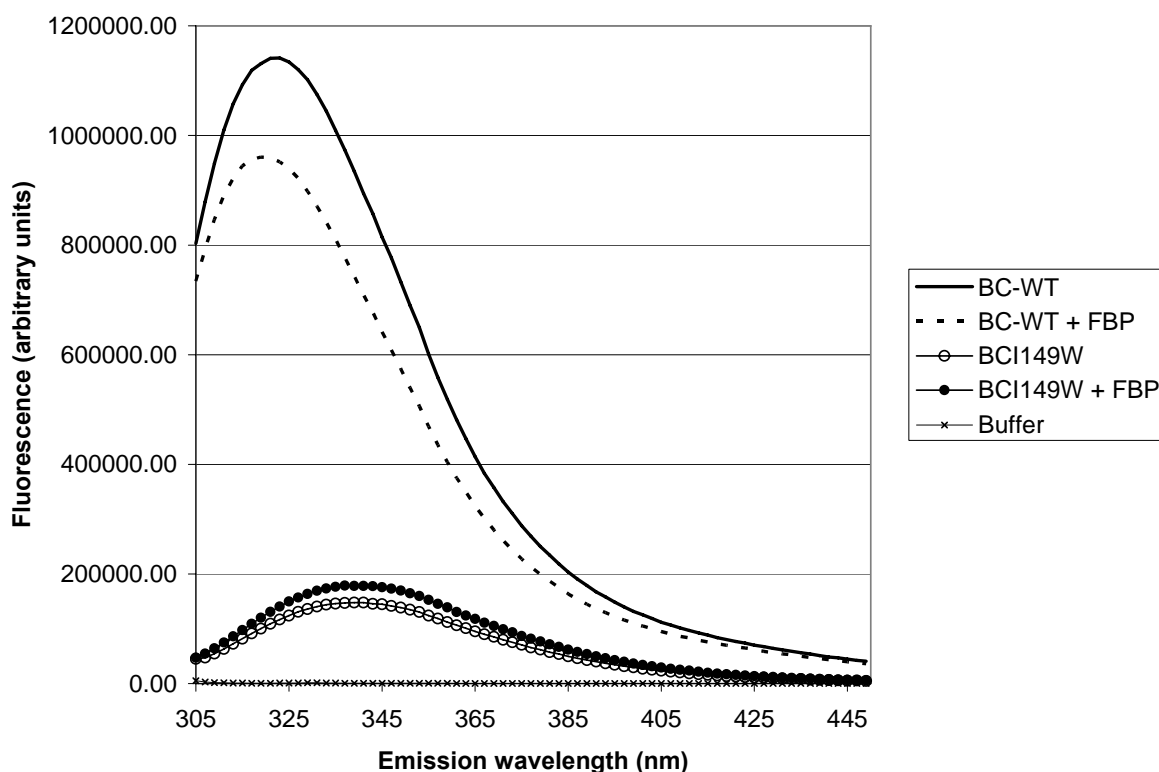


Figure 5.9 Fluorescence emission spectra of the *B. cereus* wild-type aldolase and its mutant BC149W in the presence or absence of FBP

The excitation wavelength was 295 nm, the step size was 2 nm, and the integration time was 0.5 s. The buffer was 50 mM Hepes, 5 μ M ZnCl₂, pH 7.3. The enzyme concentration was 1 mM for BC-WT and 24 μ M for BC149W, and the concentration of FBP was 5.3 mM. The emission peak is at 323 nm for the *B. cereus* wild-type enzyme in the absence of FBP, and the peak is slightly blue-shifted (to 319 nm) in the presence of the substrate. No shift is observed for the fluorescence emission peak of the mutant in these conditions.

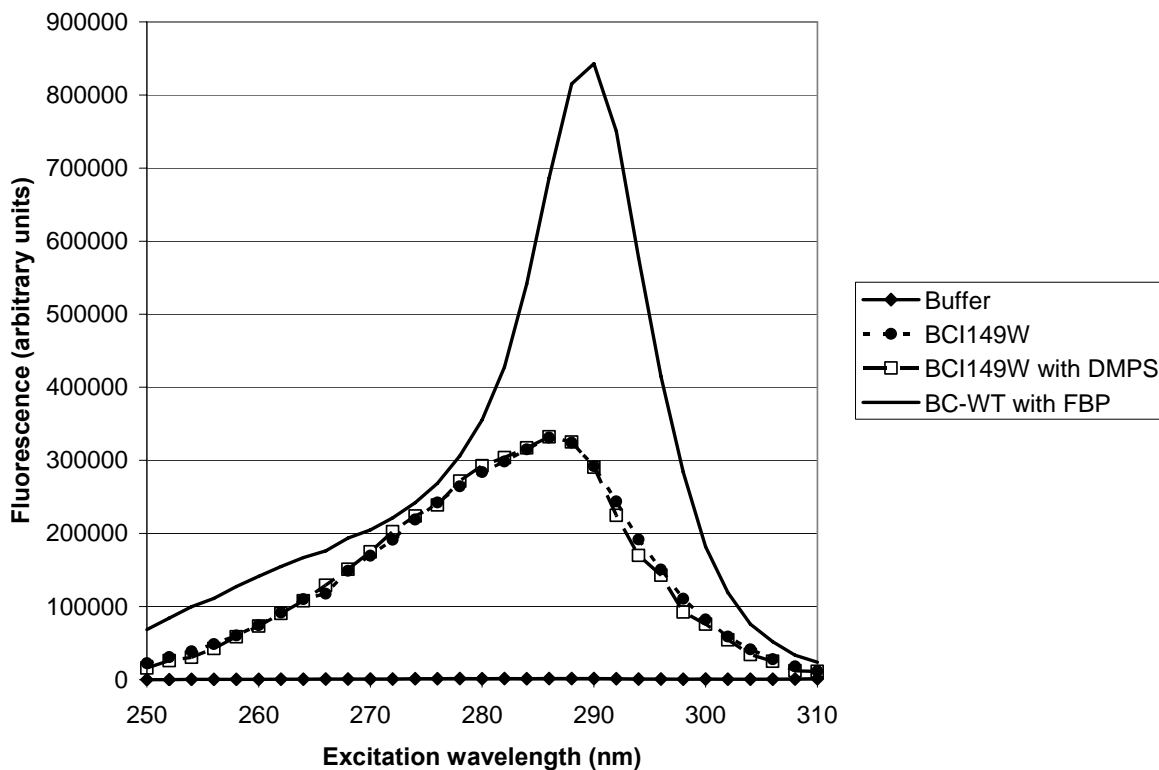


Figure 5.10 Fluorescence emission spectra of the wild-type aldolase from *B. cereus* (BC-WT) and of the mutant BCI149W in the presence of FBP or DMPS, in function of the excitation wavelength.

The emission was recorded at 350 nm, and the integration time was 0.5 s. The buffer consisted of 50 mM HEPES, 5 μ M ZnCl₂, pH 7.3, and the enzyme concentration was 1 mM for BC-WT and 24 μ M for BCI149W. The concentration of FBP was 5.3 mM and the concentration of DMPS was 5 mM.

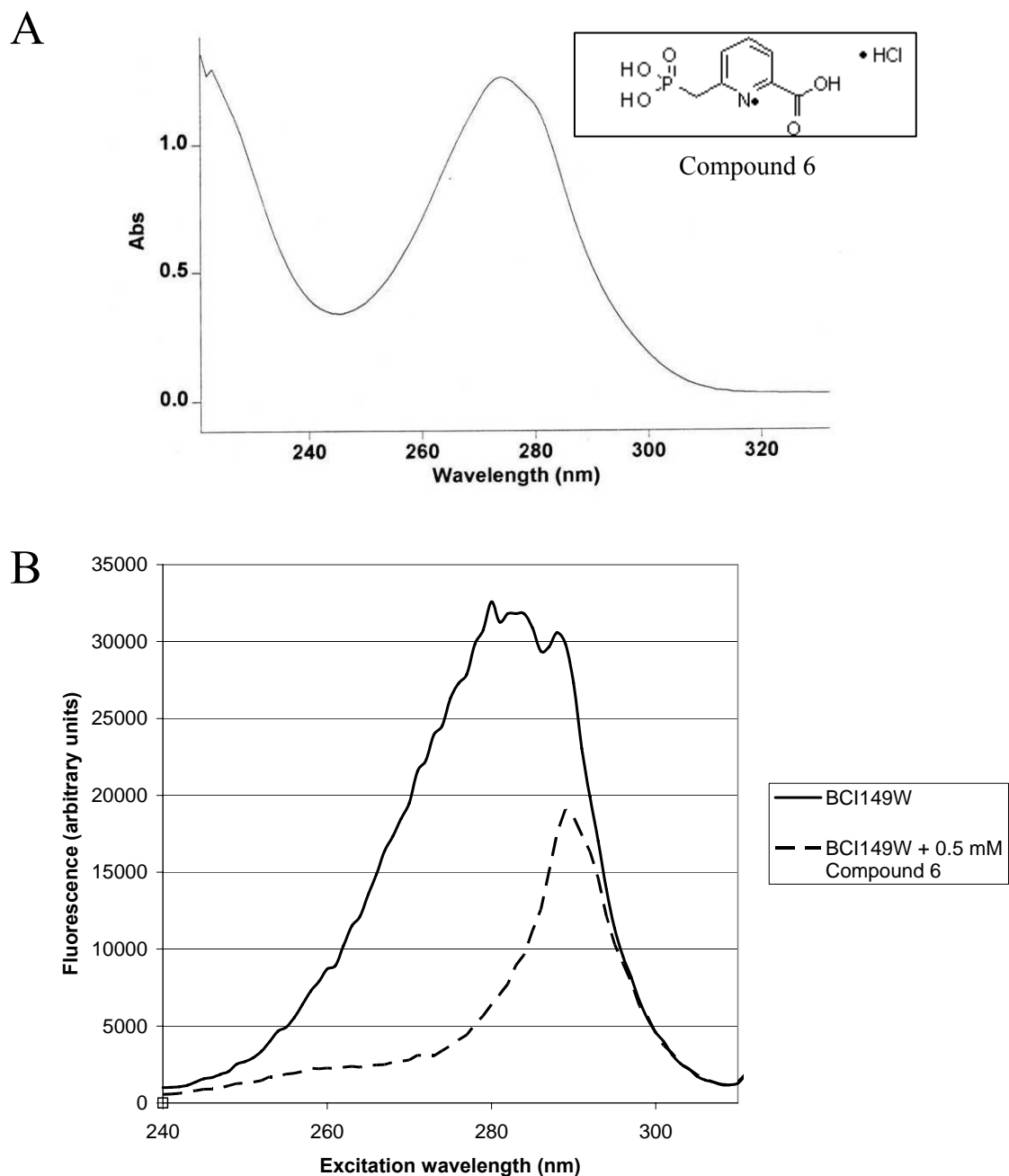


Figure 5.11 Absorption spectra of compound 6 and effect on fluorescence emission of *B. cereus* aldolase mutant I149W in function of the excitation wavelength.

Panel A: UV-Vis absorption spectra of compound 6 (insert). The DPA derivative had a concentration of 312.5 μM and was dissolved in 50 mM HEPES, pH 7.3. Panel B: Excitation spectra of the BCI149W mutant (3 μM of enzyme, dissolved in 50 mM Tris-HCl, 1 μM ZnCl_2 , pH 8.0) in the presence and absence of 0.5 mM compound 6. The emission was recorded at 350 nm, and a 1 mL quartz cuvette was used.

The emission spectra of BCI149W in the presence and absence of DMPS is shown in Figure 5.12.

No significant shift in fluorescence emission was observed in the presence of this inhibitor.

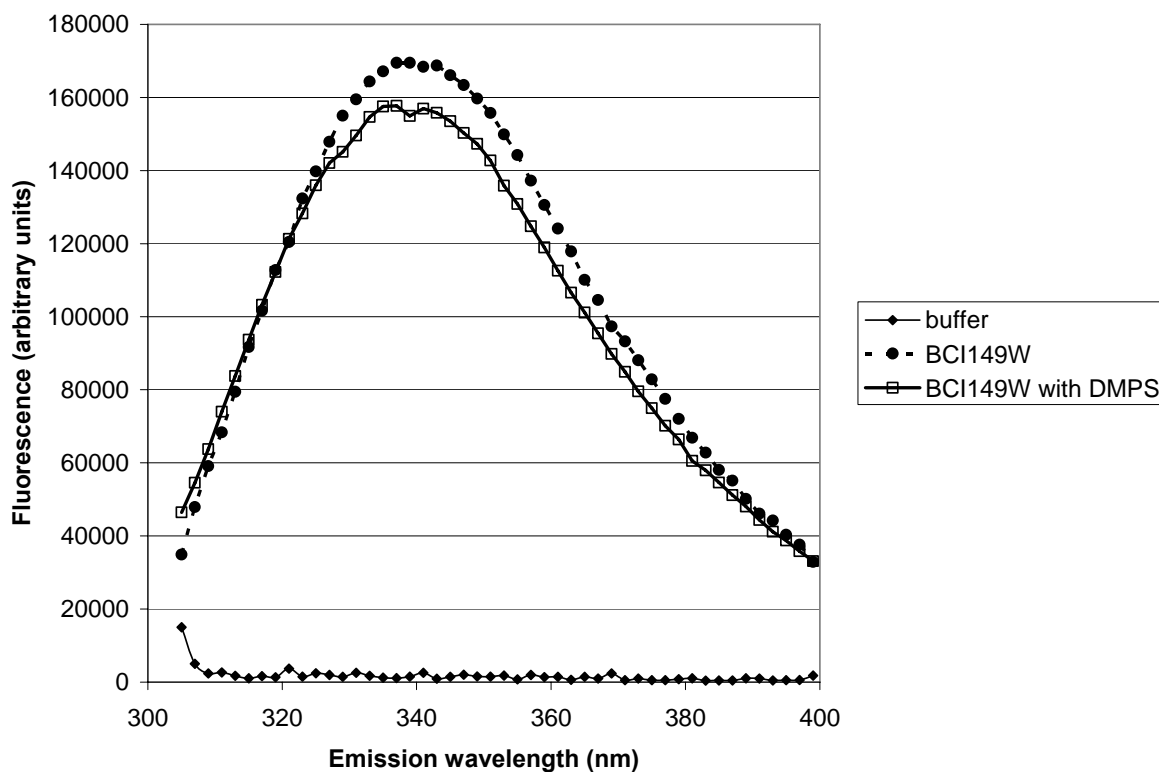


Figure 5.12 Fluorescence emission spectra of mutant BCI149W enzyme in the presence of DMPS

The excitation was done at 295 nm. The buffer consisted of 50 mM Hepes, 5 μ M ZnCl₂, pH 7.3, the enzyme concentration was 24 μ M, and the concentration of DMPS was 5 mM. The step size was 2 nm, the integration time was 0.5 seconds and 5 averages were taken for each sample.

The emission spectra of the wild-type and mutated *M. tuberculosis* aldolases are shown in Figure 5.13. The red-shift of the fluorescence emission of the mutated aldolases is consistent with the greater solvent-exposure of the inserted tryptophan residues, compared to the wild-type tryptophan residue (W130, Figure 5.1). A small shoulder is actually noticeable in the spectra of the MTY280W and MTN173W mutated aldolases around 337 nm (Figure 5.13), corresponding to the emission of the

wild-type tryptophan residue in each mutant. The emission spectra of the wild-type aldolase from *M. tuberculosis* as well as its mutants Y280W, N173W and I175W did not significantly shift upon binding of FBP or DMPS (Figure 5.14). The peak emission wavelengths of the enzymes are summarized in Table 5.4.

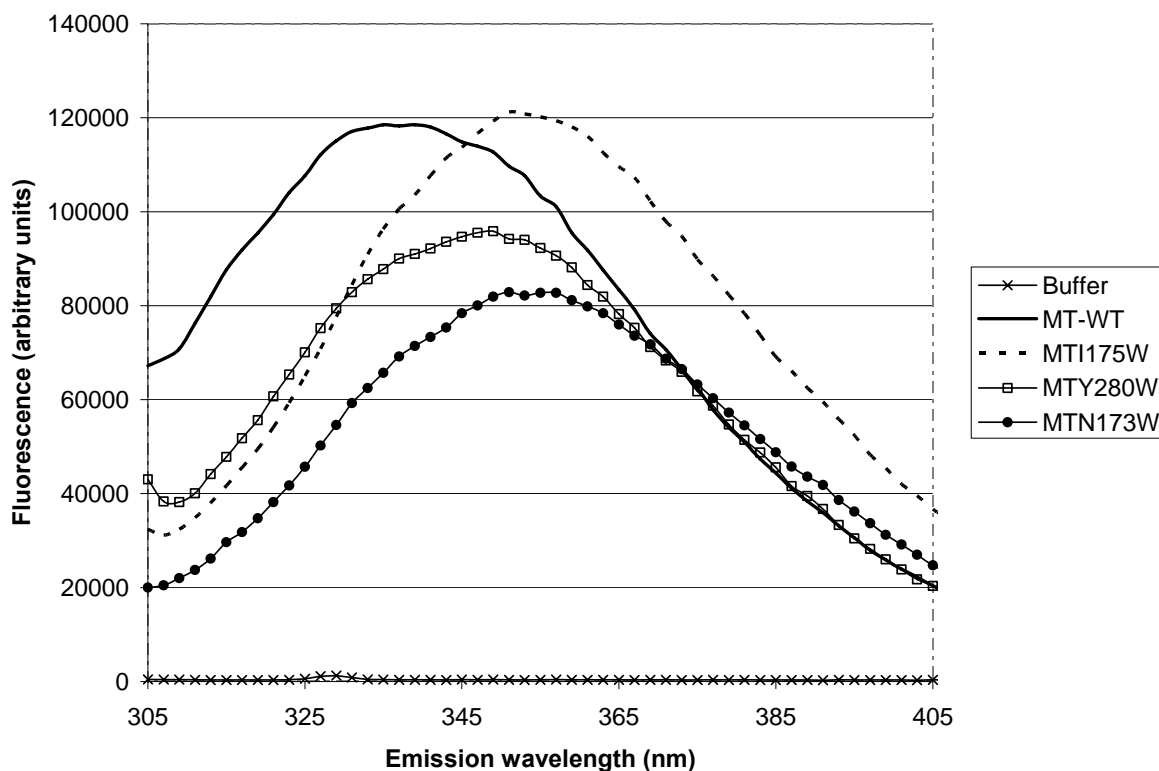


Figure 5.13 Emission spectra of the *M. tuberculosis* aldolase and its mutants

The excitation wavelength was 295 nm, and the emission spectra were recorded in 2 nm intervals. The buffer was 50 mM Hepes, pH 7.3 containing 5 μ M $ZnCl_2$. The enzyme concentration was 280 μ M for the wild-type *M. tuberculosis* aldolase (MT-WT), 94 μ M for the I175W mutant, 57 μ M for the N173W mutant, and 31 μ M for the Y280W mutant. The buffer spectrum was subtracted from the data obtained with the enzymes. The emission peak was at 337 nm for the wild-type *M. tuberculosis* aldolase; 349 nm for the Y280W mutant; and 353 nm for the I175W and the N173W mutants.

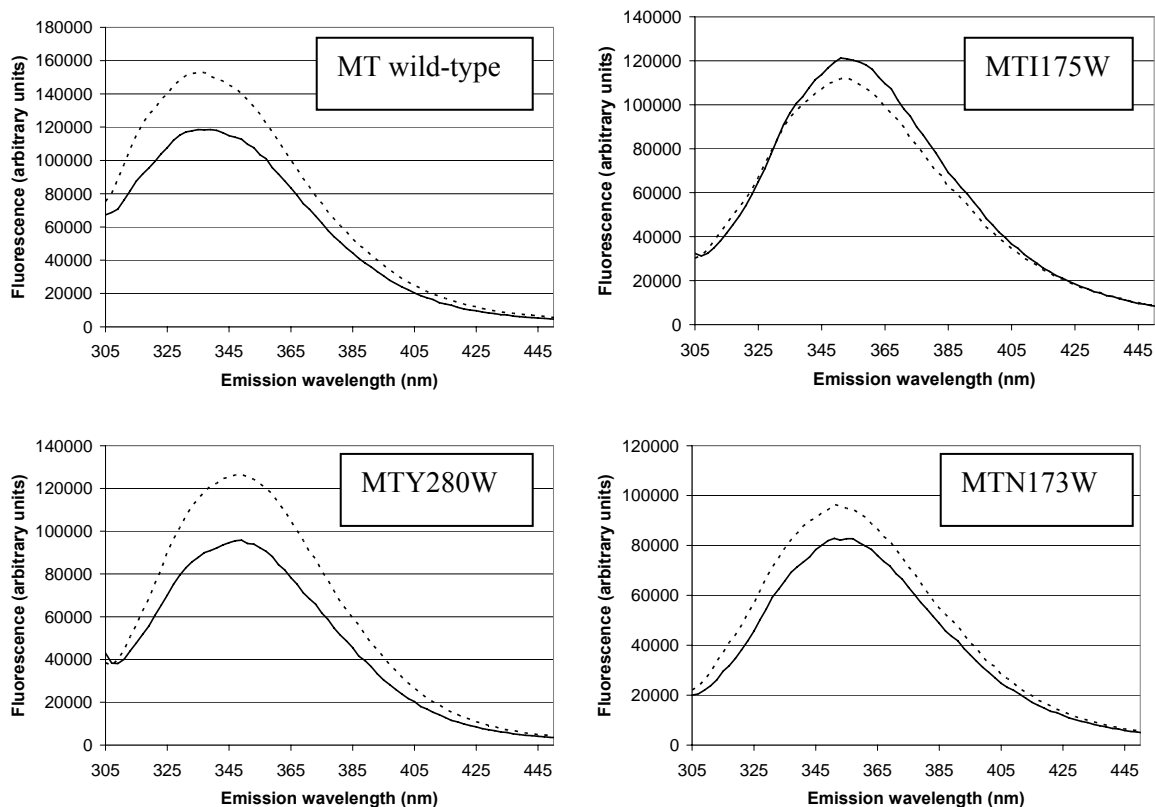


Figure 5.14 Fluorescence emission spectra of the *M. tuberculosis* aldolase and its mutants in the presence of FBP and DMPS

The spectra were taken for the enzymes alone (solid curves, also presented in Figure 5.12), and for the enzymes in the presence of 5.3 mM FBP and 4.2 mM DMPS (dashed curves). The excitation wavelength was 295 nm. The enzyme concentrations are described in Figure 5.12. The enzyme concentrations were lower after the addition of FBP and DMPS (see section 5.2.4), and the fluorescence intensity for these curves was adjusted proportionally to this dilution. The emission peaks were not significantly shifted from the values obtained after addition of FBP and DMPS (Fig. 5.12).

Table 5.4 Peak fluorescence emission wavelengths of the native and mutated Class II FBP aldolases from *B. cereus* and *M. tuberculosis*

The excitation wavelength was 295 nm and the buffer was 50 mM Hepes pH 7.3, with 5 μ M ZnCl₂ added. The concentration of FBP was 5.3 mM and the concentration of DMPS was 4.2 mM.

	Emission peak without FBP	Emission peak with FBP (*), or FBP and DMPS (†)
	(nm)	(nm)
<i>B. cereus</i> Wild-Type	323	319*
BCI149W	339	339*
<i>M. tuberculosis</i> Wild-Type	337	337†
MTN173W	353	351†
MTI175W	351	353†
MTY280W	349	349†

5.3.3 Time-resolved fluorescence

The preliminary time-resolved results obtained are shown in Table 5.5 and Figure 5.16. The *B. cereus* wild-type aldolase and BCI149W mutant aldolase were analyzed before and after the addition of 5.3 mM FBP (final concentration). No significant change in fluorescence lifetime could be detected for the BCI149W mutant, and only a very small decrease (0.1 ns) was observed for the wild-type *B. cereus* aldolase in the presence of FBP. *M. tuberculosis* aldolase and its mutants were analyzed before and after the addition of 5.3 mM FBP and 4.2 mM DMPS. Significant changes in fluorescence lifetime were observed in the presence of FBP for all enzymes except the MTN173W mutant. The fluorescence lifetime decreased by 0.2 and 0.6 ns in the presence of FBP for the wild-type and MTI175W enzymes respectively; but increased by 0.3 ns for the MTY280W mutant. The subsequent addition of DMPS did not cause significant changes in fluorescence lifetimes.

Chapter 5 Preliminary work on enzyme loop dynamics

The use of a 3-exponential equation did not significantly improve the χ^2 values (these values ranged between 0.99 and 1.274 with a 3-exponential equation, compared with 1.057 to 1.458 with a 2-exponential equation). A 4-exponential equation could not be used as the background noise was too high (low resolution, yielding arbitrary results for the decay constants). The results obtained using a 320 nm cut-off emission filter with the *M. tuberculosis* wild-type aldolase and its mutants are also shown, as the filter improved the signal-to-noise ratio significantly. Without the use of the 320 nm cut-off emission filter, approximately 99% of the signal (see amplitudes α associated with each of the decay constants τ) was due to noise and emissions with a lifetime shorter than 0.5 ns, which is the resolution limit using this pulsed LED source. The time-resolved analysis was actually limited by the high background noise obtained with the pulsed LED source used for excitation, which displays low resolution (pulse width ~ 0.5 ns). The light source pulse width (~ 0.5 ns) overlapped significantly with the expected lifetimes of the excited states of the tryptophan residues, which are usually between 0.3 ns and 10 ns (Beechem and Brand 1985)). When the 320 nm filter was used (Table 5.5, enzyme samples marked with an asterix), the amplitude attributed to this “noise” diminished slightly (94% to 97% of the signal). The mutant Y280W had the lowest signal-to-noise ratio since it had a concentration 2- and 3 times lower than for N173W and I175W, respectively, as described in section 5.2.4. It is relevant to note that the analysis of the signal coming from the buffer alone yielded results very similar to those obtained with the enzyme solutions, albeit with an amplitude 3 to 5 times lower than the protein samples for the lifetimes above 0.5 ns (Table 5.5 and Figure 5.16 panel D). This “buffer” signal was later attributed to contaminants in the 90 μ l quartz cuvette, which affected all of the time-resolved fluorescence results. The same cuvette filled with buffer alone did not give a significant signal in steady-state fluorescence experiments (see Figures 5.9, 5.12 and 5.13), but the time-resolved apparatus is much more sensitive to the presence of trace contaminants. Based on the rate of detection in photons per second, the emission signal from the

Chapter 5 Preliminary work on enzyme loop dynamics

M. tuberculosis wild-type and mutant aldolases was only 25% to 47% more intense than the signal from the buffer alone in the time-resolved experiments done using the 320 nm emission filter, which illustrates the extent of the light scattering by the less-than-ideally cleaned 90 μ l cuvette. The results still appear reliable for the fluorescence lifetimes above 0.5 ns, as the sample analysis produced nearly identical τ_1 values with and without the use of the 320 nm emission filter. As mentioned above, this filter increased the intensity (α_1) of the τ_1 fluorescence lifetime signal by a factor four to six (Table 5.5, see enzyme samples marked with an asterix).

Table 5.5 Time-resolved decay constants and associated amplitudes

τ_n represent the fluorescent lifetimes and α_n represent the percentage contribution of fluorescence lifetime decay measurements. A 2-exponential function was fitted to the signal (photon count in function of time) recorded for each sample excited at 298 nm by a pulsed light-emitting diode (LED) source (PLS-295, PicoQuant GmbH, Berlin, Germany). The χ^2 values are indicated, and the quality of the fits was verified by visual inspection of the residuals (see Figure 5.15). The FBP concentration was 5.3 mM and the DMPS concentration was 4.2 mM. The buffer was composed of 50 mM Hepes, 5 μ M ZnCl₂, pH 7.3. *An emission filter (320 nm) was used for samples marked with an asterix.

Enzyme	τ_1 (ns)	τ_2 (ns)	α_1 (%)	α_2 (%)	χ^2
BC	4.54 ± 0.02	0.101 ± 0.005	4.00 ± 0.02	96 ± 5	1.295
BC + FBP	4.45 ± 0.02	0.101 ± 0.005	4.00 ± 0.02	96 ± 4	1.300
BCI149W	4.11 ± 0.03	0.097 ± 0.004	1.00 ± 0.01	99 ± 4	1.267
BCI149W+FBP	4.13 ± 0.03	0.103 ± 0.004	1.00 ± 0.01	99 ± 4	1.251
MT	3.90 ± 0.05	0.121 ± 0.003	1.00 ± 0.01	99 ± 2	1.237
MT+FBP	3.67 ± 0.04	0.094 ± 0.004	1.00 ± 0.01	99 ± 4	1.217
MT+FBP+DMPS	3.76 ± 0.04	0.109 ± 0.003	1.00 ± 0.01	99 ± 3	1.167
MT+FBP+DMPS*	3.77 ± 0.03	0.189 ± 0.004	4.00 ± 0.04	96 ± 2	1.425
MTI175W	4.17 ± 0.05	0.080 ± 0.004	1.00 ± 0.01	99 ± 4	1.231
MTI175W+FBP	3.61 ± 0.04	0.090 ± 0.003	1.00 ± 0.01	99 ± 4	1.247
MTI175W+FBP+DMPS	3.63 ± 0.04	0.098 ± 0.003	1.00 ± 0.01	99 ± 3	1.251
MTI175W+FBP+DMPS*	3.69 ± 0.03	0.221 ± 0.004	6.00 ± 0.05	94 ± 2	1.458
MTN173W	4.02 ± 0.05	0.092 ± 0.003	1.00 ± 0.01	99 ± 4	1.230
MTN173W+FBP	3.98 ± 0.05	0.086 ± 0.004	1.00 ± 0.01	99 ± 5	1.173
MTN173W+FBP+DMPS	4.06 ± 0.05	0.096 ± 0.004	1.00 ± 0.01	99 ± 4	1.155
MTN173W+FBP+DMPS*	3.94 ± 0.03	0.181 ± 0.004	5.00 ± 0.04	95 ± 2	1.274
MTY280W	3.78 ± 0.07	0.068 ± 0.003	0.268 ± 0.006	100 ± 5	1.201
MTY280W+FBP	4.11 ± 0.07	0.076 ± 0.003	0.291 ± 0.006	100 ± 4	1.251
MTY280W+FBP+DMPS	4.07 ± 0.06	0.079 ± 0.003	0.415 ± 0.007	100 ± 4	1.194
MTY280W+FBP+DMPS*	4.09 ± 0.03	0.128 ± 0.005	3.00 ± 0.02	97 ± 3	1.316
Buffer	2.9 ± 0.1	0.100 ± 0.006	0.19 ± 0.01	100 ± 6	1.129
Buffer+FBP	2.6 ± 0.1	0.087 ± 0.004	0.22 ± 0.01	100 ± 4	1.057
Buffer*	2.42 ± 0.06	0.123 ± 0.004	1.00 ± 0.04	99 ± 3	1.117

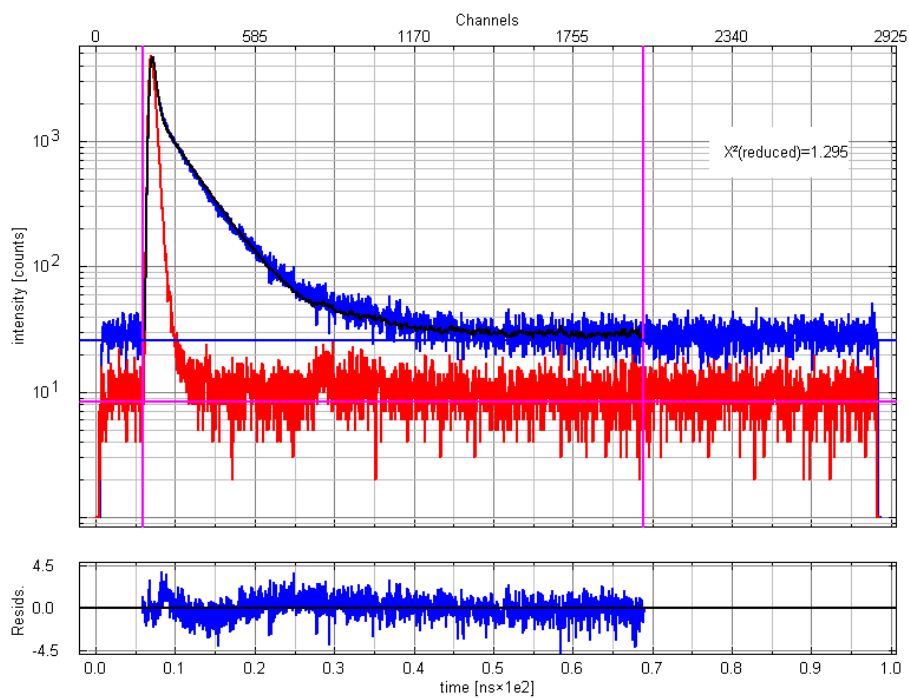
(Following pages)

Figure 5.15 Time-resolved fluorescence

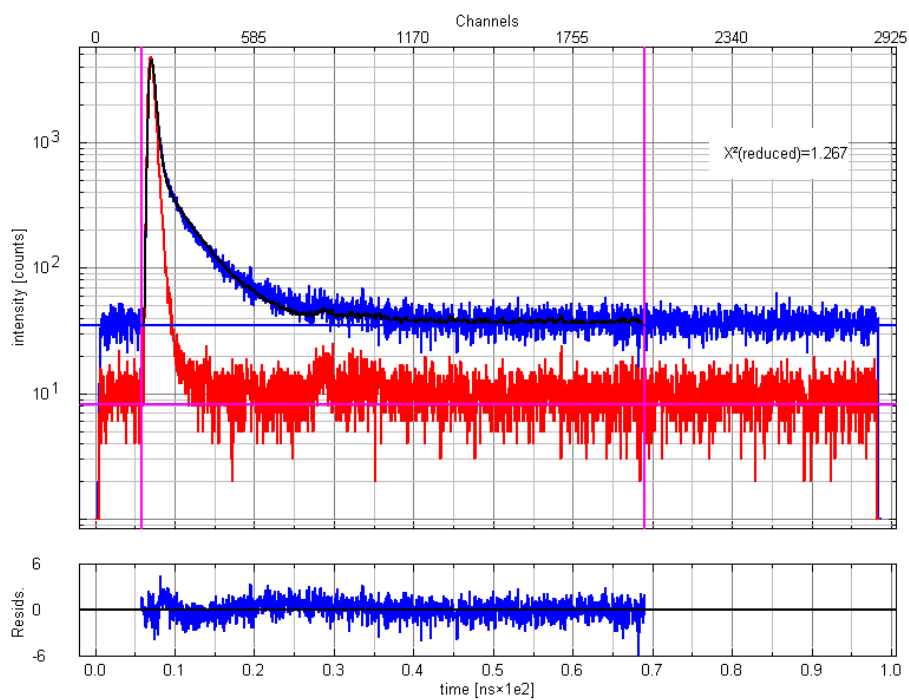
The results are shown for the *B. cereus* aldolase (1 mM, Panel A) and its mutant I149W (24 μ M, Panel B), for the *M. tuberculosis* aldolase mutant I175W (47 μ M) in the presence of 5.3 mM FBP and 4.2 mM DMPS (Panel C) and for the enzyme buffer alone (50 mM Hepes, 5 μ M ZnCl₂, pH 7.3, Panel D). The top charts represent the photon count in function of time (34 ps per channel). The red trace is the instrument response function obtained with the light-scattering colloidal silica solution (Ludox), and the (top) blue traces were obtained with the protein samples. The recordings were stopped at a photon count of 5,000 excepted for the instrument response function in panels C and D, which was stopped at a photon count of 10,000. The goodness-of-fit can be judged by the plot of the residuals obtained after fitting a 2-exponential function (black trace) is shown under each graph, with the corresponding time units indicated. The data was analyzed over a total of 64 ns, and the analysis limits are indicated by the pink vertical lines. The quality of the fit is also indicated by the χ^2 value shown on the graphs. A 320 nm filter was used to reduce the background noise in Panels C and D. The data was analyzed and the graphics produced using the PicoQuant FluoroFit software (Berlin, Germany).

Chapter 5 Preliminary work on enzyme loop dynamics

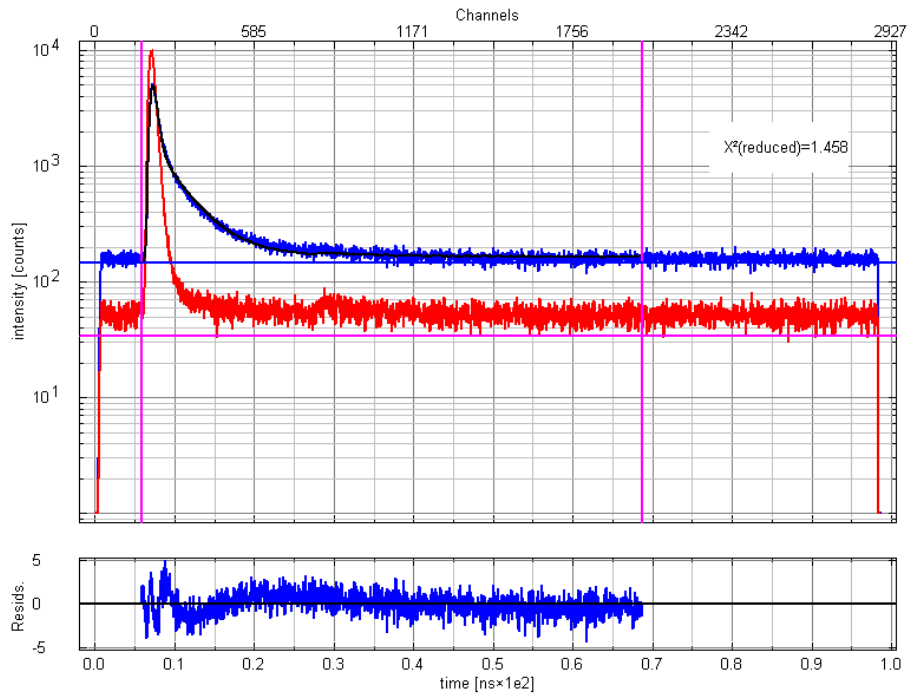
A



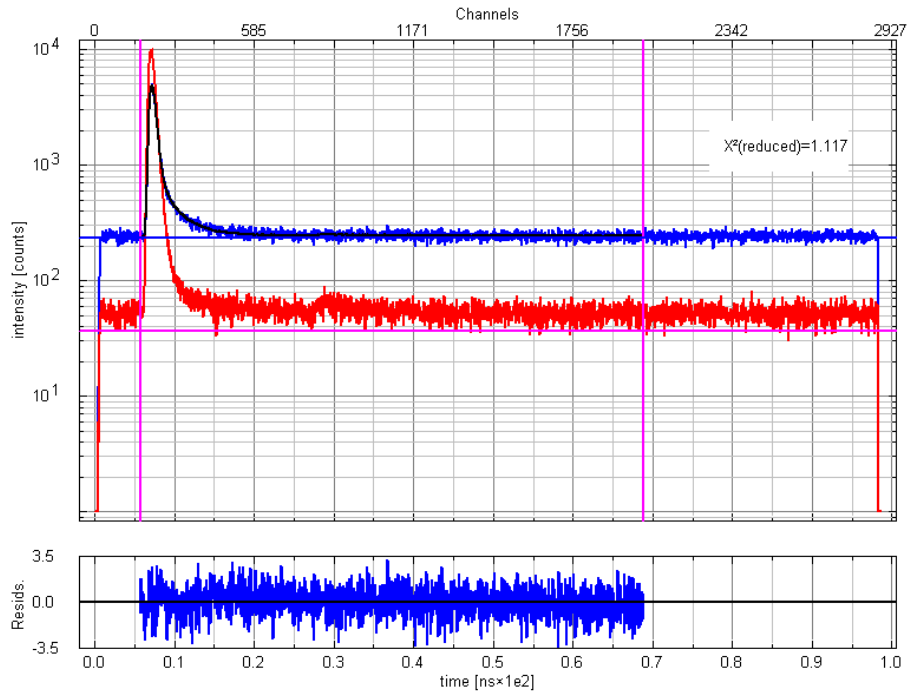
B



C



D



5.4 Discussion

Tryptophan residues were introduced in specific positions in FBP aldolases in attempts to monitor loop movements upon ligand binding. In total three tryptophan residues were introduced in *M. tuberculosis* FBP aldolase, and 1 each in *B. cereus*, *H. pylori*, and *P. aeruginosa* FBP aldolases. Both the native and mutant *H. pylori* aldolases were found to be unstable and are therefore not characterized further. Kinetic analysis was performed on the other mutants and the kinetic parameters obtained were similar to their native counterparts except for Y280W and F202W mutants of *M. tuberculosis* and *P. aeruginosa* aldolases, respectively. The presence of impurities in some mutated enzymes preparations in comparison with their wild-type counterparts, particularly for MTY280W (Figure 5.6), may have contributed to the decrease in turnover number. The residue Y280 of *M. tuberculosis* aldolase is located in the dimer interface of the enzyme and it is near the C6 phosphate binding site of the active site. Sequence alignment of the *M. tuberculosis* aldolase with other FBP aldolases reveal that several other Class II type A aldolases, such as that from *E. coli*, have a tryptophan residue in that position (Figure 5.3). However, *M. tuberculosis* differs from the other type A aldolases in that it is a tetramer instead of a dimer (Ramsaywak *et al.* 2004; see also section 3.4). Therefore the interface between subunits may be different (see modeled *M. tuberculosis* aldolase in Figure 5.1, where the dimerization arm, comprising the Y280 residue, is significantly different than that of the *E. coli* aldolase shown in inset), and substitution to a bulkier tryptophan residue may negatively impact the conformation of the protein and it is thus less catalytically efficient. This mutant however was deemed to have retained enough catalytic activity for the fluorescence studies. The residue F202 of the *P. aeruginosa* aldolase is located in the small mobile loop which includes a divalent metal ligand (Figure 5.2 B), and the rapid loss of activity of the purified enzyme could be due to a decreased metal affinity. This inactivated enzyme was not used for fluorescence studies. The other mutants, which all featured tryptophan residues introduced in the

large catalytic loop, have similar kinetic parameters as their native enzyme, suggesting that introduction of tryptophan residues in this loop did not adversely affect the conformation of the enzyme.

Fluorescence studies were performed on the *B. cereus* and *M. tuberculosis* enzymes with addition of the substrate FBP and inhibitor DMPS. Fluorescence studies were also attempted with compound 6 (see Chapter 4), however the absorption and emission spectra of this compound overlap with that of tryptophan of the enzymes (Figure 5.10) and it is therefore not possible to use tryptophan fluorescence to monitor enzyme conformation change upon binding of compound 6. The wild-type *M. tuberculosis* and *B. cereus* aldolases each contain a single native tryptophan residue, and upon addition of FBP, there is a noticeable quenching of tryptophan fluorescence. In the *B. cereus* aldolase, the native tryptophan residue is in the dimer interface of the subunits (Figure 5.2C) and since the active site of the enzyme is made up by residues of both subunits (Figure 1.13), ligand binding may cause conformational change that resulted in a change in environment of the tryptophan residue. In the *B. cereus* I149W mutant, the maximal fluorescence emission wavelength is red shifted by 18 nm compared to the wild-type enzyme. This is consistent with relative higher solvent exposure at position 149 (in the large catalytic loop) of the enzyme. Upon FBP binding, the mutant showed an increase in fluorescence emission, while binding of DMPS showed quenching of fluorescence. In the native *M. tuberculosis* aldolase, it is surprising that the native tryptophan residue is also quenched upon binding of FBP and the inhibitor DMPS, although the tryptophan residue is located in the hydrophobic core of the TIM barrel, which is not near the active site. The three tryptophan mutants in the *M. tuberculosis* aldolase all showed a red shift in fluorescence emission relative to the wild-type. Again this may be due to the higher solvent exposure in the introduced tryptophans. Addition of FBP and DMPS causes quenching of the tryptophan fluorescence in two of the mutants Y280W and N173W, similar to what is observed in the wild-type enzyme. In contrast, the presence of FBP

Chapter 5 Preliminary work on enzyme loop dynamics

and DMPS causes an increase in fluorescence in the mutant I175W. The unique response of this mutant to the presence of ligands could in the future be further characterized by replacing the native *M. tuberculosis* tryptophan by an isoleucine residue (W130I mutation), since isoleucine is relatively common in this position for both type A and B aldolases, according to the sequence alignment presented in Figure 1.17. The I175W-W130I mutant could then be used for stopped-flow fluorescence studies to monitor ligand binding. In a similar way, the *B. cereus* I149W mutant could be further characterized by mutation of the native W30 to another residue, possibly a phenylalanine. The changes in fluorescence upon ligand binding for this mutant could also be monitored using a stopped-flow spectrophotometer.

The tryptophan mutants of the *B. cereus* and *M. tuberculosis* enzymes were also analyzed using time-resolved fluorescence to monitor the possibility of loop movements upon binding of ligands. It is expected that proteins have at least one distinct fluorescence lifetime for each of its tryptophan residues, related to the environment of these residues. In our study, only a two-exponential function could be used to analyze the data because of high background noise. In addition, the lifetimes of 0.5 ns or less could not be resolved because of the long pulse width (~0.5 ns) of the light-emitting diode used as the excitation source. In spite of these limitations, some differences in fluorescence lifetimes could be detected for several enzymes in the presence of FBP. The enzyme which showed the largest difference in fluorescence lifetime upon FBP binding was the *M. tuberculosis* aldolase I175W mutant, with a decrease from 4.2 ns to 3.6 ns for the longer lifetime component. The wild-type *M. tuberculosis* and the mutant Y280W also respectively displayed a decrease of 0.2 ns and an increase of 0.3 ns in fluorescence lifetime (longer component) upon FBP binding. In contrast, the *B. cereus* enzymes had similar lifetimes (within 0.1 ns) before and after the addition of substrate.

In the future, it would be interesting to repeat these experiments with a better light source, and better enzyme samples (with increased purity). Pulsed diode LED has low resolution and is less

powerful (at most 80 μ W) than a pulsed diode laser light source, which have a pulse width as low as 50 ps, and power up to 150 mW. The excitation wavelength of 298 nm that was used in these experiments is also sub-optimal and an excitation wavelength of 292 nm or even 295 nm would have significantly increased the fluorescence emission signal from the aldolases (see Figure 5.11). Light sources with such lower wavelengths were unfortunately not available for these experiments. It would also be interesting to do time-resolved fluorescence with the double mutant proposed above (*M. tuberculosis* I175W-W130I), where the signal from the native tryptophan would be eliminated.

These fluorescence studies were attempted with the goal of obtaining real time information on loop movements upon ligand binding, in order to discover if the loops conformation is indeed affected by the presence of the ligand. It was also hoped that, even if the loop movements are not dependent upon the presence of the ligand, as was suggested previously (Hilcenko, 2003), the presence of a ligand in the active site would cause detectable changes in fluorescence from tryptophan residues introduced in the vicinity of the active site. This in turn could be insightful to learn how inhibitors bind to the active site, and possibly to guide further inhibitor design based on the response of the loop(s). Loops cannot be easily modeled, particularly when based on enzyme models generated using crystal structures of other enzymes. These types of fluorescence experiments could be complementary to the inhibition assays, especially in the case of metal-binding inhibitors where complexing or non-complexing inhibition can occur. A difference in fluorescence emission intensity or a difference in fluorescence lifetime for an active-site tryptophan residue in the presence of the inhibitor could help confirm the inhibition model determined using kinetic analysis. In other words, the tryptophan fluorescence could help to distinguish between an inhibitor remaining bound in the active site, and one that is chelating the catalytic metal out of the enzyme's active site. Further studies will be needed to assess if some of the mutants described in the present study can be used to guide future inhibitor design.

Chapter 6

Original contributions and recommendations

6.1 Conclusions

The objective of this multidisciplinary project is to rationally design Class II FBP aldolase inhibitors that can be used as new antimicrobial agents. Inhibitors that are substrate analogues, may also act on the human Class I aldolases with associated toxicity. The approach taken in this thesis was to start with metal-binding compounds which will be specific for metal-dependent Class II enzymes, but would not affect the Class I FBP aldolase activity. These compounds contained different functional groups which may improve their affinity for the active site of the Class II FBP aldolases. The development of new generations of inhibitory compounds was to be guided by kinetic analysis and structural analysis of target enzymes with bound inhibitors. This doctoral project served to put in place the foundation for a long-term study using the Class II FBP aldolases from several microorganisms as templates for metal-chelating inhibitor development.

The goals of this doctoral project as stated in section 1.7 were to: 1) clone, express, and purify several Class II FBP aldolases from pathogenic microorganisms, 2) to characterize these enzymes and determine their susceptibility to inhibition by a range of synthetic inhibitors; 3) to gain a better understanding of the reaction mechanism of the Class II adolases; 4) to investigate possible links between structural features such as mobile loops and the kinetic and inhibition parameters; and 5) to make recommendations for rational inhibitor design. Several of these goals have been achieved and significant progress has been made towards novel inhibitor development during this project, as will be summarized in the following section.

6.2 Original contributions to research

The Class II aldolases from *P. aeruginosa*, *B. cereus*, *M. grisea*, *H. pylori*, *S. pneumoniae*, and *H. influenzae* were successfully cloned and overexpressed in *E. coli*. The active recombinant enzymes from *M. tuberculosis*, *P.aeruginosa*, *B. cereus*, *M. grisea*, *E. coli* and *H. pylori* were purified, often in gram-scale quantities from *E. coli* cells grown in a bench-top fermentor. It is relevant to point out that the aldolase from *M. grisea* had, to our knowledge, never been purified previously. The purification yields of the Class II aldolases from *M. tuberculosis*, *B. cereus*, and *P. aeruginosa* were improved significantly over those reported for the purifications from the original host.

The recombinant enzymes were characterized in terms of their metal ion specificity, stability and kinetic parameters to allow a thorough interpretation of the inhibition kinetics results. The enzymes were also tested in the presence of various organic solvents and at elevated temperatures to assess their potential as catalysts for aldol condensation in organic synthesis. This was the widest parallel investigation of the substrate specificity and catalytic efficiency of evolutionarily divergent Class II FBP aldolases.

Several metal-chelating compounds were tested as Class II FBP aldolase inhibitors, and a kinetic model of the inhibition by the most potent compounds, DPA, DMPS, compounds **6** and **13** was proposed. The compounds likely form an unstable ternary complex with the catalytic metal ion and the active site amino acid residues. The compound DMPS was modeled into the crystal structure of the *E. coli* aldolase active site, and a novel inhibitor structure (AK4) based on this compound was proposed as the next step towards the generation of a potent lead inhibitory compound.

In order to study the structure-function relationship of the active site mobile loops of the Class II FBP aldolases, six mutants were generated by replacing active site and loop residues with tryptophan

residues. Five of these mutants were purified and their kinetic properties were compared with those of the wild-type enzymes. These inserted tryptophan residues were used as fluorescent probes to monitor enzyme movements upon substrate and inhibitor binding. The preliminary results of the equilibrium fluorescence studies indicate that the tryptophan residues introduced in the large catalytic loop of the *M. tuberculosis* and *B. cereus* aldolases increase in fluorescence upon substrate binding. This indicates that stopped-flow kinetic studies using fluorescence could be performed in the future to monitor loop movements during catalysis, and possibly to monitor inhibitor binding.

6.3 Recommendations

The following future studies are recommended in light of the results obtained in this doctoral project:

1. It may be useful to express the enzyme with a C-terminal affinity tag and compare the results with those presented here, now that the optimal specific activity of the native recombinant enzymes has been determined. If the C-terminally tagged enzymes have similar properties to the native recombinant enzymes, the purification methods could be significantly improved in terms of both yields and time. This was done successfully with the *M. tuberculosis* aldolase, as was recently reported (Rukseree *et al.* 2008).

2. Crystal structures of the enzymes with bound inhibitors will be helpful. Future generations of inhibitors could then be designed by combining these small compounds using linkers of appropriate length with the metal-binding compounds identified in the present study, to obtain higher-affinity compounds. These high affinity inhibitors should then be screened for host toxicity and protection against disease. As discussed in Chapter 1, it is expected that only the very potent inhibitors that eliminate more than 95% of the Class II FBP aldolase activity *in vivo* will demonstrate a protective effect against the targeted pathogens. An alternative approach is to use High Throughput Screening (HTS), which would allow the building of a database of molecules with at least moderate affinity for

Chapter 6 Original contributions and recommendations

the Class II aldolase that can be combined with metal affinity functional groups to increase specificity. After the submission of this thesis, a structure of the *M. tuberculosis* Class II aldolase was published (Pegan *et al.* 2009). This should be very useful for future inhibitor design.

3. Since the Class II enzymes' dimerization is essential for activity, inhibitors can be designed to destabilize this interface as was demonstrated with HIV-1 reverse transcriptase (Sluis-Cremer *et al.* 2000). The heat-sensitive FBP aldolase found in the *ts8* mutant of the *E. coli* strain JS8 has a Val-to-Gly mutation at position 300 which is a conserved hydrophobic residue in the dimerization arm of the enzyme (Singer *et al.* 1991a) (Figure 6.1). This mutation may reduce the stability of the dimer, which needs to be intact for catalysis to occur since the active site is composed of residues from both subunits (see Figure 1.11). This indicates that a dimer-destabilizing inhibitor could strongly influence the enzyme's catalytic capabilities.

4. The aldolases could be tested for their capacity to utilize different aldehydes in aldol condensation with DHAP. This would be helpful for inhibitor design and for the use of Class II aldolases as catalysts in organic synthesis. A protocol to monitor the condensation activity of the aldolases using a direct colorimetric assay would be useful. A stopped assay using a colorimetric reagent to detect the triose phosphates has been adapted for 96-well plates recently (Rukseree *et al.* 2008). The development of such an assay, suitable for use in neutral pH conditions at room temperature, may also be more suitable than the coupled assay for HTS.

5. The native tryptophan residue (W130) of the *M. tuberculosis* catalytic loop mutant I175W could be replaced by an isoleucine residue. This double mutant can be used for transient kinetic analysis using stopped-flow to monitor loop movements during catalysis. The double mutant is expected to display an increase in fluorescence upon substrate binding according to the preliminary steady-state results obtained with the mutant I175W relative to those obtained with the wild-type *M. tuberculosis*

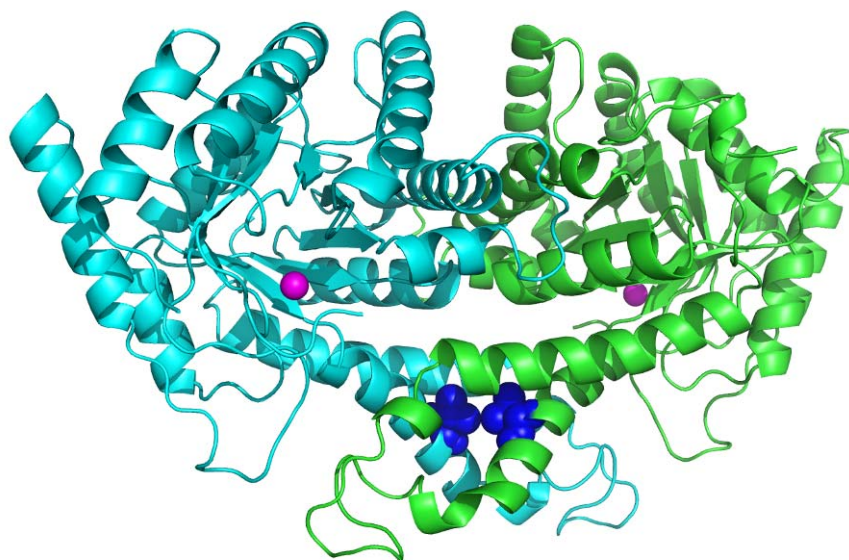


Figure 6.1 Location of the Val-to-Gly substitution in the heat-sensitive *E. coli* Class II FBP aldolase (*ts8* mutation).

The mutation is in the dimerization arm of the enzyme (Val₃₀₀ residue in dark blue, shown in space-fill format). The two different subunits are shown in cyan and green, with the catalytic Zn²⁺ shown as pink spheres. The illustration was produced with PyMOL (DeLano Scientific LLC) using the *E. coli* aldolase structure (PDB ID: 1B57).

aldolase. It would be interesting to test if such a change in fluorescence occurs upon binding of a potent inhibitor (such as PGH) to the active site. Similar experiments could be done after creating a *B. cereus* aldolase double mutant with a single tryptophan in the mobile loop (for example, I149W-W30F double mutation).

In conclusion, it bears repeating that antibacterial and antifungal discovery is a risky, long and difficult endeavor. Enzymes' properties and mechanism were studied in-depth since the 1930s, but it is still difficult to predict enzyme structure and kinetic behavior in the absence of an already well-

Chapter 6 Original contributions and recommendations

characterized homologous enzyme. Even though antimicrobial drug resistance is an increasing concern, pharmaceutical companies have all but abandoned this field of research in the last few years, in favor of the development of drugs for the treatment of the much more profitable chronic diseases. Although protein-ligand interaction predictions are constrained by our limited knowledge, the multidisciplinary collaborative efforts presented here are the best chance for drug discovery in an academic setting.

Appendix A

Plasmids, aldolase genes, and protein sequences

Vector pT7-5

Nucleotide ID=AY230150

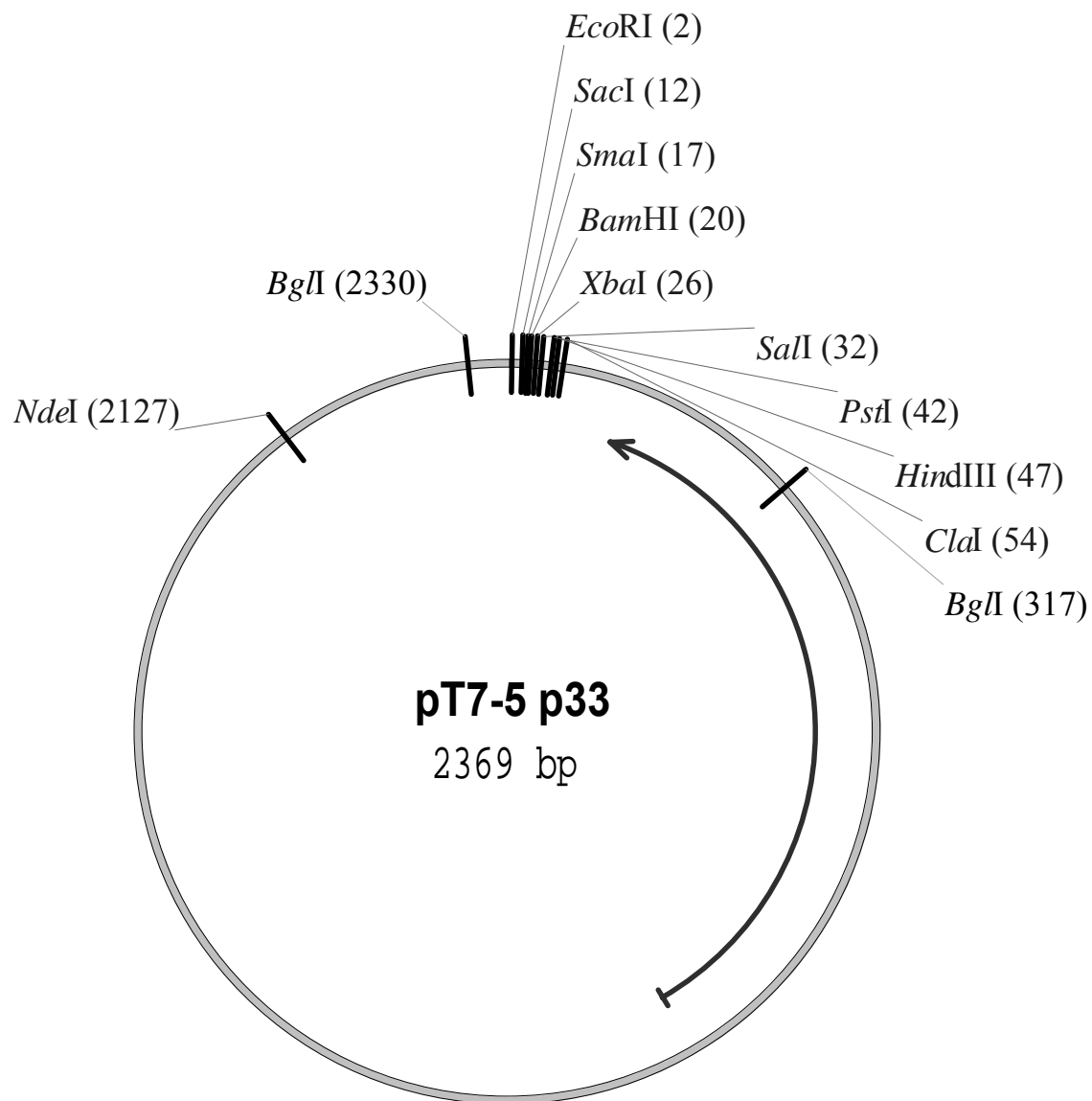


Figure 6.2 Map of plasmid pT7-5

Appendix A

Nucleotide sequence and restriction sites of pT7-5:

	SacI ~~~~~	SmaI ~~~~~	XbaI ~~~~~	PstI ~~~~~	
	EcoRI ~~~~~		BamHI ~~~~~		Sali ~~~~~
					HindIII ~
1	GAATTCGAGC	TCGCCCAGGG	ATCCTCTAGA	GTCGACCTGC	AGCCCAAGCT
	HindIII ~				
	ClaI ~~~~~				
51	TATCGATGAT	AAGCTGTCAA	ACATGAGAAT	TAAATCAATC	TAAAGTATAT
101	ATGAGTAAAC	TTGGTCTGAC	AGTTACCAAT	GCTTAATCAG	TGAGGCACCT
151	ATCTCAGCGA	TCTGTCTATT	TCGTTCATCC	ATAGTTGCCT	GACTCCCCGT
201	CGTGTAGATA	ACTACGATAC	GGGAGGGCTT	ACCATCTGGC	CCCAGTGCTG
251	CAATGATACC	GCGAGACCCA	CGCTCACCGG	CTCCAGATTT	ATCAGCAATA
		BglI ~~~~~			
301	AACCAGCCAG	CCGGAAGGGC	CGAGCGCAGA	AGTGGTCCTG	CAACTTTATC
351	CGCCTCCATC	CAGTCTATTA	ATTGTTGCCG	GGAAGCTAGA	GTAAGTAGTT
401	CGCCAGTTAA	TAGTTTGCGC	AACGTTGTTG	CCATTGCTAC	AGGCATCGTG
451	GTGTCACGCT	CGTCGTTTGG	TATGGCTTCA	TTCAGCTCCG	GTTCCCAACG
501	ATCAAGCGCA	GTTACATGAT	CCCCATGTT	GTGCAAAAAA	GCGGTTAGCT
551	CCTTCGGTCC	TCCGATCGTT	GTCAGAAGTA	AGTTGGCCGC	AGTGTTATCA
601	CTCATGGTTA	TGGCAGCACT	GCATAATTCT	CTTACTGTCA	TGCCATCCGT
651	AAGATGCTTT	TCTGTGACTG	GTGAGTACTC	AACCAAGTCA	TTCTGAGAAT
701	AGTGTATGCG	GCGACCGAGT	TGCTCTTGCC	CGGCGTCAAC	ACGGGATAAT
751	ACCGCGCCAC	ATAGCAGAAC	TTTAAAAGTG	CTCATCATTG	GAAAACGTTT
801	TTCGGGGCGA	AAACTCTCAA	GGATCTTACC	GCTGTTGAGA	TCCAGTTCGA
851	TGTAACCCAC	TCGTGCACCC	AACTGATCTT	CAGCATCTTT	TACTTTCACC
901	AGCGTTTCTG	GGTGAGCAAA	AACAGGAAGG	CAAAATGCCG	CAAAAAAGGG
951	AATAAGGGCG	ACACGGAAAT	GTTGAATACT	CATACTCTTC	CTTTTTCAAT
1001	ATTATTGAAG	CATTTATCAG	GGTATTGTG	TCATGAGCGG	ATACATATTT
1051	GAATGTATTT	AGAAAAATAA	ACAAATAGGG	GTCCGCGCA	CATTTCCCCG
1101	AAAAGTGCCA	CCTGACGTCT	AAGAAACCAT	TATTATCATG	ACATTAACCT
1151	ATAAAAATAG	GCGTATCACG	AGGCCCTTTC	GTCTTCAAGA	ATAAAAAGGAT
1201	CTAGGTGAAG	ATCCTTTTTG	ATAATCTCAT	GACCAAAATC	CCTTAACGTG
1251	AGTTTTCGTT	CCACTGAGCG	TCAGACCCCG	TAGAAAAGAT	CAAAGGATCT
1301	TCTTGAGATC	CTTTTTTTCT	GCGCGTAATC	TGCTGCTTGC	AAACAAAAAA
1351	ACCACCGCTA	CCAGCGGTGG	TTTGTTTGCC	GGATCAAGAG	CTACCAACTC
1401	TTTTTCCGAA	GGTAACTGGC	TTCAGCAGAG	CGCAGATACC	AAATACTGTC
1451	CTTCTAGTGT	AGCCGTAGTT	AGGCCACCAC	TTCAAGAACT	CTGTAGCACC
1501	GCCTACATAC	CTCGCTCTGC	TAATCCTGTT	ACCAGTGGCT	GCTGCCAGTG
1551	GCGATAAGTC	GTGTCTTACC	GGGTTGGACT	CAAGACGATA	GTTACCGGAT
1601	AAGGCGCAGC	GGTCGGGCTG	AACGGGGGGT	TCGTGCACAC	AGCCCAGCTT
1651	GGAGCGAACG	ACCTACACCG	AACTGAGATA	CCTACAGCGT	GAGCTATGAG
1701	AAAGCGCCAC	GCTTCCCGAA	GGGAGAAAGG	CGGACAGGTA	TCCGGTAAGC

1751 GGCAGGGTCG GAACAGGAGA GCGCACGAGG GAGCTTCCAG GGGGAAACGC
 1801 CTGGTATCTT TATAGTCCTG TCGGGTTTCG CCACCTCTGA CTTGAGCGTC
 1851 GATTTTTGTG ATGCTCGTCA GGGGGGCGGA GCCTATGGAA AAACGCCAGC
 1901 AACCGGCCT TTTTACGGTT CCTGGCCTTT TGCTGGCCTT TTGCTCACAT
 1951 GTTCTTTCCT GCGTTATCCC CTGATTCTGT GGATAACCGT ATTACCGCCT
 2001 TTGAGTGAGC TGATACCGCT CGCCGCAGCC GAACGACCGA GCGCAGCGAG
 2051 TCAGTGAGCG AGGAAGCGGA AGAGCGCCTG ATGCGGTATT TTCTCCTTAC

NdeI

~~~~~

2101 GCATCTGTGC GGTATTTTAC ACCGCATATG GTGCACTCTC AGTACAATCT  
 2151 GCTCTGATGC GCTACGTGAC TGGGTCATGG CTGCGCCCCG ACACCCGCCA  
 2201 ACACCCGCTG ACGCGCCCTG ACGGGCTTGT CTGCTCCCGG CATCCGCTTA  
 2251 CAGACAAGCT GTGACCGTCT CCGGGAGCTG CATGTGTCAG AGGTTTTTAC

BglI

~~~~~

2301 CGTCATCACC GAAACGCGCG AGGCCAGCT GGCTTATCGA AATTAATACG
 2351 ACTCACTATA GGGAGACCG

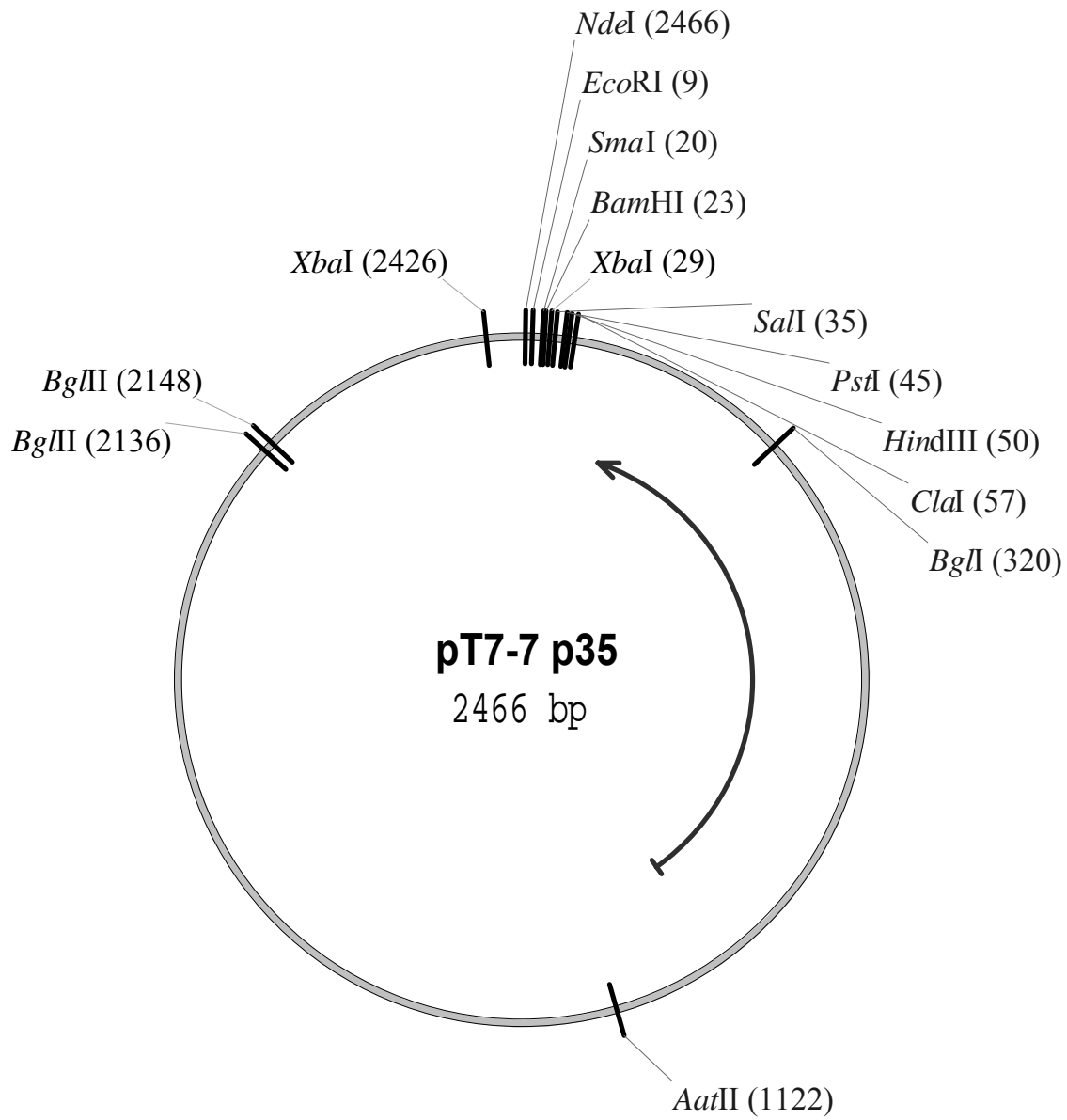


Figure 6.3 Map of plasmid pT7-7

	NdeI	EcoRI	SmaI	BamHI	XbaI	SalI	PstI	Hind
	~~~	~~~~~	~~~~~	~~~~~	~~~~~	~~~~~	~~~~~	
1	ATGGCTAGAA	TTCGCGCCCG	GGGATCCTCT	AGAGTCGACC	TGCAGCCCAA			
	HindIII							
	~~~~~							
		ClaI						
	~~~~~							
51	GCTTATCGAT	GATAAGCTGT	CAAACATGAG	AATTAAATCA	ATCTAAAGTA			
101	TATATGAGTA	AACTTGGTCT	GACAGTTACC	AATGCTTAAT	CAGTGAGGCA			
151	CCTATCTCAG	CGATCTGTCT	ATTTTCGTTCA	TCCATAGTTG	CCTGACTCCC			
201	CGTCGTGTAG	ATAACTACGA	TACGGGAGGG	CTTACCATCT	GGCCCCAGTG			
251	CTGCAATGAT	ACCGCGAGAC	CCACGCTCAC	CGGCTCCAGA	TTTATCAGCA			
		BglI						
		~~~~~						
301	ATAAACCAGC	CAGCCGGAAG	GGCCGAGCGC	AGAAGTGGTC	CTGCAACTTT			
351	ATCCGCCTCC	ATCCAGTCTA	TTAATTGTTG	CCGGAAGCT	AGAGTAAGTA			
401	GTTCCGCAAGT	TAATAGTTTG	CGCAACGTTG	TTGCCATTGC	TACAGGCATC			
451	GTGGTGTAC	GCTCGTCGTT	TGGTATGGCT	TCATTCAGCT	CCGGTTCCCA			
501	ACGATCAAGG	CGAGTTACAT	GATCCCCCAT	GTTGTGCAAA	AAAGCGGTTA			
551	GCTCCTTCGG	TCCTCCGATC	GTTGTCAGAA	GTAAGTTGGC	CGCAGTGTTA			
601	TCACTCATGG	TTATGGCAGC	ACTGCATAAT	TCTCTTACTG	TCATGCCATC			
651	CGTAAGATGC	TTTTCTGTGA	CTGGTGAGTA	CTCAACCAAG	TCATTCTGAG			
701	AATAGTGTAT	GCGGCGACCG	AGTTGCTCTT	GCCCGGCGTC	AACACGGGAT			
751	AATACCGCGC	CACATAGCAG	AACTTTAAAA	GTGCTCATCA	TTGGAAAACG			
801	TTCTTCGGGG	CGAAAACCTCT	CAAGGATCTT	ACCGCTGTTG	AGATCCAGTT			
851	CGATGTAACC	CACTCGTGCA	CCCAACTGAT	CTTCAGCATC	TTTTACTTTC			
901	ACCAGCGTTT	CTGGGTGAGC	AAAAACAGGA	AGGCAAAATG	CCGCAAAAAA			
951	GGGAATAAGG	GCGACACGGA	AATGTTGAAT	ACTCATACTC	TTCCTTTTTT			
1001	AATATTATTG	AAGCATTAT	CAGGGTTATT	GTCTCATGAG	CGGATACATA			
1051	TTTGAATGTA	TTTAGAAAAA	TAAACAAATA	GGGGTTCCGC	GCACATTTC			
		AatII						
		~~~~~						
1101	CCGAAAAGTG	CCACCTGACG	TCTAAGAAAC	CATTATTATC	ATGACATTAA			
1151	CCTATAAAAA	TAGGCGTATC	ACGAGGCCCT	TTCGTCTTCA	AGAATAAAAAG			
1201	GATCTAGGTG	AAGATCCTTT	TTGATAATCT	CATGACCAAA	ATCCCTTAAC			
1251	GTGAGTTTTT	GTTCCACTGA	GCGTCAGACC	CCGTAGAAAA	GATCAAAGGA			
1301	TCTTCTTGAG	ATCCTTTTTT	TCTGCGCGTA	ATCTGCTGCT	TGCAAACAAA			
1351	AAAACCACCG	CTACCAGCGG	TGGTTTGTTT	GCCGGATCAA	GAGCTACCAA			
1401	CTCTTTTTTCC	GAAGTAACT	GGCTTCAGCA	GAGCGCAGAT	ACCAAATACT			
1451	GTCTTCTAG	TGTAGCCGTA	GTTAGGCCAC	CACTTCAAGA	ACTCTGTAGC			
1501	ACCGCCTACA	TACCTCGCTC	TGCTAATCCT	GTTACCAGTG	GCTGCTGCCA			
1551	GTGGCGATAA	GTCGTGTCTT	ACCGGGTTGG	ACTCAAGACG	ATAGTTACCG			
1601	GATAAGGCGC	AGCGGTCGGG	CTGAACGGGG	GTTTCGTGCA	CACAGCCCAG			
1651	CTTGGAGCGA	ACGACCTACA	CCGAACGAG	ATACCTACAG	CGTGAGCTAT			
1701	GAGAAAGCGC	CACGCTTCCC	GAAGGGAGAA	AGGCGGACAG	GTATCCGGTA			

Appendix A

```
1751 AGCGGCAGGG TCGGAACAGG AGAGCGCACG AGGGAGCTTC CAGGGGGAAA
1801 CGCCTGGTAT CTTTATAGTC CTGTCGGGTT TCGCCACCTC TGACTTGAGC
1851 GTCGATTTTT GTGATGCTCG TCAGGGGGGC GGAGCCTATG GAAAAACGCC
1901 AGCAACGCGG CCTTTTACG GTTCCTGGCC TTTTGCTGGC CTTTGTCTCA
1951 CATGTTCTTT CCTGCGTTAT CCCCTGATTC TGTGGATAAC CGTATTACCG
2001 CCTTTGAGTG AGCTGATACC GCTCGCCGCA GCCGAACGAC CGAGCGCAGC
2051 GAGTCAGTGA GCGAGGAAGC GGAAGAGCGC CTGATGCGGT ATTTTCTCCT
                               BglII           BglII
                               ~~~~~~           ~~~~~~
2101 TACGCATCTG TGCGGTATTT CACACCGCAT AGGAAGATCT TCCGGAAGAT
 BglII
 ~~
2151 CTTCCTATGG TGCACCTCTCA GTACAATCTG CTCTGATGCG CTACGTGACT
2201 GGGTCATGGC TGCGCCCCGA CACCCGCCAA CACCCGCTGA CGCGCCCTGA
2251 CGGGCTTGTC TGCTCCCGGC ATCCGCTTAC AGACAAGCTG TGACCGTCTC
2301 CGGGAGCTGC ATGTGTCAGA GGTTTTCACC GTCATCACCG AAACGCGCGA
2351 GGCCCAGCGA TTCGAACTTC TGATAGACTT CGAAATTAAT ACGACTCACT
 XbaI
                               ~~~~~~
2401 ATAGGGAGAC CACAACGGTT TCCCTCTAGA AATAATTTTG TTTAACTTTA
    NdeI
    ~~~
2451 AGAAGGAGAT ATACAT
```



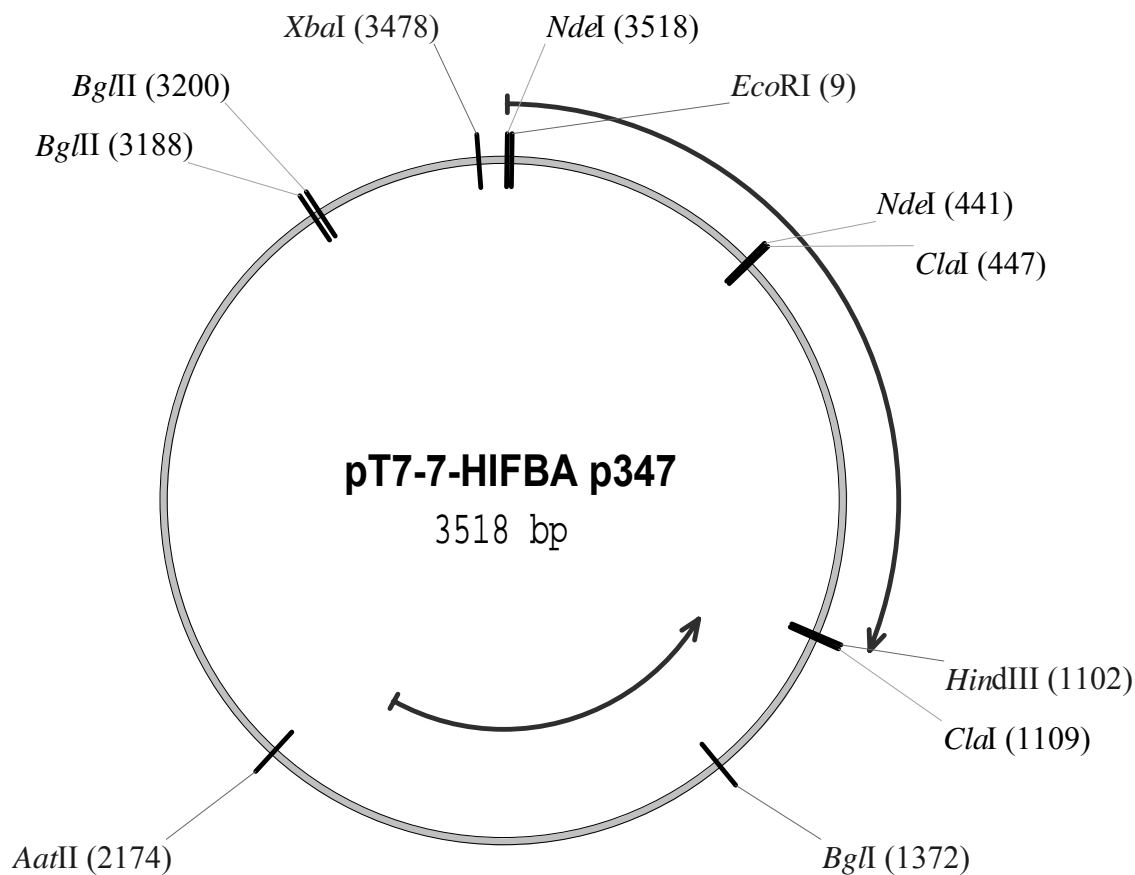


**Figure 6.4 Map of plasmid pT7-7/HIFBA**

Fructose-bisphosphate aldolase [*Haemophilus influenzae* Rd KW20]

Other Aliases: HI0524

GeneID: 949539

Amino acid sequence:

```

1- MAKLLDIVKP GVVVTGEDVQK VFAYAKEHNF AIPAVNCVGS DSVNAVLETA ARVKAPVIIQ
60- FSNGGAIFYA GKGIKPTSGT RPDVLGAIAG AKQVHTLAKE YGVPVILHTD HAAKLLPWI
120- DGLLLDAGEKH FAETGRPLFS SHMIDLSEES MEENMAICRE YLARMDKMG TLEIEIGITG
180- GEEDGVDNSD VDESRLYTQP SDVLYVYDQL HPVSPNFTVA AAFGNVHGVY KPGNVKPKPS
240- ILGESQEFVS KERNLPAKPI NFVFHGGSGS SREEIREAIG YGAIKMNIDT DTQWASWNGI
300- LNFYKANEAY LQGQLGNPEG PDAPNKYYD PRVWLRKMEE SMSKRLEQSF EDLNCVDVL

```

Appendix A

Below is the nucleotide sequence of the *H. influenzae* aldolase gene, starting from the *NdeI* restriction site of plasmid pT7-7 and ending at the *HindIII* restriction site of this plasmid. The gene was cloned using the *EcoRI* and *HindIII* sites, which results in the protein being expressed with 5 extra amino acids from the pT7-7 plasmid at the N-terminus (a.a. sequence MARIL). The *H. influenzae* aldolase gene's original start and stop codons are shown in **bold**):

```

 NdeI EcoRI
      ~~~   ~~~~~~
1    ATGGCTAGAA TTCTGATGGC TAAATTATTA GATATTGTGA AACCCGGTGT
51   TGTAACAGGC GAAGATGTGC AAAAAGTTTT TGCTTATGCT AAAGAGCATA
101  ACTTTGCTAT TCCTGCCGTA AACTGTGTGG GTTCAGACTC CGTTAATGCC
151  GTGTTAGAAA CTGCTGCACG CGTAAAAGCA CCAGTGATTA TCCAATTTTC
201  AAATGGTGGC GCAGCGTTCT ACGCAGGTAA AGGTATCAAA CCAACGAGTG
251  GTACTCGTCC TGATGTGCTT GGTGCGATTG CTGGAGCGAA ACAGGTTTCAT
301  ACTTTAGCGA AAGAATACGG TGTGCCTGTT ATTCTTCATA CTGATCACGC
351  AGCGAAAAAA TTATTACCTT GGATCGACGG TTTATTAGAT GCAGGCGAAA
                                           ClaI
                                           ~~~~~~
 NdeI
                                           ~~~~~~
401  AACATTTTGC CGAAACGGGT CGTCCACTTT TCTCTTCACA TATGATCGAT
451  TTATCTGAAG AGTCAATGGA AGAAAATATG GCAATCTGTC GTGAATACCT
501  CGCTCGTATG GATAAAATGG GGATGACCCT TGAAATCGAA ATTGGCATT
551  CTGGTGCCGA AGAAGACGGC GTTGATAACT CTGATGTTGA TGAATCACGT
601  TTATATACAC AACCTTCTGA TGTGCTTTAT GTTTACGATC AATTGCATCC
651  AGTAAGCCCT AACTTTACCG TTGCTGCTGC ATTCGGTAAC GTACACGGTG
701  TTTACAAACC AGGTAATGTA AAATTAAAC CATCTATTTT AGGTGAATCA
751  CAAGAGTTTCG TTTCTAAAGA ACGCAATCTT CCTGCAAAC CAATTAATTT
801  CGTATTCCAC GGTGGTTCAG GTTCTAGCCG CGAAGAAATC CGCGAAGCAA
851  TTGGCTACGG TGCAATCAAA ATGAACATTG ATACTGATAC GCAATGGGCA
901  TCTTGGAATG GTATTTTGAA TTTCTATAAA GCAAATGAAG CATATCTTCA
951  AGGTCAATTA GGTAACCCTG AAGGCCCAGA TGCACCAAAC AAAAAATACT
1001 ACGACCCACG TGTTTGTTTA CGTAAAATGG AAGAATCTAT GTCTAAACGC
1051 TTAGAGCAAT CTTTCGAAGA CTTAAATTGT GTTGATGTTT TATAATCCAC
HindIII
~~~~~
1101 AAGCTT

```

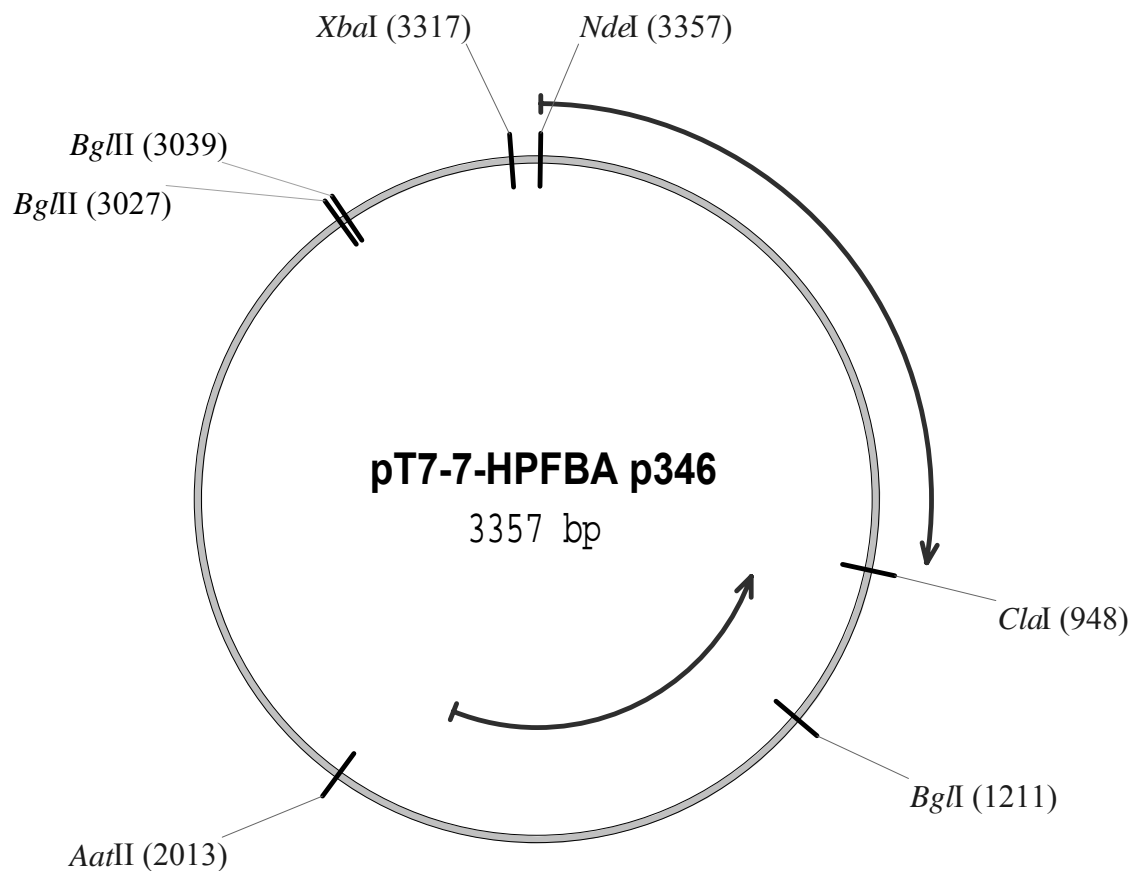


**Figure 6.5** Map of plasmid pT7-7/HPFBA

fructose-bisphosphate aldolase (tsr) [*Helicobacter pylori* 26695]

Other Aliases: HP0176

GeneID: 900140

Amino acid sequence:

```

1- MLVKGNEILL KAHKEGYGVG AFNFVNFEML NAIFEAGNEE NSPLFIQTSE GAIKYMGIDM
60- AVGMVKTMCE RYPHIPVALH LDHGTTFESC EKAVKAGFTS VMIDASHHAF EENLELTSKV
120- VKMAHNAGVS VEAELGRLMG IEDNISVDEK DAVLVNPKEA EQFVKESQVD YLAPAIGTSH
180- GAFKFKGEPK LDFERLQEVK RLTNIPVLVH GASAI PDNVR KSYLDAGGDL KGSKGVPFEF
240- LQESVKGGIN KVNTD TDLRI AFIAEVRKVA NEDKSQFDLR KFFSPAQLAL KNVVKERMKL
300- LGSANKI

```

Appendix A

Below is the nucleotide sequence of the amplified *H. pylori* aldolase gene cloned in the restriction sites *NdeI* and *ClaI* of plasmid pT7-7:

```

 NdeI
      ~~~
1    ATGTTAGTTA AAGGCAATGA AATTTTATTG AAAGCCCATA AAGAAGGTTA
51   TGGGGTGGGG GCGTTTAATT TCGTGAATTT TGAAATGCTA AACGCTATTT
101  TTGAAGCAGG AAATGAGGAA AATCCCCGC  TTTTCATTCA AACGAGTGAG
151  GGAGCGATCA AATACATGGG GATTGATATG GCGGTAGGCA TGGTGAAAAC
201  CATGTGCGAA CGCTACCCGC ACATTCCTGT AGCCTTACAC CTAGATCATG
251  GCACGACTTT TGAAAGCTGT GAAAAAGCCG TGAAAGCGGG TTTCACTTCT
301  GTGATGATTG ATGCGTCTCA TCATGCTTTT GAAGAAAATT TGGAATTGAC
351  TTCTAAAGTG GTCAAAATGG CGCATAACGC TGGGGTGAGC GTGGAAGCGG
401  AGCTGGGGCG TTTGATGGGG ATTGAAGACA ATATTTTCAGT AGATGAAAAA
451  GACGCGGTGT TAGTGAATCC TAAAGAAGCG GAGCAGTTTG TCAAAGAATC
501  TCAAGTGGAT TACTTAGCCC CAGCTATTGG GACAAGCCAC GGAGCGTTTA
551  AATTTAAGGG CGAGCCAAA  TTGGATTTTG AACGCTTGCA AGAAGTCAAA
601  AGGCTCACTA ATATCCCTTT AGTTTTGCAT GGAGCGAGCG CGATACCAGA
651  TAATGTGAGA AAATCTTATT TGGACGCTGG AGGCGATTTG AAAGGCTCTA
701  AGGGCGTGCC TTTTGAATTT TTACAAGAAT CCGTGAAAGG GGGGATCAAT
751  AAGGTCAATA CTGACACGGA TTTAAGGATC GCTTTCATCG CAGAAGTGCG
801  CAAGGTGGCC AATGAAGATA AGAGCCAATT TGATTTGAGG AAGTTTTTTT
851  CTCCGGCCCA ATTAGCGCTT AAAAAATGTGG TCAAAGAGCG CATGAAACTT
                                     ClaI
                                     ~~~~~
901 TTGGGCAGCG CTAATAAAAT TTAATCAACA AGGAAAGAGT GTAACATCGA
 ClaI
 ~
951 T
```

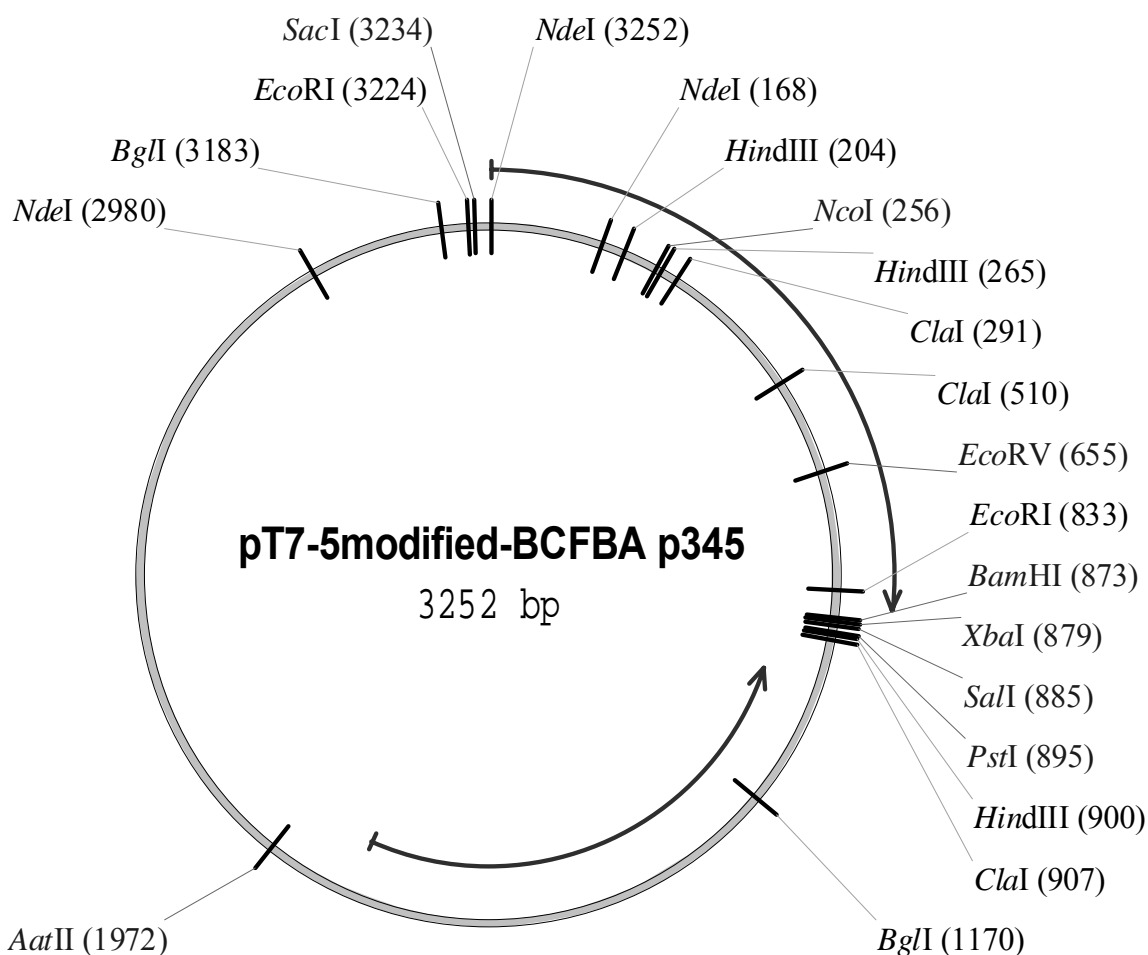


**Figure 6.6 Map of plasmid pT7-5/BCFBA**

Fructose-bisphosphate aldolase [*Bacillus cereus* ATCC 10987]

Other Aliases: BC5335

GeneID: 1207675

Amino acid sequence:

```

1- MPLVSMKEML NKALEGKYAV GQFNMMNLEW TQAILAAAE EKSPVILGVS EGAARHMTGF
60- KTVVAMVKAL IEEMNITVPV AIHLDHGSSF EKCKEIDAG FTSVMIDASH HPFEENVETT
120- KKVVEYAHAR NVSVEAELGT VGGQEDDVIA EGVYADPAE CKHLVEATGI DCLAPALGSV
180- HGPYKGEPNL GFAEMEQRD FTGVPLVLHG GTGIPTADIE KAISLGTSKI NVNTENQIEF
240- TKAVREVLNK DQEVYDPRKF IGPRDAIKA TVIGKIREFG SNGKA

```

Appendix A

Nucleotide sequence and restriction sites of the plasmid pT7-5/BCFBA (plasmid modified to include the ribosome binding site present in the plasmid pT7-7):

Containing the Class II fructose biphosphate aldolase from *Bacillus cereus* ATCC 10987 (GeneID 2748113) inserted *SacI*-*Bam*HI in pT7-5, but with added RBS in primer to make it like pT7-7. An *Nde*I site was also added at the start codon position. The stop codon is shown in bold.

```

NdeI
~~~
1  ATGCCTTTAG TTTCTATGAA AGAAATGCTA AACAAAGCAC TAGAAGGAAA
51 ATACGCAGTT GGTCAATTCA ACATGAACAA CTTAGAGTGG ACTCAAGCTA
101 TCTTAGCTGC TGCGGAAGAA GAAAAATCTC CTGTAATCCT AGGTGTATCT
      NdeI
      ~~~~~~
151 GAGGGTGCAG CTCGTCATAT GACTGGTTTC AAAACAGTTG TAGCTATGGT
 HindIII
      ~~~~~~
201 TAAAGCTTTA ATCGAAGAAA TGAACATCAC TGTTCTGTGTA GCGATTCACC
      NcoI      HindIII      ClaI
      ~~~~~~      ~~~~~~      ~~~~~~
251 TTGACCATGG TTCAAGCTTC GAAAAATGTA AAGAAGCAAT CGATGCAGGT
301 TTCACATCTG TAATGATCGA CGCTTCTCAC CACCCATTCG AAGAAAACGT
351 AGAAACTACT AAAAAAGTAG TAGAATACGC ACACGCTCGT AACGTATCTG
401 TTGAAGCTGA GCTTGGAACA GTTGGCGGAC AAGAAGACGA CGTAATCGCT
451 GAAGGCGTAA TTTACGCTGA CCCAGCTGAG TGTAAGCACC TTGTTGAAGC
 ClaI
      ~~~~~~
501 AACAGGTATC GATTGCCTAG CTCCAGCTTT AGGTTCTGTA CACGGTCCTT
551 ACAAAGGTGA GCCTAACTTA GGATTCGCTG AAATGGAACA AGTTCGTGAC
601 TTCACTGGCG TACCTTTAGT ATTACACGGT GGTACTGGTA TCCCAACTGC
      EcoRV
      ~~~~~~
651 TGATATCGAA AAAGCTATCT CTTTAGGTAC TTCAAAAATC AACGTAAACA
701 CTGAGAACCA AATTGAGTTT ACAAAGCTG TTCGTGAAGT ATTAACAAA
751 GACCAAGAAG TTTACGATCC TCGTAAATTT ATCGGACCTG GCCGCGACGC
 EcoRI
      ~~~~~~
801 TATCAAAGCA ACTGTTATTG GTAAAATTCG CGAATTCGGT TCTAACGGTA
      XbaI      PstI
      ~~~~~~      ~~~~~~
 BamHI SalI HindIII
      ~~~~~~      ~~~~~~      ~~~
851 AAGCGTAAGA ATAAAATTCC GGGATCCTCT AGAGTCGACC TGCAGCCCAA

```

## HindIII

~~~~~

ClaI

~~~~~

901	GCTTATCGAT	GATAAGCTGT	CAAACATGAG	AATTAAATCA	ATCTAAAGTA
951	TATATGAGTA	AACTTGGTCT	GACAGTTACC	AATGCTTAAT	CAGTGAGGCA
1001	CCTATCTCAG	CGATCTGTCT	ATTTCGTTCA	TCCATAGTTG	CCTGACTCCC
1051	CGTCGTGTAG	ATAACTACGA	TACGGGAGGG	CTTACCATCT	GGCCCCAGTG
1101	CTGCAATGAT	ACCGCGAGAC	CCACGCTCAC	CGGCTCCAGA	TTTATCAGCA

## BglI

~~~~~

| | | | | | |
|------|-------------|-------------|------------|------------|------------|
| 1151 | ATAAACCAGC | CAGCCGGAAG | GGCCGAGCGC | AGAAGTGGTC | CTGCAACTTT |
| 1201 | ATCCGCCTCC | ATCCAGTCTA | TTAATTGTTG | CCGGGAAGCT | AGAGTAAGTA |
| 1251 | GTTTCGCCAGT | TAATAGTTTG | CGCAACGTTG | TTGCCATTGC | TACAGGCATC |
| 1301 | GTGGTGTAC | GCTCGTCGTT | TGGTATGGCT | TCATTCAGCT | CCGGTTCCCA |
| 1351 | ACGATCAAGG | CGAGTTACAT | GATCCCCCAT | GTTGTGCAAA | AAAGCGGTTA |
| 1401 | GCTCCTTCGG | TCCTCCGATC | GTTGTCAGAA | GTAAGTTGGC | CGCAGTGTTA |
| 1451 | TCACTCATGG | TTATGGCAGC | ACTGCATAAT | TCTCTTACTG | TCATGCCATC |
| 1501 | CGTAAGATGC | TTTTCTGTGA | CTGGTGAGTA | CTCAACCAAG | TCATTCTGAG |
| 1551 | AATAGTGTAT | GCGGCGACCG | AGTTGCTCTT | GCCCGGCGTC | AACACGGGAT |
| 1601 | AATACGCGC | CACATAGCAG | AACTTTAAAA | GTGCTCATCA | TTGGAAAACG |
| 1651 | TTCTTCGGGG | CGAAAACCTCT | CAAGGATCTT | ACCGCTGTTG | AGATCCAGTT |
| 1701 | CGATGTAACC | CACTCGTGCA | CCCAACTGAT | CTTCAGCATC | TTTTACTTTC |
| 1751 | ACCAGCGTTT | CTGGGTGAGC | AAAAACAGGA | AGGCAAAATG | CCGCAAAAAA |
| 1801 | GGGAATAAGG | GCGACACGGA | AATGTTGAAT | ACTCATACTC | TTCCTTTTTT |
| 1851 | AATATTATTG | AAGCATTAT | CAGGGTTATT | GTCTCATGAG | CGGATACATA |
| 1901 | TTTGAATGTA | TTTAGAAAAA | TAAACAAATA | GGGGTCCGC | GCACATTTCC |

AatII

~~~~~

1951	CCGAAAAGTG	CCACCTGACG	TCTAAGAAAC	CATTATTATC	ATGACATTAA
2001	CCTATAAAAA	TAGGCGTATC	ACGAGGCCCT	TTCGTCTTCA	AGAATAAAAAG
2051	GATCTAGGTG	AAGATCCTTT	TTGATAATCT	CATGACCAA	ATCCCTTAAC
2101	GTGAGTTTTT	GTTCCACTGA	GCGTCAGACC	CCGTAGAAAA	GATCAAAGGA
2151	TCTTCTTGAG	ATCCTTTTTT	TCTGCGCGTA	ATCTGCTGCT	TGCAAACAAA
2201	AAAACCACCG	CTACCAGCGG	TGGTTTGT	GCCGGATCAA	GAGCTACCAA
2251	CTCTTTTTCC	GAAGGTAACT	GGCTTCAGCA	GAGCGCAGAT	ACCAAATACT
2301	GTCCCTCTAG	TGTAGCCGTA	GTTAGGCCAC	CACTTCAAGA	ACTCTGTAGC
2351	ACCGCCTACA	TACCTCGCTC	TGCTAATCCT	GTTACCAGTG	GCTGCTGCCA
2401	GTGGCGATAA	GTCGTGTCTT	ACCGGGTTGG	ACTCAAGACG	ATAGTTACCG
2451	GATAAGGCGC	AGCGGTCGGG	CTGAACGGGG	GGTTCGTGCA	CACAGCCCAG
2501	CTTGAGCGA	ACGACCTACA	CCGAACGAG	ATACCTACAG	CGTGAGCTAT
2551	GAGAAAGCGC	CACGCTTCCC	GAAGGGAGAA	AGGCGGACAG	GTATCCGGTA
2601	AGCGGCAGGG	TCGGAACAGG	AGAGCGCACG	AGGGAGCTTC	CAGGGGGAAA
2651	CGCCTGGTAT	CTTTATAGTC	CTGTCGGGTT	TCGCCACCTC	TGACTTGAGC
2701	GTCGATTTTT	GTGATGCTCG	TCAGGGGGGC	GGAGCCTATG	GAAAAACGCC
2751	AGCAACGCGG	CCTTTTTACG	GTTCCCTGGC	TTTTGCTGGC	CTTTTGCTCA
2801	CATGTTCTTT	CCTGCGTTAT	CCCCTGATTC	TGTGGATAAC	CGTATTACCG
2851	CCTTTGAGTG	AGCTGATACC	GCTCGCCGCA	GCCGAACGAC	CGAGCGCAGC

*Appendix A*

```
2901  GAGTCAGTGA GCGAGGAAGC GGAAGAGCGC CTGATGCGGT ATTTTCTCCT
      NdeI
      ~~~~~~
2951 TACGCATCTG TGCGGTATTT CACACCGCAT ATGGTGCACT CTCAGTACAA
3001 TCTGCTCTGA TGCCTACGT GACTGGGTCA TGGCTGCGCC CCGACACCCG
3051 CCAACACCCG CTGACGCGCC CTGACGGGCT TGTCTGCTCC CGGCATCCGC
3101 TTACAGACAA GCTGTGACCG TCTCCGGGAG CTGCATGTGT CAGAGGTTTT
 BglI
      ~~~~~~
3151  CACCGTCATC ACCGAAACGC GCGAGGCCCA GCTGGCTTAT CGAAATTAAT
      SacI
      ~~~~~~
 EcoRI NdeI
      ~~~~~~
3201  ACGACTCACT ATAGGGAGAC CGGAATTCGA GCTCTAAGAA GGAGATATAC
      NdeI
      ~
3251  AT
```



Below is an alignment of the *B. cereus* FBP aldolase gene sequence (GeneID 2748113), showing the nucleotides that differ from the *B. anthracis* str. 'Ames Ancestor' aldolase gene (GeneID 2815030). The amino acid sequence is identical for both genes.

Query line: >ref|NC_003909.8| *Bacillus cereus* ATCC 10987, complete genome  
 gb|AE017194.1| *Bacillus cereus* ATCC 10987, complete genome  
 Length=5224283

Sbjct line: >ref|NC_007530.2| *Bacillus anthracis* str. 'Ames Ancestor', complete genome  
 gb|AE017334.2| *Bacillus anthracis* str. 'Ames Ancestor', complete genome  
 Length=5227419

Features in this part of subject sequence:  
 fructose-bi sphosphate aldolase

Score = 1568 bits (849), Expect = 0.0  
 Identities = 855/858 (99%), Gaps = 0/858 (0%)  
 Strand=Plus/Minus

```

Query 1      ATGCCTTTAGTTTCTATGAAAGAAATGCTAAACAAAGCACTAGAAGGAAAATACGCAGTT 60
Sbjct 5064417 ATGCCTTTAGTTTCTATGAAAGAAATGCTAAACAAAGCACTAGAAGGAAAATACGCAGTT
5064358

Query 61     GGTCAATTCAACATGAACAACCTAGAGTGGACTCAAGCTATCTTAGCTGCTGCGGAAGAA 120
Sbjct 5064357 GGTCAATTCAACATGAACAACCTAGAGTGGACTCAAGCTATCTTAGCTGCTGCGGAAGAA
5064298

Query 121    GAAAAATCTCCTGTAATCCTAGGTGTATCTGAGGGTGCAGCTCGTCATATGACTGGTTTC 180
Sbjct 5064297 GAAAAATCTCCTGTAATCCTAGGTGTATCTGAGGGTGCAGCTCGTCATATGACTGGTTTC
5064238

Query 181    AAAACAGTTGTAGCTATGGTTAAAGCTTTAATCGAAGAAATGAACATCACTGTTCTCTGTA 240
Sbjct 5064237 AAAACAGTTGTAGCTATGGTTAAAGCTTTAATCGAAGAAATGAACATCACTGTTCTCTGTA
5064178

Query 241    GCGATTCACCTTGACCATGGTTCAAGCTTCGAAAAATGTAAAGAAGCAATCGATGCAGGT 300
Sbjct 5064177 GCGATTCACCTTGACCATGGTTCAAGCTTCGAAAAATGTAAAGAAGCAATCGATGCAGGT
5064118

Query 301    TTCACATCTGTAATGATCGACGCTTCTCACCACCCATTTCGAAGAAAACGTAGAACTACT 360
Sbjct 5064117 TTCACATCTGTAATGATCGACGCTTCTCACCACCCATTTCGAAGAAAACGTAGAACTACT
5064058

Query 361    AAAAAAGTAGTAGAATACGCACACGCTCGTAACGTATCTGTTGAAGCTGAGCTTGGAACA 420
Sbjct 5064057 AAAAAAGTAGTAGAATACGCACACGCTCGTAACGTATCTGTTGAAGCTGAGCTTGGAACA
5063998

Query 421    GTTGGCGGACAAGAAGACGACGTAATCGCTGAAGGCCTAATTTACGCTGACCCAGCTGAG 480
Sbjct 5063997 GTTGGCGGACAAGAAGACGACGTAATCGCTGAAGGCCTAATTTACGCTGACCCAGCTGAG
5063938
  
```

*Appendix A*

Query	481	TGTAAGCACCTTGTTGAAGCAACAGGTATCGATTGCCTAGCTCCAGCTTTAGGTTCTGTA	540
Sbj ct	5063937	TGTAAGCACCTTGTTGAAGCAACAGGTATCGATTGCCTAGCTCCAGCTTTAGGTTCTGTA	
	5063878		
Query	541	CACGGTCCTTACAAAGGTGAGCCTAACTTAGGATTCGCTGAAATGGAACAAGTTCGTGAC	600
Sbj ct	5063877	CACGGTCCTTACAAAGGTGAGCCTAACTTAGGATTCGCTGAAATGGAACAAGTTCGTGAC	
	5063818		
Query	601	TTCACTGGCGTACCTTTAGTATTACACGGTGGTACTGGTATCCCAACTGCTGATATCGAA	660
Sbj ct	5063817	TTCACTGGTGTACCTTTAGTATTACACGGTGGTACTGGTATCCCAACTGCTGATATCGAA	
	5063758		
Query	661	AAAGCTATCTCTTTAGGTACTTCAAAAATCAACGTAAACACTGAGAACCAAATGAGTTTT	720
Sbj ct	5063757	AAAGCTATCTCTTTAGGTACTTCAAAAATCAACGTAAACACTGAGAACCAAATCGAGTTTT	
	5063698		
Query	721	ACAAAAGCTGTTTCGTGAAGTATTAACAAAGACCAAGAAGTTTACGATCCTCGTAAATTT	780
Sbj ct	5063697	ACAAAAGCTGTTTCGTGAAGTATTAACAAAGACCAAGAAGTTTACGATCCTCGTAAATTT	
	5063638		
Query	781	ATCGGACCTGGCCGCGACGCTATCAAAGCAACTGTTATTGGTAAAATTCGCGAATTCGGT	840
Sbj ct	5063637	ATCGGACCTGGCCGCGACGCTATCAAAGCTACTGTTATTGGTAAAATTCGCGAATTCGGT	
	5063578		
Query	841	TCTAACGGTAAAGCGTAA	858
Sbj ct	5063577	TCTAACGGTAAAGCGTAA	5063560

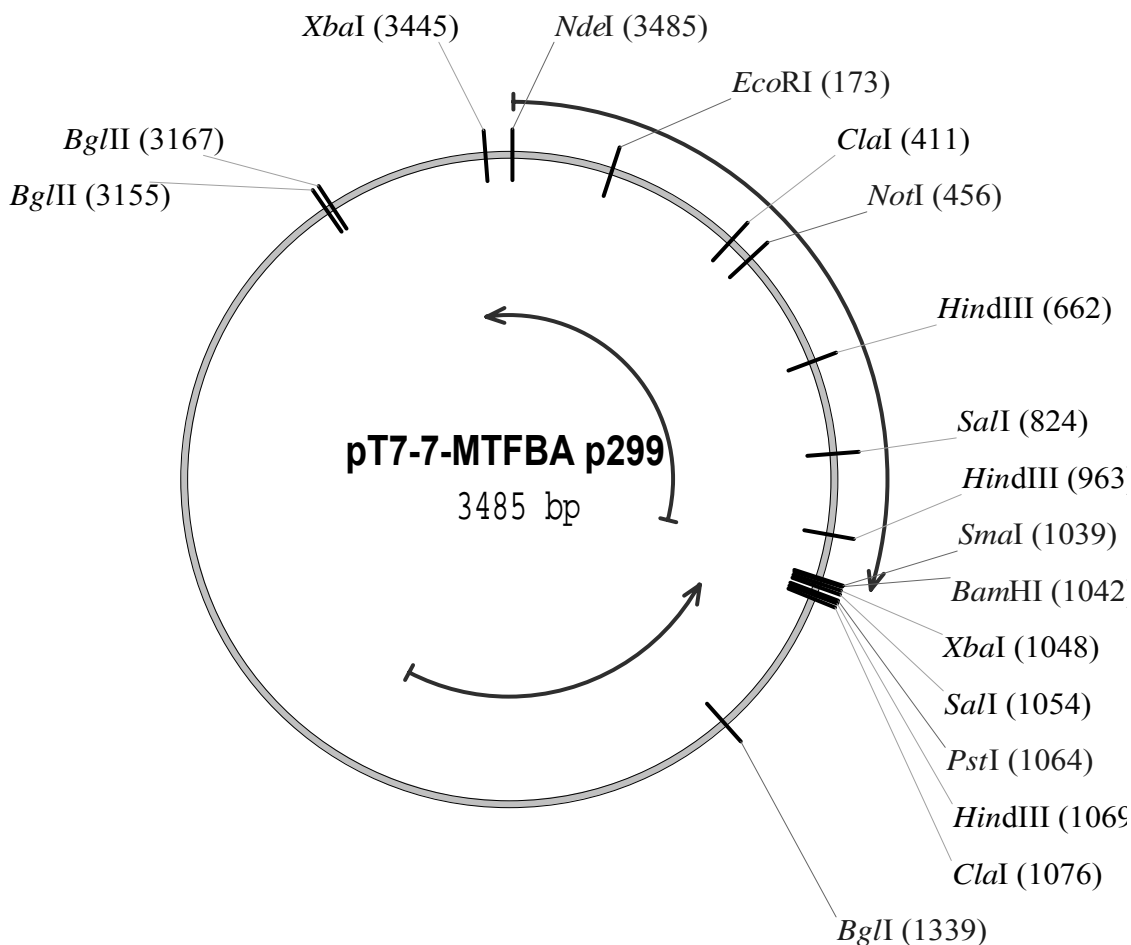


**Figure 6.7 Map of plasmid pT7-7/MTFBA**

FBP aldolase *Mycobacterium tuberculosis* H37Rv

Other Aliases: Rv0363c

GeneID: 886474

Amino acid sequence:

```

1-  MPIATPEVYA  EMLGQAKQNS  YAFPAINCTS  SETVNAAIKG  FADAGSDGII  QFSTGGAIEFG
60-  SGLGVKDMVT  GAVALAEFTH  VIAAKYPVNV  ALHTDHCPKD  KLDSYVRPLL  AISAQRVSKG
120- GNPLFQSHMW  DGSVAPIDEN  LAIAQELLKA  AAAAKIILEI  EIGVVGGEED  GVANEINEKL
180- YTSPEDFEKT  IEALGAGEHG  KYLLAATFGN  VHGVYKPGNV  KLRPDILAQG  QQVAAAKLGL
240- PADAKPFDFV  FHGGSGSLKS  EIEEALRYGV  VKMNVDTDTQ  YAFTRPIAGH  MFTNYDGVLK
300- VDGEVGVKKV  YDPRSYLKKA  EASMSQRVVQ  ACNDLHCAGK  SLTH

```

Appendix A

Amplified *M. tuberculosis* gene cloned in the restriction sites *NdeI* and *SmaI* of plasmid pT7-7:

```

NdeI
~~~
1 ATGCCTATCG CAACGCCCGA GGTCTACGCG GAGATGCTCG GTCAGGCCAA
51 ACAAAACTCG TACGCTTTCC CGGCTATCAA CTGCACCTCC TCGGAAACCG
101 TCAACGCCGC GATCAAAGGT TTCGCCGACG CCGGCAGTGA CGGAATCATC
 EcoRI
      ~~~~~
151 CAGTTCTCGA CCGGTGGCGC AGAATTCGGC TCCGGCCTCG GGGTCAAAGA
201 CATGGTGACC GGTGCGGTCC CTTTGGCGGA GTTCACCCAC GTTATCGCGG
251 CCAAGTACCC GGTCAACGTG GCGCTGCACA CCGACCACTG CCCCAGGAC
301 AAGTTGGACA GCTATGTCCG GCCCTTGCTG GCGATCTCGG CGCAACGCGT
351 GAGCAAAGGT GGCAATCCTT TGTTCCAGTC GCACATGTGG GACGGCTCGG
      ClaI
      ~~~~~
401 CAGTGCCAAT CGATGAGAAC CTGGCCATCG CCCAGGAGCT GCTCAAGGCG
 NotI
      ~~~~~
451 GCGGCGGCCG CCAAGATCAT TCTGGAGATC GAGATCGGCG TCGTCGGCGG
501 CGAAGAGGAC GGCGTGGCGA ACGAGATCAA CGAGAAGCTG TACACCAGCC
551 CGGAGGACTT CGAGAAAACC ATCGAGGCGC TGGGCGCCGG TGAGCACGGC
601 AAATACCTGC TGGCCGCGAC GTTCGGCAAC GTGCATGGCG TCTACAAGCC
      HindIII
      ~~~~~
651 CGGCAACGTC AAGCTTCGCC CCGACATCCT TGCGCAAGGG CAACAGGTGG
701 CGGCGGCCAA GCTCGGACTG CCGGCCGACG CCAAGCCGTT CGACTTCGTG
751 TTCCACGGCG GCTCGGGTTC GCTTAAGTCG GAGATCGAGG AGGCGCTGCG
 SalI
      ~~~~~
801 CTACGGCGTG GTGAAGATGA ACGTCGACAC CGACACCCAG TACGCGTTCA
851 CCCGCCCGAT CGCCGGTCAC ATGTTACCA  ACTACGACGG AGTGCTCAAG
901 GTCGATGGCG AGGTGGGTGT CAAGAAGGTC TACGACCCGC GCAGCTACCT
      HindIII
      ~~~~~
951 CAAGAAGGCC GAAGCTTCGA TGAGCCAGCG GGTCGTTTCA GCGTGCAATG
 SmaI
      ~~~~~
1001 ACCTGCACTG CGCCGGAAAG TCCCTAACCC ACTAACCCGG GG

```

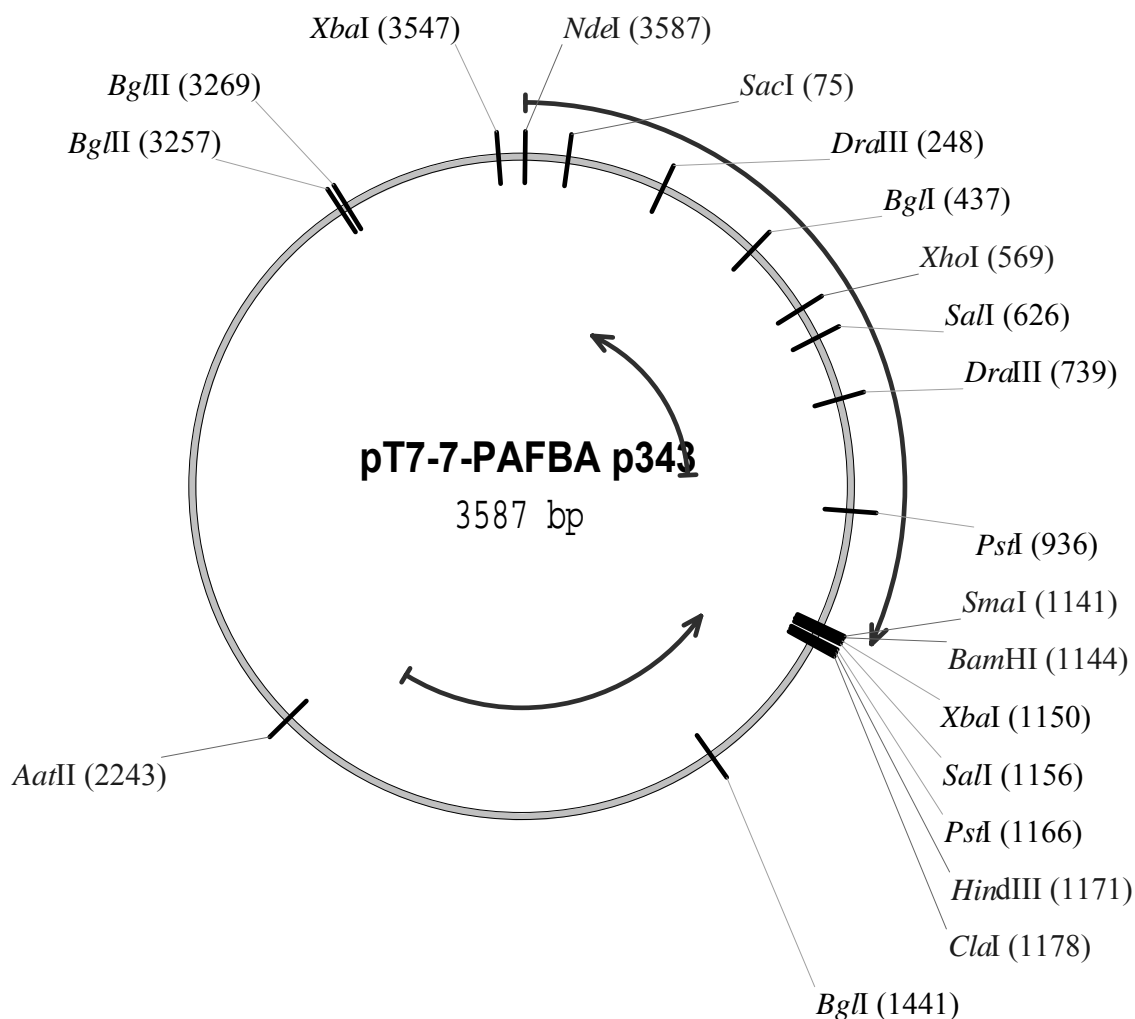


**Figure 6.8 Map of plasmid pT7-7/PAFBA**

fructose-1,6-bisphosphate aldolase [*Pseudomonas aeruginosa* PAO1]

Other Aliases: PA0555; GeneID: 880792

Amino acid sequence:

```

1-  MALISMRQML  DHAAEFGYGV  PAFNVNMLEQ  MRAIMEAADK  TDSPVIVQAS  AGARKYAGAP
60-  FLRHLILAAI  EEFPHIPVVM  HQDHGTSPDV  QORSIQLGFS  SVMMDGSLRE  DGKTPADYDY
120- NVRVTQQTVA  FAHACGVSVE  GELGCLGSLE  TGMAGEEDGV  GAEGVLDHSQ  LLTDPEEAAD
180- FVKKTKVDAL  AIAIGTSHGA  YKFTKPPTGD  TLSIQRIKEI  HARIPDTHLV  MHGSSSVPQD
240- WLAIINEYGG  EIKETYGVPV  EEIVEGIKYG  VRKVNIDTDL  RLASTGAIRR  FLAQNPFSEF
300- PRKYFSKTVE  AMRDICIARY  EAFGTAGNAS  KIKPISLEGM  FQRYARGELD  PKVN

```

Appendix A

Amplified *P. aeruginosa* gene cloned in the restriction sites *NdeI* and *SmaI* of plasmid pT7-7:

```

NdeI
~~~
1 ATGATGCTCC CGGTAGTAAG GTCAATTGGC GTGGAACCTG AGGGCAAGGA
 SacI
                               ~~~~~
51  ATGCATGGGT  GTCTTCAGCG  AGCTCGGTCT  CAAGCCCGGC  GTCCTCTACG
101 GCGAGGAGGT  CTACAAGCTG  TTTGAGCACG  CCAAGAAGAA  TGTCTACGCC
151 ATTCCTGCCA  TCAACGTGAC  CTCGTCGTCC  ACCATTATCG  CCTCCCTTGA
                               DraIII
                               ~~~~~
201 GGCCGCCCGC GACTCCAAGT CCCCATCAT CCTGCAAATG TCACAAGGTG
251 GTGCCGCCTA CTTCGCCGGC AAGGGTGTCT CCAACACCAA CCAGGAGGCC
301 TCGATCGCTG GTGCCGTTGC TGCCGCCAC TTCATCCGCT CGATTGCTCC
351 CATCTACGGC GTCCCGGTGC TCCTTCACAC CGACCACTGC GCCAAGAAGC
 BglI
                               ~~~~~
401 TCCTCCCGTG  GCTCGACGGC  ATGCTCGATG  CCGACGAGGC  TTTCCACAAG
451 GAGAACGGCA  CCCCTCTGTT  CAGCTCGCAC  ATGATCGACC  TGTCTGAGGA
501 GCCCCGTGAC  TGGAACATCG  AGACCACTGC  CAAGTACCTC  AAGCGTGCTG
                               XhoI
                               ~~~~~
551 CCCCCATGAA GCAGTGGCTC GAGATGGAGA TTGGTCTGAC CGGTGGTGAG
 SalI
                               ~~~~~
601 GAGGATGGTG  TCAACAACGA  GGATGTGCAC  AACAACTCCC  TCTACACCCA
651 GCCCCGAGGAC  ATCTTTGCCA  TCCACCAGGC  CCTGAGCCCC  ATCTCCAAGT
                               DraIII
                               ~~~~~
701 ACTTCTCCAT CGCCGCAGGC TTCGGCAACG TCCACGGCGT GTACAAGCCC
751 GGCAACGTTT GTCTTCACCC TGAGCTGCTT GACAAGCACC AGAAGTACGT
801 TATTGAGAAG CTCGGCTGCG AGGAGAAGAA GCCTATCTTC TTCGTCTTCC
851 ACGGTGGCTC CGGCTCCGGC GACTCCGAGT TCCAGGAGGC CATCAGCTAC
 PstI
                               ~~~~~
901 GGTGTCATCA  AGGTCAACCT  CGACACTGAC  CTGCAGTGGG  CCTACCTGAG
951 CGGTATCCGT  GACTACGTCA  CCAGCAAGAT  CGAGTACCTC  AACTCGCAGG
1001 TCGGCAACCC  TGACGGCGCT  GACAAGCCCA  ACAAGAAGTA  CTACGACCCC
1051 CGCGTCTGGG  TTCGTGAGGG  TGAGAAGACC  ATGAAGGCC  GCATCCAGCA
                               SmaI
                               ~~~ ~~~
1101 GGCTCTGAAG GTCTTCAACG CCGAGAACAC CATCTAACCC GGG

```

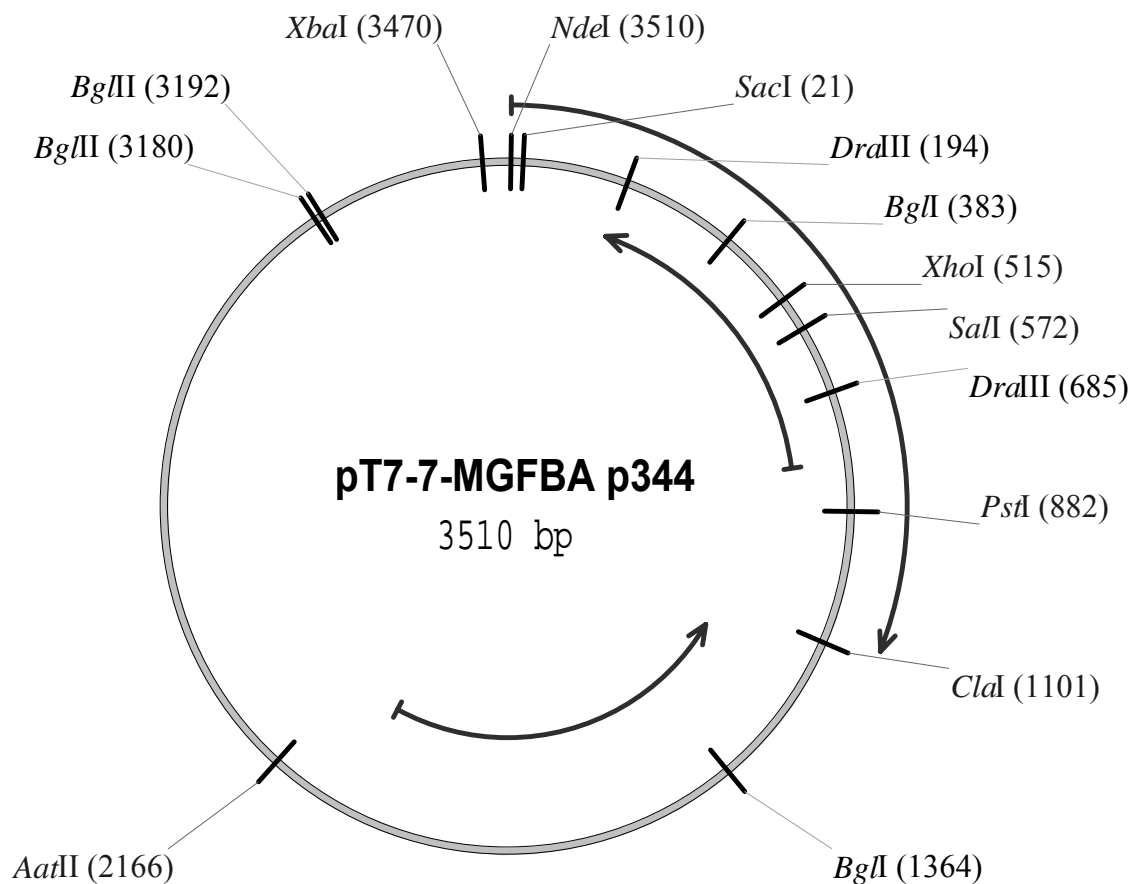


**Figure 6.9 Map of plasmid pT7-7/MGFBA**

*Magnaporthe grisea* 70-15/protein_id="EAA48565.1" replaced by EDK03188

db_xref="GI:38101632" replaced by Gene ID 2674368

Below is the aldolase amino acid sequence from the BAC vector (primers starting from position 6741 and ending at position 8153 the GenBank sequence no. **AACU01001388**):

```

1- MGVFSELGLK PGVLYGEEVY KLFEHAKKNV YAIPAINVTS SSTIIASLEA ARDSKSPIIL
60- QMSQGGAAAYF AGKGVSNNTQ EASIAGAVAA AHFIRSIAPI YGVPVVLHTD HCAKLLLPWL
120- DGMLDADEAF HKENGTPLFS SHMIDLSEEP RDWNIETTAK YLKRAAPMKQ WLEMEIGLTG
180- GEEDGVNNED VDNNSLYTQP EDIFAIHQAL SPISKYFSIA AGFGNVHGVY KPGNVRLHPE
240- LLDKHQKYVI EKLGCCEKKP IFFVFHGGSG SGDSEFQEAI SYGVIVNLD TDLQWAYLSG
300- IRDYVTSKIE YLNSQVGNPD GADKPNKYY DPRVWVREGE KTMKARIQQA LKVFNAENTI

```

Appendix A

Amplified *M. grisea* gene cloned in the restriction sites *NdeI* and *ClaI* of plasmid pT7-7, with all introns removed:

```

 NdeI SacI
      ~~~              ~~~~~
1    ATGGGTGTCT  TCAGCGAGCT  CGGTCTCAAG  CCCGGCGTCC  TCTACGGCGA
51   GGAGGTCTAC  AAGCTGTTTG  AGCACGCCAA  GAAGAATGTC  TACGCCATTC
101  CTGCCATCAA  CGTGACCTCG  TCGTCCACCA  TTATCGCCTC  CCTTGAGGCC
                                           DraIII
                                           ~~~~~
151 GCCCGCGACT CCAAGTCCCC CATCATCCTG CAAATGTCAC AAGGTGGTGC
201 CGCCTACTTC GCCGGCAAGG GTGTCTCCAA CACCAACCAG GAGGCCTCGA
251 TCGCTGGTGC CGTTGCTGCC GCCCACTTCA TCCGCTCGAT TGCTCCCATC
301 TACGGCGTCC CGGTCGTCTT TCACACCGAC CACTGCGCCA AGAAGCTCCT
 BglI
                                           ~~~~~
351  CCCGTGGCTC  GACGGCATGC  TCGATGCCGA  CGAGGCTTTC  CACAAGGAGA
401  ACGGCACCCC  TCTGTTCAGC  TCGCACATGA  TCGACCTGTC  TGAGGAGCCC
451  CGTGACTGGA  ACATCGAGAC  CACTGCCAAG  TACCTCAAGC  GTGCTGCCCC
                                           XhoI
                                           ~~~~~
501 CATGAAGCAG TGGCTCGAGA TGGAGATTGG TCTGACCGGT GGTGAGGAGG
 SalI
                                           ~~~~~
551  ATGGTGTCAA  CAACGAGGAT  GTCGACAACA  ACTCCCTCTA  CACCCAGCCC
601  GAGGACATCT  TTGCCATCCA  CCAGGCCCTG  AGCCCCATCT  CCAAGTACTT
                                           DraIII
                                           ~~~~~
651 CTCCATCGCC GCAGGCTTCG GCAACGTCCA CGGCGTGTAC AAGCCCGGCA
701 ACGTTCGTCT TCACCCTGAG CTGCTTGACA AGCACCAGAA GTACGTTATT
751 GAGAAGCTCG GCTGCGAGGA GAAGAAGCCT ATCTTTTTTCG TCTTCCACGG
801 TGGCTCCGGC TCCGGCGACT CCGAGTTCCA GGAGGCCATC AGCTACGGTG
 PstI
                                           ~~~~~
851  TCATCAAGGT  CAACCTCGAC  ACTGACCTGC  AGTGGGCCTA  CCTGAGCGGT
901  ATCCGTGACT  ACGTCACCAG  CAAGATCGAG  TACCTCAACT  CGCAGGTCGG
951  CAACCCTGAC  GCGCGTGACA  AGCCCAACAA  GAAGTACTAC  GACCCCGCG
1001 TCTGGGTTCG  TGAGGGTGAG  AAGACCATGA  AGGCCCGCAT  CCAGCAGGCT
                                           ClaI
                                           ~~~
1051 CTGAAGGTCT TCAACGCCGA GAACACCATC TAAATTCCCA CGCAACCTAT
 ClaI
      ~~~~
1101 CGAT

```



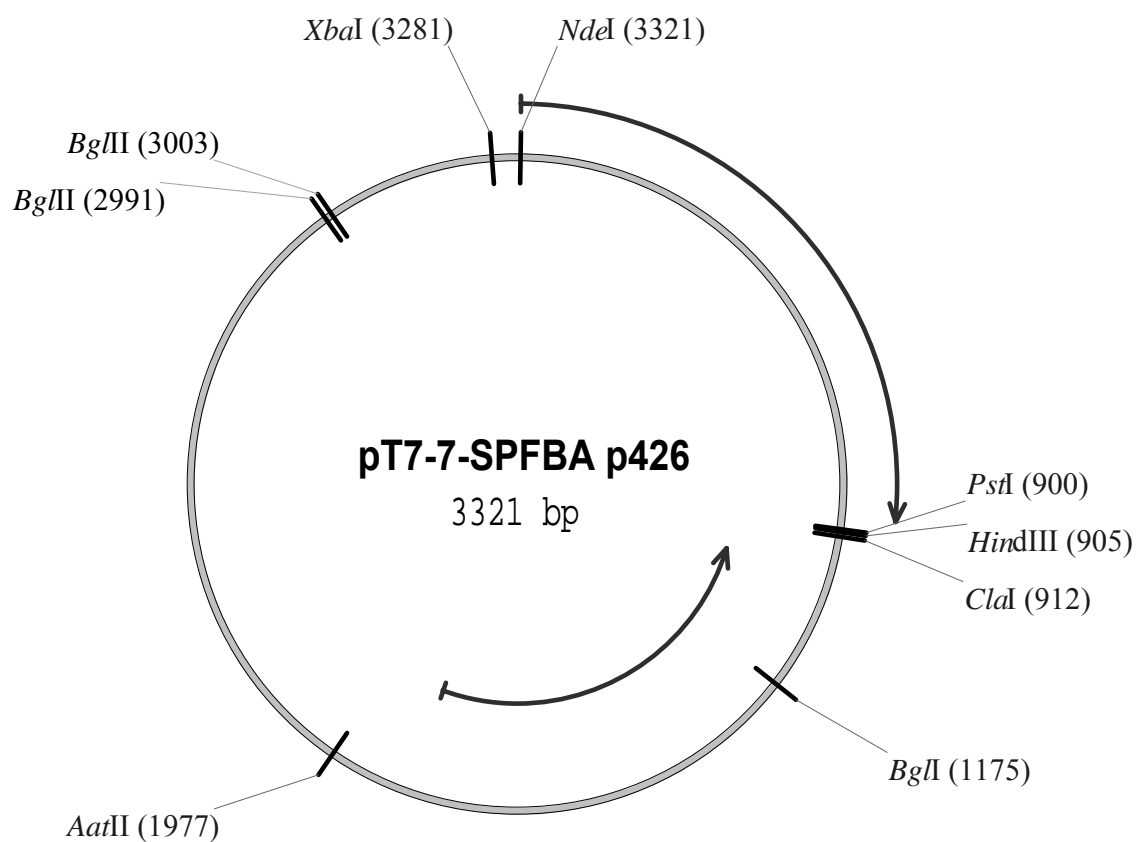


**Figure 6.10 Map of plasmid pT7-7/SPFBA**

*Streptococcus pneumoniae* aldolase

CDS 9890-10771; label=spr0530; protein_id="AAK99334.1"; db_xref="GI:15458104";

Gene ID: 933499

Amino acid sequence:

```

1-  MAIVSAEKFV QAARDNGYAV GGFNTNNLEW TQAILRAAEA KKAPVLIQTS MGAAKYMGGY
60-  KVARNLIANL VESMGITVPV AIHLDHGHYE DALECIEVGY TSIMFDGSHL PVEENLKLAK
120- EVVEKAHAKG ISVEAEVGTI GGEEDGIIGK GELAPIEDAK AMVETGIDFL AAGIGNIHGP
180- YPVNWEGLDL DHLQKLTEAL PGFPPIVLHGG SGIPDEQIQ AAIKLGVAKVN VNTECQIAFA
240- NATRKFARDY EANEAEYDKK KLFDPKFLA DGVKAIQASV EERIDVFGSE GKA

```

Appendix A

Amplified *S. pneumoniae* gene cloned in the restriction sites *NdeI* and *PstI* of plasmid pT7-7:

```

      NdeI
      ~~~
1 ATGGCAATCG T TTCAGCAGA AAAATTTGTC CAAGCAGCCC GTGACAACGG
51 TTATGCAGTT GGTGGATTTA ACACAAACAA CCTTGAGTGG ACTCAAGCTA
101 TCTTGCGCGC AGCAGAAGCT AAAAAAGCTC CAGTTTTGAT CCAAACCTCA
151 ATGGGTGCTG CTAAATACAT GGGTGGTTAC AAAGTTGCTC GCAACTTGAT
201 CGCTAACCTT GTTGAATCAA TGGGTATCAC TGTACCAGTA GCTATCCACC
251 TTGACCACGG TCACTACGAA GATGCACTTG AGTGTATCGA AGTTGGTTAT
301 ACTTCAATCA TGTTTGACGG TTCACACCTT CCAGTTGAAG AAAACCTTAA
351 ATTGGCTAAA GAAGTTGTTG AAAAAGCACA CGCTAAAGGT ATCTCAGTAG
401 AAGCTGAAGT TGGTACTATC GGTGGTGAAG AAGACGGAAT CATCGGTAAA
451 GGTGAATTGG CTCCAATCGA AGACGCTAAA GCAATGGTTG AAACTGGTAT
501 CGACTTCTTG GCAGCTGGTA TCGGTAACAT CCACGGCCCT TACCCAGTAA
551 ACTGGGAAGG TCTTGACCTT GACCACTTGC AAAAATTGAC AGAAGCTCTT
601 CCAGGATTCC CAATCGTATT GCACGGTGGA TCAGGTATTC CTGATGAGCA
651 AATCCAAGCA GCTATCAAAC TTGGTGTTGC CAAAGTTAAC GTTAACACAG
701 AATGCCAAAT CGCATTCGCT AACGCAACTC GTAAATTTGC TCGTGACTAC
751 GAAGCAAACG AAGCAGAATA CGACAAGAAA AAACCTTTCG ACCCACGTAA
801 ATTCTTGGCT GACGGTGTA AAGCTATCCA AGCATCGGTT GAAGAACGTA
 PstI
                                     ~~~~~
851  TCGACGTATT CGGTTTCAGAA GGTAAGCAT AAAGCATAAT CTAGCTGCAG

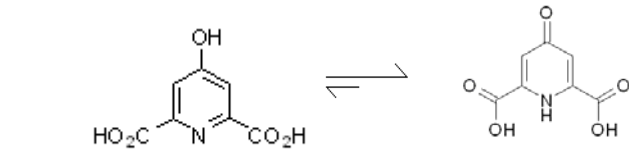
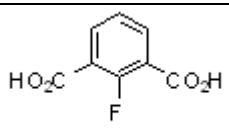
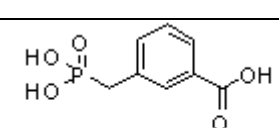
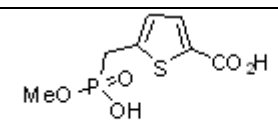
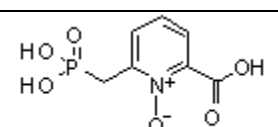
```

## Appendix B

### Synthesized inhibitory compounds codes and molecular weights

**Table 6.1 Synthesized inhibitory compounds names and structures**

Most DPA derivatives were synthesized as pyridinium chlorides, except for compounds 5 and 7 which were synthesized as pyridine N-oxides.

Compound	Laboratory code	Molecular weight (g/mol)	Structure and name
1	GD-A2	201.13	 <p>4-hydroxypyridine-2,6-dicarboxylic acid      Chelidamic acid</p>
2	GD-A3	184.12	 <p>2-fluoroisophthalic acid</p>
3	GD-A4	216.13	 <p>3-(phosphonomethyl)benzoic acid</p>
4	GD-A5	236.18	 <p>5-((hydroxy(methoxy)phosphoryl)methyl)thiophene-2-carboxylic acid</p>
5	GD-A6	233.12	 <p>N-oxide of 6-(phosphonomethyl)picolinic acid</p>

Appendix B

Table 6.1 (continued)

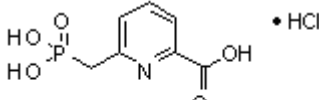
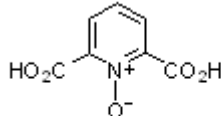
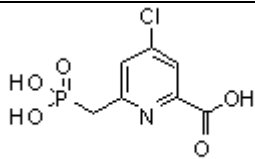
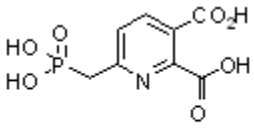
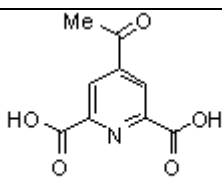
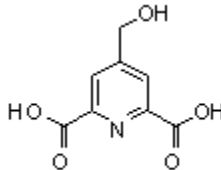
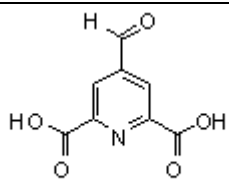
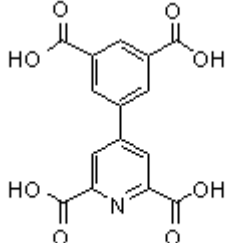
Compound	Laboratory code	Molecular weight (g/mol)	Structure and name
6	GD-A7 or MS191	253.58	 <p>6-(phosphonomethyl)picolinic acid (pyridinium chloride)</p>
7	GD-A8	183.2	 <p>N-oxide of pyridine-2,6-dicarboxylic acid</p>
8	MS183	288.02	 <p>4-chloro-6-(phosphonomethyl)picolinic acid</p>
9	MS213	373.13	 <p>6-(phosphonomethyl)pyridine-2,3-dicarboxylic acid</p>
10	TR04-83B	209.16	 <p>4-acetylpyridine-2,6-dicarboxylic acid</p>
11	TR04-107B	225.2	 <p>4-(hydroxymethyl)pyridine-2,6-dicarboxylic acid</p>

Table 6.1 (continued)

Compound	Laboratory code	Molecular weight (g/mol)	Structure and name
12	TR04-113	231.59	 <p>4-formylpyridine-2,6-dicarboxylic acid</p>
13	AK3	331.24	 <p>4-(3,5-dicarboxyphenyl)pyridine-2,6-dicarboxylic acid</p>



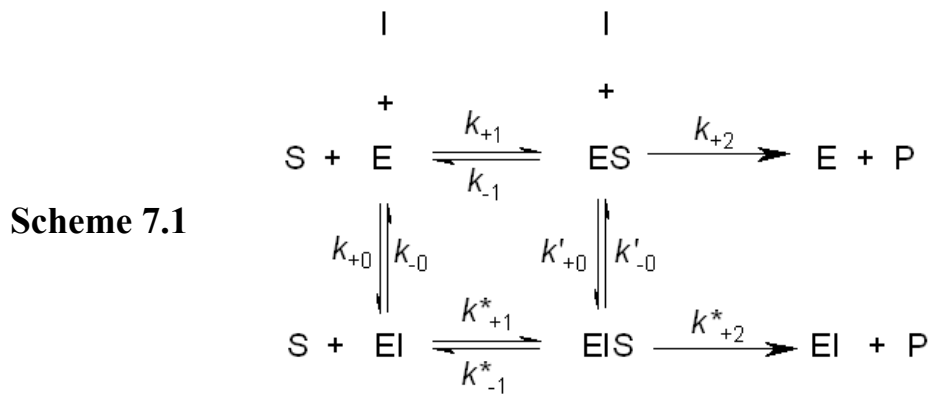
## Appendix C

### Derivation of time-dependent irreversible inhibition equations

The difference between reversible and irreversible inhibition is that in the case of the former, there is a fractional enzymatic activity at steady-state, whereas for irreversible inhibition, there is complete inhibition of the enzyme.

The following demonstration is a partial rendition of the article “Kinetics of substrate reaction during irreversible modification of enzyme activity”, published by C. L. Tsou (1988).

General Scheme applicable to reversible and irreversible inhibition by the modifier I:



The  $K_M$  and  $K^*_M$  Michaelis constants are described by **Equations 7.1 and 7.2**:

$$K_M = \frac{k_{+2} + k_{-1}}{k_{+1}} \qquad K^*_M = \frac{k^*_{+2} + k^*_{-1}}{k^*_{+1}}$$

*Appendix C*

It is assumed that  $[S] \gg [E]_0$  and  $[I] \gg [E]_0$  and that the inhibition reactions are relatively slow compared to the establishment of the steady-state of the enzymatic reaction. In that case the enzyme concentrations are defined by **Equations 7.3 to 7.6**:

$$[ES] = \frac{[E_T][S]}{K_M + [S]} \quad [E] = \frac{[E_T]K_M}{K_M + [S]}$$

$$[EIS] = \frac{[E^*_T][S]}{K^*_M + [S]} \quad [EI] = \frac{[E^*_T]K^*_M}{K^*_M + [S]}$$

Where the total concentrations of the uninhibited and inhibited enzymes are defined by **Equations 7.7 and 7.8**, respectively:

$$[E_T] = [E] + [ES] \quad \text{and} \quad [E^*_T] = [EI] + [EIS]$$

If  $[E]_0$  is the total concentration, then:

**Equation 7.9:**

$$-\frac{d[E_T]}{dt} = \left\{ \frac{[I](k_{+0}K_M + k'_{+0}[S])}{K_M + [S]} + \frac{k_{-0}K^*_M + k'_{-0}[S]}{K^*_M + [S]} \right\} [E_T] - \frac{[E]_0(k_{-0}K^*_M + k'_{-0}[S])}{K^*_M + [S]}$$

This equation can be written in the form:

$$-\frac{d[E_T]}{dt} = (A[I] + B)[E_T] - B[E]_0$$

**Equation 7.9b:**



where  $A$  and  $B$  are the apparent rate constants for the binding of the inhibitor and the backward reaction, respectively. For irreversible inhibition where both  $k_{-0}$  and  $k'_{-0}$  equal zero:

**Equation 7.10:**

$$-\frac{d[E_T]}{dt} = \frac{[I][E_T](k_{+0}K_M + k'_{+0}[S])}{K_M + [S]}$$

From these equations, an expression for the substrate reaction in the presence of the inhibitor can be obtained. For inhibitors resulting in the complete suppression of enzyme activity, that is EIS is inactive, and therefore  $k_{+2} = 0$ :

**Equation 7.11:**

$$\frac{d[P]}{dt} = \frac{k_{+2}[E]_0[S]}{(K_M + [S])(A[I] + B)} \{ B + A[I]e^{-(A[I] + B)t} \}$$

The integration is possible if the conditions are such that the change in  $[S]$  does not significantly affect the ratio  $[E]/[ES]$  and  $[EI]/[EIS]$ . This condition is easily met **when the enzyme is effectively saturated with the substrate**. Experimentally, if without the inhibitor, the same extent of substrate reaction has not led to significant change in the initial reaction rate, it can be considered that the ratio  $[E]/[ES]$  remains constant. Unless EI has a significantly higher affinity for S than the unmodified enzyme, it can also be assumed that  $[EI]/[EIS]$  hasn't changed. The integration of the above equation from  $P=0$  at  $t=0$  gives the product concentration at time  $t$ :

Appendix C

Equation 7.12: 
$$[P] = \frac{V}{A[I] + B} \left\{ Bt + \frac{A[I]}{A[I] + B} [1 - e^{-(A[I] + B)t}] \right\}$$

For irreversible inhibition,  $B = 0$ ,

Equation 7.13 
$$[P] = \frac{V}{A[I]} (1 - e^{-A[I]t})$$

and the product formed,  $[P]_{\infty}$  when  $t$  approaches infinity:

Equation 7.14 
$$[P]_{\infty} = \frac{V}{A[I]}$$

For very-tight-inhibitor binding, the off-rate becomes very small compared even to a slow on-rate and when  $B$  approaches zero, the inhibition can be virtually treated as irreversible.

**Determination of the type of inhibition**

In competitive, noncompetitive, and uncompetitive irreversible inhibitions, as for reversible inhibitions, substrate binding prevents, does not affect, or promotes inhibitor binding, respectively.

The effect of substrate concentration on the apparent rate constant  $A$  for the binding of the inhibitor can be used as the criteria for the characterization of different types of substrate competition. The three types of substrate competition in irreversible inhibition can be distinguished by suitable plots of  $A$  and  $[S]$ .

For competitive irreversible inhibition, where  $I$  does not bind to  $ES$  ( $k'_{+0}=0$ ):

$$A = \frac{k_{+0}}{1 + [S]/K_M}$$

**Equation 7.15a:**

For noncompetitive irreversible inhibition, where  $I$  does not affect  $ES$  binding ( $k_{+0} = k'_{+0}$ ):

$$A = k_{+0}$$

**Equation 7.15b:**

For uncompetitive irreversible inhibition, where  $I$  binds to  $ES$  only ( $k_{+0}=0$ ):

$$A = \frac{k'_{+0}[S]}{K_M + [S]}$$

**Equation 7.15c:**

Thus, while  $A$  is independent of  $[S]$  for noncompetitive inhibition, a plot of  $1/A$  versus  $[S]$  gives a straight line for competitive inhibition and for uncompetitive inhibition a straight line is obtained from the plot of  $1/A$  versus  $1/[S]$ , giving the value of the rate constant for the modification step from the ordinate intercepts.



## References

- Adam, D. (2002) Global antibiotic resistance in *Streptococcus pneumoniae*. *J Antimicrob Chemother* 50 Suppl, 1-5.
- Akerley, B.J., Rubin, E.J., Novick, V.L., Amaya, K., Judson, N. and Mekalanos, J.J. (2002) A genome-scale analysis for identification of genes required for growth or survival of *Haemophilus influenzae*. *Proc Natl Acad Sci U S A* 99, 966-71.
- Alpuche, C., Garau, J. and Lim, V. (2007) Global and local variations in antimicrobial susceptibilities and resistance development in the major respiratory pathogens. *Int J Antimicrob Agents* 30 Suppl 2, S135-8.
- Andreini, C., Banci, L., Bertini, I. and Rosato, A. (2006) Counting the Zinc-Proteins Encoded in the Human Genome. *J Proteome Res* 5, 196-201.
- Aparicio, R., Ferreira, S.T. and Polikarpov, I. (2003) Closed conformation of the active site loop of rabbit muscle triosephosphate isomerase in the absence of substrate: evidence of conformational heterogeneity. *J Mol Biol* 334, 1023-41.
- Aung, H.P., Bocola, M., Schleper, S. and Rohm, K.H. (2000) Dynamics of a mobile loop at the active site of *Escherichia coli* asparaginase. *Biochim Biophys Acta* 1481, 349-59.
- Azéma, L., Lherbet, C., Baudoin, C. and Blonski, C. (2006) Cell permeation of a *Trypanosoma brucei* aldolase inhibitor: Evaluation of different enzyme-labile phosphate protecting groups. *Bioorg Med Chem Lett* 16, 3440-3443.
- Bai, N.J., Pai, M.R., Murthy, P.S. and Venkitasubramanian, T.A. (1974) Effect of oxygen tension on the aldolases of *Mycobacterium tuberculosis* H37Rv. *FEBS Lett* 45, 68-70.
- Bai, N.J., Pai, M.R., Murthy, P.S. and Venkitasubramanian, T.A. (1975) Fructose 1,6 diphosphate aldolase of *Mycobacterium tuberculosis* H37Rv. *Indian J Biochem Biophys* 12, 181-183.
- Bai, N.J., Pai, M.R., Murthy, P.S. and Venkitasubramanian, T.A. (1982) Fructose-bisphosphate aldolases from mycobacteria. *Methods Enzymol* 90 Pt E, 241-250.
- Baldwin, S.A., Perham, R.N. and Stribling, D. (1978) Purification and characterization of the class-II D-fructose 1,6-bisphosphate aldolase from *Escherichia coli* (Crookes' strain). *Biochem J* 169, 633-41.
- Banerjee, P.C., Darzins, A. and Maitra, P.K. (1987) Gluconeogenic mutations in *Pseudomonas aeruginosa*: genetic linkage between fructose-bisphosphate aldolase and phosphoglycerate kinase. *J Gen Microbiol* 133, 1099-107.
- Banerjee, P.C., Vanags, R.I., Chakrabarty, A.M. and Maitra, P.K. (1985) Fructose 1,6-bisphosphate aldolase activity is essential for synthesis of alginate from glucose by *Pseudomonas aeruginosa*. *J Bacteriol* 161, 458-60.

## References

- Bang, S.S. and Baumann, P. (1978) Properties of fructose-1,6-diphosphate phosphatase and fructose-1,6-diphosphate aldolase from *Pseudomonas putida*. *Curr Microbiol* 1, 5-9.
- Bardsley, W.G. and Childs, R.E. (1974) Inhibition of enzymes by metal ion-chelating reagents. Theory and new graphical methods of study. *Biochem J* 137, 55-60.
- Beechem, J.M. and Brand, L. (1985) Time-resolved fluorescence of proteins. *Annu Rev Biochem* 54, 43-71.
- Belasco, J.G. and Knowles, J.R. (1983) Polarization of substrate carbonyl groups by yeast aldolase: investigation by Fourier transform infrared spectroscopy. *Biochemistry* 22, 122-9.
- Berry, A. and Marshall, K.E. (1993) Identification of zinc-binding ligands in the Class II fructose-1,6-bisphosphate aldolase of *Escherichia coli*. *FEBS Letters* 318, 11-16.
- Black, J.G. (1999). Microbiology, Principles and Explorations, Fourth Edition. Upper Saddle River, N.J., Prentice-Hall, Inc.
- Blom, N.S., Tetreault, S., Coulombe, R. and Sygusch, J. (1996) Novel active site in *Escherichia coli* fructose 1,6-bisphosphate aldolase. *Nat Struct Biol* 3, 856-62.
- Blonski, C., De Moissac, D., Perie, J. and Sygusch, J. (1997) Inhibition of rabbit muscle aldolase by phosphorylated aromatic compounds. *Biochem J* 323 ( Pt 1), 71-7.
- Blonski, C., Gefflaut, T. and Perie, J. (1998) Kinetic and spectroscopic study of slow-binding inhibition processes in aldolase. *J Phys Org Chem* 11, 793-802.
- Blostein, R. and Rutter, W.J. (1963) Comparative Studies of Liver and Muscle Aldolase. II. Immunochemical and Chromatographic Differentiation. *J Biol Chem* 238, 3280-5.
- Bock, A. and Neidhardt, F.C. (1966a) Isolation of a Mutant of *Escherichia coli* with a Temperature-sensitive Fructose-1,6-Diphosphate Aldolase Activity. *J Bacteriol* 92, 464-469.
- Bock, A. and Neidhardt, F.C. (1966b) Properties of a Mutant of *Escherichia coli* with a Temperature-sensitive Fructose-1,6-Diphosphate Aldolase. *J Bacteriol* 92, 470-476.
- Boles, E. and Zimmermann, F.K. (1993) *Saccharomyces cerevisiae* phosphoglucose isomerase and fructose bisphosphate aldolase can be replaced functionally by the corresponding enzymes of *Escherichia coli* and *Drosophila melanogaster*. *Curr Genet* 23, 187-191.
- Bonman, J.M., Khush, G.S. and Nelson, R.J. (1992) Breeding Rice for Resistance to Pests. *Annu Rev Phytopathol* 30, 507-528.
- Bradford, M.M. (1976) A rapid and sensitive method for the quantitation of microgram quantities of protein utilizing the principle of protein dye binding. *Anal Biochem* 72, 248-254.

## References

- Brouillard, J.E., Terriff, C.M., Tofan, A. and Garrison, M.W. (2006) Antibiotic selection and resistance issues with fluoroquinolones and doxycycline against bioterrorism agents. *Pharmacotherapy* 26, 3-14.
- Brown, E.D. and Wright, G.D. (2005) New targets and screening approaches in antimicrobial drug discovery. *Chem Rev* 105, 759-74.
- Brown, L.M. (2000) *Helicobacter pylori*: epidemiology and routes of transmission. *Epidemiol Rev* 22, 283-97.
- Camus, J.C., Pryor, M.J., Medigue, C. and Cole, S.T. (2002) Re-annotation of the genome sequence of *Mycobacterium tuberculosis* H37Rv. *Microbiology* 148, 2967-73.
- Carneiro, L.C., De Faria, F.P., Felipe, M.S.S., Pereira, M. and De Almeida Soares, C.M. (2005) *Paracoccidioides brasiliensis* presents two different cDNAs encoding homologues of the fructose 1,6-biphosphate aldolase: Protein isolation, cloning of the cDNAs and genes, structural, phylogenetic, and expression analysis. *Fungal Genet Biol* 42, 51-60.
- Choi, J.H., Jung, H.Y., Kim, H.S. and Cho, H.G. (2000) PhyloDraw: a phylogenetic tree drawing system. *Bioinformatics* 16, 1056-8.
- Choi, K.H. and Tolan, D.R. (2004) Presteady-state kinetic evidence for a ring-opening activity in fructose-1,6-(bis)phosphate aldolase. *J Am Chem Soc* 126, 3402-3.
- Chong, C.R. and Auld, D.S. (2000) Inhibition of carboxypeptidase A by D-penicillamine: mechanism and implications for drug design. *Biochemistry* 39, 7580-8.
- Clamp, M., Cuff, J., Searle, S.M. and Barton, G.J. (2004) The Jalview Java alignment editor. *Bioinformatics* 20, 426-7.
- Cole, S.T., Brosch, R., Parkhill, J., Garnier, T., Churcher, C., Harris, D., Gordon, S.V., Eiglmeier, K., Gas, S., Barry, C.E., 3rd, Tekaia, F., Badcock, K., Basham, D., Brown, D., Chillingworth, T., Connor, R., Davies, R., Devlin, K., Feltwell, T., Gentles, S., Hamlin, N., Holroyd, S., Hornsby, T., Jagels, K., Krogh, A., Mclean, J., Moule, S., Murphy, L., Oliver, K., Osborne, J., Quail, M.A., Rajandream, M.A., Rogers, J., Rutter, S., Seeger, K., Skelton, J., Squares, R., Squares, S., Sulston, J.E., Taylor, K., Whitehead, S. and Barrell, B.G. (1998) Deciphering the biology of *Mycobacterium tuberculosis* from the complete genome sequence. *Nature* 393, 537-44.
- Collins, K.D. (1974) An activated intermediate analogue. The use of phosphoglycolohydroxamate as a stable analogue of a transiently occurring dihydroxyacetone phosphate-derived enolate in enzymatic catalysis. *J Biol Chem* 249, 136-42.
- Concha, N.O., Janson, C.A., Rowling, P., Pearson, S., Cheever, C.A., Clarke, B.P., Lewis, C., Galleni, M., Frere, J.M., Payne, D.J., Bateson, J.H. and Abdel-Meguid, S.S. (2000) Crystal structure of the IMP-1 metallo beta-lactamase from *Pseudomonas aeruginosa* and its complex with a mercaptocarboxylate inhibitor: binding determinants of a potent, broad-spectrum inhibitor. *Biochemistry* 39, 4288-98.

## References

- Conway, T. (1992) The Entner-Doudoroff pathway: history, physiology and molecular biology. *FEMS Microbiol Rev* 9, 1-27.
- Cooper, S.J., Leonard, G.A., Mcsweeney, S.M., Thompson, A.W., Naismith, J.H., Qamar, S., Plater, A., Berry, A. and Hunter, W.N. (1996) The crystal structure of a class II fructose-1,6-bisphosphate aldolase shows a novel binuclear metal-binding active site embedded in a familiar fold. *Structure* 4, 1303-1315.
- Cornish-Bowden, A. (1995). Analysis of Enzyme Kinetic Data. Oxford, Oxford Science Publications.
- Da Fonseca, C.A., Jesuino, R.S., Felipe, M.S., Cunha, D.A., Brito, W.A. and Soares, C.M. (2001) Two-dimensional electrophoresis and characterization of antigens from *Paracoccidioides brasiliensis*. *Microbes Infect* 3, 535-42.
- Dandekar, T., Schuster, S., Snel, B., Huynen, M. and Bork, P. (1999) Pathway alignment: application to the comparative analysis of glycolytic enzymes. *Biochem J* 343 Pt 1, 115-24.
- Dax, C., Coincon, M., Sygusch, J. and Blonski, C. (2005) Hydroxynaphthaldehyde phosphate derivatives as potent covalent Schiff base inhibitors of fructose-1,6-bisphosphate aldolase. *Biochemistry* 44, 5430-43.
- Dax, C., Duffieux, F., Chabot, N., Coincon, M., Sygusch, J., Michels, P.A. and Blonski, C. (2006) Selective irreversible inhibition of fructose 1,6-bisphosphate aldolase from *Trypanosoma brucei*. *J Med Chem* 49, 1499-502.
- Dean, R.A., Talbot, N.J., Ebbole, D.J., Farman, M.L., Mitchell, T.K., Orbach, M.J., Thon, M., Kulkarni, R., Xu, J.R., Pan, H., Read, N.D., Lee, Y.I., Carbone, I., Brown, D., Yeon, Y.O., Donofrio, N., Jun, S.J., Soanes, D.M., Djonovic, S., Kolomlots, E., Rehmeier, C., Li, W., Harding, M., Kim, S., Lebrun, M.H., Bohnert, H., Coughlan, S., Butler, J., Calvo, S., Ma, L.J., Nicol, R., Purcell, S., Nusbaum, C., Galagan, J.E. and Dirren, B.W. (2005) The genome sequence of the rice blast fungus *Magnaporthe grisea*. *Nature* 434, 980-986.
- Dreyer, M.K. and Schulz, G.E. (1996) Refined high-resolution structure of the metal-ion dependent L-fuculose-1-phosphate aldolase (class II) from *Escherichia coli*. *Acta Crystallogr D Biol Crystallogr* 52, 1082-91.
- Fernandez-Arenas, E., Molero, G., Nombela, C., Diez-Orejas, R. and Gil, C. (2004a) Contribution of the antibodies response induced by a low virulent *Candida albicans* strain in protection against systemic candidiasis. *Proteomics* 4, 1204-1215.
- Fernandez-Arenas, E., Molero, G., Nombela, C., Diez-Orejas, R. and Gil, C. (2004b) Low virulent strains of *Candida albicans*: Unravelling the antigens for a future vaccine. *Proteomics* 4, 3007-3020.
- Fessner, W.-D. (2004). Enzyme-catalyzed Aldol Additions, in: Modern aldol reactions, Weinheim : Wiley-VCH.



## References

- Fessner, W.-D. and Walter, C. (1997). Enzymatic C-C bond formation in asymmetric synthesis. *Bioorg Chem*: 97-194.
- Fessner, W.D., Schneider, A., Held, H., Sinerius, G., Walter, C., Hixon, M. and Schloss, J.V. (1996) The mechanism of class II, metal-dependent aldolases. *Angew Chem Int Ed Engl* 35, 2219-2221.
- Fluegge, K., Schweier, O., Schiltz, E., Batsford, S. and Berner, R. (2004) Identification and immunoreactivity of proteins released from *Streptococcus agalactiae*. *Eur J Clin Microbiol Infect Dis* 23, 818-24.
- Fonvielle, M., Coincon, M., Daher, R., Desbenoit, N., Kosieradzka, K., Barilone, N., Gicquel, B., Sygusch, J., Jackson, M. and Therisod, M. (2008) Synthesis and biochemical evaluation of selective inhibitors of class II fructose bisphosphate aldolases: towards new synthetic antibiotics. *Chemistry* 14, 8521-9.
- Fonvielle, M., Weber, P., Dabkowska, K. and Therisod, M. (2004) New highly selective inhibitors of class II fructose-1,6-bisphosphate aldolases. *Bioorg Med Chem Lett* 14, 2923-6.
- Franceschi, F. and Duffy, E.M. (2006) Structure-based drug design meets the ribosome. *Biochem Pharmacol* 71, 1016-25.
- Frey, T., Newlin, L.L. and Atherly, A.G. (1975) Strain of *Escherichia coli* with a temperature-sensitive mutation affecting ribosomal ribonucleic acid accumulation. *J Bacteriol* 121, 923-32.
- Gage, T.B. (1993) The decline of mortality in England and Wales 1861 to 1964: decomposition by cause of death and component of mortality. *Popul Stud (Camb)* 47, 47-66.
- Gage, T.B. (2005) Are modern environments really bad for us?: revisiting the demographic and epidemiologic transitions. *Am J Phys Anthropol Suppl* 41, 96-117.
- Galkin, A., Kulakova, L., Melamud, E., Li, L., Wu, C., Mariano, P., Dunaway-Mariano, D., Nash, T.E. and Herzberg, O. (2007) Characterization, kinetics, and crystal structures of fructose-1,6-bisphosphate aldolase from the human parasite, *Giardia lamblia*. *J Biol Chem* 282, 4859-67.
- Garrity, J.D., Pauff, J.M. and Crowder, M.W. (2004) Probing the dynamics of a mobile loop above the active site of L1, a metallo-beta-lactamase from *Stenotrophomonas maltophilia*, via site-directed mutagenesis and stopped-flow fluorescence spectroscopy. *J Biol Chem* 279, 39663-70.
- Gavalda, S., Braga, R., Dax, C., Vigroux, A. and Blonski, C. (2005) N-Sulfonyl hydroxamate derivatives as inhibitors of class II fructose-1,6-diphosphate aldolase. *Bioorg Med Chem Lett* 15, 5375-7.
- Gefflaut, T., Blonski, C., Perie, J. and Willson, M. (1995) Class I aldolases: substrate specificity, mechanism, inhibitors and structural aspects. *Prog Biophys Mol Biol* 63, 301-40.

## References

- Gerdes, S.Y., Scholle, M.D., Campbell, J.W., Bala?Zsi, G., Ravasz, E., Daugherty, M.D., Somera, A.L., Kyrpides, N.C., Anderson, I., Gelfand, M.S., Bhattacharya, A., Kapatral, V., D'souza, M., Baev, M.V., Grechkin, Y., Mseeh, F., Fonstein, M.Y., Overbeek, R., Baraba?Si, A.L., Oltvai, Z.N. and Osterman, A.L. (2003) Experimental determination and system level analysis of essential genes in *Escherichia coli* MG1655. *J Bacteriol* 185, 5673-5684.
- Gerstein, M. and Levitt, M. (1997) A structural census of the current population of protein sequences. *Proc Natl Acad Sci U S A* 94, 11911-6.
- Giaever, G., Chu, A.M., Ni, L., Connelly, C., Riles, L., Véronneau, S., Dow, S., Lucau-Danila, A., Anderson, K., Andre, B., Arkin, A.P., Astromoff, A., El Bakkoury, M., Bangham, R., Benito, R., Brachat, S., Campanaro, S., Curtiss, M., Davis, K., Deutschbauer, A., Entian, K.D., Flaherty, P., Foury, F., Garfinkel, D.J., Gerstein, M., Gotte, D., Güldener, U., Hegemann, J.H., Hempel, S., Herman, Z., Jaramillo, D.F., Kelly, D.E., Kelly, S.L., Kötter, P., Labonte, D., Lamb, D.C., Lan, N., Liang, H., Liao, H., Liu, L., Luo, C., Lussier, M., Mao, R., Menard, P., Ooi, S.L., Revuelta, J.L., Roberts, C.J., Rose, M., Ross-Macdonald, P., Scherens, B., Schimmack, G., Shafer, B., Shoemaker, D.D., Sookhai-Mahadeo, S., Storms, R.K., Strathern, J.N., Valle, G., Voet, M., Volckaert, G., Wang, C.Y., Ward, T.R., Wilhelmy, J., Winzeler, E.A., Yang, Y., Yen, G., Youngman, E., Yu, K., Bussey, H., Boeke, J.D., Snyder, M., Philippsen, P., Davis, R.W. and Johnston, M. (2002) Functional profiling of the *Saccharomyces cerevisiae* genome. *Nature* 418, 387-391.
- Giavazzi, R. and Taraboletti, G. (2001) Preclinical development of metalloproteasins inhibitors in cancer therapy. *Crit Rev Oncol Hematol* 37, 53-60.
- Glass, J.I., Assad-Garcia, N., Alperovich, N., Yooseph, S., Lewis, M.R., Maruf, M., Hutchison, C.A., 3rd, Smith, H.O. and Venter, J.C. (2006) Essential genes of a minimal bacterium. *Proc Natl Acad Sci U S A* 103, 425-30.
- Guex, N. and Peitsch, M.C. (1997) SWISS-MODEL and the Swiss-PdbViewer: an environment for comparative protein modeling. *Electrophoresis* 18, 2714-23.
- Hall, D.R., Bond, C.S., Leonard, G.A., Ian Watt, C., Berry, A. and Hunter, W.N. (2002) Structure of tagatose-1,6-bisphosphate aldolase. Insight into chiral discrimination, mechanism, and specificity of class II aldolases. *J Biol Chem* 277, 22018-22024.
- Hall, D.R., Kemp, L.E., Leonard, G.A., Marshall, K., Berry, A. and Hunter, W.N. (2003) The organization of divalent cations in the active site of cadmium *Escherichia coli* fructose-1,6-bisphosphate aldolase. *Acta Crystallogr D Biol Crystallogr* 59, 611-4.
- Hall, D.R., Leonard, G.A., Reed, C.D., Watt, C.I., Berry, A. and Hunter, W.N. (1999) The crystal structure of *Escherichia coli* class II fructose-1,6-bisphosphate aldolase in complex with phosphoglycolohydroxamate reveals details of mechanism and specificity. *J Mol Biol* 287, 383-394.
- Hao, J. (2003). Protein engineering of aldolases. Ph.D. thesis, University of Leeds, U.K.: 225 pages.

## References

- Hao, J. and Berry, A. (2004) A thermostable variant of fructose bisphosphate aldolase constructed by directed evolution also shows increased stability in organic solvents. *Protein Eng Des Sel* 17, 689-97.
- Harris, C.E., Kobes, R.D., Teller, D.C. and Rutter, W.J. (1969) The molecular characteristics of yeast aldolase. *Biochemistry* 8, 2442-54.
- Healy, M.J. and Christen, P. (1973) Mechanistic probes for enzymatic reactions. Oxidation-reduction indicators as oxidants of intermediary carbanions (studies with aldolase, aspartate aminotransferase, pyruvate decarboxylase, and 6-phosphogluconate dehydrogenase). *Biochemistry* 12, 35-41.
- Henderson, I., Garcia-Junceda, E., Liu, K.K., Chen, Y.L., Shen, G.J. and Wong, C.H. (1994) Cloning, overexpression and isolation of the type II FDP aldolase from *E. coli* for specificity study and synthetic application. *Bioorg Med Chem* 2, 837-843.
- Hilcenko, C. (2003). Multi-dimensional nuclear magnetic resonance studies of the dynamics and mechanism of FBP-aldolase. Ph.D. thesis, University of Leeds, U.K.: 263 pages.
- Hill, H.A.O., Lobb, R.R. and Sharp, S.L. (1976) Metal replacement studies in *Bacillus stearothermophilus* aldolase and a comparison of the mechanisms of class I and class II aldolases. *Biochem J* 153, 551-560.
- Himmelhoch, S.R., Sober, H.A., Vallee, B.L., Peterson, E.A. and Fuwa, K. (1966) Spectrographic and chromatographic resolution of metalloproteins in human serum. *Biochemistry* 5, 2523-30.
- Hirose, J. and Kidani, Y. (1981) Coordination chemical studies on metalloenzymes. IX. Properties of the ternary complex between cobalt(II)-bovine carbonic anhydrase and bidentate ligands. *J Inorg Biochem* 14, 313-26.
- International Human Genome Sequencing Consortium (2004) Finishing the euchromatic sequence of the human genome. *Nature* 431, 931-45.
- Ishihama, Y., Schmidt, T., Rappsilber, J., Mann, M., Hartl, F.U., Kerner, M.J. and Frishman, D. (2008) Protein abundance profiling of the *Escherichia coli* cytosol. *BMC Genomics* 9, 102.
- Izard, T. and Sygusch, J. (2004) Induced fit movements and metal cofactor selectivity of class II aldolases: Structure of *Thermus aquaticus* fructose-1,6-bisphosphate aldolase. *J Biol Chem* 279, 11825-11833.
- Joint Commission on Biochemical Nomenclature (1984) IUPAC-IUB Joint Commission on Biochemical Nomenclature (JCBN). Nomenclature and symbolism for amino acids and peptides. Recommendations 1983. *Biochem J* 219, 345-73.
- Jacobs, M.A., Alwood, A., Thaipisuttikul, I., Spencer, D., Haugen, E., Ernst, S., Will, O., Kaul, R., Raymond, C., Levy, R., Chun-Rong, L., Guenther, D., Bovee, D., Olson, M.V. and Manoil, C. (2003) Comprehensive transposon mutant library of *Pseudomonas aeruginosa*. *Proc Natl Acad Sci U S A* 100, 14339-44.

## References

- Jafri, N.S., Hornung, C.A. and Howden, C.W. (2008) Meta-analysis: sequential therapy appears superior to standard therapy for *Helicobacter pylori* infection in patients naive to treatment. *Ann Intern Med* 148, 923-31.
- Jagannathan, V., Singh, K. and Damodaran, M. (1956) Carbohydrate metabolism in citric acid fermentation. 4. Purification and properties of aldolase from *Aspergillus niger*. *Biochem J* 63, 94-105.
- Jayanthi Bai, N., Ramachandra Pai, M., Suryanarayana Murthy, P. and Venkitasubramanian, T.A. (1975) Pathways of carbohydrate metabolism in *Mycobacterium tuberculosis* H37Rv1. *Can J Microbiol* 21, 1688-91.
- Joerger, A.C., Mueller-Dieckmann, C. and Schulz, G.E. (2000) Structures of l-fuculose-1-phosphate aldolase mutants outlining motions during catalysis. *J Mol Biol* 303, 531-43.
- Kadonaga, J.T. and Knowles, J.R. (1983) Role of mono- and divalent metal cations in the catalysis by yeast aldolase. *Biochemistry* 22, 130-6.
- Kaper, J.B., Nataro, J.P. and Mobley, H.L. (2004) Pathogenic Escherichia coli. *Nat Rev Microbiol* 2, 123-40.
- Kaufmann, S.H. (2007) The contribution of immunology to the rational design of novel antibacterial vaccines. *Nat Rev Microbiol* 5, 491-504.
- Knox, W.E., Stumpf, P.K., Green, D.E. and Auerbach, V.H. (1948) The Inhibition of Sulfhydryl Enzymes as the Basis of the Bactericidal Action of Chlorine. *J Bacteriol* 55, 451-8.
- Kobayashi, K., Ehrlich, S.D., Albertini, A., Amati, G., Andersen, K.K., Arnaud, M., Asai, K., Ashikaga, S., Aymerich, S., Bessieres, P., Boland, F., Brignell, S.C., Bron, S., Bunai, K., Chapuis, J., Christiansen, L.C., Danchin, A., Debarbouille, M., Dervyn, E., Deuring, E., Devine, K., Devine, S.K., Dreesen, O., Errington, J., Fillinger, S., Foster, S.J., Fujita, Y., Galizzi, A., Gardan, R., Eschevins, C., Fukushima, T., Haga, K., Harwood, C.R., Hecker, M., Hosoya, D., Hullo, M.F., Kakeshita, H., Karamata, D., Kasahara, Y., Kawamura, F., Koga, K., Koski, P., Kuwana, R., Imamura, D., Ishimaru, M., Ishikawa, S., Ishio, I., Le Coq, D., Masson, A., Mael, C., Meima, R., Mellado, R.P., Moir, A., Moriya, S., Nagakawa, E., Nanamiya, H., Nakai, S., Nygaard, P., Ogura, M., Ohanan, T., O'reilly, M., O'rourke, M., Pragai, Z., Pooley, H.M., Rapoport, G., Rawlins, J.P., Rivas, L.A., Rivolta, C., Sadaie, A., Sadaie, Y., Sarvas, M., Sato, T., Saxild, H.H., Scanlan, E., Schumann, W., Seegers, J.F., Sekiguchi, J., Sekowska, A., Seror, S.J., Simon, M., Stragier, P., Studer, R., Takamatsu, H., Tanaka, T., Takeuchi, M., Thomaidis, H.B., Vagner, V., Van Dijl, J.M., Watabe, K., Wipat, A., Yamamoto, H., Yamamoto, M., Yamamoto, Y., Yamane, K., Yata, K., Yoshida, K., Yoshikawa, H., Zuber, U. and Ogasawara, N. (2003) Essential *Bacillus subtilis* genes. *Proc Natl Acad Sci U S A* 100, 4678-83.
- Kobes, R.D., Simpson, R.T., Vallee, R.L. and Rutter, W.J. (1969) A functional role of metal ions in a class II aldolase. *Biochemistry* 8, 585-8.

## References

- Krishnamurthy, V.M., Kaufman, G.K., Urbach, A.R., Gitlin, I., Gudiksen, K.L., Weibel, D.B. and Whitesides, G.M. (2008) Carbonic anhydrase as a model for biophysical and physical-organic studies of proteins and protein-ligand binding. *Chem Rev* 108, 946-1051.
- Kroemer, M., Merkel, I. and Schulz, G.E. (2003) Structure and catalytic mechanism of L-rhamnulose-1-phosphate aldolase. *Biochemistry* 42, 10560-8.
- Kulkarni, R.R., Parreira, V.R., Sharif, S. and Prescott, J.F. (2007) Immunization of broiler chickens against *Clostridium perfringens*-induced necrotic enteritis. *Clin Vaccine Immunol* 14, 1070-7.
- Labbe, G., Bezaire, J., Groot, S.D., How, C., Rasmusson, T., Yaeck, J., Jervis, E., Dmitrienko, G.I. and Guy Guillemette, J. (2007) High level production of the *Magnaporthe grisea* fructose 1,6-bisphosphate aldolase enzyme in *Escherichia coli* using a small volume bench-top fermentor. *Protein Expr Purif* 51, 110-119.
- Laemmli, U.K. (1970) Cleavage of structural proteins during the assembly of the head of bacteriophage T4. *Nature* 227, 680-685.
- Larkin, M.A., Blackshields, G., Brown, N.P., Chenna, R., Mcgettigan, P.A., Mcwilliam, H., Valentin, F., Wallace, I.M., Wilm, A., Lopez, R., Thompson, J.D., Gibson, T.J. and Higgins, D.G. (2007) Clustal W and Clustal X version 2.0. *Bioinformatics* 23, 2947-8.
- Lee, J.H., Bae, J., Kim, D., Choi, Y., Im, Y.J., Koh, S., Kim, J.S., Kim, M.K., Kang, G.B., Hong, S.I., Lee, D.S. and Eom, S.H. (2006) Stereoselectivity of fructose-1,6-bisphosphate aldolase in *Thermus caldophilus*. *Biochem Biophys Res Commun* 347, 616-25.
- Lessie, T.G. and Phibbs, P.V., Jr. (1984) Alternative pathways of carbohydrate utilization in pseudomonads. *Annu Rev Microbiol* 38, 359-88.
- Lewis, D.J. and Lowe, G. (1973) Phosphoglycolohydroxamic acid: An inhibitor of class I and II aldolases and triosephosphate isomerase. A potential antibacterial and antifungal agent. *J Chem Soc Chem Commun* 713-715.
- Lewis, D.J. and Lowe, G. (1977) Inhibition of fructose-1,6-bisphosphate aldolase from rabbit muscle and *Bacillus stearothermophilus*. *Eur J Biochem* 80, 119-33.
- Leytus, S.P., Toledo, D.L. and Mangel, W.F. (1984) Theory and experimental method for determining individual kinetic constants of fast-acting, irreversible proteinase inhibitors. *Biochim Biophys Acta* 788, 74-86.
- Ling, E., Feldman, G., Portnoi, M., Dagan, R., Overweg, K., Mulholland, F., Chalifa-Caspi, V., Wells, J. and Mizrachi-Nebenzahl, Y. (2004) Glycolytic enzymes associated with the cell surface of *Streptococcus pneumoniae* are antigenic in humans and elicit protective immune responses in the mouse. *Clin Exp Immunol* 138, 290-8.
- Lobo, Z. (1984) *Saccharomyces cerevisiae* aldolase mutants. *J Bacteriol* 160, 222-6.

## References

- Lyczak, J.B., Cannon, C.L. and Pier, G.B. (2002) Lung infections associated with cystic fibrosis. *Clin Microbiol Rev* 15, 194-222.
- Machajewski, T.D. and Wong, C.H. (2000) The catalytic asymmetric aldol reaction. *Angew Chem Int Ed Engl* 39, 1352-1374.
- Marino, M., Hoffmann, T., Schmid, R., Moßbitz, H. and Jahn, D. (2000) Changes in protein synthesis during the adaptation of *Bacillus subtilis* to anaerobic growth conditions. *Microbiology* 146, 97-105.
- Marks, G.T., Harris, T.K., Massiah, M.A., Mildvan, A.S. and Harrison, D.H.T. (2001) Mechanistic Implications of Methylglyoxal Synthase Complexed with Phosphoglycolohydroxamic Acid As Observed by X-ray Crystallography and NMR Spectroscopy. *Biochemistry* 40, 6805-6818.
- Marques, H.H., Zouain, C.S., Torres, C.B., Oliveira, J.S., Alves, J.B. and Goes, A.M. (2008) Protective effect and granuloma down-modulation promoted by RP44 antigen a fructose 1,6 bisphosphate aldolase of *Schistosoma mansoni*. *Immunobiology* 213, 437-46.
- Marsh, J.J. and Lebherz, H.G. (1992) Fructose-bisphosphate aldolases: an evolutionary history. *Trends Biochem Sci* 17, 110-3.
- Mccarthy, J.S., Wieseman, M., Tropea, J., Kaslow, D., Abraham, D., Lustigman, S., Tuan, R., Guderian, R.H. and Nutman, T.B. (2002) *Onchocerca volvulus* glycolytic enzyme fructose-1,6-bisphosphate aldolase as a target for a protective immune response in humans. *Infect Immun* 70, 851-8.
- Mcnamara, D. and El-Omar, E. (2008) Helicobacter pylori infection and the pathogenesis of gastric cancer: a paradigm for host-bacterial interactions. *Dig Liver Dis* 40, 504-9.
- Menz, G.L., Hazell, S.L. and Burns, B.P. (1994) The Entner-Doudoroff pathway in *Helicobacter pylori*. *Arch Biochem Biophys* 312, 349-56.
- Meyerhof, O. (1948) New investigations on enzymatic glycolysis and phosphorylation. *Experientia* 4, 169-176.
- Meyerhof, O., Lohmann, K. and Schuster, P. (1936) On the aldolase, a carbon-knotting enzyme. II. Announcement: Aldol-condensation of dioxyacetone-phosphoric acid with glycerine-aldehyde. *Biochemische Zeitschrift* 286, 319-335.
- Mildvan, A.S., Kobes, R.D. and Rutter, W.J. (1971) Magnetic resonance studies of the role of the divalent cation in the mechanism of yeast aldolase. *Biochemistry* 10, 1191-204.
- Mitchell, C., Morris, P.W., Lum, L., Spiegelman, G. and Vary, J.C. (1992) The amino acid sequence of a *Bacillus subtilis* phosphoprotein that matches an orfY-tsr coding sequence. *Mol Microbiol* 6, 1345-9.

## References

- Monaghan, R.L. and Barrett, J.F. (2006) Antibacterial drug discovery--then, now and the genomics future. *Biochem Pharmacol* 71, 901-9.
- Morrison, J.F. and Walsh, C.T. (1988) The behavior and significance of slow-binding enzyme inhibitors. *Adv Enzymol Relat Areas Mol Biol* 61, 201-301.
- Munagala, N., Basus, V.J. and Wang, C.C. (2001) Role of the flexible loop of hypoxanthine-guanine-xanthine phosphoribosyltransferase from *Tritrichomonas foetus* in enzyme catalysis. *Biochemistry* 40, 4303-11.
- Nagano, N., Orengo, C.A. and Thornton, J.M. (2002) One fold with many functions: The evolutionary relationships between TIM barrel families based on their sequences, structures and functions. *J Mol Biol* 321, 741-765.
- Nakahara, K., Yamamoto, H., Miyake, C. and Yokota, A. (2003) Purification and characterization of class-I and class-II fructose-1,6-bisphosphate aldolases from the cyanobacterium *Synechocystis* sp. PCC6803. *Plant and Cell Physiology* 44, 326-333.
- Nathan, C. (2004) Antibiotics at the crossroads. *Nature* 431, 899-902.
- Neidhardt, F.C. and Magasanik, B. (1960) Studies on the role of ribonucleic acid in the growth of bacteria. *Biochim Biophys Acta* 42, 99-116.
- O'brien, R.J. and Nunn, P.P. (2001) The need for new drugs against tuberculosis: Obstacles, opportunities, and next steps. *Am J Respir Crit Care Med* 163, 1055-1058.
- Oerke, E.-C., and Dehne, H.-W. (2004) Safeguarding production—losses in major crops and the role of crop protection. *Crop Protection* 23, 275-285.
- Ohyoshi, E., Hamada, Y., Nakata, K. and Kohata, S. (1999) The interaction between human and bovine serum albumin and zinc studied by a competitive spectrophotometry. *J Inorg Biochem* 75, 213-218.
- Palm, J.E., Weiland, M.E., Griffiths, W.J., Ljungstrom, I. and Svard, S.G. (2003) Identification of immunoreactive proteins during acute human giardiasis. *J Infect Dis* 187, 1849-59.
- Pasqualotto, A.C. and Denning, D.W. (2008) New and emerging treatments for fungal infections. *J Antimicrob Chemother* 61 Suppl 1, i19-30.
- Pegan, S.D., Rukseere, K., Franzblau, S.G. and Mesecar, A.D. (2009) Structural basis for catalysis of a tetrameric class IIa fructose 1,6-bisphosphate aldolase from *Mycobacterium tuberculosis*. *J Mol Biol* 386, 1038-53.
- Peitsch, M.C. (1995) Protein Modeling by E-Mail. *Bio-Technology* 13, 658-660.
- Pelzer-Reith, B., Wiegand, S. and Schnarrenberger, C. (1994) Plastid class I and cytosol class II aldolase of *Euglena gracilis*. Purification and characterization. *Plant Physiology* 106, 1137-1144.

## References

- Pezza, J.A., Choi, K.H., Berardini, T.Z., Beernink, P.T., Allen, K.N. and Tolan, D.R. (2003) Spatial clustering of isozyme-specific residues reveals unlikely determinants of isozyme specificity in fructose-1,6-bisphosphate aldolase. *J Biol Chem* 278, 17307-13.
- Plater, A.R., Zgiby, S.M., Thomson, G.J., Qamar, S., Wharton, C.W. and Berry, A. (1999) Conserved residues in the mechanism of the *E. coli* class II FBP-aldolase. *J Mol Biol* 285, 843-855.
- Plaumann, M., Pelzer-Reith, B., Martin, W.F. and Schnarrenberger, C. (1997) Multiple recruitment of class-I aldolase to chloroplasts and eubacterial origin of eukaryotic class-II aldolases revealed by cDNAs from *Euglena gracilis*. *Curr Genet* 31, 430-438.
- Pompliano, D.L., Peyman, A. and Knowles, J.R. (1990) Stabilization of a reaction intermediate as a catalytic device: definition of the functional role of the flexible loop in triosephosphate isomerase. *Biochemistry* 29, 3186-94.
- Portnoi, M., Ling, E., Feldman, G., Dagan, R. and Mizrahi-Nebenzahl, Y. (2006) The vaccine potential of *Streptococcus pneumoniae* surface lectin- and non-lectin proteins. *Vaccine* 24, 1868-73.
- Qamar, S., Marsh, K. and Berry, A. (1996) Identification of arginine 331 as an important active site residue in the Class II fructose-1,6-bisphosphate aldolase of *Escherichia coli*. *Protein Science* 5, 154-161.
- Ramsaywak, P.C. (2003). The development of an expression system for fructose 1,6-bisphosphate aldolase II. Waterloo, Ont., University of Waterloo Dept. of Chemistry: xvii, 141 leaves.
- Ramsaywak, P.C., Labbe, G., Siemann, S., Dmitrienko, G.I. and Guillemette, J.G. (2004) Molecular cloning, expression, purification, and characterization of fructose 1,6-bisphosphate aldolase from *Mycobacterium tuberculosis* - A novel Class II A tetramer. *Protein Expr Purif* 37, 220-228.
- Rodaki, A., Young, T. and Brown, A.J. (2006) Effects of depleting the essential central metabolic enzyme fructose-1,6-bisphosphate aldolase on the growth and viability of *Candida albicans*: implications for antifungal drug target discovery. *Eukaryot Cell* 5, 1371-7.
- Roe, J.H., Epstein, J.H. and Goldstein, N.P. (1949) A photometric method for the determination of insulin in plasma and urine. *J Biol Chem* 178, 839-45.
- Rogers, M. and Keeling, P.J. (2004) Lateral transfer and re-compartmentalization of calvin cycle enzymes of plants and algae. *J Mol Evol* 58, 367-375.
- Rose, I.A., O'connell, E.L. and Mehler, A.H. (1965) Mechanism of the Aldolase Reaction. *J Biol Chem* 240, 1758-65.
- Rose, I.A. and Rieder, S.V. (1958) Studies on the mechanism on the aldolase reaction; isotope exchange reactions of muscle and yeast aldolase. *J Biol Chem* 231, 315-29.



## References

- Rosenblum, G., Meroueh, S.O., Kleifeld, O., Brown, S., Singson, S.P., Fridman, R., Mobashery, S. and Sagi, I. (2003) Structural basis for potent slow binding inhibition of human matrix metalloproteinase-2 (MMP-2). *J Biol Chem* 278, 27009-15.
- Rosenkrands, I., Slayden, R.A., Crawford, J., Aagaard, C., Barry, C.E., 3rd and Andersen, P. (2002) Hypoxic response of *Mycobacterium tuberculosis* studied by metabolic labeling and proteome analysis of cellular and extracellular proteins. *J Bacteriol* 184, 3485-91.
- Rukseree, K., Thammarongtham, C. and Palittapongarnpim, P. (2008) One-step purification and characterization of a fully active histidine-tagged Class II fructose-1,6-bisphosphate aldolase from *Mycobacterium tuberculosis*. *Enzyme Microb Technol* 43, 500-506.
- Rutter, W.J. (1964) Evolution of Aldolase. *Fed Proc* 23, 1248-57.
- Rutter, W.J. and Ling, K.H. (1958) The mechanism of action of fructose diphosphate aldolase. *Biochim Biophys Acta* 30, 71-9.
- Sadoff, H.L., Hitchins, A.D. and Celikkol, E. (1969) Properties of fructose 1,6-diphosphate aldolases from spores and vegetative cells of *Bacillus cereus*. *J Bacteriol* 98, 1208-18.
- Saiman, L. and Siegel, J. (2004) Infection control in cystic fibrosis. *Clin Microbiol Rev* 17, 57-71.
- Sakharkar, K.R., Sakharkar, M.K. and Chow, V.T. (2004) A novel genomics approach for the identification of drug targets in pathogens, with special reference to *Pseudomonas aeruginosa*. *In Silico Biol* 4, 355-60.
- Salama, N.R., Shepherd, B. and Falkow, S. (2004) Global transposon mutagenesis and essential gene analysis of *Helicobacter pylori*. *J Bacteriol* 186, 7926-35.
- Sambrook, J., Fritsch, E.F. and Maniatis, T. (1989). Molecular Cloning, a Laboratory Manual, Second Edition. Plainview, NY, Cold Spring Harbor Laboratory Press.
- Sánchez, L.B., Horner, D.S., Moore, D.V., Henze, K., Embley, T.M. and Müller, M. (2002) Fructose-1,6-bisphosphate aldolases in amitochondriate protists constitute a single protein subfamily with eubacterial relationships. *Gene* 295, 51-59.
- Sasseti, C.M., Boyd, D.H. and Rubin, E.J. (2001) Comprehensive identification of conditionally essential genes in mycobacteria. *Proc Natl Acad Sci U S A* 98, 12712-7.
- Sasseti, C.M., Boyd, D.H. and Rubin, E.J. (2003) Genes required for mycobacterial growth defined by high density mutagenesis. *Mol Microbiol* 48, 77-84.
- Sauve, V. and Sygusch, J. (2001a) Crystallization and preliminary X-ray analysis of native and selenomethionine fructose-1,6-bisphosphate aldolase from *Thermus aquaticus*. *Acta Crystallogr D Biol Crystallogr* 57, 310-3.

## References

- Sauve, V. and Sygusch, J. (2001b) Molecular cloning, expression, purification, and characterization of fructose-1,6-bisphosphate aldolase from *Thermus aquaticus*. *Protein Expr Purif* 21, 293-302.
- Scamuffa, M.D. and Caprioli, R.M. (1980) Comparison of the mechanisms of two distinct aldolases from *Escherichia coli* grown on gluconeogenic substrates. *Biochimica et Biophysica Acta* 614, 583-590.
- Schmid, R., Uhlemann, E.M., Nolden, L., Wersch, G., Hecker, R., Hermann, T., Marx, A. and Burkovski, A. (2000) Response to nitrogen starvation in *Corynebacterium glutamicum*. *FEMS Microbiology Letters* 187, 83-88.
- Schneider, D.A. and Gourse, R.L. (2003a) Changes in *Escherichia coli* rRNA promoter activity correlate with changes in initiating nucleoside triphosphate and guanosine 5' diphosphate 3'-diphosphate concentrations after induction of feedback control of ribosome synthesis. *J Bacteriol* 185, 6185-91.
- Schneider, D.A. and Gourse, R.L. (2003b) Changes in the concentrations of guanosine 5'-diphosphate 3'-diphosphate and the initiating nucleoside triphosphate account for inhibition of rRNA transcription in fructose-1,6-diphosphate aldolase (fda) mutants. *J Bacteriol* 185, 6192-4.
- Schoevaart, R., Van Rantwijk, F. and Sheldon, R.A. (2000) Stereochemistry of nonnatural aldol reactions catalyzed by DHAP aldolases. *Biotechnol Bioeng* 70, 349-52.
- Schoevaart, R., Van Rantwijk, F. and Sheldon, R.A. (2001) Facile enzymatic aldol reactions with dihydroxyacetone in the presence of arsenate. *J Org Chem* 66, 4559-62.
- Schray, K.J., Fishbein, R., Bullard, W.P. and Benkovic, S.J. (1975) The anomeric form of D-fructose 1,6-bisphosphate used as substrate in the muscle and yeast aldolase reactions. *J Biol Chem* 250, 4883-7.
- Schreyer, R. and Bock, A. (1973) Phenotypic suppression of a fructose-1,6-diphosphate aldolase mutation in *Escherichia coli*. *J Bacteriol* 115, 268-76.
- Schwede, T., Kopp, J., Guex, N. and Peitsch, M.C. (2003) SWISS-MODEL: An automated protein homology-modeling server. *Nucleic Acids Res* 31, 3381-5.
- Schwelberger, H.G., Kohlwein, S.D. and Paltauf, F. (1989) Molecular cloning, primary structure and disruption of the structural gene of aldolase from *Saccharomyces cerevisiae*. *Eur J Biochem* 180, 301-8.
- Seoane, G. (2000) Enzymatic C-C bond-forming reactions in organic synthesis. *Curr Org Chem* 4, 283-304.
- Shao, P.L., Huang, L.M. and Hsueh, P.R. (2007) Recent advances and challenges in the treatment of invasive fungal infections. *Int J Antimicrob Agents* 30, 487-95.

## References

- Siemann, S., Brewer, D., Clarke, A.J., Dmitrienko, G.I., Lajoie, G. and Viswanatha, T. (2002) IMP-1 metallo-beta-lactamase: Effect of chelators and assessment of metal requirement by electrospray mass spectrometry. *Biochimica et Biophysica Acta - General Subjects* 1571, 190-200.
- Siemann, S., Clarke, A.J., Viswanatha, T. and Dmitrienko, G.I. (2003) Thiols as classical and slow-binding inhibitors of IMP-1 and other binuclear metallo-beta-lactamases. *Biochemistry* 42, 1673-83.
- Singer, M., Rossmiessl, P., Cali, B.M., Liebke, H. and Gross, C.A. (1991a) The *Escherichia coli* ts8 mutation is an allele of *fda*, the gene encoding fructose-1,6-diphosphate aldolase. *J Bacteriol* 173, 6242-8.
- Singer, M., Walter, W.A., Cali, B.M., Rouviere, P., Liebke, H.H., Gourse, R.L. and Gross, C.A. (1991b) Physiological effects of the fructose-1,6-diphosphate aldolase ts8 mutation on stable RNA synthesis in *Escherichia coli*. *J Bacteriol* 173, 6249-57.
- Sluis-Cremer, N., Dmitrienko, G.I., Balzarini, J., Camarasa, M.J. and Parniak, M.A. (2000) Human immunodeficiency virus type 1 reverse transcriptase dimer destabilization by 1-[Spiro[4"-amino-2",2" -dioxo-1",2" -oxathiole-5",3'-[2', 5'-bis-O-(tert-butylidimethylsilyl)-beta-D-ribofuranosyl]]]-3-ethylthymine. *Biochemistry* 39, 1427-33.
- Soanes, D.M., Skinner, W., Keon, J., Hargreaves, J. and Talbot, N.J. (2002) Genomics of phytopathogenic fungi and the development of bioinformatic resources. *Mol Plant Microbe Interact* 15, 421-7.
- Song, J.H., Ko, K.S., Lee, J.Y., Baek, J.Y., Oh, W.S., Yoon, H.S., Jeong, J.Y. and Chun, J. (2005) Identification of essential genes in *Streptococcus pneumoniae* by allelic replacement mutagenesis. *Mol Cells* 19, 365-74.
- Sterner, R. and Hocker, B. (2005) Versatility, stability, and evolution of the (beta alpha)(8)-barrel enzyme fold. *Chem Rev* 105, 4038-4055.
- Stribling, D. and Perham, R.N. (1973) Purification and characterization of two fructose diphosphate aldolases from *Escherichia coli* (Crookes' strain). *Biochem J* 131, 833-41.
- Su, C.H., Merlie, J.P. and Goldfine, H. (1975) Rapid cessation of phospholipid synthesis in fructose-1,6-diphosphate aldolase mutants of *Escherichia coli*. *J Bacteriol* 122, 565-9.
- Szwergold, B.S., Ugurbil, K. and Brown, T.R. (1995) Properties of fructose-1,6-bisphosphate aldolase from *Escherichia coli*: an NMR analysis. *Arch Biochem Biophys* 317, 244-52.
- Tabor, S. and Richardson, C.C. (1985) A bacteriophage T7 RNA polymerase/promoter system for controlled exclusive expression of specific genes. *Proc Natl Acad Sci U S A* 82, 1074-1078.
- Takayama, S., Mcgarvey, G.J. and Wong, C.H. (1997) Microbial aldolases and transketolases: new biocatalytic approaches to simple and complex sugars. *Annu Rev Microbiol* 51, 285-310.

## References

- Talbot, N.J. (2003) On the trail of a cereal killer: Exploring the biology of *Magnaporthe grisea*. *Annu Rev Microbiol* 57, 177-202.
- Tamames, B., Sousa, S.F., Tamames, J., Fernandes, P.A. and Ramos, M.J. (2007) Analysis of zinc-ligand bond lengths in metalloproteins: trends and patterns. *Proteins* 69, 466-75.
- Thomson, G.J., Howlett, G.J., Ashcroft, A.E. and Berry, A. (1998) The *dhnA* gene of *Escherichia coli* encodes a Class I fructose bisphosphate aldolase. *Biochem J* 331, 437-445.
- Tomas, C.A., Beamish, J. and Papoutsakis, E.T. (2004) Transcriptional Analysis of Butanol Stress and Tolerance in *Clostridium acetobutylicum*. *J Bacteriol* 186, 2006-2018.
- Trach, K., Chapman, J.W., Piggot, P., Lecoq, D. and Hoch, J.A. (1988) Complete sequence and transcriptional analysis of the *spo0F* region of the *Bacillus subtilis* chromosome. *J Bacteriol* 170, 4194-208.
- Tsou, C.L. (1988) Kinetics of substrate reaction during irreversible modification of enzyme activity. *Adv Enzymol Relat Areas Mol Biol* 61, 381-436.
- Valjevac, S., Hilaire, V., Lisanti, O., Rami se, F., Hernandez, E., Cavallo, J.D., Pourcel, C. and Vergnaud, G. (2005) Comparison of minisatellite polymorphisms in the *Bacillus cereus* complex: a simple assay for large-scale screening and identification of strains most closely related to *Bacillus anthracis*. *Appl Environ Microbiol* 71, 6613-23.
- Van Den Bergh, E.R., Baker, S.C., Riggers, R.J., Terpstra, P., Woudstra, E.C., Dijkhuizen, L. and Meijer, W.G. (1996) Primary structure and phylogeny of the Calvin cycle enzymes transketolase and fructosebisphosphate aldolase of *Xanthobacter flavus*. *J Bacteriol* 178, 888-93.
- Veiga-Crespo, P., Ageitos, J.M., Poza, M. and Villa, T.G. (2007) Enzybiotics: a look to the future, recalling the past. *J Pharm Sci* 96, 1917-24.
- Verhees, C.H., Kengen, S.W., Tuininga, J.E., Schut, G.J., Adams, M.W., De Vos, W.M. and Van Der Oost, J. (2003) The unique features of glycolytic pathways in Archaea. *Biochem J* 375, 231-46.
- Voet, D. and Voet, J.G. (2004). Biochemistry, John Wiley and Sons, Inc.
- Von Der Osten, C.H., Sinskey, A.J., Barbas, C.F., Pederson, R.L., Wang, Y.F. and Wong, C.H. (1989) Use of a recombinant bacterial fructose-1,6-diphosphate aldolase in aldol reactions: preparative syntheses of 1-deoxynojirimycin, 1-deoxymannojirimycin, 1,4-dideoxy-1,4-imino-D-arabinitol, and fagomine. *J Am Chem Soc* 111, 3924-3927.
- Wellcome Trust Sanger Institute (2008). Pathogen Genomics. Cambridge, U.K. <http://www.sanger.ac.uk/Projects/Pathogens/>
- Walsh, C. (2003) Where will new antibiotics come from? *Nat Rev Microbiol* 1, 65-70.

## References

- Walsh, C. and Wright, G. (2005) Introduction: antibiotic resistance. *Chem Rev* 105, 391-4.
- Wang, J., Tolan, D.R. and Pagliaro, L. (1997) Metabolic compartmentation in living cells: structural association of aldolase. *Exp Cell Res* 237, 445-51.
- Wang, W. and Malcolm, B.A. (1999) Two-stage PCR protocol allowing introduction of multiple mutations, deletions and insertions using QuikChange Site-Directed Mutagenesis. *Biotechniques* 26, 680-2.
- Warburg, O. and Christian, W. (1943) Isolation and cristalization of the fermentative enzyme zymohexase. *Biochemische Z* 314, 149-176.
- Wehmeier, U.F. (2001) Molecular cloning, nucleotide sequence and structural analysis of the *Streptomyces galbus* DSM40480 *fda* gene: The *S. galbus* fructose-1,6-bisphosphate aldolase is a member of the class II aldolases. *FEMS Microbiol Lett* 197, 53-58.
- Wen, J., Nelson, S.W., Honzatko, R.B., Fromm, H.J. and Petrich, J.W. (2001) Environment of tryptophan 57 in porcine fructose-1,6-bisphosphatase studied by time-resolved fluorescence and site-directed mutagenesis. *Photochem Photobiol* 74, 679-85.
- Whitesides, G.M. and Krishnamurthy, V.M. (2005) Designing ligands to bind proteins. *Quarterly Reviews of Biophysics* 38, 385-395.
- Whiting, G.C., Rijpkema, S., Adams, T. and Corbel, M.J. (2004) Characterisation of adsorbed anthrax vaccine by two-dimensional gel electrophoresis. *Vaccine* 22, 4245-51.
- World Health Organization (2004). World Health Report 2004 - Changing History. <http://www.who.int/whr/2004/en/>
- Wilkins, J.C., Homer, K.A. and Beighton, D. (2002) Analysis of *Streptococcus mutans* proteins modulated by culture under acidic conditions. *Appl Environ Microbiol* 68, 2382-2390.
- Willard, J.M. and Gibbs, M. (1968a) Purification and characterization of the fructose diphosphate aldolases from *Anacystis is nidulans* and *Saprospira thermalis*. *Biochimica Biophys ACTA* 151, 438-448.
- Willard, J.M. and Gibbs, M. (1968b) Role of Aldolase in Photosynthesis. II Demonstration of Aldolase Types in Photosynthetic Organisms. *Plant Physiol* 43, 793-798.
- Williams, G.J., Domann, S., Nelson, A. and Berry, A. (2003) Modifying the stereochemistry of an enzyme-catalyzed reaction by directed evolution. *Proc Natl Acad Sci U S A* 100, 3143-8.
- Williams, J.C. and Mcdermott, A.E. (1995) Dynamics of the flexible loop of triosephosphate isomerase: the loop motion is not ligand gated. *Biochemistry* 34, 8309-19.
- Winslow, R.M. (1971) A consequence of the *rel* gene during a glucose to lactate downshift in *Escherichia coli*. The rates of ribonucleic acid synthesis. *J Biol Chem* 246, 4872-7.

## References

- Wommer, S., Rival, S., Heinz, U., Galleni, M., Frere, J.M., Franceschini, N., Amicosante, G., Rasmussen, B., Bauer, R. and Adolph, H.W. (2002) Substrate-activated zinc binding of metallo-beta-lactamases: Physiological importance of the mononuclear enzymes. *J Biol Chem* 277, 24142-24147.
- Wong, C.H., Halcomb, R.L., Ichikawa, Y. and Kajimoto, T. (1995) Enzymes in Organic-Synthesis - Application to the Problems of Carbohydrate-Recognition .1. *Angew Chem Int Ed Engl* 34, 412-432.
- Yin, Z., Stead, D., Selway, L., Walker, J., Riba-Garcia, I., McInerney, T., Gaskell, S., Oliver, S.G., Cash, P. and Brown, A.J. (2004) Proteomic response to amino acid starvation in *Candida albicans* and *Saccharomyces cerevisiae*. *Proteomics* 4, 2425-36.
- Zgiby, S., Plater, A.R., Bates, M.A., Thomson, G.J. and Berry, A. (2002) A functional role for a flexible loop containing Glu182 in the class II fructose-1,6-bisphosphate aldolase from *Escherichia coli*. *J Mol Biol* 315, 131-140.
- Zgiby, S.M., Thomson, G.J., Qamar, S. and Berry, A. (2000) Exploring substrate binding and discrimination in fructose 1,6- bisphosphate and tagatose 1,6-bisphosphate aldolases. *Eur J Biochem* 267, 1858-1868.
- Zhu, Y., Chen, H., Fan, J., Wang, Y., Li, Y., Chen, J., Fan, J., Yang, S., Hu, L., Leung, H., Mew, T.W., Teng, P.S., Wang, Z. and Mundt, C.C. (2000) Genetic diversity and disease control in rice. *Nature* 406, 718-22.